NanoScience and Technology

Sergey Bulyarskiy
Alexandr Saurov *Editors*

Doping of Carbon Nanotubes

Springer

NanoScience and Technology

The series NanoScience and Technology is focused on the fascinating nano-world, mesoscopic physics, analysis with atomic resolution, nano and quantum-effect devices, nanomechanics and atomic-scale processes. All the basic aspects and technology-oriented developments in this emerging discipline are covered by comprehensive and timely books. The series constitutes a survey of the relevant special topics, which are presented by leading experts in the field. These books will appeal to researchers, engineers, and advanced students.

More information about this series at http://www.springer.com/series/3705

Sergey Bulyarskiy · Alexandr Saurov
Editors

Doping of Carbon Nanotubes

Springer

Editors
Sergey Bulyarskiy
Institute Nanotechnology
of Microelectronics
Russian Academy of Sciences
Moscow
Russia

Alexandr Saurov
Institute Nanotechnology
of Microelectronics
Russian Academy of Sciences
Moscow
Russia

ISSN 1434-4904 ISSN 2197-7127 (electronic)
NanoScience and Technology
ISBN 978-3-319-55882-0 ISBN 978-3-319-55883-7 (eBook)
DOI 10.1007/978-3-319-55883-7

Library of Congress Control Number: 2017937503

Printed on acid-free paper

This Springer imprint is published by Springer Nature
The registered company is Springer International Publishing AG
The registered company address is: Gewerbestrasse 11, 6330 Cham, Switzerland

Preface

The main trend in the nanoelectronics is connected with hybrid structure creation and production using carbon nanotubes (CNT), which have been specially developed up for silicon integral circuits. In this case one can naturally combine modern microelectronic achievements with the CNT advantages and thus produce large-scale integrated circuits (LSIC) with several new and unique properties. This method adds additional possibilities to the production and use of new devices with built-in microwave range receivers and emitters for irradiation, cold emission, etc., as well as various magnetic, chemical, and biological sensors for use in LSIC. Thus, a new direction has emerged for the general development of microelectronics. This development is known as silicon–carbon nanoelectronics and allows the combination, within a single crystal, of the properties of both silicon and carbon structures, widening the characteristics of the usual planar LSIC and/or unique carbon structures. The approach extends and magnifies the possibilities of digital treatment of information and signals.

The characteristics of CNTs are very important to practical usage: they can conduct an electric current of very high density (up to value 10^9 A/cm^2), emit electrons from their ends at low temperatures (cold electron emission), radiate light, etc. However, to combine CNT growth with existing silicon planar technologies it is necessary to know how their properties can be controlled and regulated. Property control of CNTs is connected mainly with the doping and adsorption of the various atoms and molecules.

This book provides information regarding the control of the electronic properties of CNTs. It is shown that doping and adsorption lead to a change in the electronic structure of the tubes as well as to the appearance of impurity states in the HOMO–LUMO gap. The book presents thermodynamic calculations for the formation of impurities and defects in the interaction of the nanotubes with hydrogen, oxygen, nitrogen, and boron. These calculations are based on the thermodynamic theory of self-organization of defects in solids, which was developed by the authors of this book. This model allows the calculation of results of self-organization of structural elements in multicomponent systems, including CNTs and clusters and precipitates in condensed matter, and also assists understanding the formation of nanodroplet

catalysts for the growth of CNTs. This model is adapted to the doping of carbon nanotubes. The authors provide specific calculations for doping carbon nanotubes with oxygen, hydrogen, nitrogen, and boron. They compare their thermodynamic calculations with many experimental results that are presented in the scientific literature. In particular entropy and enthalpy of the introduction of impurities in carbon nanotubes are calculated after comparing their calculations with experimental data. The possible directions for technological processes of optimization, as well as the perspectives of *p–n* transition creation by CNT arrays are pointed out. Although the scientific literature has accumulated a large empirical knowledge of doping nanotubes, one problem is the lack of a theoretical model for analysis. This book overcomes this. Analysis of a large number of experiments, based on the theoretical model, allows for an understanding of the processes of doping carbon nanotubes.

The book is a collective monograph written by the specialists of the Russian Academy of Sciences Microelectonics Nanotechologies Institute. It contains six chapters. In Chap. 1 the general problems associated with nanotube properties and control are considered, especially in connection to their doping and adsorption. In Chap. 2, the thermodynamics of these processes is studied and some equations are derived, connecting the doping admixture concentrations with the technological process conditions and features of the doping atom interactions with a graphene lattice. Chapter 3 is devoted especially to hydrogen that can be regarded as an etalon element, allowing the consideration and the undertaking of many experiments and calculations or approval of various experiments and technologies, connected with doping. The problem of a limiting degree for CNTs being filled by hydrogen is considered in connection with hydrogen energetics. Chapters 4 and 5 are devoted to main, widely used, technological admixture atoms (oxygen and nitrogen), playing an important role in a CNT property regulation. In the last, Chap. 6 the problem of nanotube doping by acceptors (including boron) is considered, as well as the perspectives of the *p–n* transitions creation on CNT arrays.

We hope that the book help the scientists, students, and post-graduates to gain orientation in the field of CNT property regulation problems as well as gaining knowledge about CNT doping regularities and the arising structure characteristics in connection with used technological process conditions.

The edition was supported by RF Ministry of Education and Science under the framework of the State Program of scientific research support.

Moscow, Russia

Prof. Alexandr Saurov
Academician of the Russian Academy of Sciences

Contents

Contributors

Alexandr S. Basaev Institute Nanotechnology of Microelectronics, Russian Academy of Sciences, Moscow, Russia

Darya A. Bogdanova Institute Nanotechnology of Microelectronics, Russian Academy of Sciences, Moscow, Russia

Sergey Bulyarskiy Institute Nanotechnology of Microelectronics, Russian Academy of Sciences, Moscow, Russia

Alexandr Pavlov Institute Nanotechnology of Microelectronics, Russian Academy of Sciences, Moscow, Russia

Alexandr Saurov Institute Nanotechnology of Microelectronics, Russian Academy of Sciences, Moscow, Russia

Abstract

This book provides information regarding the control of the electronic properties of carbon nanotubes. It is shown that doping and adsorption lead to a change in the tubes electronic structure as well as the appearance of impurity states in the HOMO–LUMO gap. The book presents thermodynamic calculations of the formation of impurities and defects in the interaction of the nanotubes with hydrogen, oxygen, nitrogen, and boron. These calculations are based on the thermodynamic theory of the self-organization of defects in solids, which was developed by the authors of this book. This model allows the calculation of results of the self-organization processes of structural elements in multi-component systems, including carbon nanotubes, clusters and precipitates in condensed matter, as well as providing an understanding of the formation of nanodroplet catalysts for growth of carbon nanotubes. This model in the book is adapted for the doping of carbon nanotubes. The authors provide specific calculations for doping carbon nanotubes with oxygen, hydrogen, nitrogen, and boron. They compare their thermodynamic calculations with many experimental results that are presented in the scientific literature. In particular the entropy and enthalpy of the introduction of impurities in carbon nanotubes are calculated after comparing calculations with experimental data. Possible directions for technological process optimization, as well as the perspectives of p–n transition creation by carbon nanotube arrays are indicated. Although the scientific literature has accumulated a large empirical knowledge of nanotube doping, this book analyzes a large number of experiments, based on theoretical models, allowing an understanding of the processes of doping carbon nanotubes. The book is intended for students, post-graduates, and researchers, connected with various investigations and applications in the field of nanoelectronics in general.

This edition was supported by RF Ministry of Education and Science under the framework of the State Program for scientific research support.

Chapter 1
Adsorption and Doping as Methods for the Electronic Regulation Properties of Carbon Nanotubes

Alexandr Saurov

Abstract This chapter contains general information about the doping of carbon nanotubes, which allows the reader better understand the main problem addressed in the book. It examines the interaction of gas molecules with the graphene lattice, discusses the differences between physical and chemical adsorption, as well as the differences between chemical adsorption and doping.

This chapter contains general information about the doping of carbon nanotubes, which allows the reader better understand the main problem addressed in the book. It examines the interaction of gas molecules with the graphene lattice, discusses the differences between physical and chemical adsorption, as well as the differences between chemical adsorption and doping.

Carbon nanotubes (CNT) are worthy of special attention from researchers and developers of modern electronic devices [1, 2] for their unique mechanical, electrical, and optical properties, which they exhibit in numerous experiments and applications [1]. They have branched surfaces (achieving hundreds of square meters per gram), that define their high sorption ability [2, 3], allowing CNT to adsorb great amounts of inert gases, hydrogen, metals, water, etc. Studies of adsorption process reveal their nature and characteristic parameters and is now one of most significant problems facing nanotechnology in general [4, 5]. Another important problem of CNT is connected with capillary phenomena, when the various substances are "drawn in" to the tubes [6]. This effects their study both theoretically [7] and experimentally [8–10]. This is important not only as an investigation of theses interesting objects, but also as an instrument of nanotube electrical property control and regulation.

Single-wall carbon nanotube (SWNT) properties depend on both their structure and morphology (chiral vector, length, diameter, the presence of closed or open ends, defects, etc.). The method of growing CNTs with certain and planned

A. Saurov (✉)
Institute Nanotechnology of Microelectronics, Russian Academy of Sciences, Moscow, Russia
e-mail: a.saurov@tcen.ru

S. Bulyarskiy and A. Saurov (eds.), *Doping of Carbon Nanotubes*, NanoScience and Technology, DOI 10.1007/978-3-319-55883-7_1

architectures should allow access to tubes with the required properties. Note, that the technique of growing CNTs and their refinement is permanently improving. Perhaps this problem will be solved in near future, although even now we can influence the growth of SWNT structures. We have effective methods, allowing the introduction of defects into CNT [11], to open the closed ends and cuts the tubes, decreasing their length [12–14].

It is sufficiently difficult to divide doping and adsorption processes for CNTs, because the CNT (just as the graphene plane itself) presents a continuous and entire surface. Therefore, the usual doping notion (an introducing of an admixture into the substance) is not applicable. We must initially define a special notion known as "CNT doping" as a process, when an admixture atom substitutes the basic atom in a carbon network node. This definition is near to the common doping notion, but is also near to the notion of "chemisorption", when an admixture atom creates chemical bonds with the basic substance atoms, located at a surface. Nevertheless, we consider that the adsorption process includes all processes where a foreign atom interacts with a carbon network surface, but does not substitute the lattice atom.

It seems likely that in the CNT case it is impossible to use the notion of free charge carrier concentration to assess the results of doping. For example, oxygen adsorption favors the whole concentration growth in nanotubes, but oxygen does not replace the lattice carbon atoms and does not even form any chemical bonds with these atoms [2, 15, 16]. This is because the oxygen interaction with a CNT is a typical example of physical adsorption, which cannot change the CNT conductance. It is connected with the fact that CNTs under adsorption change their electron structure and consequently their main corresponding properties [17, 18].

The studies and understanding of these processes, as well as development of adequate mathematical models can form a grounding for new perspective technologies, allowing the production of new devices on CNT bases. The adsorption and doping processes are now the main tools for CNT property control and regulation.

Doping and encapsulation. In classic microelectronics for material electronic properties, doping is used (i.e., an impurity atom is introduced into the sample volume). The impurity atoms introduced into the CNT arrays can occur in the graphene lattice or occupy the inter-wall channels, thus we name it "volume doping". For the SWNT the problem of doping is more complicated, because the SWNT presents a graphite sheet, being rolled up into a cylinder, i.e., into a continuous surface. We can consider an impurity introduced into the hollow nanotube inner space as "volume doping", i.e., for SWNT this encapsulation process can be considered as a variant of volume doping. Moreover, the usual substitution doping, when one carbon network atom is replaced by an admixture atom, must be considered and named as "surface doping".

Doping and adsorption. The doping affects on the electronic structure and the conductance of nanotubes but this influence dose not exclude the others local methods of CNT electronic property modification. We can change the structure and the conductance of SWNT by adsorption of any atoms. Adsorption can have a physical or chemical nature (chemisorption). For example, some experiments are

demonstrating that even weak physical adsorption of oxygen and nitrogen on a CNT can change their conductance. Chemisorption with the formation of an adsorbent new covalent or ionic bond with a nanotube is a more powerful tool for influencing SWNT properties. Even hydrogen (which in a physically adsorbed state practically has no influence on CNT conductance) in a chemisorbed state sufficiently affects their resistance. Chemisorption influence on tube conductance is comparable with a doping influence, but can be more easily realized practically.

Doping and chemisorption. The separation of chemisorption and adsorption for SWNT seems to be a conditional one. In both cases are formed some new chemical bonds between the adsorbed atom and the nanotube carbon network. As this takes place, so proceeds a sufficient change of the systems' electronic spectra and properties, as well as charge transport. For example, for nitrogen doping on SWNT we have two well-known doping mechanisms with near energy parameters: first, classical substitution (graphite-type) doping; second, pyridine-type doping. The chemisorption of the impurity atoms can be realized on both external and internal surfaces of a nanotube, and the case of internal chemisorption can be considered as volumetric adsorption.

The adsorption can have an accentuated applied meaning, for example, as a process allowing the design of hydrogen storage. The first investigation of CNT adsorptive abilities in respect to hydrogen gave very optimistic results. For example, Dillon obtained a value of 5–10 wt% [19], Chen obtained 10–20 wt% [20], whilst in other work [21–24] values of more than 8 wt% at 80 K and 10 MPa have been achieved. Note also, that the physical adsorption efficiency is connected with tube curvature [25] and an intensive adsorption runs into the tubes and pores, formed by tube bunches [21, 26–28], not considering the defect influence [22, 29].

The adsorption process plays an important role in the mechanisms of charge carrier transfer or carrier emission, and therefore the adsorption parameters must be defined to create any controlling technologies. The main method used to define these parameters are studies of the adsorption process kinetics, and particularly the gravimetric measurements under desorption. To obtain a definition of the adsorbed atoms or molecules energies and numbers it was first necessary to develop a general thermodynamic model of adsorption. In this book, such a model is generated on the basis of the Gibbs free energy minimization method studies [30–32]. The foundations of our calculation are described in several publications [33, 34].

The adsorption processes on carbon nanotubes have some important peculiarities in comparison with the adsorption on a volume substance. First, the tubes are charged and therefore there can appear with strong electric fields at their ends. Second, the nanotube surface has strong inner elastic stresses. Moreover, in a multilayer CNT every tube has its own field of elastic stresses, which increase with a decrease in tube radius. Hence, the adsorption processes in single-wall and multi-wall nanotubes are different in their features and respectively this difference must be taken into account in theoretical models and calculation algorithms for the adsorption process parameters in these cases. In general, the CNTs in terms of their structure are placed between graphene and fullerene [1, 6].

A detailed review of CNT adsorption is presented in a survey by Eletzky [6]. Adsorption theoretical models have been developed by [35]. Calculations [15, 16] have shown that for any adsorption type, the forbidden zone width narrows, but this effect is weaker for physical adsorption case. At high adsorbate, concentrations appear at discrete levels, splitting off from corresponding zones, with their positions changing with changes in the adsorbate donor–acceptor properties and concentrations. It is obvious, that this situation affects the CNT optical and electric properties, and this effect can be used for practical purposes. Thus, adsorption changes the electronic properties of the "CNT–adsorbate" system, and this can be used to create various types of sensor.

The authors of one piece of research [36] obtained analogous results. In particular, they showed that under physical adsorption of the complex organic molecules there proceeds a localization of the charge carriers on CNT, which defines some change in the nano-conductor resistance. The energy spectrum depends on the molecular system rigidity. A crystallization of the coating leads to a step-wise rigidity change with a step-wise growth of CNT conductance. The theoretical calculations were affirmed by the results obtained by the molecular dynamics method [37]. The adsorbed addend can be movable ones [36], and it was affirmed by Monte-Carlo experiments.

From the scientific literature data we can conclude that at low temperatures (up to 150 K) the adsorption is mainly physical in character with stable bonds between carbon and adsorbent not being formed. The physical adsorption is usually caused by various natural forces (van der Waals interactions, electrostatic polarization, etc.), characterized by an absence of exchange interaction, peculiar to the chemisorption. Under physical adsorption processes of the molecule decomposition into atoms, along with their recharging, does not occur, hence we can neglect the electronic processes. Note, that hydrogen physical adsorption is observed at low temperatures (up to 80 K) and its content is no more than 1.2 wt% of hydrogen. Such a small value of physical adsorption is connected with the fact that chemical bonds are not forming.

Chemisorption is characterized by the formation of covalent or ionic bonds, as well as an adsorbate changing theirs charge. The adsorptive abilities of nanotubes increasing in this case, but the adsorption process itself is more complicated, because for chemical bond formation the adsorbate must overcome a potential barrier. If the adsorbate (i.e., as for the case of hydrogen) exists in a molecular form, it must be transformed in an atomic form. At the same time the forces holding the adsorbate in place are stronger under chemisorption, something which arises from the amount of adsorbed substance. These properties make chemisorption a prospective process for hydrogen energetics in general (i.e., for creating hydrogen storage devices with working temperatures, exceeding the room temperature).

Investigations of the graphite paramagnets [38] and adsorptive characteristics [39] have shown that the nature of bond hybridization is changing for the adsorbent atom, on which the adsorption proceeds: namely $sp^2\pi$-hybridization transforms into s^2p^2-hybridization. This means that one of the carbon σ-bonds is being torn apart, whilst the two free bonds join the two hydrogen atoms (formed after the molecule

dissociates). There are also suggestions of other mechanisms of CNT electric property change.

References

1. S.V. Bulyarskiy, *Uglerodnye nanotrubky: techologya, upravlenie svoystvami, primenenie* (Streshen, Ulyanovsk, 2011), 479 p (Rus.)
2. A. Tchernatinsky, B. Nagabhinrava, S. Desai et al., Adsorption oxygen molecules on individual Carbon single-walled nanotubes. arXiv: cond-mat/0502012 (2005)
3. H. Ulbricht, G. Moos, T. Hertel, Physisorption of molecular oxygen on single-walled Carbon nanotubes bundles and graphite. arXiv: cond-mat/0204525 (2005)
4. S.V. Bulyarskiy, A.S. Basaev, Thermodynamics and kinetics of adsorption of atoms and molecules with carbon nanotubes. ZhETF **135**(4), 788–799 (2009)
5. S.V. Bulyarskiy, A.S. Basaev, Adsorption by carbon nanotubes. Nano Microsyst. **12**(116), 16–55 (2009)
6. V.A. Eletskiy, Sorption properties of carbon nanostructures. Adv. Phys. Sci. **174**(11), 1191–1231 (2004)
7. M.R. Pederson, J.Q. Broughton, Phys. Rev. Lett. **69**, 2689 (1992)
8. P.M. Ajayan, S. Iijima, Nature **361**, 333 (1993)
9. T.W. Ebbesen, Annu. Rev. Mater. Sci. **24**, 235 (1994)
10. T.W. Ebbesen, Phys. Today **49**(6), 26 (1996)
11. M.S. Fuhrer, J. Nygard, L. Shih, M. Forero, Y.G. Yoon, H.J. Choi, J. Ihm, S.G. Louie, A. Zettl, P.L. McEuen, Crossed nanotube junctions. Science **288**(5465), 494–497 (2000)
12. K.J. Ziegler, Z. Gu, J. Shaver, Z. Chen et al., Cutting single-walled carbon nanotubes. Nanotechnology **16**(7), 539–544 (2005)
13. K.J. Ziegler, Z. Gu, H. Peng, E.L. Flor, R.H. Hauge, R.E. Smalley, Controlled oxidative cutting of single-walled carbon nanotubes. J. Am. Chem. Soc. **127**(5), 1541–1547 (2005)
14. C. Wang, S. Guo, X. Pan, W. Chen, X. Bao, Tailored cutting of carbon nanotubes and controlled dispersion of metal nanoparticles inside their channels. J. Mater. Chem. **18**, 5782–5786 (2008)
15. S.J. Tans, A.R.M. Verchueren, C. Dekker, Nature **93**, 49–54 (1998)
16. R. Martel, T. Scmidt et al., Appl. Phys. Lett. **73**, 2447–2454 (1998)
17. O.B. Tomilin, U.U. Murumin, Adsorption on the graphene surface of carbon nanotubes and their energy spectrum. Phys. Solid State **48**(3), 563–571 (2006)
18. O.B. Tomilin, P.V. Avramov, A.A. Kuzovov, S.G. Ovchinikov, G.L. Pashkov, Connection the chemical properties of carbon nanotubes with their atomic and electronic structure. Phys. Solid State **46**(6), 1143–1146 (2004)
19. A.C. Dillon, K.M. Jonse, T.A. Bekkedhai, C.H. Kiang, Storage of hydrogen in single-walled carbon nanotubes. Nature **386**, 377–379 (1997)
20. P. Chen, X. Wu, J. Lin, K.L. Tan, High uptake by alkali-doped carbon nanotubes under ambient pressure and moderate temperatures. Science **285**, 91–99 (1999)
21. K.K. Murata, K. Kaneko, Adsorption mechanism of supercritical hydrogen in internal and interstitial nanospaces of single-wall carbon nanohorn assembly. J. Phys. Chem. B. **106**, 1132–1138 (2002)
22. V. Gayathri, R. Geetha, Hydrogen adsorption in defected carbon nanotubes. Adsorption **13**, 53–60 (2007)
23. Y. Ye, C.C. Ahn, C. Witham, B. Fultz, J. Liu, A.G. Rinzler, D. Colbert, K.A. Smith, R.E. Smalley, Hydrogen adsorption and cohesive energy of single-walled carbon nanotubes. Appl. Phys. Lett. **74**, 2307–2309 (1999)

24. C. Liu, Y.Y. Fan, M. Liu, H.T. Conga, H.M. Cheng, M.S. Dresselhaus, Hydrogen in single-walled carbon nanotubes at room temperature. Science **286**, 1127–1132 (1999)
25. R.F. Cracknell, Simulation of hydrogen adsorption in carbon nanotubes. Mol. Phys. **100**, 2079–2086 (2002)
26. J. Cheng, X. Yuan, L. Zhao, D. Huang, Review of hydrogen storage in inorganic fullerene-like nanotubes. Carbon **42**, 2019–2037 (2004)
27. S.V. Bulyarsky, V.P. Oleinicov, Thermodynamics of defect interaction in compound semiconducters. Phys. Stat. Sol. (b) **146**, 439–453 (1988)
28. K. Tada, S. Furuya, K. Watanabe, Ab initio study of hydrogen adsorption to single-walled carbon nanotubes. Phys. Rev. B. **63**, 155–179 (2001)
29. V. Gayathri, R. Geetha, Hydrogen adsorption in defected carbon nanotubes. Adsorption **13**, 53–59 (2007)
30. S.V. Bulyarskiy, V.P. Oleinicov, Thermodynamically evaluation of point defect density and impurity solubility in component semiconductor. Phys. Stat. Sol. (b) **141**, K7–K10 (1987)
31. S.V. Bulyarskiy, V.V. Fistul, *The Thermodynamics and Kinetics of the Interaction of Defects in Semiconductors* (Science, Moscow, 1997), 351 p
32. S.V. Bulyarskiy, V.V. Svetuhin, *Physical Basis of Defect Management in Semiconductors* (Ulianovsk, 2003), 385 p (Rus.)
33. B. Trepnel, *Chemisorption* (M.: Moscow, 1958), 327 p
34. Y.S. Nechaev, O chemosorbtchii i phyzicheskoy sorbtcii vodoroda uglerodnymi nanostructurami. Alternativnaya energetica i ecologya **2**(22), 64–73 (2005). (Rus.)
35. F.F. Volkinshteyn, Physical Chemistry of Semiconductor Surfaces. (Science, Moscow, 1973), 399 p (Rus.)
36. V.A. Lykah, E.S. Syrkin, Influence of adsorbed molecules on the spectrum of carriers in a semiconductor nanowire. Semiconductors **39**, 610–615 (2005)
37. A. Proykova, in *Molecular Dynamic Simulation of Gas Adsorption and Absorption in Nanotubes*, Carbon Nanotubes (Springer, Berlin, 2006), pp 187–207
38. Y.A. Zarifayntc, J. Phys. Chem. **38**, 2655–2664 (1964)
39. V.F. Kisilev, O.V. Krylov, *Adsorption Processes on the Surface of Semiconductors and Dielectrics* (Science, Moscow, 1978), 255 p (Rus.)

Chapter 2
Thermodynamics and Kinetics of Adsorption and Doping of a Graphene Plane of Carbon nanotubes and Graphene

Sergey Bulyarskiy and Alexandr S. Basaev

Abstract This chapter presents a theoretical introduction to the problem of doping carbon nanotubes (CNTs) and graphene. It examines the basic concepts of thermodynamics, such as thermodynamic systems, balance the internal energy, and free energy.

This chapter presents a theoretical introduction to the problem of doping carbon nanotubes (CNTs) and graphene. It examines the basic concepts of thermodynamics, such as thermodynamic systems, balance the internal energy, and free energy. Kinetics of thermodynamic processes and basic equations that describe them are discussed in this chapter. We show the method for determining the kinetic coefficients of the interaction of the gases with the matter and discuss the conduction of experiments that allow the calculation of kinetic coefficients. We describe a method for determining the concentration of defects that arise upon the doping of CNTs and graphene. This method consists of describing the Gibbs free energy of the thermodynamic system, which consists of carbon material placed in a certain gas environment. The search for minimum Gibbs energy allows us to find the desired concentration of defects. The method of analysis of results from experiments on desorption substances is analyzed in detail and the calculation of kinetic coefficients is given in practice, when several desorption processes overlap. This chapter provides concrete examples of the application of the theoretical approaches described above. The problem of calculating the distribution of nanoparticle catalyst size is resolved and changes in nanoparticle size after the annealing process due to the phenomenon of coalescence are analyzed. A system of equations for growth of nanotubes is identified and solved. It takes into account the impact of the temperature gradient in the reactor on the rate of growth of nanotubes,

S. Bulyarskiy (✉) · A.S. Basaev
Institute Nanotechnology of Microelectronics, Russian Academy of Sciences, Moscow, Russia
e-mail: bulyar2954@mail.ru

A.S. Basaev
e-mail: a.basaev@tcen.ru

S. Bulyarskiy and A. Saurov (eds.), *Doping of Carbon Nanotubes*, NanoScience and Technology, DOI 10.1007/978-3-319-55883-7_2

and the allowance for the formation, on the surface of catalyst nanoparticles, of intermetallic compounds and the buffer layer of pyrolysis residues which slow down the growth of CNTs.

2.1 The Equilibrium of Thermodynamic Systems

Classical thermodynamics can only describe systems in thermodynamic equilibrium and processes connecting states of equilibrium. The ***thermodynamic system*** is a particular amount of a substance, contained within definable boundaries. The objects of our study are the graphene and carbon nanotube. They grow or are subjected to annealing at a certain temperature and a certain composition of a gas medium. In this chapter, graphene and nanotubes will be called crystals. Graphene is a 2D crystal, which is a flat graphene nanoribbon. A CNT is an allotrope of carbon with a cylindrical nanostructure. The nanotube arises from a graphene nanoribbon folding into a tube. The axis of this structure is defined by crystallographic direction. This direction is called a chiral vector which connects two crystallographically equivalent sites on a 2D graphene sheet. Graphene and nanotubes have a certain symmetry arrangement of carbon atoms. Therefore, they may be referred as crystals.

Our thermodynamic system is a crystal that is in equilibrium with the surrounding gas environment, kept at a constant temperature and constant pressure. Pressure P, volume V, and temperature T, and number of particles N, are examples of thermodynamic properties of a system. The thermodynamic state of a system is determined if the thermodynamic properties of the system are known.

The types of thermodynamic system are: an open system which can exchange matter and energy with its surroundings; a closed system which can only exchange energy with its surroundings; an isolated system which can exchange *neither* energy *nor* matter with its surroundings. Our system is impervious to the exchange of matter with the surroundings, hence the system is closed. Boundaries that separate the system may be real material boundaries (vessel wall) or imagined. Imaginary boundaries determine a certain volume, in which the thermodynamic parameters (temperature, pressure, number of particles) are kept constant. The aim of the macroscopic thermodynamic approach is to find the equilibrium concentration of defects of a particular type in the crystal. All thermodynamics are based on studies of systems. When we speak of processes and cycles, we have to bear in mind that these occur in systems with well-defined boundaries. The laws of thermodynamics will provide relations among thermodynamic properties.

A thermodynamic property may be any general quantity that has a unique value for each thermodynamic state of a substance. There are thermodynamic properties and some functions that define the thermodynamic state of the system. A state function only depends on the state of the system and does not depend on the way in which the state has been achieved. The change of state parameters and state functions is solely determined by the initial state and final state of the system.

The function of the thermodynamic state is known as thermodynamic potential. We will use the following functions: U—internal energy; S—entropy; $H = U + PV$—enthalpy; $G = H - TS$—Gibbs energy.

For an infinitesimal, quasistatic (reversible) process, occurring in a closed system, we write the first law as [1]:

$$\delta Q_{\text{rev}} = \mathrm{d}U + P\mathrm{d}V \tag{2.1}$$

where δQ_{rev} is an amount of heat that is transferred to the system in a reversible process; $\mathrm{d}U$ is a change in the internal energy; and $P\mathrm{d}V$ is thermodynamic work. Work and heat are quantities that represent the exchange of energy between a system and its surroundings; work and heat are assumed to be positive when energy is transferred to the system.

The differential change in the internal energy is then given by:

$$\mathrm{d}U = \delta Q_{\text{rev}} - P\mathrm{d}V \tag{2.2}$$

Both terms on the right-hand side of (2.2) depend on each other. But their difference is the differential of a thermodynamic property and does not depend on heat and work. The internal energy is defined by a differential expression, provided by the first law. That is, only difference in internal energy is defined. The internal energy in integrated form is then only determined to within a constant, which may be chosen to be zero at an arbitrary point. The main contribution to the internal energy of the crystal gives the energy of chemical bonds between atoms and the energy of the lattice vibrations.

The definition of entropy is usually given on the basis of the second law of thermodynamics. In our case it is better to use the definition of Plank [2]. The number of states at a given energy is related to a quantity, called the entropy of the system, S. The entropy of a crystal with a defect consists of a configurational and a vibrational part: $S = S_{\text{conf}} + \Delta S_{\text{v}}$.

$$S_{\text{conf}} = k_{\text{B}} \ln \Omega \tag{2.3}$$

where Ω is the number of microstates that implements the macroscopic state of the systems.

Variation of vibrational entropy change is [3]:

$$\Delta S_{\text{v}} = k_{\text{B}} \ln(\nu_{\text{i}}/\nu_{\text{d}}) \tag{2.4}$$

where ν_{i} is the oscillation frequency of the ideal crystal lattice and ν_{d} is the frequency of vibrations of the crystal lattice with a defect.

The Gibbs free energy is:

$$G = H - TS \tag{2.5}$$

The free energy G of a system is defined by the system enthalpy H minus the product of the temperature T and the entropy S.

Suppose we keep the volume and energy of a system constant but allow the number of particles to change. If the temperature and pressure are not allowed to change, then the entropy must change as well as the number of states that modify the system. Alternately, changing the number of particles at constant volume and entropy must change the energy of the system and other thermodynamic potentials as each atom also adds a unit of chemical potential to the system.

$$H = TS + \sum_i \mu_i N_i \quad G = \sum_i \mu_i N_i \tag{2.6}$$

The chemical potential is the Gibbs free energy per each particle.

$$\mu_i = \frac{\partial G}{\partial N_i} \tag{2.7}$$

There are two types of thermodynamic variable: an intensive variable is a state variable whose value is independent of the size of the chosen system (e.g., temperature T, pressure P); an extensive variable is a state variable whose value is proportional to the size of the chosen system (e.g., amount of substance N, volume V). The chemical potential is the intensity value.

Equilibrium in a thermodynamic system assumes that the established temperature and pressure and all the thermodynamic processes are stationary. The variation that takes the system out of balance, satisfies the Clausius inequality in this case:

$$\mathrm{d}U + P\delta V - T\mathrm{d}S > 0 \tag{2.8}$$

Our system is closed. In this case the variation of internal energy and volume are available as $\mathrm{d}U = 0, \delta V = 0$. The inequality (2.8) implies conditions for a change of entropy.

$$\mathrm{d}S < 0 \tag{2.9}$$

Formula (2.9) is equivalent to the statement: at equilibrium, the entropy of the system is maximized, if the volume and the internal energy remain constant. If the entropy and volume are constant, the internal energy is maximized ($\delta V = 0, \mathrm{d}S = 0 \rightarrow \mathrm{d}U > 0$). As pessure is constant, different variations that bring the system out of balance should have a maximum energy which represents not only its internal energy but its energy with some addition of potential energy, i.e., its enthalpy. By substituting the enthalpy change in the Clausius inequality (2.8) we get:

$$T\mathrm{d}S - \mathrm{d}H + V\delta P + \delta V\delta P < 0 \tag{2.10}$$

After reasoning similar to that above, we obtain equilibrium conditions at constant pressure:

$$(\mathrm{d}S)_{H,P} < 0, \quad (\mathrm{d}H)_{S,P} > 0 \tag{2.11}$$

From (2.10) it follows that at equilibrium there must be a minimum of Gibbs free energy:

$$(\mathrm{d}G)_{H,T} > 0. \tag{2.12}$$

Thus, in equilibrium, the Gibbs free energy of a thermodynamic system takes a minimum value. Therefore, any variation leads to the fact that this value increases.

2.2 Thermodynamic and Kinetic Approaches to the Description of Thermodynamic Systems

2.2.1 Kinetics Equations

Physical kinetics deals with the rates of thermodynamic processes, factors which influence the rates, and the explanation of the rates in terms of the reaction mechanisms of the processes. In kinetics, the time variable is introduced and rate of change of concentration of reactants or products is a function of time. We must bring the system out of thermodynamic equilibrium, to study the kinetics of a process.

We consider the thermodynamic system of a solid state (nanotubes or graphene) and an outer gaseous medium. A solid is exchanging with the external environment by particles. We used the kinetic model, based on the main notions of Langmuir's theory, described in several works [4, 5]:

- The particles are emitted or captured from the environment at the certain adsorption sites; $N_{\alpha i}^{\beta}$ is the concentration of particles, captured on β-type solids, α is the type of particles, and i is the type of place that captures them.
- The particles do not interact with one another.
- N_i^{β} is the concentration of the i-type absorption sites. It is a constant value, defined by the sample fabrication prehistory.
- Every adsorption center binds only one molecule.

It is necessary to consider, in the framework of Langmuir's theory, the adsorption kinetics as a whole. The rate of adsorption reaction is defined as a change in number of molecules of reactant or product per unit time:

$$\frac{dN_{\alpha i}^{\beta}}{dt} = c_{\alpha}^{\beta} N_{\alpha}\left(N_{i}^{\beta} - N_{\alpha i}^{\beta}\right) - e_{\alpha}^{\beta} N_{\alpha i}^{\beta}, \tag{2.13}$$

where N_α is the concentration of particles in gaseous phase, defining an adsorbate partial pressure; c_α^β is the probability of adsorbate capture by β-type adsorption centers for the unitary concentration of the adsorbate in gaseous phase; and e_α^β is the probability of the particle emission or desorption from β-type adsorption centers.

To solve (2.13), it is necessary to know the concrete values of the kinetic coefficients, which define the particles capture and emission (adsorption and desorption) process probabilities. In equilibrium state the right-hand side of (2.13) becomes zero, and substituting the concentration of particles in gaseous phase (N_α) in this equation, we obtain the expression of a desorption probability:

$$e_{\alpha}^{\beta} = c_{\alpha}^{\beta} N^{\alpha} \exp\left(-g_{\alpha}^{\beta}/kT\right). \tag{2.14}$$

where g_α^β is the partial Gibbs free energy of a particle that occupies a place of type N_i^β; k is the Boltzmann constant; and T is absolute temperature.

The kinetic equation (2.26) can be written as:

$$\frac{dN_{\alpha i}^{\beta}}{dt} = c_{\alpha}^{\beta} N_{\alpha} N_{i}^{\beta} - \left(c_{\alpha}^{\beta} N_{\alpha} + e_{\alpha}^{\beta}\right) N_{\alpha i}^{\beta} = C - \frac{N_{\alpha i}^{\beta}}{\tau} \tag{2.15}$$

where $C = c_\alpha^\beta N_\alpha N_i^\beta$ is constant, if N_α and N_i^β are constant; and τ is a relaxation time of the process. The relaxation time has the following physical meaning: the time during which the concentration of particles at certain places is reduced 2.73 times (base of the natural logarithm).

The general expression (2.15) allows investigation of the transition from a non-equilibrium thermodynamic system state to an equilibrium state.

2.2.2 Solutions of Equations of Physical Kinetics

Solution of (2.15) depends on the conditions of the process. We consider two special cases:

1. Emission or desorption of particles into a vacuum ($N_i^\beta = 0$, when $t = 0$ is $N_{\alpha i}^\beta = N_{\alpha i0}^\beta$)

$$\frac{dN_{\alpha i}^{\beta}}{dt} = -\frac{N_{\alpha i}^{\beta}}{\tau} \rightarrow N_{\alpha i}^{\beta} = N_{\alpha i0}^{\beta} \exp\left(-\frac{t}{\tau}\right) \tag{2.16}$$

2. Particles, captured by the adsorption site at a low temperature ($e_\alpha^\beta = 0$, $\tau^{-1} = c_\alpha^\beta N_\alpha$; when $t = 0$ is $N_{\alpha i0}^\beta = 0$)

$$\frac{dN_{\alpha i}^{\beta}}{dt} = C - \frac{N_{\alpha i}^{\beta}}{\tau} \rightarrow N_{\alpha i}^{\beta}\left[1 - \exp\left(-\frac{t}{\tau}\right)\right] \tag{2.17}$$

2.2.3 The Kinetic Coefficients

Kinetic processes occur when a thermodynamic system is driving toward a state of equilibrium. The study of this process makes it possible to calculate the kinetic coefficients, which characterize the probability of capture or emission of particles from certain sites of a solid. It is important to regard these probabilities. Capture of particles is a result of their diffusion to a certain site of a solid, where they come to react. The result of the reaction is its localization on the site. There are two stages of the process: diffusion and reaction. Since these steps proceed sequentially, the kinetic coefficient is presented as:

$$c_{\alpha}^{\beta} = \frac{V}{\tau_{\alpha}^{\text{dif}} + \tau_{\alpha}^{\text{reac}}} \tag{2.18}$$

where V is the unit volume; $\tau_{\alpha}^{\text{dif}}$ is the diffusion time; and $\tau_{\alpha}^{\text{reac}}$ is the time of the reaction flow.

The diffusion time ($\tau_{\alpha}^{\text{dif}}$) is found from the well-known relationship of Smolukhovsky:

$$\frac{V}{\tau_{\alpha}^{\text{dif}}} = 4\pi R_{\alpha} D_{\alpha} \tag{2.19}$$

where R_{α} is the free path of particle type α before its capture and D_{α} is the diffusion coefficient of the particles.

The reaction time of the particles with the capture site can be found from the relationship:

$$\frac{V}{\tau_{\alpha}^{\text{reac}}} = \frac{S_{\alpha}^{\beta} D_{\alpha}}{R_{\alpha}} \exp\left\{-\frac{E_{\alpha}^{\beta}}{kT}\right\} \tag{2.20}$$

where S_{α}^{β} is the cross-section of the particle interaction with the place of its localization and E_{α}^{β} is the repulsive potential energy barrier that prevents the capture of particles.

We combine formulas (2.19) and (2.20), and get:

$$c_{\alpha}^{\beta} = \frac{4\pi R_{\alpha} D_{\alpha} S_{\alpha}^{\beta} \exp\left(-E_{\alpha}^{\beta}/kT\right)}{4\pi R_{\alpha}^{2} + S_{\alpha}^{\beta} \exp\left(-E_{\alpha}^{\beta}/kT\right)} \tag{2.21}$$

Formula (2.21) is useful for the preliminary assessment of kinetic coefficients. However, formulas (2.19) and (2.20) are approximate. Therefore, it is necessary to calculate the kinetic coefficients of the experiment.

The kinetic experiments were performed at a constant temperature. In this case, all the coefficients of formulas (2.16) and (2.17) are constant. An overview of the results of such experiments is shown in Fig. 2.1. The curves of the change of concentration of adsorbed particles allow us to find the relaxation time. Typically, this time is reduced with increasing temperature. The relaxation time can be found by means of a tangent from the beginning of the experimental curve to the *x*-axis (Fig. 2.1a, b). The accuracy of the tangent is small. To find a more accurate relaxation time it is necessary to build curves in semi-logarithmic coordinates.

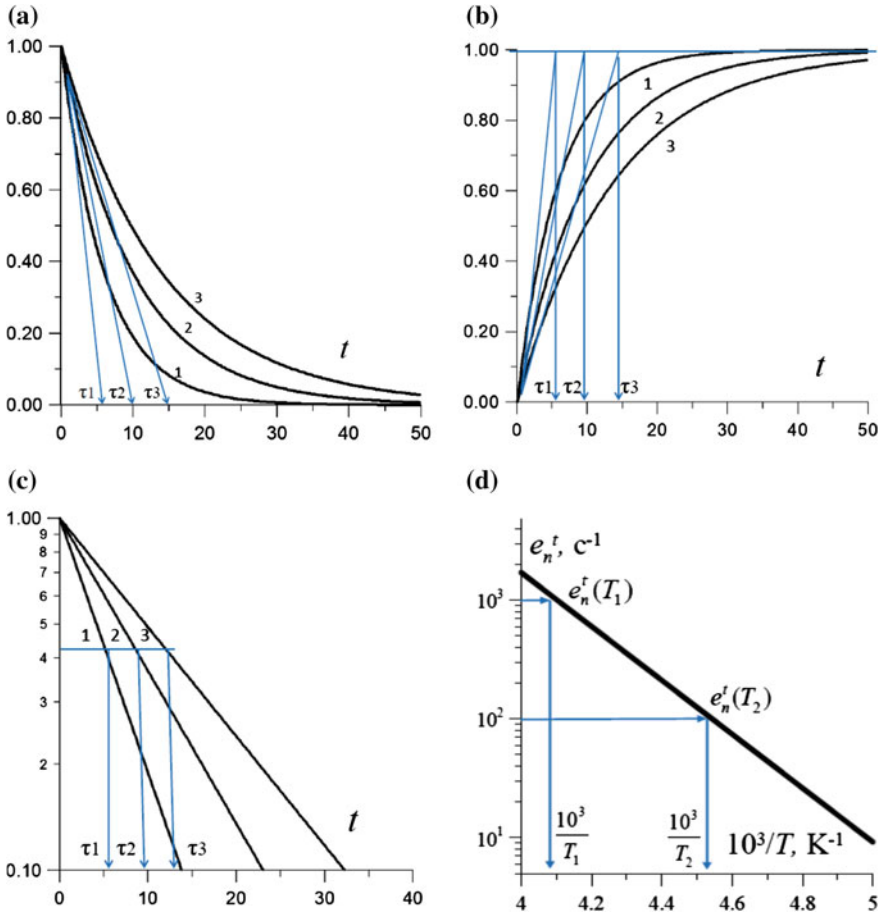

Fig. 2.1 Modeling relaxation kinetic curves at different temperatures ($T1 > T2 > T3$); **a** calculation of formula (2.28) in linear coordinates; **b** calculation of formula (2.29) in linear coordinates; **c** calculation of formula (2.28) in linear coordinates; **d** temperature dependence of the probability of particle emission

We draw a line parallel to the x-axis from the point 0.434 on the y-axis to the kinetic curves. The projections of the points of intersection on the x-axis are the kinetic constants. Then we drop a perpendicular to the axis of time and find the relaxation time. The probability of emission of the adsorbed particles is equal to τ^{-1}. We then build this value into the Areniusa coordinates. The slope allows identification of the activation energy (2.22), which then permits the calculation of the capture ratio according to formula (2.23).

$$E_{\alpha}^{\beta} = k\frac{T_1 T_2}{T_1 - T_2}\ln\left(\frac{e_{\alpha}^{\beta}(T_1)}{e_n^t(T_2)}\right) \tag{2.22}$$

$$c_{\alpha}^{\beta} = e_{\alpha}^{\beta}(T_i)\exp\left(E_{\alpha}^{\beta}/kT_i\right)/N^{\alpha} \tag{2.23}$$

2.2.4 Kinetic Processes in Carbon Nanostructures

We have considered the kinetic processes at a constant temperature. Such processes are rarely used in experimental practice. This is due to the fact that the time of inertial heating of a solid state is comparable to the relaxation time of the transport process. In this case, the experiment is not accurate because of large systematic measurement errors.

However, calculations using formulas (2.16)–(2.23) are very important in the analysis of technological experiments devoted to carbon nanostructures. These calculations make it possible to estimate the length of time during which the thermodynamic system comes to equilibrium. This interval is comparable to the magnitude of 3τ. If the experiment time is more than this value, then processing of the experimental results can completed using thermodynamic formulas. We will show in Sects. 2.6 and 2.7 of this chapter that the thermodynamic approach can be used to analyze the results of physical adsorption and chemisorption at high temperatures.

Solids lose mass when heated. This is due to the emission of particles from their surface. One can overcome the inertia of heating by heating at a low constant rate. This method is known as thermal gravimetric analysis (TGA). This has become standard in the technology of CNTs. The theory of this method is analyzed in Sect. 2.9. The practice of its application is given in Chaps. 3–5.

2.2.5 Role and Limits of the Thermodynamic Approach with Regard to the Process of Doping Carbon Nanostructures

The results of thermodynamic calculations are values of doping impurity concentrations and defects that may arise, provided that the system has come to

thermodynamic equilibrium, or an alloying process is under equilibrium conditions. These concentrations are expressed as a simple formula, if the impurity or defect is not ionized:

$$N = N^{\beta} \exp(-g/kT) \tag{2.24}$$

where N^{β} represents concentrations of sites that the impurity or defect may take and g is the free energy of the process of introducing an impurity or defect formation.

Formula (2.24) becomes more complicated if the impurity in a solid is ionized or if occurs a formation occurs with several defects, which interact with each other. These situations will be calculated subsequently. However, formula (2.24) resembles the Boltzmann distribution. Exact thermodynamic formulas really connect with the energy of the introduction to the solid, concentrations of other impurities, as well as the conditions under which it occurs: temperature, pressure, gas composition, ionization of several donor or acceptor defects, as well as other factors. Thermodynamic formulas are accurate when they describe the conditions of equilibrium that occur in most cases. These formulas reflect the probability of reaching the impurity concentration value if the balance in the system is not achieved.

We can conclude that each of the approaches in thermodynamic and kinetic have their own place in the development of technology for obtaining carbon nanostructures. They complement each other and allow a deeper understanding of ongoing technological processes.

2.3 Description of Defect Formation in Crystals

Crystalline solids contain different types of structural defects. If the imperfection is limited to one structural or lattice site and its immediate vicinity the imperfection is termed a point defect [6]. It can be seen in numerous experimental observations evidencing defects in CNTs such as vacancies [7], inclusions, and topological (Stone–Walles) defects [8] as well as dopants [7]. Defects in nanotubes have attracted great attention, both theoretically and experimentally, because of their potential use in a great variety of applications.

The formation of crystal defects can be studied in various ways [6, 9].

2.3.1 The Quasi-chemical Reaction Method

Such a method is described in detail in the books by Krőger [6]. This method has several names: the quasi-chemical reaction, the material balance method, and the mass-action law. However, they all have the exact same physical nature, which is set out below. There is a separation of the formation of defects into several stages.

Each stage is described by the chemical reaction occurring in the solid body and on its surface, for example:

$$\sum_i v_i Y_i = \sum_j v_j Z_j \tag{2.25}$$

where Y is the chemical symbol of the molecules (the defect or quasi-molecule complex in the solid state) which react; Z is the chemical symbol of the molecules that occur after the end of the reaction; v is the mole fraction of the substance; and i and j are indices of the molecules, both joined and formed by the reaction.

It is believed that the reactions take place under conditions that are close to balanced. A change in the Gibbs free energy after completion of the reaction is zero at equilibrium:

$$\Delta G = \sum_i v_i \mu_i - \sum_j v_j \mu_j = 0 \tag{2.26}$$

where μ is the chemical potential of the reagents. From (2.26) we get:

$$\sum_i v_i \mu_i = \sum_j v_j \mu_j \tag{2.27}$$

Now, assigns each structural element of the lattice of the solid (impurities or point defects, and so on) to the chemical potential, which is determined by the equation:

$$\mu_i = \mu_i^0 + kT \ln X_i, \tag{2.28}$$

where μ_i^0 is the chemical potential of the material of which the defect comprises, under standard conditions and X_i is the concentration of the defects of i-type.

Formula (2.28) is valid, if the defect and the substance in which it is formed, are an ideal solid solution. If the defect interacts with the substance, the solid solution is regular. In this case we must use the activity instead of concentration:

$$a_i = \gamma_i X_i \quad \text{and} \quad \mu_i = \mu_i^0 + kT \ln a_i, \tag{2.29}$$

where γ_i is the activity coefficient that takes into account the interaction of the defect with the lattice material, where it is formed.

We substitute formula (2.28) into (2.27) and get an expression for calculating the defect density in the case of the ideal solid solution:

$$\frac{\prod_j (X_j)^{v_j}}{\prod_i (X_i)^{v_i}} = \exp\left[\frac{1}{kT}\left(\sum_i v_i \mu_i^0 - \sum_j v_j \mu_j^0\right)\right] = K_{id}(T), \tag{2.30}$$

where $K_{id}(T)$ is the quasi-chemical reaction equilibrium constant, which describes the formation of a defect in a solid of the ideal solid solution.

If we substitution (2.29) into (2.27), we obtain the concentration of defects in the regular approximation:

$$\frac{\prod_j (X_j)^{\nu_j}}{\prod_i (X_i)^{\nu_i}} = \frac{\prod_j (\gamma_i)^{\nu_j}}{\prod_j (\gamma_j)^{\nu_i}} \exp\left[\frac{1}{kT}\left(\sum_i \nu_i \mu_i^0 - \sum_j \nu_j \mu_j^0\right)\right] = K_{\text{reg}}(T) \tag{2.31}$$

where $K_{id}(T)$ is the quasi-chemical reaction equilibrium constant, which describes the formation of a defect in a solid of the regular solid solution.

This method is applied as follows:

- Model of defect formation, described by a system of quasi-chemical reactions in solids and on its surface.
- An attempt is made to find the equilibrium constant (2.30) or (2.31) of the experiment.
- Calculation of the concentration of defects.

This method is developed and well used in many scientific papers [6]. It has repeatedly been used successfully, especially for the chalcogenide semiconductors. However, this method has certain disadvantages:

- The parameters of the problem are the equilibrium constants. They are not known. These constants cannot always be expressed in terms of chemical potentials. The following example shows the problems. Vacancy is the absence of an atom in its place. The question arises, what is the chemical potential of the vacancy? It does not have a simple physical meaning in the comparison with the chemical potential of the atom. A rigorous approach is required to apply the concept of chemical potential for the type of atoms, but not for the type of vacancy defects or anti-structural defects.
- The equilibrium constants appear in the final formulas for the required concentration of defects in the form of products and sums. These are constant equilibrium processes, which include several chemical reactions. These constants are not described by formulas (2.30) and (2.31). They are identified in some experiments. However, the search for them that takes place is not always successful.
- There is always a question about how much reaction is necessary to describe a model for a specific task. What kinds of reactions are chosen for the model? How many initial equations are there? These important questions pre-determine the answer to the problem that will be solved.

2.3.2 The Gibbs Free Energy Search Minimum Method

This method has been proposed in several works [10, 11]. Its application has allowed the solution of a number of important tasks for semiconductors [9] and CNTs [12]. This approach is derived from (2.12) and (2.26). This method requires writing the Gibbs free energy of the system and finding its minimum. The minimum of Gibbs free energy corresponds to the state of thermodynamic equilibrium. One can identify the equilibrium concentration of defects during the process of finding the minimum energy.

The Gibbs free energy search minimum method will be described in detail in this and the following chapters. The advantages of this method surpass the method quasi-chemical reactions.

A solution to the problem of the concentration of defects comprises: the partial Gibbs free energies of the formation of defects; the energy of defect ionization; consideration of the donor's or acceptor's nature; the concentration in the lattice sites of a solid, which they may occupy; and the temperature and pressure of the process gases in the reactor. These values have a clear physical meaning. They can be determined experimentally or calculated theoretically.

The problem is solved in its general form considering the number of defects, the number of different places they may occupy, the solid lattice structure, and the composition of the gas mixture in the reactor not being limited. The problem of selection of the initial set of chemical reactions is absent. Here the parameters of the substances that are in the experiment are used. The influence of defects on each other is detected in the course of solving the problem.

The method of compiling the equation for the Gibbs free energy of a thermodynamic system containing a solid with defects will be used and analyzed in detail in this chapter and chaps. 3, 4, 5.

2.4 The Thermodynamics of Physical Adsorption of Carbon Nanotubes and Graphene

Adsorption is a phenomenon which occurs on an interface as part of a two-phase system, resulting in the solid phase surface being enriched by molecules from a gaseous phase. The ***adsorbate*** are a molecule of matter that is adsorbed by a solid; ***adsorbent*** in turn, is the substance which is adsorbing the molecules from gaseous phase.

A distinction must be made between physical and chemical adsorption, although it is not easy to divide these processes. For example, the hydrogen adsorption on CNTs often is characterized by energies, being intermediate between typical values of physical and chemical adsorptions, and therefore it is difficult to use standard energy criterion for their mechanisms division or definition [1]. Usually physical adsorption is called an association process, where no presentation is apparent of processes of chemical bond destruction or formation, and where the adsorbent and

graphene lattice interaction proceeds via van der Waals type forces, etc. On the contrary, for chemisorption it is characteristic to identify the formation of new covalent and ionic bonds with a dissociation nature and the charge transfer between adsorbate and adsorbent.

2.4.1 Objects of Research: CNTs and Graphene

Allotropic forms of carbon have attracted the attention of scientists around the world. The material that is of primary interest is graphene, which pushed CNTs into second place. A graphene lattice makes it possible to generate various forms of carbon: graphene, nanotubes, fullerenes [13]. Graphene is a honeycomb lattice of carbon atoms. Graphite can be viewed as a stack of graphene layers. Carbon nanotubes are rolled-up cylinders of graphene. Fullerenes C60 are molecules consisting of wrapped graphene achieved via the introduction of pentagons on the hexagonal lattice. This forms a united type of lattice. Carbon, the elementary constituent of graphene and graphite, is the 6th element in the periodic table. In its atomic ground state, its 6 electrons are in the configuration $1s^2 2s^2 2p^2$, i.e. 2 electrons fill the inner shell 1*s*, which is close to the nucleus and which is irrelevant for chemical reactions, whereas 4 electrons occupy the outer shell of the 2*s* and 2*p* orbitals. Because the 2*p* orbitals ($2p_x$, $2p_y$, and $2p_z$) are roughly 4 eV higher than the 2*s* orbital, it is energetically favorable to put 2 electrons in the 2*s* orbital and only 2 of them in the 2*p* orbitals. By superposition of the 2*s* and two 2*p* orbitals, which we may choose to be the $|2p_x\rangle$ and the $|2p_y\rangle$ states, one obtains the planar sp^2 hybridization.

The adsorbed molecules are arranged over the chemical bonds of the graphene lattice. They hold the force of van der Waals in the case of physical adsorption. These molecules may be inside single-walled nanotubes or between layers of multi-walled tubes.

2.4.2 Differences Between Physical and Chemical Adsorption

Although the physical and chemical adsorption is not connected with great energetics or charge transfers, it can in some cases strongly affect CNT properties. It was shown in several theoretical and experimental studies, that molecular hydrogen adsorption does not change CNTs. On the other hand it is known that nitrogen and oxygen, under physical adsorption, can change the width of the HOMO–LUMO zone and type of a conductance of *n*- or *p*-type. Adsorption can transform a semi-conductive CNT into a metallic CNT.

Table 2.1 Comparison of physical and chemical adsorption parameters

Interaction parameters	Physical adsorption	Chemical adsorption
Type of the chemical bonds	van der Waals bonds	Chemical covalent bonds
Temperature range of the physical phenomenon appearance	Approximate temperature range 0–100 K	Approximate temperature range above 100 K
Activation energies of adsorption processes	Adsorption energy is low, as a rule, a few tenths of a meV	Adsorption energy values from a few tenths to single units of eV
Charge exchange between adsorbate and adsorbent	Charge exchange is absent	Charge exchange is possible in some processes

The chemisorption of the various substances is rarely realized in practice, and therefore it is weakly studied compared with physical adsorption. However, it gives the possibility to change the material energy spectrum and form new, strong bonds, and therefore is an effective and important tool for CNT property modification. The mechanism of chemisorption influence on the SWNT conductance is very complicated. First, during chemisorption we often see a charge transfer between the adsorbates and nanotubes. Second, chemisorption usually deforms the nanotube carbon framework, and the arising stresses also change the tube's electronic properties, with the deformations for a finite length SWNT being sufficient. The main features of these two described adsorption types are presented in Table 2.1.

Therefore, nanotubes have many non-equivalent places for adsorption. Moreover, adsorption (both, physical and chemical) and doping change the electronic properties of nanotubes. This is therefore an important tool in the control of tube characteristics and regulation after their synthesis.

The thermodynamic model of adsorption in CNTs was developed in Bulyarskiy and Basaev [14, 15, 16]. In this model one situation is considered where the CNT surrounding medium is presented with an α-type adsorbate. This can exist in molecular or atomic form (the latter we will call particles), however, (in spite of the particles aggregate state) the medium with given conditions can hold any certain amount of particles. In a gaseous phase, it corresponds to a condensation start point, but in solution it corresponds to saturation. The limiting number of particles, N^{α}, which can be held in the outer media, we call place number, but the real number of particles in the gaseous phase, N_{α}^{g}, is smaller. The upper index shows the place held by a particle, and the lower index indicates the particle type. In condensed liquid phase, all places are occupied by particles, and therefore these two numbers are equal. In an ideal gas the particle concentration can be expressed through pressures by the relationship:

$$N^{\alpha} = p_s^{\alpha}/kT, \quad N_{\alpha}^{g} = p^{\alpha}/kT, \tag{2.32}$$

where p^{α} is the partial pressure of the α-type adsorbate and p_s^{α} is the partial pressure of its saturated vapor.

Thus, the gaseous phase formally can be divided to small volumes, each of which can hold only one gaseous molecule. A second molecules appearance induces an excessive particle condensation process. This approach we will call a cell model for the gaseous molecules. This was developed initially by Bulyarskiy [9–11].

The particle is connected with a capture at some place (site) on the adsorbing surface. The number of atomic sites is equal, N^{β}. The number of adsorbate particles, being captured on these sites, we denote as N_{α}^{β}, and such notation shows that the molecule or atom of an "α"-type substance takes place over a "β"-type chemical bond.

These processes proceed with some probability, which counts very little in the thermodynamic equilibrium conditions, but is defined the kinetics processes. The adsorbate capture (adsorption) at a given place is accompanied by a free energy change at a value equal to the Gibbs partial free energy.

The method used is based on the Gibbs free energy minimization [9–11], and it is supposed that there is equilibrium in the system, i.e., the temperature and pressure are equalizing and all kinetic processes become stationary ones. In this case, for the constant temperature and pressure values the Gibbs free energy is:

$$G = H - TS. \tag{2.33}$$

This must have some minimum. Let us present the Gibbs free energy in the form:

$$G = G^{g}(N_{\alpha}) + G^{S}(N_{\alpha}), \tag{2.34}$$

where G^{g} is the gaseous phase free energy; N_{α} is a summary number of the α particles in both gaseous and condensed phases; and G^{S} is the free energy of the system, containing the nanotubes with adsorbed molecules or atoms on them (by physical adsorption).

2.4.3 The Conservation Law of Place Number

Conservation laws for place and particle numbers play an important role for the considered solutions to these problems, as does as the law of charge conservation. The processes of the two "independent" adsorbate particles arranged on a CNT are not really "independent". Conservation laws, listed below, establish the relationship between these processes.

The term "place" here and in the sections below indicate one of the following situations:

- A site of a carbon atom in the node of crystal lattice. This case is suitable for doping and for chemisorption.
- A site on the π-bond, that corresponds to chemisorption only.
- A position above the chemical bond. This case corresponds to physical adsorption.

The conservation laws for place number can be written down for both gaseous and condensed phases. Their number corresponds to the various place types, which are contained in the gaseous and condensed phases. For gaseous phase, the number of place types coincides with the number of atom and molecule types, which can be adsorbed. Each conservation law contains all the structural units, occupying the given types of places (i.e., α-type). These laws have the form:

$$\varphi^{\alpha} = \lambda^{\alpha}\left(N^{\alpha} - N_{\alpha}^{g} - N_{0}^{\alpha}\right), \tag{2.35}$$

where N_{α}^{g} is the molecule number in gaseous phase, occupying the α-type sites. Such a molecule concentration defines the adsorbate partial pressure (2.32); and N_{0}^{α} is the number of sites in gaseous phase that remain free.

For the condensed phase, the conservation laws have a similar form. Their amount corresponds to the adsorption place number:

$$\varphi^{\beta} = \lambda^{\beta}\left(N^{\beta} - \sum_{\alpha} N_{\alpha}^{\beta} - N_{0}^{\beta}\right), \tag{2.36}$$

where N_{0}^{β} is the number of adsorption places, that remain free.

The summation sign denotes that on one place there can be adsorbed different molecules. The α index runs all possible parameters for all molecule types that can be adsorbed on given sites.

2.4.4 The Laws of Conservation of Particle Number

The number of such laws is equal to the adsorbed α-type particle variants. The balance is defined by the lower index, and the equation has the form:

$$\varphi_{\alpha} = \lambda_{\alpha}\left(N_{\alpha} - N_{\alpha}^{\beta} - N_{\alpha}^{g}\right), \tag{2.37}$$

where the index β is running all possible values, corresponding to the number of place types, on which the physical adsorption can take place.

2.4.5 Free Energy of the Systems

The system as a whole is closed, and is limited by the reactor volume, where the thermodynamic equilibrium is established and where the temperature and pressure remain constant. Our thermodynamic system includes two subsystems, describing

the gaseous and condensed phases. These phases exchange by particles, and as a result, thermodynamic equilibrium is established, after which both subsystems becomes quasi-closed, and we can apply to them all thermodynamic laws.

Let us consider the subsystem, relating to the gaseous phase. To every molecule sort we can ascribe a certain partial thermodynamic potential, its value depends on how the molecule appeared in the system. First, a molecule amount is entered in the system before the moment when chemical equilibrium is reached. In this case the work, corresponding to the molecule's transport from the outer (with respect to reactor) medium, is equal to the chemical potential of the given molecule type. Second, the adsorbates can appear as a result of the pyrolysis of other substances, and in this case, we must take into account the free energy of the molecule pyrolysis. Both cases can be considered by introducing and using the value of the molecules free energy in its gaseous phase $g^{\alpha}_{\alpha g}$. Thus, the free energy of a given subsystem can be written as:

$$G\left(N^g_\alpha\right) = g^g_\alpha N^g_\alpha - kT \ln W^g, \tag{2.38}$$

where W^g is the thermodynamic probability of the subsystem, connected to the gaseous phase. This probability equals the number of possible adsorbate rearrangements over a phase's possible sites:

$$W^g = \prod_\alpha \frac{N^\alpha!}{N^g_\alpha!(N^\alpha - N^g_\alpha)!}. \tag{2.39}$$

The analogous relationships can be written for the condensed phase subsystem taking the form:

$$G\left(N^\beta_\alpha\right) = g^\beta_\alpha N^\beta_\alpha - kT \ln W^S, \tag{2.40}$$

where W^S is the thermodynamic probability of the subsystem, connected with the condensed phase, which equals:

$$W^g = \prod_\alpha \frac{N^\beta!}{N^\beta_\alpha!\left(N^\beta - N^\beta_\alpha\right)!}. \tag{2.41}$$

The minimization will be carried out by the Lagrange indefinite multipliers method. The functional for this operation was obtained by summation of the subsystems (2.8) and (2.10) free energies with condition (2.4)–(2.7).

$$\Phi = g^\beta_\alpha N^\beta_\alpha + g^g_\alpha N^g_\alpha - kT \ln\left(W^g * W^S\right) + \varphi^\alpha + \varphi^\beta + \varphi_\alpha = 0. \tag{2.42}$$

Using Stirling's formula for the factorial changes we obtain:

$$\Phi = g_\alpha^\beta N_\alpha^\beta + g_\alpha^g N_\alpha^g - kT\left\{\begin{array}{l}\sum\limits_\alpha \left[N^\alpha \ln N^\alpha - N_\alpha^g \ln N_\alpha^g - \left(N^\alpha - N_\alpha^g\right)\ln\left(N^\alpha - N_\alpha^g\right)\right] \\ + \sum\limits_\beta \left[N^\beta \ln N^\beta - N_\alpha^\beta \ln N_\alpha^\beta - \left(N^\beta - N_\alpha^\beta\right)\ln\left(N^\beta - N_\alpha^\beta\right)\right]\end{array}\right\}$$
$$+ \lambda^\alpha\left(N^\alpha - N_\alpha^g - N_0^\alpha\right) + \lambda^\beta\left(N^\beta - \sum_\alpha N_\alpha^\beta - N_0^\beta\right) + \lambda_\alpha\left(N_\alpha - N_\alpha^\beta - N_\alpha^g\right) = 0 \tag{2.43}$$

Let us take derivatives of the functional (2.43) with respect to the place numbers N^α and N^β. Setting them equal to zero, we receive an equation system for the Lagrange indefinite multipliers (λ^α and λ^β) in the form:

$$\lambda^\alpha = kT\left[\ln N^\alpha - \ln\left(N^\alpha - \sum_\alpha N_\alpha^g\right)\right], \tag{2.44}$$

$$\lambda^\beta = kT\left[\ln N^\beta - \ln\left(N^\beta - \sum_\alpha N_\alpha^\beta\right)\right]. \tag{2.45}$$

The meaning of the derivative of the functional with respect to the particle number is the given substance chemical potential μ_α [3, 9], therefore differentiating (2.43) with respect to the particle number, we obtain:

$$\lambda_\alpha = \mu_\alpha = \mu_\alpha^0 + kT\ln(a_\alpha), \tag{2.46}$$

where μ_α^0 is the standard chemical potential of element α and a_α is this element activity in the gaseous phase.

During the following minimization of functional (2.43), we can calculate the values of the adsorbate molecule numbers both in gaseous phase and adsorbed on the nanotube chemical bonds:

$$N_\alpha^g = a_\alpha N^\alpha \exp\left(-\frac{g_\alpha^g - \mu_\alpha^0}{kT}\right), \tag{2.47}$$

$$N_\alpha^\beta = a_\alpha N^\beta \exp\left(-\frac{g_\alpha^\beta - \mu_\alpha^0}{kT}\right). \tag{2.48}$$

Thus, the adsorbed molecule concentration is proportional to the component activity in the gaseous phase and depends on the temperature and adsorbate properties, which are defined by its partial free energies (for adsorption and

appearance in gaseous phase). Formulas (2.47) and (2.48) allow us to obtain some useful relationships.

First, we can calculate a coefficient of the adsorbate molecule distribution between gaseous and condensed phases in the form:

$$\frac{N_\alpha^\beta}{N_\alpha^g} = \frac{N^\beta}{N^\alpha}\exp\left(-\frac{g_\alpha^\beta - g_\alpha^g}{kT}\right) = kT\frac{N^\beta}{p_s^\alpha}\exp\left(-\frac{g_\alpha^\beta - g_\alpha^g}{kT}\right). \tag{2.49}$$

In the second part of relation (2.49) the Clapeyron formula (2.32) is used. The distribution coefficient is determined by saturation vapor pressure and partial Gibbs potentials.

Second, formulas (2.47) and (2.48), together with (2.49) and taking account of (2.1), allow us to obtain the adsorption isotherm equation:

$$C_\alpha^\beta = \frac{N_\alpha^\beta}{N^\beta} = p^\alpha K_\alpha^\beta, \tag{2.50}$$

where C_α^β is the concentration of atoms (α) on the site (β) of the CNTs and p^α is the partial pressure of component (α).

The equilibrium constant is:

$$K_\alpha^\beta = \frac{1}{p_s^\alpha}\exp\left(-\frac{g_\alpha^\beta - g_\alpha^g}{kT}\right).$$

Thus, the adsorption isotherm studies allow us to evaluate a difference between the partial free energies. Note, that when the adsorbate is introduced into a reactor (but does not form in the reactor), the adsorbate partial free energy is equal to its chemical potential, and hence the adsorption free energy can be defined as $G_\alpha^\beta = g_\alpha^\beta - \mu_\alpha$, and thereafter formula (2.48) takes the simple and usual form:

$$N_\alpha^\beta = N^\beta \exp\left(-\frac{G_\alpha^\beta}{kT}\right). \tag{2.51}$$

Note also, that in this explicit form the adsorption connection does not appear with the conditions of the processes, running in gaseous phase. We can not evaluate the role of activity (in the gas phase) on concentration values of defects.

Thus, in this section we analyzed the phenomenon of physical adsorption in CNTs and detected the main factors determining its quantitative parameters. The results of this section will be used to analyze the amount of hydrogen that can be held in storage—made using CNTs.

2.5 The Thermodynamics of Doping and Chemical Adsorption

Carbon nanotube doping and the atoms and molecules chemisorbed into them are joined and united by a phenomenon of charge transport, that is accompanying any new chemical bond formation. The types of the formed bonds can divide these processes. The process of doping is accompanied by rupture of bonds in the graphene lattice. If the process involves an addition of foreign atoms, molecules and radicals via π-bonds, we must call it chemisorption. Note, that from a thermodynamic point of view the nature of the formed bonds is not principal, because the bond character influences only the partial free energy value for a particular bond. The final mathematical expression is the same for doping and chemisorption. Below we will consider some problems related to the charge transfer influence on CNT property control.

Let us suppose, as in Sect. 2.1, that a system is in equilibrium, i.e., the temperature and pressure are level, all kinetic processes also become stationary and the Gibbs free energy (2.2) takes its minimal value. However, in our case in (2.3) appears a new term, describing the free energy of an electronic subsystem. Thus, we have:

$$G = G^g(N_\alpha) + G^S\left(N_\alpha^\beta\right) + G^e, \tag{2.52}$$

where G^e is the free energy of charge carriers (electrons and holes). The last term in the free energy expression characterizes a free energy fraction, relating to the particles (adsorbate atoms and molecules) changing their charge, something that can accompany the adsorption process.

It was said above, that two "independent" adsorbate particles, arranged on a CNT, are not independent. A mutual conditionality of concentrations is established due to several conservation laws, listed below.

2.5.1 The Conservation Laws for the Number of Places

We can write down many laws, as there are the various place types in nanotubes. Every conservation law contains all the structural units which can occupy given type places, e.g., for β-type we have:

$$\varphi^\beta = \lambda^\beta\left(N^\beta - \sum_\alpha N_\alpha^\beta - N_0^\beta\right), \tag{2.53}$$

where λ^β are the Lagrange indefinite multipliers.

Because we are considering the place numbers the system's total balance is established with the upper index in the formula, but the index α runs through the all values which possibly used in the model, including β.

As we did in Sect. 2.4, let us single out the conservation laws for the gaseous and condensed phases. For example, for the gaseous phase we can write:

$$\varphi^{\beta s} = N^{\beta s} - \sum_{\alpha} N_{\alpha}^{\beta s} - N_0^{\beta} = 0. \tag{2.54}$$

However, expression (2.53) is practically the same, and hence we can unite them in one system, compelling the index β to run through all values which are characteristic to the gaseous phase.

2.5.2 The Conservation Laws of Particle Number

As above, we can write down many laws, as there are the various particle types which can be adsorbed. The balance is established via the lower index, and the equation itself has the form:

$$\varphi_{\alpha} = \lambda_{\alpha}\left(N_{\alpha} - \sum_{\beta} N_{\alpha}^{\beta} - N_{\alpha}^{0}\right), \tag{2.55}$$

where λ^{β} are the Lagrange indefinite multipliers.

The index α runs through all values characteristic to the condensed phase. Note also, that the conservations laws can be written down as components of a functional, as in Sect. 2.1, and the notation form does not change the equations meaning and results.

2.5.3 The Conservation Law of Charge

Under the chemisorption and doping processes the exchange of the charge carriers proceeds between the nanotube and adsorbate particle, and therefore in the conservation law system arises an additional law of charge conservation. The law demands that the nanotube must remain neutral as a whole. This equation is a unique one in our system, but plays an important role, because it establishes a specific general balance, equalizing the charges of free carriers and ionized adsorbates:

$$\varphi_e = \lambda_e\left(n - p + \left\{\sum_{\alpha,\beta} n_{\alpha}^{\beta} - \sum_{\alpha,\beta} N_{\alpha}^{\beta} d_{\alpha}^{\beta}\right\}\left(1 - \delta_{\alpha}^{\beta}\right)\right), \tag{2.56}$$

where n_α^β is the electron number, captured on defects, that equals either the number of defects that have captured the electrons or the number of chemisorbed molecules (atoms) for which the adsorption process is accompanied by charge transport (namely, electrons); N_α^β is the number of α-*type* adsorbed particles; d_α^β takes meanings of "1" for chemisorption with electron loss (a donor process) or "0" for a processes with a hole loss (acceptor process); δ_α^β is the delta-function, introduced to take into account the fact that the components of nanotubes and media, with which the tube is interchanging, do not make a contribution to the described part of the free energy.

To calculate the equilibrium concentrations of the adsorbed particles we use the following algorithm.

(1) We must compose an equation of the Gibbs free energy for a nanotube with adsorbed particles, and also this equation must consist of two parts, namely the configuration and energetic ones.
(2) We must carry out free energy minimization, using the Lagrange indefinite multipliers method, taking into account the above described conservation laws.

In accordance with this algorithm, let us write down the Gibbs energy in the form:

$$G = H - TS = H - TS_T - kT \ln W, \tag{2.57}$$

where W is the state of thermodynamic probability [9–11] and S_T is the thermal part of the system's entropy.

To calculate the free energy of a nanotube with the adsorbate, let us introduce the Gibbs partial potential per single adsorbed particle:

$$g_\alpha^\beta = H_\alpha^\beta - TS_\alpha^\beta, \tag{2.58}$$

where H_α^β is the enthalpy and $S_{\alpha T}^\beta$ is the vibrational entropy of the particle adsorption.

It follows from the partial parameter definition, that the defect formation energy can be found using this parameter multiplication of a given particle number. For our problem, taking into account the above-stated algorithm, we can write the thermal part of the system free energy as a sum of the energies for the neutral defect formation electronic states of ionization, i.e., as the expression:

$$G = \sum_{\alpha,\beta} N_\alpha^\beta g_\alpha^\beta + \left\{ E_g \left[p - \sum_{\alpha,\beta} n_\alpha^\beta \left(1 - d_\alpha^\beta\right) \right] + \sum_{\alpha,\beta} \varepsilon_\alpha^\beta \left[\left(N_\alpha^\beta - n_\alpha^\beta\right) d_\alpha^\beta + n_\alpha^\beta \left(1 - d_\alpha^\beta\right) \right] \right\} \left(1 - \delta_\alpha^\beta\right), \tag{2.59}$$

where ε_α^β is the particle ionization energy; and the indices α and β are running all values, thereby accounting for both the CNT atoms and the particles of media, into the system free energy where the nanotube is located.

We can use the expression for the thermodynamic probability from several works [9–11]:

$$W = \frac{(N_C)^n}{n!}\frac{(N_v)^p}{p!}\prod_{\alpha,\beta}\frac{N^\beta!\left(r_\alpha^\beta\right)^{n_\alpha^\beta}\left(R_\alpha^\beta\right)^{N_\alpha^\beta - n_\alpha^\beta}}{n_\alpha^\beta!\left(N_\alpha^\beta - n_\alpha^\beta\right)!}, \tag{2.60}$$

where $N_{c(v)}$ is the effective state density into the conductance zone (in valence zone); $n(p)$ are the concentrations of free electrons (holes); and r_α^β $\left(R_\alpha^\beta\right)$ is a degeneration factor of the filled (unfilled) electron state of the defect.

This probability accounts for the possible permutations of both the electrons and holes (over the states of the nanotube permitted zones) and the adsorbates over the adsorption places or their possible re-charging under the capture process on the nanotube.

As was said above, the search for the free energy extreme will be undertaken using the Lagrange indefinite multipliers method. The functional for the determination of the conditional extreme point location has the form:

$$\Phi = G - kT\ln W + \sum_\alpha \lambda_\alpha\varphi_\alpha + \sum_\alpha \lambda^\beta\varphi^\beta + \lambda_e\varphi_e, \tag{2.61}$$

where λ_α, λ^β, and λ_e are the Lagrange indefinite multipliers, that arise from the conservation laws for the particle number (2.55), places number (2.54), and charge (2.56), correspondingly. The number of Lagrange indefinite multipliers is equal to the conservation law numbers.

Substituting expressions (2.54)–(2.60) into (2.61), we obtain the formula for the functional, which must be minimized:

$$\begin{aligned}\Phi = {} & \sum_{\alpha,\beta} N_\alpha^\beta g_\alpha^\beta + \left\{E_g\left[p - \sum_{\alpha,\beta} n_\alpha^\beta\left(1 - d_\alpha^\beta\right)\right] + \sum_{\alpha,\beta}\varepsilon_\alpha^\beta\left[\left(N_\alpha^\beta - n_\alpha^\beta\right)d_\alpha^\beta + n_\alpha^\beta\left(1 - d_\alpha^\beta\right)\right]\right\}\left(1 - \delta_\alpha^\beta\right) \\ & - kT\left\{n\ln N_C - n\ln n + p\ln N_v - p\ln p + n + p + \sum_{\alpha,\beta}\left[n_\alpha^\beta\ln r_\alpha^\beta + \left(N_\alpha^\beta - n_\alpha^\beta\right)\ln R_\alpha^\beta + N_\alpha^\beta\right.\right. \\ & \left.\left. - n_\alpha^\beta\ln n_\alpha^\beta + n_\alpha^\beta - \left(N_\alpha^\beta - n_\alpha^\beta\right)\ln\left(N_\alpha^\beta - n_\alpha^\beta\right) - n_\alpha^\beta + N^\beta\ln N^\beta - N^\beta\right]\right\} \\ & + \sum_\alpha \lambda_\alpha\left(N_\alpha - \sum_\beta N_\alpha^\beta\right) + \sum_\beta \lambda^\beta\left(N^\beta - \sum_\alpha N_\alpha^\beta\right) + \lambda_e\left\{n - p + \left[\sum_{\alpha,\beta} n_\alpha^\beta - \sum_{\alpha,\beta} N_\alpha^\beta d_\alpha^\beta\right]\left(1 - \delta_\alpha^\beta\right)\right\}.\end{aligned} \tag{2.62}$$

At first glance (2.62) is very bulky and tedious, but for minimization one can take only the partial derivatives of it, and after differentiation the majority of its additives vanish (i.e., become zero). Thus, we obtain the equation system:

$$\frac{\partial \Phi}{\partial N_\alpha^\beta} = g_\alpha^\beta + \varepsilon_\alpha^\beta d_\alpha^\beta (1 - \delta_\alpha^\beta) - kT\left[\ln R_\alpha^\beta - \ln\left(N_\alpha^\beta - n_\alpha^\beta\right)\right] - \lambda_\alpha - \lambda^\beta - \lambda_e d_\alpha^\beta \left(1 - \delta_\alpha^\beta\right). \tag{2.63}$$

Formula (2.63) is namely an equations system, and the equation number equals the number of combinations which can be formed from indices α and β, corresponding to the various types of particles and places. The interactions between the defects of the system are concluded or contained in the Lagrange multipliers, whose physical meanings are yet to be considered and established.

Let us suppose that in formula (2.63) there are only indices α (corresponding to an adsorbate particle in an outer media) or β (corresponding to the nanotube carbon atoms). In this case we have $R_\alpha^\beta = 1$ and $n_\alpha^\beta = 0$, and as a result we obtain an expression connecting two (from three) Lagrange multipliers:

$$\lambda^\alpha = -\lambda_\alpha + g_\alpha^\alpha + kT \ln N_\alpha^\alpha. \tag{2.64}$$

The free energy derivative with respect to the particle number is their chemical potential and therefore: $\lambda_\alpha = \mu_\alpha$, $\lambda_\beta = \mu_\beta$. The chemical potential in a regular approximation can be expressed in the form:

$$\mu_{\alpha,\beta} = \mu_{\alpha,\beta}^0 + kT \ln a_{\alpha,\beta}, \tag{2.65}$$

where $\mu_{\alpha,\beta}^0$ is the chemical potential of the pure component and $a_{\alpha,\beta}$ is the component activity, connected with its concentration by: $a_\alpha = \gamma_\alpha X_\alpha$, where γ_α is the activity coefficient and X_α is the α-type adsorbate concentration.

Taking the derivative of expression (2.63), with respect to electrons or hole concentrations, we define a physical meaning of yet one more Lagrange multiplier:

$$\lambda_e = kT \ln \frac{n}{N_c} = -E_F, \tag{2.66}$$

i.e., the multiplier λ_e is equal to the Fermi energy value, but with the opposite sign.

The final expressions for the number of the defects and electrons captured on them have the form:

$$N_\alpha^\beta = N_\beta^\beta A_\alpha^\beta \left(1 + B_\alpha^\beta\right), \quad n_\alpha^\beta = N_\beta^\beta A_\alpha^\beta B_\alpha^\beta, \tag{2.67}$$

where:

$$A_\alpha^\beta = R_\alpha^\beta \frac{a_\alpha}{a_\beta} \exp\left\{\frac{1}{kT}\left[-g_\alpha^\beta + \left(E_F - \varepsilon_\alpha^\beta\right) d_\alpha^\beta \left(1 - \delta_\alpha^\beta\right)\right]\right\}, \tag{2.68}$$

$$B_{\alpha}^{\beta} = \frac{r_{\alpha}^{\beta}}{R_{\alpha}^{\beta}} \exp\left\{\frac{1}{kT}\left[-E_F + \varepsilon_{\alpha}^{\beta} + \left(1 - d_{\alpha}^{\beta}\right)\left(E_g - 2\varepsilon_{\alpha}^{\beta}\right)\right]\left(1 - \delta_{\alpha}^{\beta}\right)\right\}.$$

Below, formulas (2.67) and (2.68) will be derived in more detail for some concrete examples of doping and chemisorption, thereby becoming clearer.

From formula (2.67) can be derived a sufficiently simple expression for the adsorbed molecule number. The CNTs as a rule have hole-type conduction and are not degenerate, hence in this case:

$$N_{\alpha}^{\beta} = \frac{a_{\alpha}}{a_{\beta}} N_{\beta}^{\beta} \exp\left(-\frac{g_{\alpha}^{\beta}}{kT}\right)\left[\exp\left(\frac{E_g - \varepsilon_{\alpha}^{\beta} - E_F}{kT}\right) + 1\right]. \tag{2.69}$$

It follows from formula (2.69), that the number of one type of adsorbed particles is connected with the concentration of all other adsorbed atoms for the following reasons. First, let us note that a number of empty adsorption places, N_{β}^{β}, depends on the total defect number. For the defect formation in a usual solid body this number tends to the lattice basic atom number (that as a rule is sufficiently greater than the defect number), but under adsorption of various types of particle in nanotubes there arises a competition for adsorption places. In such a situation it is necessary to use the place number conservation law. A mutual connection between the N_{β}^{β} defect with other defects is expressed by: $N_{\beta}^{\beta} = N^{\beta} - \sum_{\alpha \neq \beta} N_{\alpha}^{\beta}$. Second, a connection is established through the Fermi energy, which depends on all adsorbate numbers. For example, an acceptors introduction into the CNT immediately leads to a growth in the donor admixtures number.

Formula (2.69) is correct in all cases. However, under physical adsorption, adsorbates re-charging are practically absent and therefore the activation energy for the electron or the hole can be turned to infinity. For this case, the expression in square brackets in formula (2.69) becomes equal to "1". Let us note also, that under adsorption the carbon atom number in the nanotube does not change and the defect number is small compared with the basic cell number, thus, we have $a_{\beta} \to 1$. Taking into account all these conditions, we can write the following expression for several types of particles adsorption:

$$N_{\alpha}^{\beta} = \frac{N_{\alpha}}{N^{\alpha}}\left(N^{\beta} - \sum_{\alpha \neq \beta} N_{\alpha}^{\beta}\right) \exp\left(-\frac{g_{\alpha}^{\beta}}{kT}\right). \tag{2.70}$$

For one type of atom adsorption we get:

$$N_{\alpha}^{\beta} = \frac{N_{\alpha}}{N^{\alpha}}\left(N^{\beta} - N_{\alpha}^{\beta}\right) \exp\left(-\frac{g_{\alpha}^{\beta}}{kT}\right). \tag{2.71}$$

From (2.71) we can obtain the expression for Langmuir's isotherm [17–19]:

$$N_\alpha^\beta = \frac{N^\beta N_\alpha \exp\left(-\frac{g_\alpha^\beta}{kT}\right)}{N_\alpha \exp\left(-\frac{g_\alpha^\beta}{kT}\right) + N^\alpha} = \frac{Kp}{1+Kp} N^\beta, \tag{2.72}$$

where $K = \frac{1}{p_s^z} \exp\left(-\frac{g_\alpha^\beta}{kT}\right)$ is the equilibrium constant and p is the pressure.

Formulas (2.69)–(2.71) allow calculation of the adsorbed particle concentrations for all cases of monomolecular adsorption.

The results of this section are generic and can be can be used in all cases when doping or chemical adsorption is studied. However, the derivation of the formulas appears complicated at first reading. Therefore, these findings are dismantled again in Chaps. 3–6 for simple examples.

2.6 Kinetics of Doping Carbon Nanotubes and Graphene

Kinetics of reactions in the solid state are well developed. Information on this subject can be found in numerous monographs and textbooks, i.e., [20]. The theoretical part of the problem is easily solved both analytically and numerically. An example of solving this problem is shown below.

Task: doping CNTs or graphene during treatment in an atmosphere of doping atom vapor. At time $t = 0$ the nanotube is placed in an atmosphere which consists of an ideal gas of dopant. It is supposed that the chemical bonds between carbon atoms of the solid are broken by heating. The probability of this process is denoted by e_c. The concentration of the resulting vacancies is denoted by N_v^c. This process is described by the kinetic equation:

$$\frac{\mathrm{d}N_v^c}{\mathrm{d}t} = -c_c N_c^g N_v^c + e_c\left(N_c^{\mathrm{cnt}} - N_v^c\right) \tag{2.73}$$

where c_c is the probability of capture of carbon from the gas phase on the vacancies of the lattice; N_c^g is the carbon concentration in the gas phase; and N_c^{cnt} is the concentration of carbon in the lattice sites. The solid body only exists in impurity pairs and the carbon in the gas phase is practically absent ($N_c^g \to 0$). Then:

$$\frac{\mathrm{d}N_v^c}{\mathrm{d}t} = e_c\left(N_c^{\mathrm{cnt}} - N_v^c\right) \tag{2.74}$$

The impurity concentration in the gas phase (N_a^g) can be calculated using the Clapeyron equation:

$$N_a^g = p_a/kT, \tag{2.75}$$

where: p_a is the partial pressure of the impurity gas in vapor phase. Capture of the impurity by vacancy and emission of the impurities is a process occurring simultaneously. It is described by the kinetic equation:

$$\frac{dN_a^c}{dt} = c_a N_v^c N_a^g - e_a N_a^c \tag{2.76}$$

where c_a is the probability of an impurity atom being captured from the gas phase to a vacancy; and e_a is the probability of impurity emission from the solid to the gaseous phase. The problem is solved with initial conditions, $N_v^c(0) = 0$, $N_a^c(0) = 0$. A full joint solution of (2.74) and (2.76) is very cumbersome. Therefore, the results are presented in Fig. 2.2. Analytical results are presented in the following conditions:

$$N_v^c = N_c^{\text{cnt}}[1 - \exp(-e_c t)] \quad N_a^c = \frac{c_a p_a N_c^{\text{cnt}}}{e_a kT}[1 - \exp(-e_c t)], \quad \text{then } e_c \ll e_a \tag{2.77}$$

Kinetics is limited by a slower process, namely, by the formation of carbon vacancies.

$$N_v^c = N_c^{\text{cnt}}[1 - \exp(-e_c t)] \quad N_a^c = \frac{c_a p_a N_c^{\text{cnt}}}{e_a kT}[1 - \exp(-e_a t)], \quad \text{then } e_c \gg e_a \tag{2.78}$$

Kinetics is also limited by an impurity atom being captured from the gas phase.

One knows that the energy gap of the C–C bond is 4.2 eV [12]. Energy needed to create vacancies of carbon atoms in a graphene lattice should be greater than this

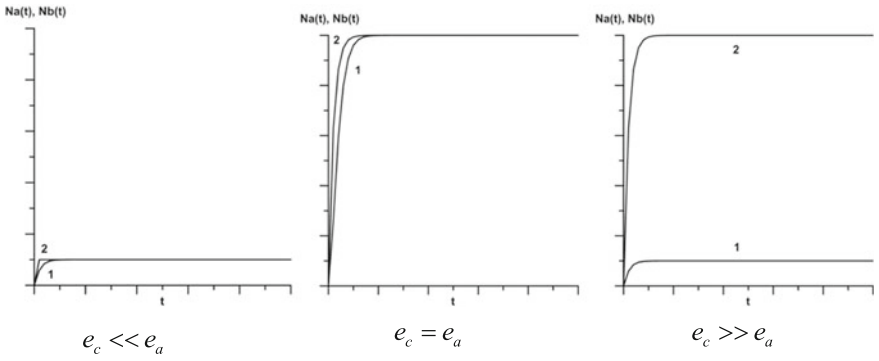

Fig. 2.2 Kinetics of doping CNTs or graphene during annealing in impurity vapor. (1) N_v^c; (2) N_a^c

value. An experiment was undertaken [21] permitting the evaluation of this energy. The authors [12] annealed nanotubes for 5 h at a temperature of 2500 K. The annealing led to the formation of about 1% vacancies that chemisorbed hydrogen further. This data allows the estimation of the emission rate of carbon atoms. It was calculated at 5×10^{-7} s. We calculate the coefficient of capture using formula (2.21), assuming that the nanotube is surrounded by an ideal gas and the capture is limited only by the diffusion process ($C_c = 1.2$ cm^3 s^{-1}). The concentration of nanotube atoms was $10^{17} \div 10^{18}$ cm^{-3}. The value of these variables allows estimation of the energy of carbon vacancies to be 10 eV. The calculations, presented in Chap. 3, give a value of the energy of hydrogen desorption that is about 2.7–3 eV. Therefore, CNTs and graphene cannot chemisorb hydrogen when they are annealed in an atmosphere of this gas. Instead, one uses graphene in hydrogen plasma. The plasma lowers the energy of the process and makes it possible.

Kinetics of processes is complicated and time consuming, so research work in this direction for nanotubes is nearly non-existent.

2.7 Kinetics of the Desorption Process

The adsorbed atoms characteristics can be determined by studying the desorption process. At present the methods and apparatus of thermal (thermogravimetric) analysis (TGA) and differential thermogravimetric analysis (DTGA) are well developed. These methods are based on the measurements of the substance losses under heating and now are widely used for to determine the various parameters of many adsorption processes. In this connection, below we will consider in detail the connection between the parameters of desorption from a surface and some parameters, considered earlier, in previous sections.

The basis of the kinetic model used are notions of Langmuir's theory, derived in several works [1, 10]:

- Adsorption proceeding on certain adsorption centers (cites).
- Adsorbent molecules not interacting with each other.
- Adsorption center numbers being a constant value, defined by sample fabrication prehistory.
- Every adsorption center binding to only one molecule.

Let us consider under the framework of Langmuir's theory the adsorption kinetics as a whole. The equation of the adsorption has the form:

$$\frac{\mathrm{d}N_{\alpha i}^{\beta}}{\mathrm{d}t} = c_{\alpha i}^{\beta} N_{\alpha} \left(N_i^{\beta} - N_{\alpha i}^{\beta} \right) - e_{\alpha i}^{\beta} N_{\alpha i}^{\beta}, \tag{2.79}$$

where $N_{\alpha i}^{\beta}$ is the concentration of adsorbate atoms, captured on i-type places; N_i^{β} is the concentration of i-type places; N_{α} is the concentration of adsorbate in gaseous

phase, defining an adsorbate partial pressure; $c_{\alpha i}^{\beta}$ is the probability of adsorbate capture by the i-type adsorption centers for the unitary concentration of the adsorbate in gaseous phase; and $e_{\alpha i}^{\beta}$ is the probability of the adsorbate desorption.

In order to solve (2.79), it is necessary to know concrete values of the kinetic coefficients, which define the gas adsorption and desorption process probabilities. In equilibrium state the right-hand side of (2.79) becomes zero, and substituting in this equation the adsorbate concentration (2.71), we obtain for a desorption probability the expression:

$$e_{\alpha i}^{\beta} = c_{\alpha i}^{\beta} N^{\alpha} \exp\left(-g_{\alpha i}^{\beta}/kT\right). \tag{2.80}$$

Experiments connected with gas desorption are usually carried out under continuous pumping out and, therefore, the pressure of the adsorbed gas is equal to zero (and the molecule concentration, $N_{\alpha} = 0$). Equation (2.25) is simplified to the form:

$$\frac{\mathrm{d}N_{\alpha}}{\mathrm{d}t} = \sum_{i=1}^{m} \frac{\mathrm{d}N_{\alpha i}^{\beta}}{\mathrm{d}t} = -\sum_{i=1}^{m} v_{\alpha i}^{\beta} N_{\alpha i}^{\beta} \exp\left(-\frac{g_{\alpha i}^{\beta}}{kT}\right) \mathrm{d}t, \tag{2.81}$$

where $v_{\alpha i}^{\beta} = c_{\alpha i}^{\beta} N^{\alpha}$ and $g_{\alpha i}^{\beta}$ is the adsorption partial free energy, introduced by (2.19).

In formula (2.81) summing is carried out over the number of places the adsorbate atoms are captured, and therefore in (2.81) it is enough to study a desorption process for only one type of such a place.

The nanotubes are usually annealed at high vacuum conditions and temperatures 1000–1200 °C during several hours before measurements. This is done to remove from the samples the amorphous graphite, low-molecular complexes, and undesirable adsorbates. After annealing the temperature is decreasing and the nanotubes are saturated by adsorbate under a specific temperature. After that the cryostat with the sample is cooled to helium temperatures. When an equilibrium state is reached, the samples are heating at a constant rate (i.e., at γ = 0.25 K/s). In these tests the sample temperatures changed linearly with time: $T = T_0 + \gamma t$, where T_0 is the heating start temperature, chosen as a rule long before the desorption process starts. During the heating process the amount of de-adsorbed substance is recorded. For a full description of the process under the framework of formula (2.81) it is necessary to change the function argument, i.e., to pass from argument t (time) to argument T (temperature). After the change of variables we obtain a differential equation:

$$\frac{\mathrm{d}N_{\alpha i}^{\beta}}{N_{\alpha i}^{\beta}} = -\frac{v_{\alpha i}^{\beta}}{\gamma} \exp\left(-\frac{g_{\alpha i}^{\beta}}{kT}\right) \mathrm{d}T, \tag{2.82}$$

where γ is the sample heating rate.

The solution of this equation has the form:

$$N_{\alpha i}^{\beta} = N_{\alpha 0 i}^{\beta} \exp\left[-\frac{v_{\alpha i}^{\beta} T}{\gamma} E_2\left(\frac{g_{ai}^{\beta}}{kT}\right)\right], \tag{2.83}$$

where $E_2(x)$ is the integral exponential function of second order.

Equation (2.83) allows us to obtain the kinetic coefficients: g_{ai}^{β} is the Gibbs free energy of adsorption (molecular bond) and $v_{\alpha i}^{\beta}$ is the desorption probability. The values are determined by a comparison of the analytical expression with experimental results, but practically it is more convenient to use the desorbed gases concentration derivative with respect to temperature (the DTGA method). This curve for a single process has only one maximum, but for a processes superposition—several maximums, the number of which equals the independent desorption process number. For such desorption process superposition the derivative is described by the expression:

$$\frac{\mathrm{d}N_{\alpha}}{\mathrm{d}T} = \sum_{i=1}^{m} \frac{\mathrm{d}N_{\alpha i}^{\beta}}{\mathrm{d}T} = -\sum_{i=1}^{m} \frac{v_{\alpha i}^{\beta} N_{\alpha 0 i}^{\beta}}{\gamma} \exp\left(-\frac{g_{\alpha i}^{\beta}}{kT}\right) \exp\left[-\frac{v_{\alpha i}^{\beta} T}{\gamma} E_2\left(\frac{g_{\alpha i}^{\beta}}{kT}\right)\right]. \tag{2.84}$$

For this the following conditions are taken into account:

$$\frac{\mathrm{d}E_n(x)}{\mathrm{d}x} = -E_{n-1}(x).$$

An asymptotic expansion of the function:

$$E_n(x) = \frac{\exp(-x)}{x}\left\{1 - \frac{n}{x} + \frac{n(n+1)}{x^2} - \cdots\right\},$$

We should also consider the fact that the temperature range of desorption rate derivative maximum as a rule has values $x > 30$.

The desorption probability at the peak maximum temperature with number i (i.e., at temperature T_{mi}), with a systematic error of order $k^2T^2/\left(g_{\alpha}^{\beta}\right)^2$, is equal [22]:

$$v_{\alpha i}^{\beta} = c_{\alpha i}^{\beta} N^{\alpha} = \frac{\gamma g_{\alpha i}^{\beta}}{kT_{mi}^2} \exp\left(\frac{g_{\alpha i}^{\beta}}{kT_{mi}}\right). \tag{2.85}$$

Substituting (2.85) into (2.30) and approximating the integral exponential function, we obtain the equation:

$$\frac{\mathrm{d}N_{\alpha}}{\mathrm{d}T} = \sum_{i=1}^{m} \frac{g_{\alpha i}^{\beta}}{kT_{mi}} N_{\alpha i}^{\beta} Z \exp\left[-\frac{T^2}{T_{mi}^2}\left(1 - \frac{2g_{\alpha i}^{\beta}}{kT_{mi}}\right) Z\right], \tag{2.86}$$

where $Z = \exp\left[\frac{g_{\alpha i}^{\beta}}{k}\left(\frac{1}{T_{mi}} - \frac{1}{T}\right)\right]$.

An analogous equation for a thermally stimulated desorption of electrons from traps was obtained [11]. Formula (2.86) is very convenient in order to analyze the desorption kinetics and allows, with high precision, the division of the processes of desorption onto the components and definition of desorption parameters. In this formula the maximum temperature and the peak amplitude are evaluated directly from an experimental curve, and we must select only bond energy, which can be completed with an accuracy of 1–2%.

In summary it must be stated that in this chapter the general expressions describing the adsorption processes have been derived, and will be developed and completed below given material consideration. We present specific examples of the application of this theoretical model in Chaps. 2–6.

2.8 The Thermodynamics and Kinetics of Chemical Vapor Deposition Growth of Carbon Nanotubes

The problem of the growth of CNTs is described in detail in several books, including [12, 23, 24]. Chemical vapor deposition (CVD) is the most modern method for growing arrays of carbon nanotubes for nanoelectronics. It is a chemical process, used to produce high-purity, high-performance solid materials. Although CVD offers the benefit of significantly lower synthesis temperatures than arc-discharge and laser ablation techniques, it still requires a growth temperature of 600–950 °C [23]. A further drop in temperature has been associated with the use of plasma (PECVD). Until now, this PECVD process has become the most popular method to synthesize SWCNTs and Multiwalled carbon nanotubes—MWCNTs, MWCNT arrays, and ordered SWCNT strands on various substrates [12, 23, 25].

In principle, a catalyst has a critical effect in reaction of kinetics by lowering the energetic barrier of a particular chemical reaction, neither modifying thermodynamics nor being consumed. During a standard thermal CVD or PECVD procedure, a substrate is coated with a layer of metal catalytic nanoparticles, most commonly nickel, cobalt, iron, or a combination thereof. The metal nanoparticles can also be produced in other ways, such as reduction of oxides or oxide solid solutions. The size of the catalytic nanoparticles can be controlled by patterned (or masked) deposition of the metal, annealing, or by plasma etching of a metal layer. The substrate with catalytic particles is usually heated to approximately 700 °C in a protective gas. To initiate the growth of nanotubes, two gases are bled into the reactor: a process gas (such as ammonia, nitrogen, or hydrogen) and a carbon-containing gas (such as acetylene, ethylene, ethanol, or methane) [23]. The substance and the morphology of the catalyst play an important role in the growth of CNTs. We will carry out the analysis of the formation of catalyst nanodroplets. We will examine the kinetics of the catalyst interaction with the gas phase of the reactor and what processes accompany the growth and doping of CNTs.

2.8.1 Catalyst Nanoparticles

Researchers of CNT growth (e.g., [26]) have concluded that the diameter of nanotubes is associated with the catalyst **nanoparticles** diameter, from which they growth. Nanoparticles from catalyst formation (nucleation) are complex, occurring under the influence of the several factors [12]. The sizes of nanodroplets are increasingly determined by the temperature of its synthesis, its surface tension, and the thickness of the metal film from which it is formed. We have undertakend a study of the influence of temperature of technological processes on the diameter of the catalyst particles. The results of these studies are shown in Fig. 2.3.

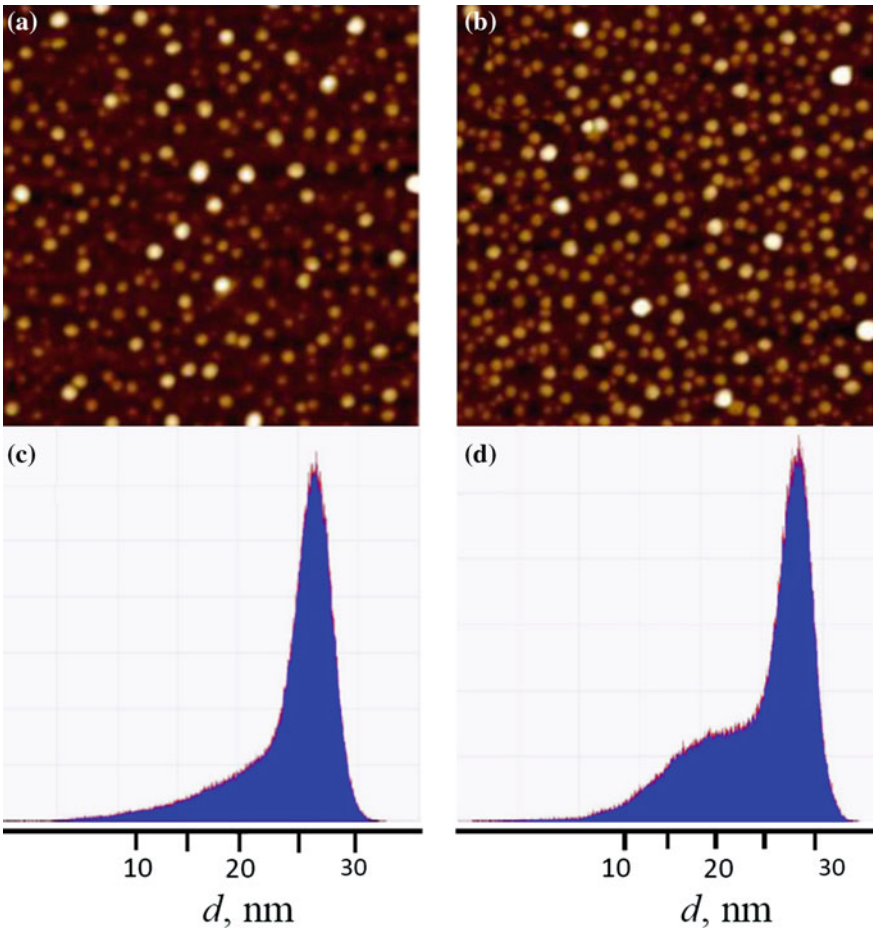

Fig. 2.3 The distribution of particles size. **a**, **b** Are a surface scans, 1 × 1 μm, produced via atomic-force microscope; **c**, **d** show the distribution of nanoparticles according to their size; **a**, **c** are immediate results after magnetron sputtering; **b**, **d** are results after annealing at 500 °C for 30 min

Here, Ti (10 nm) and Ni (2 nm) thin films were deposited by magnetron sputtering of silicon oxide on the coated silicon surface. Nanoparticles appeared immediately after deposition on the surface of the catalyst (Fig. 3.3a). Samples were annealed at 500 °C for 30 min. We studied the catalyst nanodroplets by atomic-force microscopy, ScanAsyst™. This produces high-resolution, 3D images by scanning over the sample surface. The peaks of the distribution of particles are at 28 nm size, immediately after deposition. It was found that the particle distribution changes after annealing, receiving an additional distribution of particles with a maximum of 18 nm. The phenomenon of coalescence occurs during annealing.

We constructed a thermodynamic model of the formation of the catalyst cluster to better understand the observed phenomena. The thermodynamic model, which is built below, explains the shape of the experimental nanodroplet size distribution and shows the important role played by the surface tension of the particles during formation. The theoretical distribution is obtained by calculating the minimum Gibbs free energy of the system, in which the clusters are formed by the catalyst. The surface tension of the particle catalysts are obtained after comparing experimental and theoretical distributions.

2.8.2 The Free Energy of the Particles

The free energy of the particles at a constant pressure (Gibbs energy) plays a significant role in the self-formation of the particle, its melting, and the growth of a CNT. The expression for the free energy including surface tension is given by:

$$G_k = G_i + G_S = -g_i n_i + 4\pi r_i^2 \gamma_l, \tag{2.87}$$

where g_i is the partial Gibbs **free energy** per atom in the particle; n_i is the number of atoms in the particle of the catalyst; r_i is the radius of the particle; and γ_l is the surface tension. The first term describes the connection of an additional particle to particle r. The second term is associated with the occurrence of a boundary, separating the particle from its environment. Equation (3.25) gives the free energy of the particle in gas phase.

The free energy of the particle is expressed in terms of the number of atoms within it. We assume that the particle is a sphere. This is true if the number of atoms in it is more than a few hundred. Iron in the particle of the catalyst has a body-centered lattice, which has a volume a^3, and in this volume there are 3 atoms. Accordingly, the volume of the particle is $a^3 n_i/2$. Then:

$$n_i = \left(\frac{8\pi}{3}\right)\frac{r_i^3}{a^3}; \quad r_i = \left(\frac{3}{8\pi}\right)^{1/3} a n_i^{1/3}, \tag{2.88}$$

$$G_k = -g_i n_i + 4\pi r_i^2 \gamma_l = -g_i n_i = -g_i n_i + c n_i^{2/3}, \quad c = (3)^{2/3} \pi^{1/3} a^2 \gamma_l. \tag{2.89}$$

The coalescence changes the free energy of the system, because it occurs in two types of clusters: globular particles and mono, each of which is subject to their distribution. The free energy of the system, consisting of a number of mono and globular clusters, can be written as (2.89):

$$G_k = \sum_j M_j \left(-g_j n_j + c_j n_j^{2/3} \right) + \sum_i N_i \left(-g_i n_i + c_i r_i^{2/3} \right) \tag{2.90}$$

where M_j is the concentration (number) of globular particles; N_i is the concentration (number) of independent mono particles (by independent we mean mono clusters, not part of the globules); g_j is the partial energy of attachment of particles to the globule; and g_i is the partial energy of the particle attachment to an independent mono particle.

It is important to note that each particle can take one of three locations: in free state, as part of an independent mono particle, or as part of the globule.

2.8.3 The Laws of Conservation for the Number of Sites and Particles

For each phase we can provide the number of sites (N^{Fe}) for particles of a certain type and number of particles (N_{Fe}) that occupy them. In a condensed liquid phase, all the sites are filled with particles, so the two numbers are equal. In an environment of ideal gas, these numbers can be expressed in terms of pressure:

$$N^{\mathrm{Fe}} = p_s^{\mathrm{Fe}} V^{\mathrm{Fe}} / kT, \quad N_{\mathrm{Fe}} = p^{\mathrm{Fe}} V^{\mathrm{Fe}} / kT, \tag{2.91}$$

where p_s^{Fe} is the partial vapor pressure of the atoms that make up the cluster; p^{Fe} is the partial vapor pressure at saturation; and V^{Fe} is the volume, occupied by iron atoms.

Equation (2.91) follows from the cellular model of the gas [12]. The *number of places* (N^{Fe}) is the total number of cells for the gas molecules. This number is equal to the volume of the gas that is divided by the volume of a molecule, found in the saturated vapor pressure. The law of conservation of the number of sites is:

$$N^{\mathrm{Fe}} - N_{\mathrm{Fe}} - N_0^{\mathrm{Fe}} = 0, \tag{2.92}$$

where N_0^{Fe} is the number of places in the gas phase which are free.

The law of conservation of particles in the case of a globular cluster is a different analog for mono clusters. It is necessary to enter the following parameter of

clusters: N_i is number of mono clusters containing the same number of iron particles n_i. $N_i * n_i$ is the total number of particles in these clusters, the number of particles containing iron n_i. M_j is the concentration of globular clusters, each of which contains n_j iron atoms. The total number of iron atoms in the system remains constant. The law of conservation of atoms is:

$$N_{\mathrm{Fe}} - \sum_i N_i n_i - \sum_j M_j n_j - N_{\mathrm{Fe}}^0 = 0. \tag{2.93}$$

2.8.4 Calculation of the Cluster Size Distribution

Cluster size distribution is calculated by minimizing the Gibbs free energy of the crystal by the method of undetermined multipliers of Lagranzh. This energy can be written as:

$$G = \sum_i N_i G_{ki} - kT \ln W \tag{2.94}$$

where G_{ki} is the partial Gibbs free energy of a particle containing i atoms. It is defined by (2.89) or (2.90), which is determined by the nucleation model.

In order to write the thermodynamic probability, and then go on to calculate the entropy configuration, we proceed as follows:

1. The placement of the iron atoms at the sites. These atoms are the centers of particles and globules. The probability of such a placement can be written as:

$$W^{\mathrm{Fe}} = \frac{N^{\mathrm{Fe}}!}{N_{\mathrm{Fe}}!(N^{\mathrm{Fe}} - N_{\mathrm{Fe}})!} \tag{2.95}$$

2. The placement of the particles and globules. Particles are placed at sites which are occupied by iron atoms. The probability of such a placement can be written as:

$$W = \frac{N_{\mathrm{Fe}}! \prod_i (R_i)^{N_i} \prod_j (R_j)^{M_j}}{\prod_j M_j n_j! \prod_i N_i n_i! \left(N_{\mathrm{Fe}} - \sum_i N_i n_i - \sum_i M_j n_j\right)!} \tag{2.96}$$

where R_i and R_j are the degeneration coefficients of the particles and globules, respectively. The value of these coefficients depends on the shape of the cluster. Since the particles and globules are oriented in space randomly, and they themselves have a shape close to the sphere, then the value of these coefficients is 1. Finally, the thermodynamic probability is:

$$W = \frac{N^{\mathrm{Fe}}! \prod_i (R_i)^{N_i} \prod_j (R_j)^{M_j}}{(N^{\mathrm{Fe}} - N_{\mathrm{Fe}})! \prod_j M_j n_j! \prod_i N_i n_i! \left(N_{\mathrm{Fe}} - \sum_i N_i n_i - \sum_i M_j n_j\right)!}. \tag{2.97}$$

The Gibbs free energy, whilst taking into account (2.90), is written in the form:

$$G = \sum_j M_j \left(-g_j n_j + c_j n_j^{2/3}\right) + \sum_i N_i \left(-g_i n_i + c_i r_i^{2/3}\right) - kT \ln W \tag{2.98}$$

The standard method of Lagrange multipliers involves the creation of a functional, consisting of values whose minimum is sought, and the conditions under which the minimum is reached. Equations (2.92), (2.93), (2.97), and (2.98) allow us to write the functional in the form:

$$\begin{aligned}
\Phi = & \sum_i N_i \left(-g_i n_i + c_i n_i^{2/3}\right) + \sum_i M_j \left(-g_j n_j + c_j n_j^{2/3}\right) \\
& - kT \left[N^{\mathrm{Fe}} \ln N^{\mathrm{Fe}} + \sum_i N_i \ln R_i + \sum_j M_j \ln R_j\right] \\
& - kT \left[-\left(N^{\mathrm{Fe}} - N_{\mathrm{Fe}}\right) \ln\left(N^{\mathrm{Fe}} - N_{\mathrm{Fe}}\right) - \sum_j M_j n_j \ln\left(M_j n_j\right)\right] \\
& - kT \left[-\sum_i N_i n_i \ln(N_i n_i) - \left(N_{\mathrm{Fe}} - \sum_i N_i n_i - \sum_j M_j n_j\right) \ln\left(N_{\mathrm{Fe}} - \sum_i N_i n_i - \sum_j M_j n_j\right)\right] \\
& + \lambda^{\mathrm{Fe}} \left(N^{\mathrm{Fe}} - N_{\mathrm{Fe}} - N_0^{\mathrm{Fe}}\right) + \lambda_{\mathrm{Fe}} \left(N_{\mathrm{Fe}} - \sum_i N_i n_i - \sum_j M_j n_j - N_{\mathrm{Fe}}^0\right),
\end{aligned} \tag{2.99}$$

Calculate the derivative of formula (2.99) in the number of places:

$$\frac{\partial \Phi}{\partial N^{\mathrm{Fe}}} = -kT \left[\ln\left(N^{\mathrm{Fe}}\right) - \ln\left(N^{\mathrm{Fe}} - N_{\mathrm{Fe}}\right)\right] + \lambda^{\mathrm{Fe}} = 0 \tag{2.100}$$

From (2.100), we find one of the Lagrange multipliers:

$$\lambda^{\mathrm{Fe}} = kT \ln\left(\frac{N^{\mathrm{Fe}}}{N^{\mathrm{Fe}} - N_{\mathrm{Fe}} - N_{\mathrm{Fe}}^0}\right) \tag{2.101}$$

Calculate the derivative of formula (2.99) in particles:

$$\begin{aligned}
\frac{\partial \Phi}{\partial N_{\mathrm{Fe}}} = & -kT \left[\ln\left(N^{\mathrm{Fe}} - N_{\mathrm{Fe}} - N_{\mathrm{Fe}}^0\right) - \ln\left(N_{\mathrm{Fe}} - \sum_i N_i n_i - \sum_j M_j n_j\right)\right] \\
& + \lambda_{\mathrm{Fe}} - \lambda^{\mathrm{Fe}} = \mu_{\mathrm{Fe}}
\end{aligned} \tag{2.102}$$

$$\mu_{\mathrm{Fe}} = \mu_{\mathrm{Fe}}^{0} + kT\ln(a_{\mathrm{Fe}})$$

where a_{Fe} is the activity of iron.

We then find the second Lagrange multiplier:

$$\lambda_{\mathrm{Fe}} = kT\ln\left(\frac{N^{\mathrm{Fe}}}{N_{\mathrm{Fe}} - \sum_i N_i n_i - \sum_j N_j n_j}\right) + \mu_{\mathrm{Fe}} \tag{2.103}$$

Derivatives with respect to the number of globular clusters and mono clusters are as follows:

$$\begin{aligned}\frac{\partial\Phi}{\partial n_i} &= -g_i n_i + \frac{2}{3}c_i n_i^{-1/3} - kT\left[\ln(R_i)^{n_i} - \ln(N_i n_i)^{n_i} - \ln\left(N_{\mathrm{Fe}} - \sum_i N_i n_i - \sum_j M_j n_j\right)^{n_i}\right] \\ &\quad - \lambda_{\mathrm{Fe}} N_i = 0 \\ \frac{\partial\Phi}{\partial n_j} &= -g_j n_j + \frac{2}{3}c_j n_j^{-1/3} - kT\left[\ln(R_j)^{n_j} - \ln(M_j n_j)^{n_j} - \ln\left(N_{\mathrm{Fe}} - \sum_i N_i n_i - \sum_j M_j n_j\right)^{n_j}\right] \\ &\quad - \lambda_{\mathrm{Fe}} M_j = 0\end{aligned} \tag{2.104}$$

where μ_{Fe}^{0} is the chemical potential of the iron under standard conditions, included within the enthalpy: $\Delta H = g_i + \mu_{\mathrm{Fe}}^{0}$. Substituting (2.102) and (2.103) into (2.104), we obtain the distribution of clusters, according to the number of particles.

For a single cluster:

$$N_i = a_{\mathrm{Fe}}(R_i)^{1/n_i}\frac{N^{\mathrm{Fe}}}{n_i}\exp\left[\frac{\Delta H_i - \pi^{1/3}a^2\gamma_{li}(n_i)^{-1/3}\frac{2}{3}(3)^{3/2}}{kT}\right]. \tag{2.105}$$

For globular particles:

$$M_j = a_{\mathrm{Fe}}(R_j)^{1/n_j}\frac{N^{\mathrm{Fe}}}{n_j}\exp\left[\frac{\Delta H_j - \pi^{1/3}a^2\gamma_{lj}(n_j)^{-1/3}\frac{2}{3}(3)^{3/2}}{kT}\right] \tag{2.106}$$

We then need to analyze which parameters define the characteristics of the distributions (2.105) and (2.106). The shape of the distribution is determined only by the coefficient of surface tension of mono or globular clusters. The number of clusters depends on the enthalpy of the sublimation of atoms, the reactor temperature, and the concentration of ferrocene in the gas phase. These parameters define the activity of iron in the gas phase. The temperature of the crystals is affected on

the concentration of clusters. It represents part of the exponent of (2.105) and (2.106), and also (2.92) for the number of seats.

We obtain the cluster size distribution from (2.105):

$$N_i = \frac{A}{r_i^3}\exp\left(-\frac{b}{r_i}\right) \tag{2.107}$$

where

$$A = a_{\mathrm{Fe}} N^{\mathrm{Fe}} a^3 \exp\left(\frac{\Delta H}{kT}\right), \quad b = \frac{a^3 \gamma_{ef}}{kT}. \tag{2.108}$$

The distribution reaches a maximum when the radius of the cluster takes the value:

$$r_{i\,\max} = b/3.$$

Therefore, the experimental distribution (Fig. 2.3) is a superposition of (2.105) and (2.106).

An important parameter for particle size distribution is surface tension. This value determines the maximum of the distribution. From (2.108) the surface tension follows the expression:

$$\gamma_{ef} = \frac{3kTr_{\max}}{a^3} \tag{2.109}$$

The experimental distribution, shown in Fig. 2.3, allows us to calculate the surface tension of mono particles and globules using expression (2.109). Annealing leads to the emergence of a particle distribution peak at 18 nm. We substitute this value in (2.109) and obtain $\gamma_{ef} = 4.6$ J/m^2. If the particle has a size of 18 nm then it must be in a solid state. The surface tension of solid Ni is difficult to calculate. Here we make an approximate estimation [12]:

$$\gamma_{ls} = \frac{1}{2} K \alpha_T \Delta T r_{\max} \tag{2.110}$$

where K is compressibility coefficient; α_T is the coefficient of thermal expansion; ΔT is a heating temperature of 0 °C; and $r_{\max}$ is the particle radius, which corresponds to the maximum found in the distribution.

The value of the surface tension, calculated according to the formula, is 4.4 J/m^2. Agreement between the values is good, considering experimental error and the shortcomings of formula (2.110).

One question which arises is why the nanotubes grow if the catalyst is a solid. Scanning the surface of the catalyst nanoparticles by atomic-force microscope is shown in Fig. 2.4. A nanoparticle surface may melt due to its large number of irregularities.

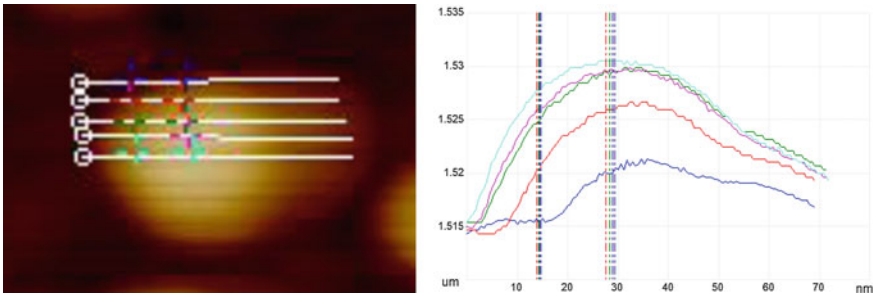

Fig. 2.4 Scanning the surface of catalyst nanoparticles using an atomic-force microscope

We have developed the thermodynamics of homogeneous catalysts and the formation of particles of the catalyst, taking into account the phenomenon of coalescence. This theory is consistent with the results of experiments on the growth of metal particles. We have shown that the phenomenon of coalescence leads to the growth of globular particles. The experimental dependence of the number of particles of a certain size allows us to calculate the surface tension of the particle material.

The coalescence model allows researchers to better understand the mechanism of formation of nanoparticles comprising the catalyst. Nanoparticle size is constantly changing with the growth of a nanotube. This should be considered when the results of growth of nanotubes are analyzed.

2.8.5 The Kinetics of the Growth of a Nanotube

Vertically aligned CNT arrays are both an important technological system and a fascinating system for studying the basic principles of nanomaterial synthesis. Nevertheless, growth deactivation and the accompanying termination mechanisms still remain a topic of nanotube synthesis science. Due to their extremely small size, however, direct characterization of various transport and conversion events occurring at the catalyst surface is not easy. Thus, investigations on growth kinetics are the first step to resolve questions about the growth mechanism.

There are a series of works devoted to the kinetics of CVD growth. One of the first [27], showed that the kinetic equations adequately described growth. A rate-equation model was developed to describe the measured kinetics in terms of activation energies and rate constants for surface carbon formation and diffusion on the catalyst nanoparticle, nanotube growth, and catalyst over-coating. In one work [28] is presented a simple model for the growth and termination of CNT arrays. This model was developed by modifying several submodels and provides a comprehensive predictive tool for the CNT growth process as a function of CNT wall number.

2.8.6 Some Experimental Results

Carbon nanotubes were synthesized by the method of PECVD installed using an Oxford Plasmalab System 100. The titanium (10–15 nm) was a buffer layer and nickel (2.4 nm) served as the catalyst. Growth occurred at temperatures of 550–650 °C. Formation of the catalysts and the array of CNTs was analyzed using a scanning electron microscope (HeliosNanoLab 650 company FEI), an atomic-force microscope (Dimension Icon firm Brucker) and an Auger Electron Spectrometer (Jamp 9510F of JEOL). The height of the array had a limit value. It grew rapidly at a first and then slowed and stopped (Fig. 2.5).

The growth of CNTs was repeated many times, experimentation results were statistically averaged and confidence intervals were found for the change of height of the array (the points in Fig. 2.5). Auger analysis revealed that in addition to carbon, nickel, titanium, and titanium carbide phases took place (Fig. 2.6). The concentration of titanium carbide decreases with etching of argon ions in the cell analysis of the Auger Electron Spectrometer. This suggests that titanium carbide is located on the catalyst surface. The experiments allow us to offer one possible mechanism for the formation of a heterogeneous catalyst. Carbides of titanium and nickel produce carbon, which penetrates into the catalyst from the reactor. Titanium carbide has a high melting temperature and is a very stable compound that is evidenced by high formation heat (−183 kJ/K) and a large free energy change (−236 kJ/K/mol). The formation of these compounds is active and continues until complete exhaustion of one of the components. Alternatively, nickel carbide is easily decomposed at the front of the formation of nanotubes, thereby, it supplies

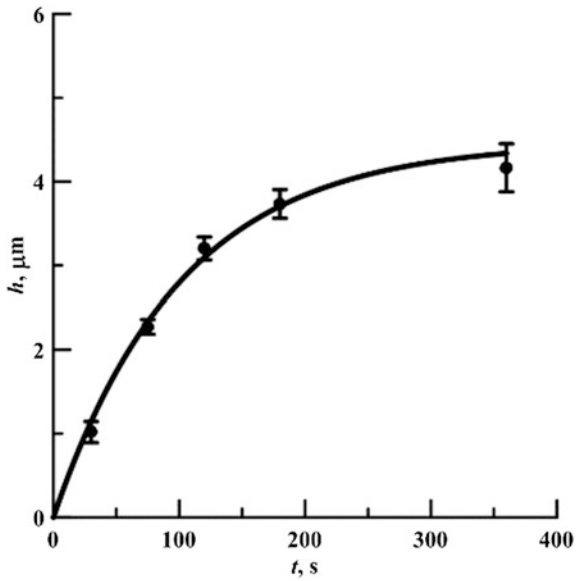

Fig. 2.5 The dependence of the height of the array of CNTs on the time of synthesis. The *points* represent experimental data, the *solid line* represents the calculation

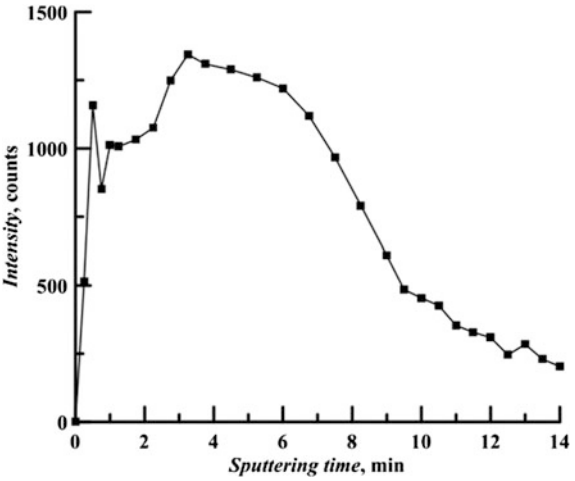

Fig. 2.6 The dependence of the intensity of the Auger peak of titanium carbide on the surface of nanoparticle ion etching time

the carbon for its growth. Titanium carbide, formed on the surface of the catalyst drops and forms a crust that creates a barrier against penetration of carbon into catalyst. It initially forms islets which eventually merge and create a crust on the surface of the catalyst. The carbon concentration in the catalyst is thus reduced, growth slows down, and stops when the crust covers the surface completely. Hydrocarbon pyrolysis products are involved in the formation of the crust, too.

One may conclude that there is great complexity in the CNT growth process. The CVD synthesis of carbon nanotubes involves a series of transport and conversion events that produce a flux of carbon material from a precursor, provided by the feed gases (or generated by gas phase reactions), to the CNT that grows from the catalyst particle. Nanotube growth processes via CVD share several common characteristics. The arriving molecules adsorb to the catalyst surface and start to decompose into carbon and hydrogen. The carbon adsorbate dissociates itself further into atomic carbons, and thereafter the carbon adatoms diffuse through the catalyst particle to the open end of the growing nanotube and finally incorporate into graphitic carbons comprising the CNT. These steps need to be included in the system of kinetic equations.

2.8.7 System of Kinetic Equations

Figure 2.7 summarizes the processes that occur on the surface of the catalyst we had considered in our attempt to explain the observed kinetics of the growth of CNTs. The basis of a system of differential equations of the kinetics can be found in research work [27]. However, the following major additions were made in our work:

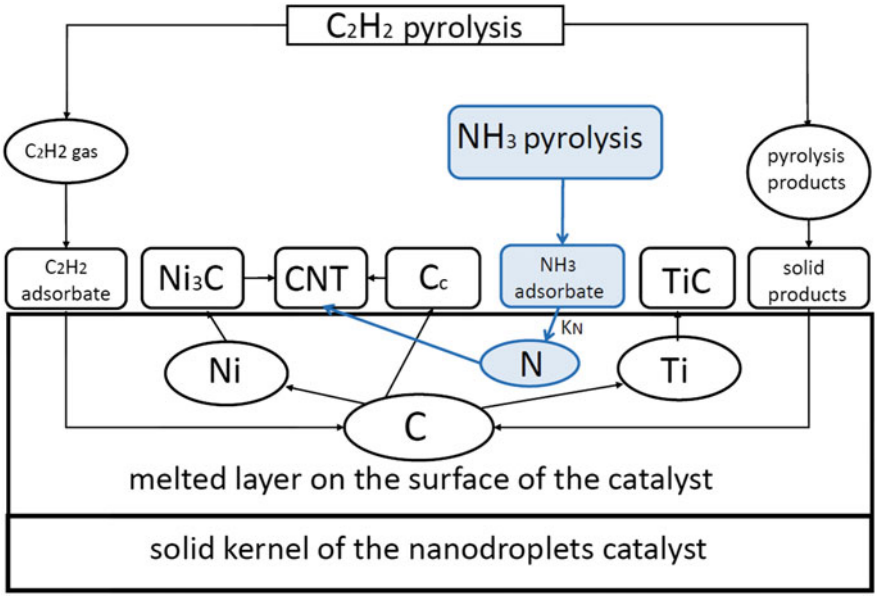

Fig. 2.7 Schematic representation of the processes responsible for growth and doping of CNTs

- Nickel carbide was formed in the melt. The process of its decomposition is the main supplier of carbon during the growth of CNTs.
- The intermetallic compounds are formed on the surface of the catalyst, such as titanium carbide.
- Dopant occurs simultaneously with the growth of nanotubes.

Hydrocarbons provide a constant flux of carbon-containing molecules, F_{c1}, to the surface of the catalyst nanoparticle. Pyrolysis products do this also, F_{c2}. The surface of the catalyst layer is molten as it contains many fine irregularities. These have a radius smaller than 1 nm, so their melting temperature is lower than the temperature in the reactor and so they melt. The thickness, Δm, of this layer is defined by the maximum number of feedstock molecules decomposed on the surface of the catalyst nanoparticle, N_C, at a particular temperature. This layer channels the diffusion of the dissolved carbon atoms, N_B, at a rate constant k_t and encourages their precipitation into a nanotube because of the much higher carbon diffusivity in the disordered layer compared to the ordered solid phase.

Carbides of titanium and nickel are formed as well. Titanium carbide has a low density, but higher melting temperature (>3000 °C) and a high stability. It forms a crust on the surface of the catalyst, which hinders the entry of carbon into the melt. This crust inhibits the growth of nanotubes. The pyrolysis products are also deposited on the catalyst surface. Some of them form an amorphous layer. This layer is a supplier of carbon into the catalyst, on the one hand, but participates in the formation of the crust which slows the growth of nanotubes, on the other.

Carbon nanotubes grow at the expense of carbon, which is supplied from the melt and TiC decay.

These processes are described by a system of kinetic equations:

$$\begin{aligned}
&\frac{dN_{C2H2}}{dt} = \tilde{F}_{c1} n \left(1 - \frac{N_{L1}}{\alpha_L S_0 n_L} - \frac{N_{TiC}}{\alpha_{TiC} S_0 n_{TiC}}\right) - k_{Ni3C} N_{C2H2} N_{Ni}^6,\\
&\frac{dN_{L1}}{dt} = \tilde{F}_{c2} n_p \left(1 - \frac{N_{L1}}{\alpha_L S_0 n_L} - \frac{N_{TiC}}{\alpha_{TiC} S_0 n_{TiC}}\right) + k_{c1} N_C - k_{d1} N_{L1},\\
&\frac{dN_{Ni3C}}{dt} = k_{Ni3C} N_{C2H2} N_{Ni}^6 - e_{Ni3C} N_{Ni3C},\\
&\frac{dN_{TiC}}{dt} = k_{TiC} N_B N_{Ti},\\
&\frac{dN_C}{dt} = e_{Ni3C} N_{Ni3C} - (k_{sb} + k_{c1}) N_C,\\
&\frac{dN_T}{dt} = k_t N_B,\\
&\frac{dN_B}{dt} = k_{sb} N_C - k_t N_B + k_{d1} N_{L1} - k_{TiC} N_B N_{Ti}, \quad N_{Ti}(t) + N_{TiC}(t) = N_{Ti}^0,\\
&\frac{dn_p}{dt} = k_{1p} n^2 - k_{2p} n_p, \quad n + 2n_p = n_0(1 - \exp(-kt)), \quad N_{Ni}(t) + 3N_{Ni3C}(t) = N_{Ni}^0,\\
&\frac{dN_{Ti}}{dt} = -k_{TiC} N_B N_{Ti},\\
&\frac{dN_{Ni}}{dt} = -k_{Ni3C} N_{C2H2} N_{Ni}^6 + e_{Ni3C} N_{Ni3C},
\end{aligned} \tag{2.111}$$

These equations must be supplemented by the initial conditions:

$$\begin{array}{llll}
N_{Ni}(0) = N_{Ni}^0; & N_{Ti}(0) = N_{Ti}^0; & N_{Ni3C}(0) = 0; & N_{TiC}(0) = 0;\\
N_{C2H2}(0) = 0; & N_C(0) = 0; & N_{L1}(0) = 0; & N_B(0) = 0;\\
N_T(0) = 0; & n_P(0) = 0; & n(0) = \tilde{n}_0 = n_0. &
\end{array} \tag{2.112}$$

where N_{C2H2} is the number of molecules of acetylene which adsorb on the surface of the catalyst nanoparticles; N_{Ti} is the number of titanium atoms in the nanoparticles of the catalyst; N_{Ni} is the number of nickel atoms in the nanoparticles of the catalyst; N_{TiC} is a number of the molecules of titanium carbide in the solid phase on the surface of the catalyst nanoparticles; N_{Ni3C} is the number of molecules of carbide nickel on the surface catalyst nanoparticles; k_{TiC} is the coefficient of the probability of formation of titanium carbide molecules; k_{Ni3C} is the coefficient of the probability of the formation of nickel carbide molecules; e_{Ni3C} is the coefficient of the probability of the nickel carbide molecules decaying; N_C is the number of carbon atoms on the surface of the catalyst nanoparticles, obtained by catalytic decomposition of acetylene molecules; N_L is the number of carbon atoms falling within a carbonaceous layer on the surface of the catalyst nanoparticles; N_B is the number of carbon atoms diffusing

in the melted surface layer, Δ_m; N_T is the number of carbon atoms falling in the melted surface layer; $n_L = 10^{15}$ atoms/sm^2 is the surface density of a monolayer of carbon atoms; α_L is the number of monolayers ($\alpha_L = 1$); $n_{\text{TiC}} = 10^{15}$ atoms/sm^2 is the surface density of a monolayer of molecules of titanium carbide on the surface of the catalyst nanoparticles; α_{TiC} is the number of monolayers of molecules of titanium carbide ($\alpha_{\text{TiC}} = 1$); $S_0 = 2\pi R^2$ is the surface area of the catalyst nanoparticles disposed on the substrate; R is the radius of catalyst nanoparticles; $\tilde{F}_{c1}\, n$, $\tilde{F}_{c2}\, n_p$ are flows of acetylene and acetylene pyrolysis products deposited on the surface of the catalyst nanoparticles; $k_{\text{TiC}} \cdot N_{\text{B}} \cdot N_{\text{Ti}}$ is the rate of reaction of the formation of titanium carbide; $k_{\text{Ni3C}} \cdot N_{\text{C2H2}} \cdot N_{\text{Ni}}^6$ is the rate of reaction of the formation carbide nickel; and $e_{\text{Ni3C}} \cdot N_{\text{Ni3C}}$ is the rate of decay of nickel carbide.

The kinetic coefficients of system (2.111) are temperature dependent and are determined by the following expressions:

$$
\begin{aligned}
&\tilde{F}_{c1} = \frac{1}{4} S_0 \sqrt{\frac{k_{\text{B}} T}{2\pi m}} p_1 \exp\left(-\frac{E_{a1}}{k_{\text{B}} T}\right),\\
&\tilde{F}_{c2} = \frac{1}{4} S_0 \sqrt{\frac{k_{\text{B}} T}{2\pi M}} p_2 \exp\left(-\frac{E_{a2}}{k_{\text{B}} T}\right)\\
&\frac{k_{1p}}{k_{2p}} = P \exp\left(-E_p / k_{\text{B}} T\right),\\
&k_{\text{sb}} = B \exp\left(-\frac{E_{\text{sb}}}{k_{\text{B}} T}\right),\\
&k_{c1} = A \exp\left(-\frac{E_{c1}}{k_{\text{B}} T}\right),\\
&k_t = C \exp\left(-\frac{E_b}{k_{\text{B}} T}\right),\\
&D_{\text{Ni3C}} = D_0 \exp\left(-\frac{E_1}{k_{\text{B}} T}\right),\\
&D_{\text{TiC}} = D_0 \exp\left(-\frac{E_2}{k_{\text{B}} T}\right),\\
&k_{\text{Ni3C}} = 4\pi a D_{\text{CNi}} / V = (4\pi a D_0 / V) \exp\left(-\frac{E_1}{k_{\text{B}} T}\right),\\
&k_{\text{TiC}} = 4\pi a D_{\text{CTi}} / V = (4\pi a D_0 / V) \exp\left(-\frac{E_2}{k_{\text{B}} T}\right),\\
&e_{\text{Ni3C}} = k_{\text{Ni3C}} N \exp\left(-\frac{E_r}{k_{\text{B}} T}\right) = 4\pi a D_0 (N/V) \exp\left(-\frac{E_1}{k_{\text{B}} T}\right) \exp\left(-\frac{E_r}{k_{\text{B}} T}\right),
\end{aligned}
\tag{2.113}
$$

where T is the absolute temperature; k_{B} is the Boltzmann constant; E_{a1} is the energy of activation of the capture and catalytic decomposition of molecules of acetylene

C_2H_2 at the catalyst surface; E_{a2} is the energy of activation of the capture and catalytic decomposition of molecules of acetylene pyrolysis products (in the simplest case, molecule C_4H_4 dimers) on the catalyst surface; p_1, p_2 are the corresponding pre-exponential factors; m, M are masses of molecules of C_2H_2 and C_4H_4, respectively; E_p is the activation energy of the decomposition of the molecules in the gas phase; P is pre-exponential factor; E_{sb} is the activation energy of the penetration of carbon atoms in the molten layer; E_{c1} is the activation energy of the formation of a carbon layer; E_b is the activation energy of diffusion of carbon atoms to the place of CNT growth; A, B, C are the pre-exponential factors; $a = 0.35$ nm is the mean distance between the atoms and molecules in the molten layer; $D_0 = a^2 v/6 = 0.204$ cm^2/c, $v = 10^{15}$ 1/c is the characteristic phonon frequency; $V = (4/3)\pi R^3$ is the volume of the catalyst nanoparticles; E_1 is the activation energy of the mutual diffusion of carbon and nickel in the molten layer; E_2 is the activation energy of the mutual diffusion of carbon and titanium in the molten layer; E_r is the activation energy of molecules of nickel carbide decaying; and $N/V = 2/a^3 \approx 4.66 \times 10^{22}$ cm^{-3} is the concentration of atoms in the molten layer.

If we exclude the dependent equation, then system (2.111) takes the form:

$$\begin{aligned}
\frac{dN_{C2H2}}{dt} &= \tilde{F}_{c1} n \left(1 - \frac{N_{L1}}{\alpha_L S_0 n_L} - \frac{N_{TiC}}{\alpha_{TiC} S_0 n_{TiC}}\right) - k_{Ni3C} N_{C2H2} N_{Ni}^6, \\
\frac{dN_{L1}}{dt} &= \tilde{F}_{c2} n_p \left(1 - \frac{N_{L1}}{\alpha_L S_0 n_L} - \frac{N_{TiC}}{\alpha_{TiC} S_0 n_{TiC}}\right) + k_{c1} N_C - k_{d1} N_{L1}, \\
\frac{dN_{Ni}}{dt} &= -k_{Ni3C} N_{C2H2} N_{Ni}^6 + \frac{1}{3} e_{Ni3C} \left(N_{Ni}^0 - N_{Ni}(t)\right), \\
\frac{dN_{Ti}}{dt} &= -k_{TiC} N_B N_{Ti}, \\
\frac{dN_C}{dt} &= \frac{1}{3} e_{Ni3C} \left(N_{Ni}^0 - N_{Ni}(t)\right), \\
\frac{dN_B}{dt} &= k_{sb} N_C - k_t N_B + k_{d1} N_{L1} - k_{TiC} N_B N_{Ti}, \\
\frac{dN_T}{dt} &= k_t N_B, \\
\frac{dn_p}{dt} &= k_{1p} \left(n_0 (1 - \exp(-kt)) - 2n_p\right)^2 - k_{2p} n_p.
\end{aligned} \tag{2.114}$$

We solve system (2.114) numerically. It is assumed that coefficient $k_{d1} = 0$. This means that the transition of carbon through a barrier layer is absent.

Solution of system (2.114) can be found:

$$\begin{aligned}
N_{Ni3C}(t) &= \frac{1}{3} \left(N_{Ni}^0 - N_{Ni}(t)\right), \\
N_{TiC}(t) &= N_{Ti}^0 - N_{Ti}(t).
\end{aligned} \tag{2.115}$$

System (2.2.28) provides a solution for the height of the nanotubes. It can be estimated using formula $L(t) = N_T(t)/z$, where z is number of carbon atoms per unit length of the nanotube. The number of carbon atoms per unit length is given by a single-walled nanotubes, which can be obtained on the basis of the theory described in [23]:

$$z = \frac{4\pi d}{3\sqrt{3}d_0^2}\ (\text{SWNT}), \quad z = \frac{4\pi d}{3\sqrt{3}d_0^2} \cdot N_w\ (\text{MWNT}) \tag{2.116}$$

where d is the diameter of the CNT; d_0 is the distance between the nearest carbon atoms in the nanotube; and N_w is the number of layers in the MWCNT.

System (2.114) was solved at several temperatures in the interval 450 °C < T < 750 °C. It is possible to calculate the temperature dependence of the height of the array from its temperature rise (Fig. 2.8).

The calculation results described the experimental results well.

System (2.114) can be solved in view of the doping process, such as nitrogen, which occurs simultaneously with the growth of nanotubes. Melting is in an equilibrium state and is saturated by the particles that are in the gas phase. The concentration of these particles in the melt is determined by the distribution coefficient. We can then add to this system the following equation:

$$N_N = k_N N_{NH3} = k_N \frac{p_{NH3}}{k_B T}, \quad \frac{dN_N}{dt} = -k_{cN} N_N \tag{2.117}$$

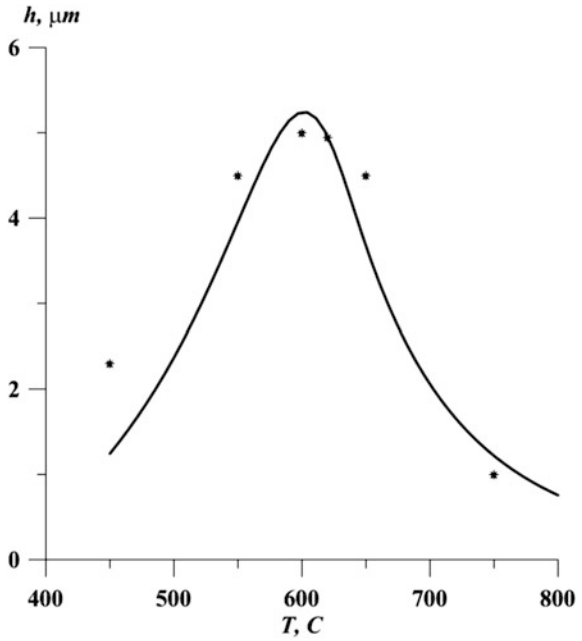

Fig. 2.8 Temperature dependence of the height of an array against temperature rise. *Points* represent experimental data. The *solid line* is the result of a numerical solution of system (2.114) at different temperatures

where N_N is the concentration of nitrogen in the melt; k_N is the coefficient of distribution of nitrogen between gas and liquid phases; p_{NH3} is the pressure of the nitrogen vapor; and k_{cN} is the probability of the capture of nitrogen, dissolved in the melt, by growing nanotubes. Dissolution of nitrogen, and its capture by a nanotube, weakly depends on other parameters of the growth process. Therefore, the use of calculation and experimental data do not make it possible to identify the influence of nitrogen on the growth of nanotubes if its concentration is low.

Growth rates of CNTs in temperatures between 550 and 900 °C, and the effect of different flow rates (concentrations) of C_2H_2 feedstock gas, were separately studied. Growth is modeled using rates of arrival of carbon on the metal catalyst surface, its dissolution into a highly disordered, 'molten' surface catalyst layer that channels diffusion to the nanotube boundary, and precipitation into a nanotube. This model agrees with the experimental data well.

2.9 Conclusion

Thermodynamics and kinetics allow a better understanding of the processes of growth of CNTs. Growth and doping of CNTs are complex physical and chemical processes so the quality of a CNT depends on many factors: the temperature and gas composition in the reactor, the catalyst, and the sequence of process steps. The interactions of the molecules and the reaction rate between them are easier to understand if we use thermodynamic and kinetic approaches to technological processes.

Catalyst substance and its surface treatment always determine the results of the growth. Thermodynamics and kinetics allow a better understanding of these processes. These two approaches are complementary to each other and should be used together for process analysis. The thermodynamic approach is used in the case where thermodynamic equilibrium can be established in the reactor. Such processes include pyrolysis processes, when the balance is provided by the constancy of temperature and speed of movement of gases in the reactor; clusters of catalysts containing a small quantity of the substance being quickly are warmed up, and reaching equilibrium. Growth is relatively slow, however, in this case it is important to investigate the kinetics of the process.

Carbon nanotubes may be doped in the growth process as well as after its completion. Thermodynamic doping allows a better understanding of what defects, and how many defects, are formed by doping. Kinetics allows us to estimate the rate of processes, which allows us to determine whether a reaction took place at the end of doping or not. The study of kinetics allows us to calculate the kinetic coefficients, which are important for the understanding of the conditions for the realization of technological doping processes. In this case, the thermodynamics and kinetics are complementary. Unfortunately, the kinetic processes are rarely studied and there is not enough information about them. This is due to the great difficulty associated with such experiments. The processes of desorption of molecules

(TGA) are an exception and have become standard methods of carbon nanotube technology.

This chapter provides the physical basis for the use of thermodynamics and kinetics for the description of the doping process. This chapter is the foundation for following chapters, where the above models are discussed and explained with specific examples.

In this chapter we have described two important results. First, we have considered the method used to calculate the concentration of defects, which is based on the minimization of the free energy of the system. This method allows the calculation of the concentration in the case of the existence of a large number of simultaneously occurring reactions and determines the influence of some defects. Second, we considered the identification of the formation of intermetallic compounds in the catalyst nanoparticle and its impact on the growth of nanotubes.

References

1. S. Carl, *Helrich Modern Thermodynamics with Statistical Mechanics* (Springer, Berlin, 2009), 402 pp. doi:10.1007/978-3-540-85418-0
2. F. Hansen, *The Science of Construction Materials* (Springer, Berlin, 2009), 386 pp. doi:10.1007/978-3-540-70898-8
3. R.A. Svelin, *Thermodynamics of Solids* (Wiley, New York, 1966), 315 pp
4. S.V. Bulyarskiy, A.S. Basaev, in *Thermodynamics and Kinetics of Adsorption of Atoms and Molecules with Carbon Nanotubes*. ZhETF, vol. 135, no. 4 (Springer, Heidelberg, 2009), pp. 788–799
5. L.J. Dunne, G. Manos, *Adsorption and Phase Behaviour in Nanochannels and Nanotubes* (Springer, Dordrecht, 2010). doi:10.1007/978-90-481-2481-7
6. F.A. Krőger, *The Chemistry of Imperfect Crystals* (North-Holland, Amsterdam; Interscience (Wiley), New York, 1964), 1039 pp
7. A. Jorio, G. Dresselhaus, M.S. Dresselhaus, *Carbon Nanotubes. Advanced Topics in the Synthesis, Structure, Properties and Applications* (Springer, Berlin, 2008), 720 pp
8. A.R. Ranjbartoreh, G. Wang, Effect of topological defects on buckling behavior of single-walled carbon nanotube. Nanoscale Res. Lett. **6**, 28 (2011)
9. S.V. Bulyarskiy, V.I. Fistul, *The Thermodynamics and Kinetics of the Interaction of Defects in Semiconductors* (Science, Moscow), 352 pp (Rus.) (1997)
10. S.V. Bulyarsky, V.P. Oleinicov, Thermodynamically evaluation of point defect density and impurity solubility in component semiconductor. Phys. Stat. Sol. (b) **141**, K7–K10 (1987)
11. S.V. Bulyarsky, V.P. Oleinicov, Thermodynamics of defect interaction in compound semiconducters. Phys. Stat. Sol. (b) **146**, 439–444 (1988)
12. S.V. Bulyarskiy, *Carbon Nanotubes: Technology, Properties Management, Application* (Ulyanovsk, 2011), 479 pp (Rus.)
13. A.H. Castro Neto, F. Guinea, N.M.R. Peres, Graphene. Phys. Rev. B **73**, 205–408 (2006)
14. S.V. Bulyarskiy, A.S. Basaev, in *Thermodynamics and Kinetics of Adsorption of Atoms and Molecules with Carbon Nanotubes*. ZhETF, vol. 135, no. 4 (2009), pp. 788–799
15. S.V. Bulyarskiy, A.S. Basaev, Adsorption by carbon nanotubes. Nano Microsyst. **12**(116), 16–55 (2009)
16. S.V. Bulyarskiy, V.V. Svetuhin, in *Physical Basis of Defect Management in Semiconductors*. Ulianovsk (2003), 385 p

17. V.F. Kisilev, O.V. Krylov, *Adsorption Processes on the Surface of Semiconductors and Dielectrics* (Science, Moscow, 1978), 255 pp (Rus)
18. G. Brown, Appl. Phys. **A76**, 457–462 (2003)
19. F.F. Volkinshteyn, *Physical Chemistry of Semiconductor Surfaces* (Science, Moscow, 1973), 399 p
20. S.K. Upadhyay, *Chemical Kinetics and Reaction Dynamics* (Springer, New York, 2006)
21. Y. Zhao, Y.-H. Kim, A.C. Dillon, M.J. Heben, S.B. Zhang, Hydrogen storage in novel organometallic buckyballs. Phys. Rev. Lett. **94**, 155–504 (2005)
22. S.V. Bulyarskiy, S.I. Radautcan, Modified method for thermally stimulated measuring of defects options. Semiconductors **15**, 1443–1448 (1981)
23. *Aligned Carbon Nanotubes. Physics, Concepts, Fabrication and Devices* (Springer, Berlin, 2013). doi:10.1007/978-3-642-30490-3
24. Y. Xu, X.-T. Yan, *Chemical Vapour Deposition* (Springer, London Limited, 2010). doi:10.1007/978-1-84882-894-0
25. A. Peigney, P. Coquay, E. Flahaut, R.E. Vandenberghe, E. De Grave, C. Laurent, A study of the formation of single- and double-walled carbon nanotubes by a CVD method. J. Phys. Chem. B **105**(40), 9699–9710 (2001)
26. E. Vanhaecke, F. Huang, Y. Yu, M. Rønning, A. Holmen, D. Chen, Catalytic consequence of the interface between iron catalysts and foils in synthesis of aligned nanocarbons on foils. Top. Catal. **54**, 986–997 (2011)
27. A.A. Puretzky, D.B. Geohegan, S. Jesse, I.N. Ivanov, G. Eres, In situ measurements and modeling of carbon nanotube array growth kinetics during chemical vapor deposition. Appl. Phys. A **81**, 223–240 (2005)
28. D.H. Lee, S.O. Kim, W.J. Lee. Growth kinetics of wall-number controlled carbon nanotube arrays. J. Phys. Chem. **114**, 3454–3458 (2010)

Chapter 3
Interaction of Hydrogen with a Graphene Plane of Carbon Nanotubes and Graphene

Sergey Bulyarskiy, Alexandr S. Basaev and Darya A. Bogdanova

Abstract Chapter 3 examines the reaction of hydrogen with CNTs. We have made an overview that describes the existing scientific literature experimental results and calculations on the interaction of hydrogen with CNTs. Review of the literature shows the prospect of using nanotubes as hydrogen storage, we continue this in the chapter, confirming the research via calculations.

Chapter 3 examines the reaction of hydrogen with CNTs. We have made an overview that describes the existing scientific literature experimental results and calculations on the interaction of hydrogen with CNTs. Review of the literature shows the prospect of using nanotubes as hydrogen storage, we continue this in the chapter, confirming the research via calculations.

Analysis of the interaction of hydrogen with a graphene plane is carried out by methods of quantum mechanics, thermodynamics, and physical kinetics. Calculation by methods of quantum mechanics allows us to establish a link between CNT size and electronic properties. The energy of electron states and the width of the HOMO–LUMO gap is reduced when the diameter and the length of the nanotube are reduced. We have performed calculations of chemical adsorption energy of hydrogen by nanotubes, as well as the energy of the formation of stone-walls defects and vacancies in a graphene lattice. We have calculated the concentration of the defects by the method of minimizing the Gibbs free energy that occurs during the physical adsorption and doping of graphene and CNTs. The partial Gibbs potential of the physical adsorption of hydrogen was also calculated.

S. Bulyarskiy (✉) · A.S. Basaev · D.A. Bogdanova
Institute Nanotechnology of Microelectronics,
Russian Academy of Sciences, Moscow, Russia
e-mail: bulyar2954@mail.ru

A.S. Basaev
e-mail: a.basaev@tcen.ru

D.A. Bogdanova
e-mail: bogdanovada8@gmai.com

S. Bulyarskiy and A. Saurov (eds.), *Doping of Carbon Nanotubes*,
NanoScience and Technology, DOI 10.1007/978-3-319-55883-7_3

Analysis of thermogravimetric experiments was made using the methods of physical kinetics and partial Gibbs potential of the chemical adsorption. It was found to be equal to 2.8 ± 0.1 eV and it is consistent with the results of calculations from quantum mechanics methods. In conclusion, we have analyzed the problem of using nanotubes as a hydrogen storage.

3.1 Adsorption by Carbon Nanotubes as a Basis for Hydrogen Storage Technology

Hydrogen is one potential source of the future, global energy [1], and therefore investigations of hydrogen energetics at present are proceeding and developing very intensively, especially in connection with hydrogen storage problems, where the main task is to collect and conserve this important product in great volumes. One method of the hydrogen storage is its adsorption on various carbon surfaces, now presented in many various allotropic forms [2]. For this purpose, modern carbon materials, such as fullerenes and CNTs, seem a very good prospect [3–12], because for example CNTs can retain and hold hydrogen even at room temperature [4]. In this connection, it is necessary to study and understand in detail the gas adsorption mechanisms in tubes, as well as to develop methods for determining its parameters or adsorptive capacitance.

The investigations of hydrogen adsorption and storage on CNTs are mainly devoted to the perspective of CNT usage as "containers" for the hydrogen storage [2]. At present, there are some different technologies for hydrogen storage and usage (e.g., hydrogen storage in compressed forms, hydrogen transformation into the metal hydrides, hydrogen adsorption on the various carbon structures surface, etc.). All these technologies have their own disadvantages. Compressed hydrogen is stored under pressure up to 2.5×10^4 Pa. Such storage requires the development of new types of storage tanks made from expensive and light composite materials. Hydrogen volumetric density (the stored hydrogen weight per unit system volume) remains very low even at the above-mentioned pressures. Moreover, this high-pressure storage method is not profitable economically due to the high cost of pressure equipment and safety issues. Sometimes hydrogen transfers into a bound state in some inter-metallic compounds, forming various metal hydrides. The hydrogen charge/discharge is carried out simply by system compression/rarefaction. The technology is very simple, but it provided only a low capacitance. Adsorption on carbon structures was considered the best prospect method for hydrogen storage but (due to the structures limited surface area and a high mass density) these carbon-adsorptive technologies have yet to reach their potential.

In the scientific literature, there are a large number of publications devoted to the various problems of hydrogen adsorption on CNT.

Many results of the adsorption on CNT are summarized in survey work [2]. There are also many experimental and theoretical investigations, devoted especially

to hydrogen accumulation into, and storage in different, CNT samples, but their data are very conflicting and contradictory. Thus, in the pioneering experimental publication of Dillon [5] it was reported, that the capacitance of the SWCNT can reach 5–10 wt% at room temperature and pressure of 4×10^4 Pa. In accordance with research data [13], this value is only actually about 3.5 wt%. In publications [14, 15] authors have reported that they reached a capacitance 4.2 wt% (at room temperature and pressure of 10–12 MPa) and even 8.25 wt% at cryogenic temperatures and pressure of 7.18 MPa. However, some authors [16] could obtain only 0.3–0.5 wt% (at room temperature), 1.23 wt% (at 77 K on SWCNT), and 0.1–0.34 wt% (at room temperature) and 0.5–3.3 wt% at 77 K on MWCNT. The experimental studies of the samples with high MWCNT content [17] showed that the maximal hydrogen capacitance is 0.3 wt% at room temperature and 2.27 wt% at lower temperatures (77 K) under pressure of 10.3 MPa. Some researchers reported that nanotubes adsorptive capacitance in regard to hydrogen increased with a growth in the purity level and with tubes being "cut" to shorter lengths. Such purified and "sectioned" SWCNTs, produced by electric arc methods and laser evaporation, held at hydrogen atmosphere at room temperature and at a 500-torr pressure demonstrated an accumulation level ranging 3.5–6.5 wt% [18–20]. Except for the usually considered hydrogen adsorption from gas phase, it is possible to achieve what is called electrochemical adsorption, and in this case a SWCNT can adsorb from 0.4 to 4 wt% of hydrogen [21, 22]. The parameters of the hydrogen accumulation in CNTs were theoretically calculated by the different quantum mechanical methods along with various numerical methods, including Monte-Carlo and density functional approaches, semi-empirical methods, etc. [23–26]. For example, in one work [27] was developed a theoretical model, predicting that the maximal adsorption capacitance on the inner and outer surfaces of nanotubes, with a diameter $\sim$14 Å, can reach 3.5 wt% at pressure up to 5×10^7 Pa and a temperature of 150 K. The authors [28] used a quantum mechanical method to model the hydrogen adsorption with a "loading" of 6.5 wt% on the CNT with different diameters and chirality. It was also shown, that hydrogen accumulation grows in CNTs which are preliminarily doped by nitrogen [29–31] (up to 9.8 wt% at 77 K [32] and 6.0 wt% at 300 K), titanium, and lithium (up to 7–8 wt%) [33–35]). A wide range of materials and measuring procedures can explain such a great dispersion of experimental data. The scattering of modeling and calculated results is connected with the approximation differences and absence of a general theory for hydrogen adsorption processes on CNTs.

One possibility for the stable chemisorption on SWCNTs was not only theoretically predicted, but was confirmed in experiments with usage of the various spectroscopic observations [36–43]. It was shown, that chemisorbed hydrogen content can be accumulated in SWCNTs up to 5.1 ± 1.2 wt%. From the studies of TGA spectra it was found that chemisorbed hydrogen is desorbed at temperatures ranging $\sim$500–600 °C [44–46]. A presence of hydrogen, being chemisorbed from a gaseous phase on CNTs and carbon nanofilaments (the structures very similar to SWNT) under moderate temperatures and pressures, is confirmed also by TGA spectra [15–17, 47, 48]. The TGA spectrum of these studies has usually as a

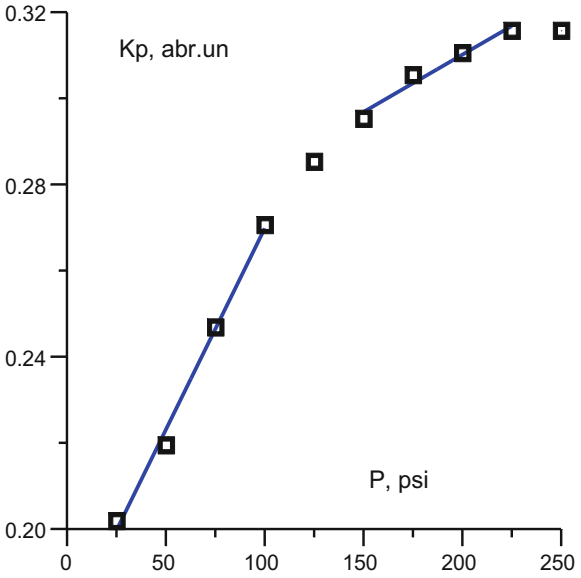

Fig. 3.1 The hydrogen physical adsorption isotherms and their approximation by formula (2.72). Points—experimental, continuous lines—approximation

minimum of two peaks. The first ordinarily can be ascribed to the physical adsorption, but the second one, a high-temperature ($T > 400$ K) peak, relates to chemisorption. It follows from the spectra analysis [15], that the chemisorption fraction is about 0.9 wt% from the total content (4.2 wt%) of captured hydrogen.

The experiments show that the adsorbed hydrogen content changes with a change in the environment media temperature and the hydrogen pressure in the system, as demonstrated by the adsorption isotherms in Fig. 3.1 [17]. It is worthy to note that the isotherm's non-linearity appears more evidently with a growth of volume of adsorbed substance. In the text below we will explain this fact and even show how these isotherms must be treated to obtain the necessary process parameters.

The developed theoretical models [5, 6], given in Chap. 2, allow the determination of the adsorption process parameters. We compared experimental data with calculations according to formula (2.72, Chap. 2). First, we calculated the part played by places, which are occupied by hydrogen atoms. We take an obvious expression for this purpose, where the difference between hydrogen and nitrogen molecular weights is taken into account. Additionally, it was proposed that under physical adsorption hydrogen is adjoined as a single molecule, but the place number equals the carbon atom number.

The part played by places, occupied by hydrogen atoms, in this case is:

$$a = wt\mu_c/\mu_{H_2}. \tag{3.1}$$

Then, a transformation was used, which must linearizes the adsorption isotherm (2.72), giving gives the expression:

$$\frac{a}{1-a} = pK = \frac{p}{p_s}\exp\left(-\frac{g_{\mathrm{H}}^{\mathrm{c}}}{kT}\right), \tag{3.2}$$

where $g_{\mathrm{H}}^{\mathrm{c}}$ is the adsorption free energy.

At the experimental dependence of Fig. 3.1 we see the two rectilinear parts, corresponding to the adsorption from different places. An approximation of these linear parts by the simplest linear dependencies of $(a_1 p + a_2)$-type allows the definition of the free energy as:

$$h_{\mathrm{H}}^{\mathrm{c}} = -kT\ln(a_1 p_s). \tag{3.3}$$

The calculated results give values of 0.012 and 0.021 eV. These parameters allow the calculation of adsorbed molecule concentrations. Therefore, the non-linearity of isotherms is related to the following two conditions. First, the hydrogen molecules are adsorbed on different places and have different bounding energies. Different slopes of adsorption isotherms can be explained by different binding energies. The molecules are adsorbing on the states with lower energies as the pressure rises. Second, CNTs are saturated with pressure increase, and in this case formula (2.72) ceases to be valid and correct, because the hydrogen content dependence on the pressure already can not be identified on an isotherm; that is a line parallel to abscissa-axis, that characterizes the CNTs saturation fact or phenomena.

It was reported in some work [2, 49] that on a SWCNT was obtained hydrogen capacitance of 4.2 wt% (at room temperature and a pressure of 10–12 MPa) and 8.25 wt% at a cryogenic temperature and a pressure of 7.18 MPa. Moreover, in these publications it was pointed put that a critical factor for hydrogen adsorption in a CNT is the inter-plane distance into the nanotubes, which equaled about 0.3 nm. A distance is characteristic to turbo-stratified graphite. In other words, the hydrogen penetrates into the space between carbon nanotubes.

If the nanotubes are sufficiently convenient and practically efficient then graphite can be used as a hydrogen absorbent [27], because it can capture hydrogen even at room temperatures and their bended surface increased the binding energy of the hydrogen molecules with carbon atoms. Moreover, during single-wall tube fabrication there often arises some “bunches” from the tight compacted triangular lattice structures in parallel stacked cylinders, the distance between them being equal to 3.4 Å, correctly corresponding to the distance between neighboring layers in graphite. Such triangular nanotube packages increases the system’s total accumulating capacitance due to the voids [50]. The adsorption can go on at both the inner and outer tube surface, as well as in the voids arising between the nanotube bunches.

The geometrical package of hydrogen molecules into SWCNTs ensures hydrogen accumulation into the material at 3.3 wt%, and the voids volume enhances this by 0.7 wt%, achieving a total accumulated hydrogen of 4 wt%.

The authors of [51] seek to find a simple and reliable criterion to define the limiting values of the adsorptive capacitance of various carbon materials.

The criterion was obtained on the basis of experimental isotherm analysis for hydrogen and other gas adsorptions at the super-crucial range. Hydrogen storage from an economic and technological point of view is justified only at temperatures above 77 K, sufficiently exceeding the hydrogen critical temperature (T_{cr} = 33 K). The transfer of the T_{cr} point on the adsorption isotherms of various gases removed the so called the polymolecular adsorption branch and therefore reaches a maximum within the range 1–10 MPa.

It was found in research [50], that a maximal value for the adsorption on the both sides of a single graphene plane equals 5 wt% at 77 K and 1.06 wt% at 293 K.

If the van der Waals sizes of hydrogen molecules and carbon atoms are considered, the a strengthening of interaction potential is observed in nanotubes with diameters below 1.1 nm. For the tubes with greater diameters this potential strengthening is not important, and their adsorption characteristic at super-crucial temperatures is not practically different from the usual adsorption on graphene. For SWCNTs the specific surface (both inner and outer) is the same as for graphene, and therefore the maximal values of the specific adsorption are the same. The volumetric hydrogen content in SWCNTs will be less than for the graphene plane adsorption, because this value will be defined by tube packaging density in the sample and by the relationship between the tubes mean diameter and hydrogen molecule diameter. It was noted also, that the samples after the synthesis consist of a great number of tubes stuck together. Their specific surface area is less than for the ideal case (with divided tubes). Therefore, the limiting specific adsorption value is smaller.

In MWCNTs, the distance between neighboring coaxial tubes (0.34 nm) is near to the inter-planar distance in graphite. For a weak adsorption attraction, the hydrogen molecules cannot penetrate into the space between the coaxial tubes, because otherwise the hydrogen molecules will be draw together with the carbon lattice at a distance, corresponding to strong repulsion. Hence, in MWCNTs, an adsorption proceeds at the inner channel surface and the tube outer surface. This leads to a sharp decrease in the maximal value for hydrogen adsorption in MWCNTs.

It was shown also, that under an oxygen plasma treatment the CNT ends open, increasing the adsorbed hydrogen volume. Some theoretical models predict a high adsorptive selectivity of CNTs in respect to the heavy hydrogen isotopes (tritium and deuterium) from isotopic mixtures at low temperatures. Hydrogen isotope selective adsorption was verified in several works [52, 53] experimentally by using adsorption isotherms on the nanoporous carbon. The authors measured the equilibrium adsorption isotherms for protium and deuterium at temperatures of 67–78 K in the pressure range from 10 Pa to 0.2 MPa.

One other variant of hydrogen storage is connected with the chemisorption. This method is similar to the metal hydrate production, but is energetically more advantageous. The problems of hydrogen chemisorption will be separately considered below.

3.2 Quantum Mechanical Calculations of Carbon Nanotube Adsorptive Characteristics

Chemisorption allows the accumulation of high amounts of the hydrogen. This is not the only use of chemisorption. Chemisorption of hydrogen on CNTs also changes the CNT electronic characteristics and hence their conductance. Unfortunately, we have not, until now, obtained the experimentally measured current–voltage characteristics of CNT samples with chemisorbed hydrogen, but there is much theoretical work underway, where (using different methods and models) the changes of SWCNT energetic spectra are predicted [54–57]. It must be noted also that in an experimental study [58] researchers marked an electrical resistance change after molecular hydrogen adsorption, which was not accompanied by a charge transfer.

In work [59] on SWCNTs arranged on gold substrate, results after treatment by low-energy hydrogen plasma were studied using scanning tunnel microscopy methods. The authors obtained images of hydrogen atoms, chemisorbed on the single-layered CNTs (11, 1) and (6, 2). The differential current–voltage characteristics showed that in the SWCNT forbidden zone were observed some symmetric and highly localized additional states, that were induced by the hydrogen plasma treatment. These states have ascribed due to the split of levels by hydrogen atoms, interacting with the graphene lattice. The theoretical part of the study was based on calculations using the well-known density functional method, showing, that the energy of a unique hydrogen chemisorption process on SWNT equals 1.5–2 eV. This energy grew with decreasing nanotube diameter. In this connection, in the middle of the HOMO–LUMO energy gap (it is an analog to the forbidden zone of a semiconductor but for macromolecules) some additional state arised. The relative position of the two hydrogen atoms on an SWNT is defined by the interaction between them during chemisorption, because their location influences the adsorption energy value, and also on the positions of the "doped" hydrogen levels relative to the middle of the HOMO–LUMO energy gap for a nanotube. The authors pointed out that a change in the mutual arrangement or relative location of the adsorbed atoms allows a change in the SWCNT properties, a fact that can be practically used in carbon nanoelectronics.

The adsorption free energy was also calculated, using quantum mechanical methods [60]. In all procedures, applied to the hydrogen adsorption theoretical description, various approximations were used. The most widely known approaches are the Monte-Carlo method, both the diffusion (DMC) and canonic variants, and the molecular dynamics (MD) methods. The DMC method [61] is based on the wave function calculations and it allows one to obtain some thermodynamic functions, the correlation functions, and the equilibrium particle density, taking into account the quantum effects. However, the algorithm realization is a very complex procedure, so that it is difficult to account for, by this method, the various temperature phenomena. The canonical Monte-Carlo method [62] takes account of the temperature effects, but in this case the dynamical equations and particle interaction potentials are used, based on classical mechanics principles, so that the quantum

effects remain unconsidered. Moreover, it is well known that all Monte-Carlo method calculations requiring computations of the configurations of vast numbers ($\approx 10^6$), making these methods very complex.

The MD method allows calculation of the atoms dynamics, using the forces of interaction, but in this method the forces (and therefore the atoms properties) were considered as classical ones and are subordinated to Newton's equations. Consequently, the many quantum effects (the atoms zero oscillations, energy level quantization, tunneling effects, etc.) cannot be accounted for and calculated using these methods. Procedures, based on MD calculations, cannot even predict a particles behavior at low temperatures, when the particle kinetic energy is smaller than the height of the potential barriers [62, 63].

In some work [27, 64] a method of the state equation was suggested for the adsorbed CNT hydrogen molecules taking account of the quantum mechanical effects, leading to energy level digitization and to a "smearing" of the adsorbed particle location between the neighboring atoms. The procedure was earlier used for the calculations of thermodynamic functions and the equilibrium density of the 1D chain of hydrogen molecules, adsorbed into super-thin SWCNT with chiralities of (3, 3) and (6, 0). In this work the introduced molecule interactions between one another were counted, as well as their interactions with the nanotube walls. For thermodynamic function calculations at non-zero temperatures there was phonon addition and an effect of particle transitions to excited levels. It was found that an adsorbent molecule motion along the narrow space (3, 3) and (6, 0) nanotube axes could be considered as a 1D motion. Next the 1D Schrödinger equation was considered for a hydrogen molecule, moving along the nanotube axis in a summary potential, created by its left and right neighbors (the same type molecules), as well as a potential created by the nanotube atoms themselves. The molecule wave function was considered as an expansion over plane waves.

These studies were developed and continued [27], where authors considered hydrogen adsorption on SWCNT of (10, 10) and (20, 20), having corresponding diameters of 13.56 and 27.13 Å. In these tubes the motion of the hydrogen molecules could not be reckoned as 1D. The authors considered the molecules as being adsorbed on the tube surface without strong covalent bounding, i.e., only due to weak van der Waals interactions (i.e., as in the case of pure physical adsorption). In their calculation it was also supposed that the hydrogen molecules must form a regular lattice that can be distorted later thanks to the thermal displacement of the molecules (which are accounted for afterwards by using photons contribution). It follows from the commensurability of the hydrogen molecules and carbon atom lattices, that the hydrogen lattice must be a hexagonal one superimposed on the nanotube surface. From Fig. 3.4 it is seen that with the outer pressure growth at different temperatures the adsorbed hydrogen molecule density demonstrates a series of phase transitions. This effect can be explained by the appearance of a quantum property for the adsorbed hydrogen molecules, because they have a set of quantum levels populated at non-zero temperatures.

Moreover, the calculations of adsorption on the tube outer surfaces were carried out too. The phase transition pressure linearly increased with temperature for the

studied tubes of both types. The adsorption on the inner surface of the tube was more intense than for the outer ones, however, at the same time, the total adsorption values (both inside and outside the SWNTs) decreased with tubes diameter growth. These dependencies are connected with an effective van der Waals potential growth for hydrogen molecules with an increase of inner tube curvature (and a decrease of the outer surface curvature, correspondingly). It was identified that the maximal adsorption value on both surfaces for tubes with diameters $\sim$14 Å can achieve 3.5 wt% at pressures up to 500 bar and T = 150 K.

Thus, the quantum mechanical calculations as a whole are in agreement with experimental results, but there are many other important problems, namely: to define the optimal conformations of both pure and doped (by chemisorption and encapsulation methods) single-wall carbon nanotubes; to detect an influence of the tube length and diameter on the energetic characteristics of nanotubes and adsorbed admixtures, etc. It is necessary also to consider hydrogen chemisorption as the most effective phenomena for resolving the hydrogen storage problem, i.e., to define the dependencies of the energetic and adsorptive characteristics on the accumulated hydrogen volumes and its influence on the SWCNT energetic gap width. These problems are solved in next section.

3.3 Modeling of Single Carbon Nanotube Properties for the Processes of Hydrogen Adsorption

We used the semi-empirical method AM1 (the so called Ostin 1 model) [65] for the calculations. In this semi-empirical method of quantum chemistry is used one special form of the Hamiltonian model, suggested by M. Dewar's group. In this model the following parameters are used: the electron energy at the free atom valence orbital; the two-centered one electron integrals; and the resonance integrals, calibrated over the heat from molecule formation in the basic electronic state. The quality of the method is sufficiently high and its results in mostly cases are near to ab initio calculations, however, they exceed the AM1 method, especially for hydrogen binding descriptions.

For investigations we selected eight *zigzag*-type SWCNTs: (n, 0). Their values ranged from 1 to 9 (with radiuses from 3.37 to 9.26 Å). We also chosefive armchair-type (n, n) SWCNTs: (3, 3), (4, 4), (5, 5), (6, 6), and (7, 7) (with radiuses 4.02, 5.43, 6.82, 8.08, and 9.41 Å, correspondingly). Dependence of the HOMO–LUMO gap on nanotube length was studied (LUMO—"lowest unoccupied molecular orbital"; HOMO—"highest occupied molecular orbital"). The length of the nanotubes was determined by the number of elementary rings (N) and the width of one unit ring. The value of N varied from 1 to 9 for (n, n)-type tubes. The N values varied from 6 to 8 for (n, 0)-type tubes.

Primarily the conformations with one hexagonal ring were considered. Later, after every additional ring supplement, the system geometry was optimized once more. In this case we considered the finite length nanotube case, when the "broken"

bounds on tube ends were "covered" by hydrogen atoms. The real tube length is always limited and therefore it is necessary to define the conditions under which we can use the results obtained by calculations from the model of infinite length tubes. It is also necessary to determine a minimal nanotube length, which allows the minimization of the influence of hydrogen atoms on chemisorption. Note, that for a transition from finite length tubes to tubes with a finite structural elemental number is worth using quantum mechanical notions of LUMO and HOMO instead of the notions of the conductance zone's bottom and ceiling, correspondingly. In this case, the energetic HOMO–LUMO gap presents an analog of the usual forbidden zone.

The results of the energetic gap calculations for (n, n)-type nanotubes demonstrates an oscillation of the HOMO–LUMO gap width with as the tube length increases (i.e., with growth of the structural unit numbers along the tube axis). Similar dependencies on length were obtained for (6, 6) and (7, 7) tubes, being consistent with other research results. These oscillations are less evident for (3, 3), (4, 4), and (5, 5) tubes, explained by the presence of stronger curvature effects in these SWCNT-type tubes. The calculations showed that the bigger the tube radius (i.e., the curvature being less), the deeper the corresponding curve was situated (i.e., the smaller its forbidden zone width).

The calculation results for (n, 0)-type tubes had a similar character, but in this case the gap width dependence on the chirality index was more pronounced (Fig. 3.2).

The authors of [66, 67] studied the dependence of the the *zigzag*-type (n, 0) tubes energetic characteristics on their length (with n values from 3 to 15), using the density functional method.

Studies of single wall carbon nanotubes with different lengths and chiralities have shown that the HOMO–LUMO gap width depends on the carbon hexagon number, which can be arranged along the tube length and perimeter, i.e., the SWCNT conductance depends not on the tube chirality, but its geometrical sizes too. The energy gap width corresponds to a semi-conductive material nature for all considered finite length nanotubes, in spite of their chirality. It is a well-known rule

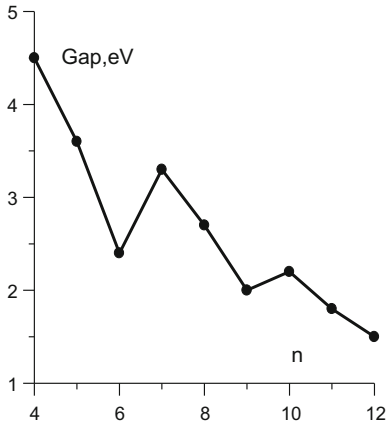

Fig. 3.2 Results of HOMO–LUMO gap width calculations. The gap width dependence on the cells number was obtained via a computer program [65] for nanotubes (6, 0)

that all *zigzag*–type (n, n) SWCNT and all SWCNT divisible by three$|n - m|$ values must have metallic conductivity. This rule is applicable with high precision only to nanotubes with sufficient length and not too small diameters. The HOMO–LUMO *energy* gap width of *armchair*-type CNTs is sufficiently more sensitive to change of length than chirality. For *zigzag*-type nanotubes the inverse situation is observed, and the sensitivity decreases with nanotube length and diameter growth.

Above it was mentioned that nanotube electrical properties depend not only on their chirality, but on their geometrical sizes too. This fact mostly explains the wide scatter of published experimental data. At the same time nanotube length and diameter changes become a new possible mechanism for modeling and creating macromolecular systems with certain electrical properties.

At present experimental studies of hydrogen adsorption are devoted to physical adsorption, although there is some work connected with chemisorption [68–78]. Molecular hydrogen is adsorbed mostly on the CNT outer surfaces. A rise of SWCNT diameters and pressures gives an increase in inner center populations [28]. However, some data show that hydrogen is partly chemisorbed under adsorption from the gas phase, using a metallic catalyst at high pressures [15]. The same process proceeds under hydrogen electrochemical accumulation into the samples [79], and in addition hydrogen accumulation by a chemisorption mechanism is sometimes preferable to physical adsorption. The point is that chemisorption has some advantages over the usual physical adsorption. First, chemisorption theoretically allows the achievement of a bigger hydrogen weight capacitance (that is very important regarding hydrogen storage fabrication). Second, the chemically adsorbed hydrogen has a stronger influence on CNT properties (such as the forbidden zone width, conductivity, etc.) than the physically adsorbed hydrogen. This fact opens up new possibilities to regulate and control nanotube characteristics. Third, the chemisorption bounding energy is bigger, than for physical adsorption, and this allows hydrogen storage under higher temperatures. Last, it must be noted that in CNT bunches some "patterns" of a hydrogen coating can cause the CNT to "unpack" [80] and this in turn can lead to the joining of two or three tubes into one tube with a bigger diameter (this effect also can be interesting from a practical point of view).

In this section, using the above described semi-empirical method (AM1), we model hydrogen chemisorption on SWCNTs of different chiral vectors and diameters. The *zigzag*-type (4, 0), (5, 0), (6, 0), (7, 0), (8, 0), and (10, 0) nanotubes, as well as the *armchair*-type (3, 3), (4, 4) and (5, 5) tubes were studied. All tube behavior was modeled for a length of $N = 5$ single cycles along the tube axis. This length gives stable conformations for the SWCNT under consideration and is enough to guarantee that the edge atoms are not contributing significantly to the electronic adsorption as a whole. It was supposed also, that for modeled nanotubes hydrogen atom "coatings" were regular (along the tube axis). It is known, that for chemisorption a paired hydrogen atom adsorption (i.e., on neighboring carbon atoms) is more preferable than an adsorption on the single atoms [81, 82], and therefore it was included in the modeling procedure.

From a logical point of view it can be supposed that when on a unique cell there are adsorbed more than one atom pair we must select such coating type "patterns"

which correspond to the maximal symmetry of the system. This assumption was proved by our calculation results.

In Fig. 3.3 are shown the four conformations for two pairs of hydrogen atoms, adsorbed on SWCNT (4, 4). The minimal energy has a conformation with index *a*. In the studies by other authors it was found that the "coating patterns" exhibiting symmetry were in fact energetically more profitable [83]. Below is presented some other data obtained for the energetically most profitable "coating patterns" (at similar coating sizes).

For the studied tubes we considered all variants of tube coatings, from minimal (2 hydrogen atoms) to total coating by hydrogen atoms. Moreover, for each case adsorption was modeled for both outer and inner SWCNT surfaces. For each "tube + adsorbate"-type system we defined the most stable conformations, the adsorption energy values, and the energy gap width.

We carried out *a geometry optimization for hydrogen's outer and inner chemisorption*. As an example in Fig. 3.4 are presented the optimized (i.e., the energetically most profitable) geometrical patterns for hydrogen adsorption on the (4, 4) nanotube's outer surface for all possible values of surface coating (coverage) degree θ (coverage is value equal to the ratio of the adsorbed hydrogen atoms number, N_H, to the carbon atoms number, N_C, i.e., $\theta = N_H/N_C$).

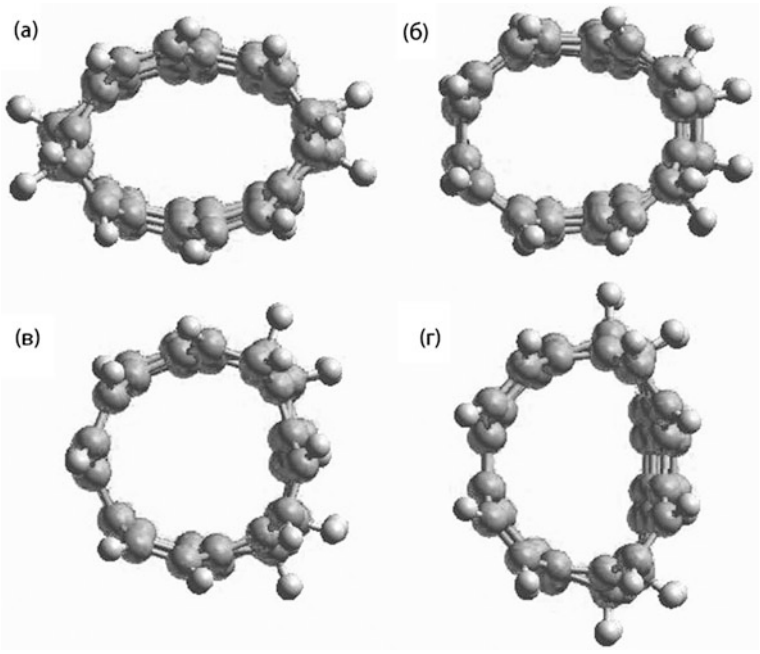

Fig. 3.3 Possible cross-sections of a nanotube (4, 4) SWCNT with two pairs of hydrogen atoms adsorbed on the single cell of the tube

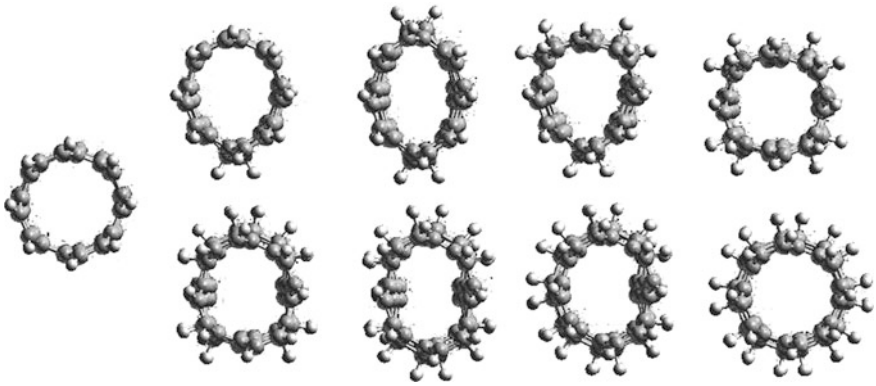

Fig. 3.4 Possible cross-section of the SWCNT (4, 4) for different variants of outer hydrogen adsorption coatings

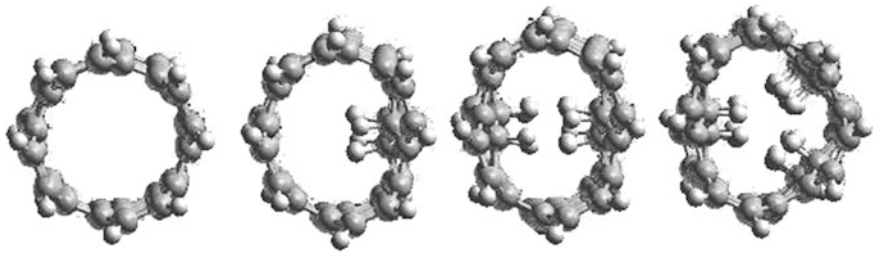

Fig. 3.5 Possible cross-section of the SWCNT (4, 4) for the different variants of inner hydrogen adsorption coatings

It is seen that when over 12 carbon atoms fit to 4 hydrogen atoms, the tube cross-section is elliptical; for absorption of 6 hydrogen atoms its form is near to a triangle; for absorption of 8 atoms its form is near to a rectangle; and for a total coating the cross-section returns to the initial circular form, but this time with a bigger mean diameter. Other researchers obtained similar results too. It will be shown below that a distortion or bending of the nanotube "graphene linen" strongly influences its energy spectrum.

Figure 3.5 presents the optimized geometrical patterns for inner hydrogen adsorption on a (4, 4) tube. It is seen that with a coating of one pair of hydrogen atoms per one unit of SWCNT cell, the carbon atoms, bounded with hydrogen, are "drawn into" the nanotube. However, in cases of 2 and 3 pairs they are "pulled out"—something which is connected with hydrogen atoms repulsion as a consequence of their coming together.

Calculations have shown that not all conformations of the H–SWCNT-system are stable. Chemisorption can cause nanotube "destruction" (if the inner coating degree becomes too great) or, in a particular case, can cause some "packing out", when we see a "nanotube opening" and becoming a curved graphite list. This final

case is observed during outer chemisorption, when the nanotube is small and hydrogen atom pairs are adsorbed very near to each other's 9th non-symmetric conformations). Such atom pairs can break the C–C chemical bonds along a zigzag-line in the tube's axis. Below we will only examine stable conformations, which do not lead to molecular system destruction.

The first important conclusion from our calculated data is the fact that all considered SWCNTs (in spite of their chirality and diameters) can be totally (in one layer) covered by hydrogen. The adsorption on their inner surfaces is not possible for all types of studied tubes. Energetically profitable situations occur only with chemisorption into tubes with diameters exceeding 5 Å, i.e., tubes with chirality from (4, 4). Moreover, under inner adsorption not all formed coatings are stable. There is a certain limitation for hydrogen amounts being adsorbed on inner surfaces. This can be explained by sufficiently small tube diameters, because as a result of a high density of accumulated hydrogen atoms they arrange themselves very near to each other. With a growth of the inner coating degree (parameter θ—coverage) these distances between the adsorbed hydrogen atom and the carbon atom, is only decreasing, and therefore a mutual repulsion between hydrogen atoms becomes more important and leads to a growth of energy in the tube + adsorbate system.

Figures 3.6 and 3.7 show the mean distances between the adsorbed hydrogen atoms and bounded nanotube lattice carbon atoms presented as plots depending on the hydrogen coating degree for outer and inner chemisorption, correspondingly.

The data shows the bond length of H–C varies from 1.12 to 1.17 Å for outer chemisorption and 1.16 to 1.195 Å for inner chemisorption. The bond length grows with an increase of parameter θ, and this fact reflects that a greater coating degree provides a repulsion of mutual hydrogen atoms that weakens the bond.

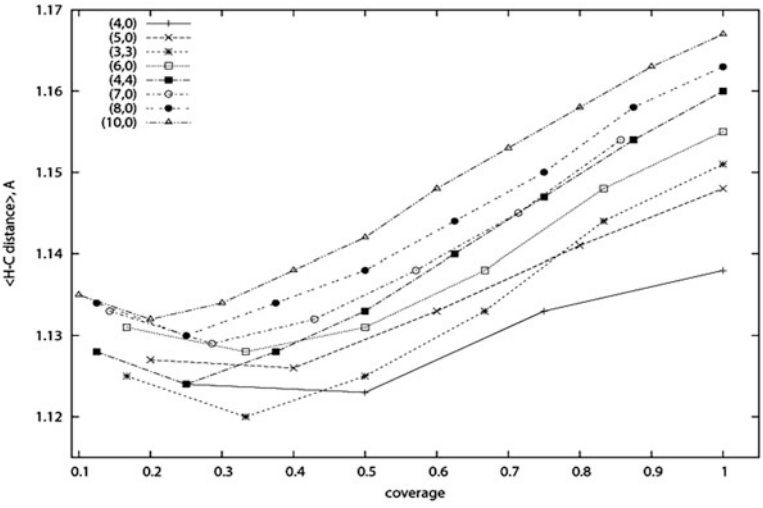

Fig. 3.6 The dependencies of the mean distances between the adsorbed hydrogen atoms and the degree of tube hydrogen coverage for outer chemisorption for tubes with different chiral vectors

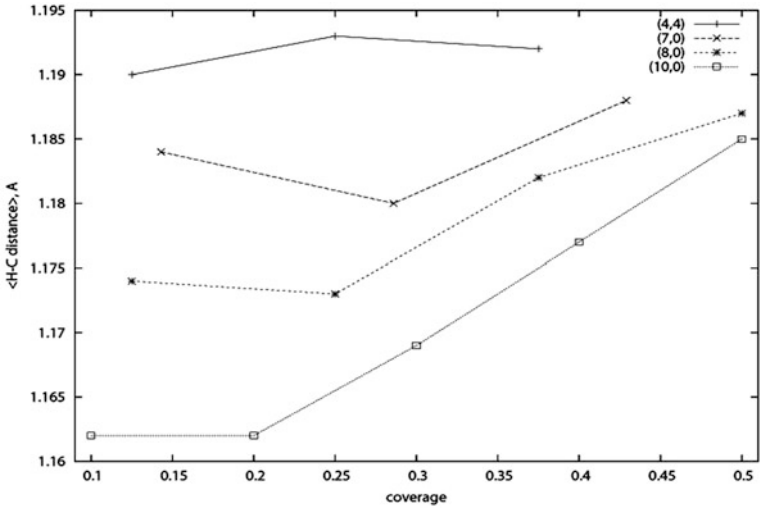

Fig. 3.7 The dependencies of the mean distances between the adsorbed hydrogen atoms and the degree of tube hydrogen coverage for inner chemisorption for tubes with different chiral vectors

We had considered also a special case of combined chemisorption (inner and outer simultaneously) for a (8, 0)-type nanotube. We found that under combined chemisorption (unlike the inner chemisorption case) there exists a stable conformation for every coating degree.

Hydrogen chemisorption energy for a SWCNT

The adsorption energy for a SWCNT was calculated as a difference between the nanotube total energy (with account the adsorbed hydrogen atoms) and total energy of a pure nanotube with adsorbed atoms:

$$E_{\text{ads}} = [E_{\text{tot}}(\text{tube} + N_{\text{H}}\text{H}) - E_{\text{tot}}(\text{tube}) - N_{\text{H}}E(\text{H})]/N_{\text{H}}, \tag{3.4}$$

where N_{H} is the total number of adsorbed H atoms; E_{tot}(tube + N_{H}H) is the total energy of the "tube + N_{H} adsorbed *H* atoms" system; E_{tot}(tube) is the total energy of a pure nanotube; and E(H) is one hydrogen atom's energy.

The deformation energy was calculated as the difference between the energy of a CNT (but deformed by hydrogen atom adsorption) and a pure nanotube:

$$E_s = E_{\text{tot}}(\text{strained tube without H}) - E_{\text{tot}}(\text{tube}), \tag{3.5}$$

where E_{tot} (strained tube without H) is the total energy of a pure tube with geometry deformed by hydrogen atom adsorption; and E_{tot}(tube + N_{H}H) and E_{tot}(tube) relate to the totally optimized geometry (below in tables and graphs the E_s value is estimated for a single carbon atom).

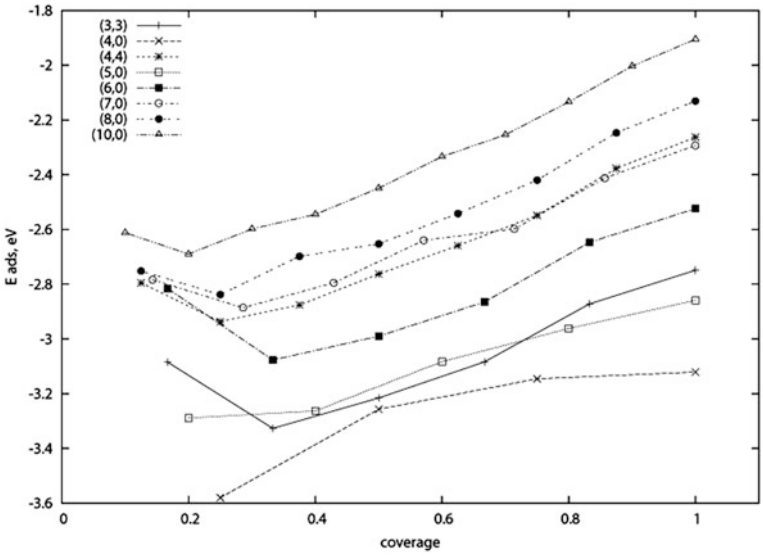

Fig. 3.8 The dependencies of the mean distances between the adsorbed hydrogen atoms and the degree of tube hydrogen coverage for inner chemisorption for tubes with different chiral vectors

The calculations were carried out for tubes with different chiral vectors and coating degrees. In Fig. 3.8 the outer adsorption energies are presented as a function of the coverage, and the data allows the following conclusions.

First, the SWCNT type (*armchair* or *zigzag*) does not change the general character of the adsorption energies dependence on coverage degree. Second, SWCNTs demonstrate that the greater the nanotube diameter, the less the adsorption energy. This can be explained due to a tubes bigger curvature for smaller diameters, leading to stronger hydrogen atom couplings on the surface of a tube. For the case of the smallest tubes (4, 0) and (5, 0) the adsorption energy is continuously rising with coverage degree, but for the tubes with big diameters this monotonic rise is violated by a minimum in the little coatings degree range. Such behavior can be explained by considering factors contributing to the adsorption energy on tube outer surfaces. This value is added from an energy change at the expense of a transition between electron shells from the sp^2-hybridization to the sp^3-hybridization—the energy of the adsorbed hydrogen atom interaction (repulsion) between one another and the energy of the tube carbon framework extension (deformation).

A hydrogen coating enlargement leads to the next sequence of processes and effects. First, the coverage degree growth increases the number of sp^3-hybridized orbitals which decreases the adsorption energy. Second, the tube is deformed more and the extension energy increased, this increases the adsorption energy. Third, the distances between the adsorbed hydrogen atoms shortens (i.e., the repulsion becomes stronger, also increasing the adsorption energy). The adsorption energy decreases initially for tubes (3, 3), (6, 0), (4, 4), (7, 0), (8, 0), and (10, 0) when

coverage degree grows. The sp^3-hybridization factor prevails. We can neglect deformation and atom repulsion. Hydrogen atom repulsion and tube deformation become most important with further growth of parameter θ. The adsorption energy increases after that. For SWCNT (4, 0) and (5, 0), with very small diameters, repulsion and deformation factors are significant even at small values of coverage degree. Therefore, their adsorption curves have absent minimums.

Let us consider an adsorption on the SWCNT inner surface. In Fig. 3.9 the dependence of the inner chemisorption energy on the hydrogen coverage degree is presented for the tubes with different chirality (and for stable conformations only). The calculations have shown that in general the adsorption energy decreases when the diameter of the nanotubes becomes smaller. Contribution of a re-hybridization prevails up to some coverage degree (parameter θ value). In this case the adsorbed hydrogen strongly deforms the tube and C–C binding length rises.

The following rise in the inner coating density leads to an energy rise on account of the strong repulsion of hydrogen atoms arranged in the tube. The maximal inner coating degree, when the tubes remain stable, is one-half for SWCNTs (8, 0) and (10, 0). Comparing the plots of the outer and inner adsorption for the same tubes, we can verify that the adsorption into tubes is energetically less profitable than on its outer surface.

Calculations have shown that in the case of combined chemisorption there always exists a stable conformation for every coverage degree in contrast to an inner chemisorption. The values of such "hybrid" adsorption energy lies between the inner and outer chemisorption values, demonstrating that mixed hydrogen chemisorption really is more preferable then inner, but less preferable compared

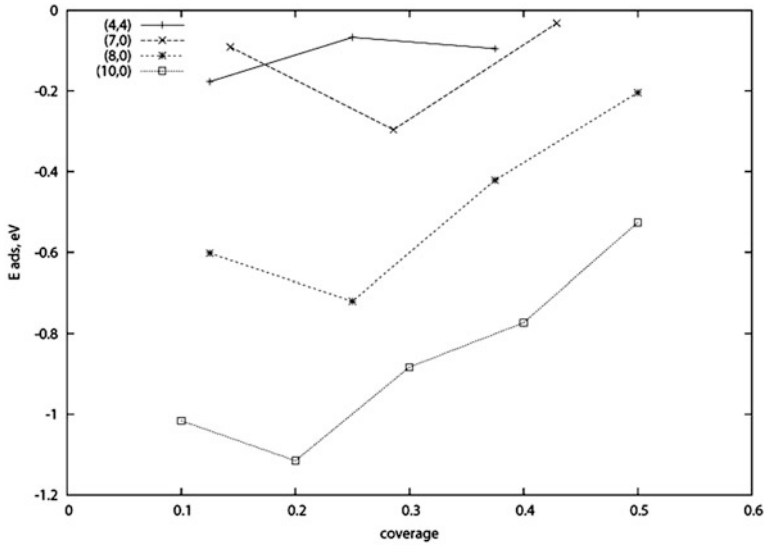

Fig. 3.9 The dependence of the deformation energy on the outer hydrogen coating for tubes with different chiral vectors

with outer chemisorption. It is also interesting that the energy of the combined type of adsorption is monotonically dumped with an increase in hydrogen coverage degree. This fact most likely demonstrates the prevailing role of one factor, connected with a sp^2–sp^3 re-hybridization over the contributions of factors connected with hydrogen atom repulsion SWCNT deformation.

SWCNT deformation energy with hydrogen chemisorption

As was shown above, the chemisorbed hydrogen can strongly deform CNTs. Let us consider first adsorption on the outer surface. In Fig. 3.10 the dependence of the deformation energy on the outer hydrogen coating is presented.

It is seen that with coating degree growth the deformation energy initially increased, but after some value of the coverage degree (>0.5) it begins to decrease. This is observed for all tubes besides (4, 0). As was said above, with a growth of adsorbed hydrogen on a tube's outer surface the tube becomes extended and deformed more intensely. An important role is played by conformation symmetry. Let us suppose that at $\theta = 1$ the adsorbed hydrogen uniformly coats the tube's total surface, but the tube cross-section remains almost circular (similar to a cross-section of a pure SWCNT) and the deformation energy is less than for coatings with lower symmetries.

The results of deformation calculations for inner chemisorption are presented in Fig. 3.11. In all cases the deformation energy increased with hydrogen coating degree growth.

Unfortunately, as was mentioned above, at present it is impossible to check the presented modeling results using experimental materials due to an absence of

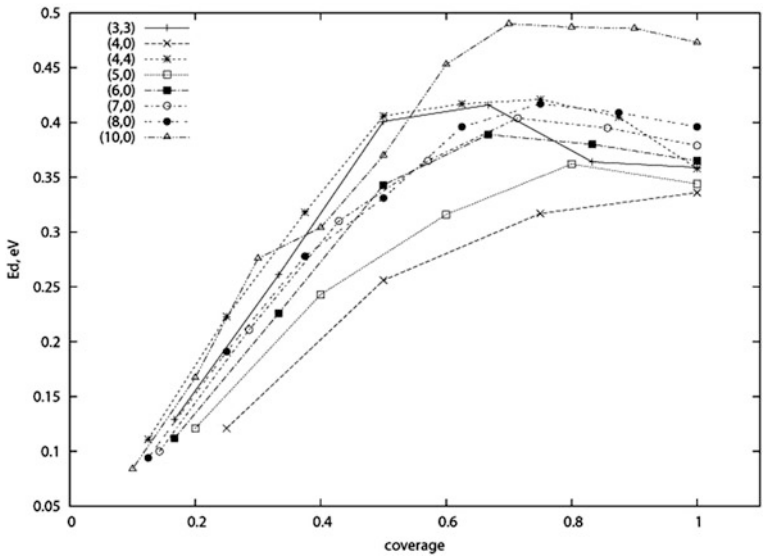

Fig. 3.10 Dependencies of the inner chemisorption energy on the hydrogen coating degree for tubes with different chiral vectors

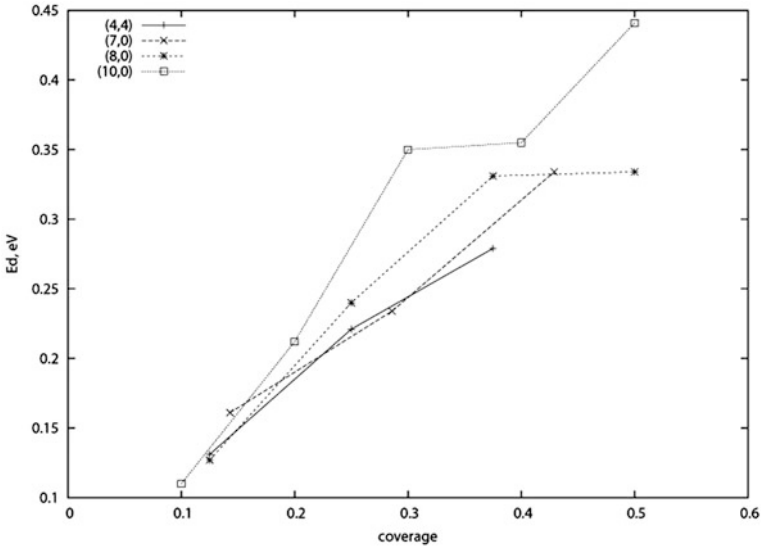

Fig. 3.11 The dependence of the deformation energy on the inner hydrogen coating for tubes with different chiral vectors

necessary experimental data relating to adsorption on a single SWCNT or even on bunch of linear tubes with similar diameters and chiralities. However, we can compare our results with data obtained by other researchers in these fields of computer modeling. The analysis of the known scientific literature shows that in general the different theoretical methods give similar results. For example, the authors of [83], modeling the atomic hydrogen adsorption on SWCNT (3, 3) and (5, 5), found that the total outer coating of tubes is stable, but the total inner coating leads to tube destruction. The results obtained for the (5, 5) tube deformation energy coincides, in magnitude order and general behavior, with the above considering our data for the nearest diameter nanotubes (8, 0) and (10, 0). However, they did not find a "fall" in the deformation curve in the total outer coating, which we explained earlier. Moreover, in their calculations the maximal deformation energy was found to be about 0.9 eV, although in our modeling it did not exceed 0.5 eV.

The problem of destruction of (6, 6) nanotubes, the unit cell which captures two hydrogen atoms, is discussed in theoretical research [83]. There is experimental data which demonstrates nanotube "joining" at high temperatures in an atomic hydrogen atmosphere. In some cases of chemisorption the C–C bonds in tubes breaks [84].

HOMO–LUMO gap behavior for hydrogen chemisorption on a SWCNT

As was mentioned above, chemisorption on a SWCNT strongly affects their energy spectrum. The calculation results confirm that the energy gap can be sufficiently changed by the action of hydrogen chemisorption, which is very important and useful

for practical applications, e.g., in nanoelectronics. The energy gap change under hydrogen chemisorption can be explained by the fact that binding hydrogen to carbon atoms in a carbon network changed their hybridization from sp^2-type to sp^3-type, and leads to π-bond removal near the Fermi level and the "opening" of an energy gap. In Figs. 3.12 and 3.13 the dependencies of the energy gap width on the outer hydrogen coating degree are presented for SWCNTs of *armchair* and *zigzag* types, correspondingly. The data show that for *armchair*-type nanotubes the forbidden zone width is large, increasing with the outer hydrogen coating degree growth, but for *zigzag*-type tubes the dependence has a more complicated character.

The results can be explained in the following way. The energy gap width dependence for the (n, 0)-type tubes strongly depends on their diameter and their ability to dump oscillations. However, chemisorbed hydrogen deforms the form of a SWCNT, naturally changing their cross-sections and the mean diameters. By the action of these tendencies, we notice the obviously non-monotonic behavior seen in the plot, arising from an overlapping of tube "extension" effect with its diameter decrease under hydrogen atom accumulation on the tube walls.

The energy gap dependence on the hydrogen coating degree is also non-monotonic for inner and combined adsorption processes.

Hydrogen chemisorption influence on SWCNT conductance

The HOMO–LUMO gap energy for macromolecules is an analog of the forbidden gap in semiconductors, and therefore the SWCNT conductance must depend on the energy gap width. This fact is very important, because in the text above it was

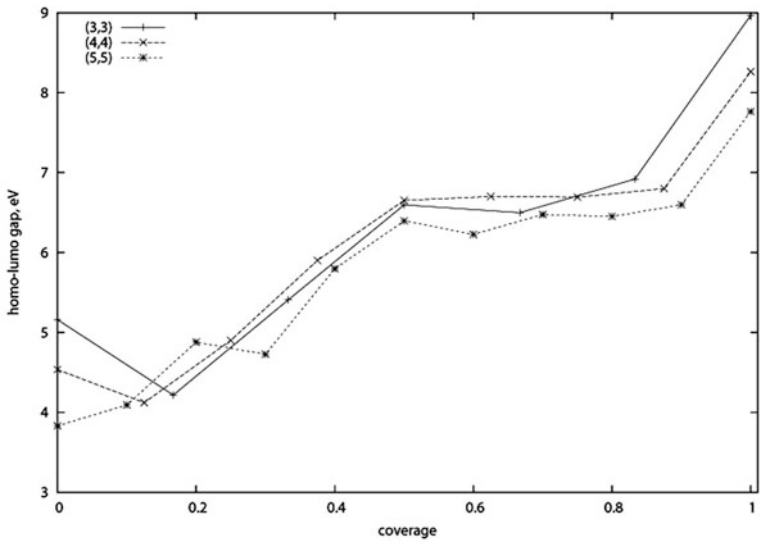

Fig. 3.12 Energy gap width dependence on outer hydrogen coverage degree for SWCNTs of (n, n) type

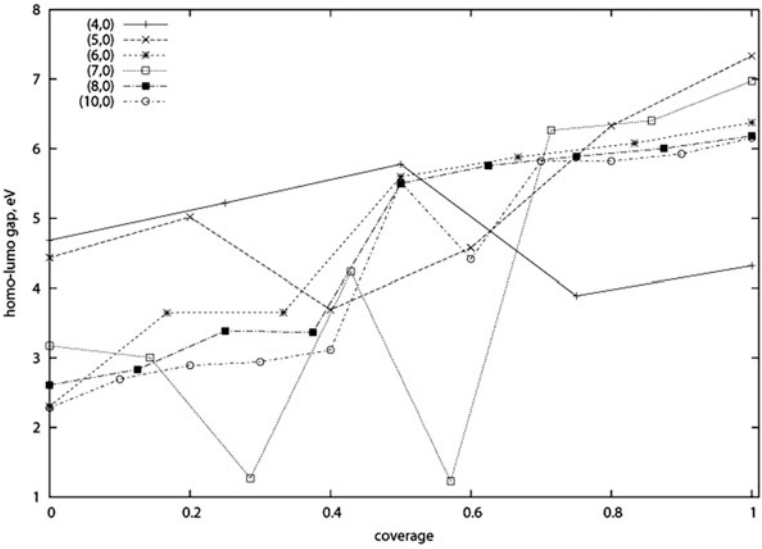

Fig. 3.13 Energy gap width dependence on outer hydrogen coverage degree for SWCNTs of (n, 0) type

shown that atomic hydrogen chemisorption can both increase and decrease the HOMO–LUMO gap width. Let us suppose that the total outer tube coating always increases the gap width, i.e., it practically always leads to a conductance decrease. On the other hand, a little coating can decrease the gap width, i.e., it can lead to an increase of conductance. In addition, conductance, G, dependence on the gap width has an exponential character:

$$G = \frac{2e^2}{h} \int_{-\infty}^{+\infty} T(E)\left(-\frac{\partial f}{\partial E}\right) dE$$

where $T(E)$ is a passage coefficient as a function of energy and $f(E)$ is the Fermi distribution function.

Even a little change in the former function $T(E)$ leads to a sufficient change (increase or decrease) in the conductance, G. For example, with normal conditions the conductance of an (8, 0) tube with two hydrogen atoms (chemisorbed per one elementary cell on the outer surface) is seven times smaller than for a pure (8, 0) nanotube. The same coverage degree (but on the inner surface of the tube) gives a conductance decrease of 3 times. If there are two hydrogen atoms (also chemisorbed per one elementary cell on the outer surface), this time on the outer surface of a (7, 0)-type SWCNT, then the conductance increases 3.7 times. Naturally, the real experimental conditions these figures are sufficiently lower, because they are obtained in the framework of an ideal model with single, straight-lined, and

defect-less SWCNTs. Moreover, we have considered only regular adsorption cases along the nanotube axis. This process is an idealization too. However, nanotube growth and modification methods are constantly developing and improving, and we can hope that in the future the controlled chemisorption on a SWCNT will allow the creation of devices with given parameters for molecular electronics, etc.

3.4 Thermodynamic Evaluations for Limiting Hydrogen Adsorption by SWCNTs

Above it was shown that chemisorption (from a general standpoint) is more preferable than physical adsorption, because of the higher bond energy, which leads to a growth of the accumulated amounts of hydrogen, etc. Therefore, we tried to estimate the maximal sorption ability of the CNT materials. It is known that the distinctive features of chemisorption are covalent or ionic bonding and the formation of the adsorbate re-charging processes [85, 86]. As a result the material's adsorptive possibilities increase, but the adsorption process itself is complicated, because to form a chemical bond the adsorbate must overcome a potential barrier connected with a breaking of chemical bonds necessary for chemisorption. If the adsorbate (as for hydrogen) is in a molecular form it must be transferred into an atomic form. At the same time the adsorbate-confining forces are stronger under chemisorption, and this fact is important for the hydrogen energetics. Therefore, in this chapter we study the thermodynamics and kinetics of hydrogen chemisorption on SWCNT, especially with the aim of defining the limiting values of CNTs adsorptive possibilities, as well as the conditions for its realization.

A model of hydrogen chemisorption

A SWNT by its nature and structure is placed between the graphite and fullerene [3, 87–90]. Because it is formed under a graphite plain convolution it preserves the sp^2 π-hybridization with bond angles being a characteristic 120°. The classical π-bond is formed by overlapping P_z-orbitals. The process of plane convolution involves changing the P_z-orbital energies. However, the same hybridization result means that nanotube surface properties are brought nearer to graphite surface properties. In this connection chemisorption characteristics must be similar. Now, there is a problem of tube energetics characteristics in general, because it depends on both tube diameter and structure (which can be single-wall, multi-wall, or bundled). Therefore, within the CNT materials there are several different places for chemisorption sites (in the nanotube interior, on their surfaces or into pores formed by tube bundles, etc.), and every such place has its own energetic.

Thus, hydrogen chemisorption is an activation process [87, 88] and is accompanied with a rapture of the carbon atom and hydrogen molecule bonds. The process is not connected with a total charge change, because the electrons are not transferred from adsorbant to adsorbent or vice versa [89]. It can be supposed,

that similar processes are proceeding also under hydrogen chemisorption on MWCNT, but these are more complicated because carbon atom arrangements on the different layers are not equivalent each other. For the MWCNT the curvature of the inner (embedded) tube is greater than that of external one, and therefore the bond rapture energy can be changed—something which must be accounted for during calculations.

The authors of experimental studies are often not interested in the adsorption energy values and therefore we can evaluate these values only occasionally, for example, using the data of TGA [68]. The chemical adsorption of atomic hydrogen and the adsorption energetic barrier dependence on the carbon atom network have been studied theoretically in [69]. As limiting cases the following two curvature radius values were considered: $r = \infty$ for graphite and $r = 3.55$ Å for C_{60} fullerene. It was established that for plane graphite the atomic hydrogen energy is not sufficient to overcome the chemisorption energetic barrier, connected with a local sp^2–sp^3 re-hybridization, i.e., the hydrogen chemisorption in this system is impossible, as opposed to single-layer nanotubes where the greater the curved graphite surface, the smaller the barrier. In some work [70], the optimal chemisorption places (sites) along with several atoms (including hydrogen) adsorption energy values were calculated by TGA-method for SWCNTs (8, 0). In this study it was supposed that hydrogen adsorbed on a carbon atom of the carbon network with energy of 2.8 eV. The authors [71] calculated the energy of a single hydrogen atom, chemisorbed on a zigzag SWCNT, with different radiuses. It was found that for (n, 0) tubes an absolute value of the bond energy monotonically decreases with radius growth. For tubes with chirality indices of $n = 7$–12 the adsorption energy was $\sim$2–3 eV. The authors [71], using quantum chemistry modeling methods, also studied a finite length tubes and those closed at the ends (10, 0) with hydrogen atoms chemisorbed on them. Results of this modeling showed that the HOMO–LUMO gap width oscillaties with these chemisorbed hydrogen atom numbers. The obtained gap width values were correspondingly: 0.75 eV for a pure tube; 0.12 eV for one atom; 0.18 eV for two; 0.06 eV for three; and 0.10 eV for twelve atoms. The oscillations were also observed for SWCNT (5, 5). Naturally, these changes in the energy gap change the SWCNT conductance too.

In [73] the results of quantum chemistry modeling are presented for regular (along tube axis) hydrogen chemisorption on chair-form SWCNT (6, 6). The authors found that the adsorption energy for one H atom (per elementary cell) was equal to 1.77 eV for the tube outer surface and 0.49 eV for its inner surface. Because the adsorption energy values are negative chemisorption on the outer surface is energetically more preferable. In addition, for infinite length metallic nanotubes arises a forbidden zone with a width of 5 eV, i.e., the tube becomes a semi-conductive one. For two hydrogen atom chemisorption (per elementary cell) on a SWCNT the authors considered two possible scenarios: 1—the hydrogen atoms being adsorbed on neighboring carbon atoms in neighboring layers; 2—being adsorbed on one layer. In the first variant the authors obtained energy values of 3 and 0.37 eV for outer and inner chemisorption,

correspondingly. In the second variant regular chemisorption does not form any stable conformation and leads to nanotube "unpacking". The authors refer to the experimental results of other researchers who had observed that under high-temperature nanotube annealing, in a hydrogen atmosphere, SWCNTs "join", forming tubes with greater diameters [73]. The same effect was observed under SWCNT electron irradiation at high temperature [74]. Some authors [72] consider cases of the SWCNT inner and outer surfaces being totally coated by chemisorbed hydrogen. For the adsorption energy in this case they obtained 0.84 and 0.30 eV, correspondingly. In all cases there was a charge transport of 0.1–0.33 eV. Thus, we conclude that hydrogen chemisorption on CNTs has a well expressed activation character. Below we will show how, with the use of so-called thermodynamic and kinetic methods, chemisorption energy and kinetic parameters can be defined. For chemisorption process analysis, we will use the Gibbs free energy minimization method, described in Sect. 2.1.

Hydrogen chemisorption in our problem proceeds from a gaseous phase, and for this system the Gibbs free energy can be presented in the form:

$$G = G^g(N_{\mathrm{H}}) + G^S(N_{\mathrm{H}}^{\mathrm{C}}) + G^e, \tag{3.6}$$

where G^g is the hydrogen free energy in gaseous phase; N_{H} is the hydrogen concentration in gaseous phase; G^S is the free energy of a CNT with adsorbed hydrogen; $N_{\mathrm{H}}^{\mathrm{C}}$ is the adsorbed hydrogen concentration; and G^e is the free energy of the charge carrier (electrons and holes)—this component characterizes a part of the free energy connected with atom and molecule re-charging, which accompanies the adsorption process.

Place number conservation law

Hydrogen chemisorption is not connected with a charge transport and therefore we can use only two conservation laws, namely the law of conservation of places and particle numbers. The charge conservation law is unnecessary in this situation.

For the problem under consideration hydrogen atoms can occupy the following two types of place.

First, hydrogen is in gaseous phase, forming hydrogen molecules. The maximal ability of a gaseous phase to retain molecules corresponds to a condensation moment, when the gas becomes a saturated vapor. Therefore, the place concentration in gaseous phase is equal to the molecule concentration the moment the gas transforms into a saturated vapor. This concentration can be calculated through saturated vapor pressure $p_s^{\mathrm{H_2}}$:

$$N^{\mathrm{H_2}} = p_s^{\mathrm{H_2}}/kT. \tag{3.7}$$

Second, relates to the sites where hydrogen can be adsorbed. These are the places on the CNT surface being formed as a result of chemical bonds raptures

between carbon atoms on the graphene plane. In accordance with the conditions of Lagrange's indefinite multiplier method, we can write down the place number conversation law in the form:

$$\varphi^{\mathrm{H}} = N^{\mathrm{H}} - N^{\mathrm{H}_2} - N^{\mathrm{HC}} = 0, \tag{3.8}$$

where N^{H} is the total concentration of places that hydrogen can occupy and N^{HC} is the concentration of places that hydrogen can occupy on the CNT. From an energetic point of view these places can differ from each other, we let $N^{\mathrm{HC}} = \sum_i N_i^{\mathrm{HC}}$, where the i index represents all values corresponding to the various adsorbate positions.

Particle number conservation law

Particle number conservation law can be written down by analogy with the places number conservation law in the form:

$$\phi_{\mathrm{H}} = N_{\mathrm{H}} - N_{\mathrm{H}_2} - N_{\mathrm{H}}^{\mathrm{C}} = 0, \tag{3.9}$$

where N_{H} is the total number of hydrogen atoms. However, because on a CNT the hydrogen atoms can occupy various and non-equivalent positions we let $N_{\mathrm{H}}^{\mathrm{C}} = \sum_i N_{\mathrm{H}i}^{\mathrm{C}}$. The double indices in this formula, as mentioned above, means that the particle (hydrogen atom) is occupying a place on a carbon bond. The meaning of the index i was also considered above.

The calculations were carried out in accordance with a procedure, described in Sect. 1.2. The thermodynamic probability takes the form:

$$W = \prod_i \frac{N_i^{\mathrm{HC}}!}{N_{\mathrm{H}i}^{\mathrm{C}}!(N_i^{\mathrm{HC}} - N_{\mathrm{H}i}^{C})!}. \tag{3.10}$$

The free energy extreme will be found using Lagrange's indefinite multi-player method. The functional for a conditional minimum search has the form:

$$\Phi = G + \sum_i \lambda_{\mathrm{H}i}\varphi_{\mathrm{H}} + \sum_i \lambda_i^{\mathrm{H}}\varphi^{\mathrm{H}}, \tag{3.11}$$

where $\lambda_{\mathrm{H}i}$ are Lagrange's indefinite multi-players, arising from the two above listed conservation laws, namely the particle number and place number, correspondingly. The number of Lagrange indefinite factors is equal to a given number of conservation laws for the system.

Substituting (3.9) and (3.10) into (3.11), we obtain the functional which can be minimized to the expression:

$$\begin{aligned}\Phi = &\sum_i N_{\mathrm{H}i}^{\mathrm{C}} g_{\mathrm{H}i}^{\mathrm{C}} - kT\Bigg\{\sum_i \Big[N_{\mathrm{H}i}^{\mathrm{C}} - N_{\mathrm{H}i}^{\mathrm{C}} \ln\left(N_{\mathrm{H}i}^{\mathrm{C}}\right) - N_{\mathrm{H}i}^{\mathrm{C}} + N_i^{\mathrm{HC}} \\ &- \left(N_i^{\mathrm{HC}} - N_{\mathrm{H}i}^{\mathrm{C}}\right) \ln\left(N_i^{\mathrm{HC}} - N_{\mathrm{H}i}^{\mathrm{C}}\right) + N_i^{\mathrm{HC}} \ln N_i^{\mathrm{HC}} - N_i^{\mathrm{HC}}\Big]\Bigg\} \\ &+ \sum_i \lambda_{\mathrm{H}i}\left(N_{\mathrm{H}} - N_{\mathrm{H}_2} - \sum_i N_{\mathrm{H}i}^{\mathrm{C}}\right) \\ &+ \sum_i \lambda_i^{\mathrm{H}}\left(N^{\mathrm{H}} - N^{\mathrm{H}_2} - \sum_i N_i^{\mathrm{HC}}\right).\end{aligned} \tag{3.12}$$

Under minimization we take the partial derivatives of this functional. However, by differentiation the majority of its additives become zero and we obtain the next system of equations:

$$\frac{\partial \Phi}{\partial N_{\mathrm{H}i}^{\mathrm{C}}} = g_i^{\mathrm{H}} - kT\left[\ln\left(N_i^{\mathrm{HC}} - N_{\mathrm{H}i}^{\mathrm{C}}\right) - \ln N_{\mathrm{H}i}^{\mathrm{C}}\right] - \lambda_{\mathrm{H}i}, \tag{3.13}$$

$$\frac{\partial \Phi}{\partial N_i^{\mathrm{HC}}} = kT\left[\ln\left(N_i^{\mathrm{HC}} - N_{\mathrm{H}i}^{\mathrm{C}}\right) - \ln N_i^{\mathrm{HC}}\right] - \lambda_i^{\mathrm{H}}. \tag{3.14}$$

In equilibrium all derivatives becom zero, and therefore formulas (3.13) and (3.14) become a system of the algebraic equations, the number of which corresponds to the number of the possible and energetically distinct places for hydrogen adsorption on a given CNT. In these formulas we also take into account an interaction between the adsorbed atoms. This is "contained in" the Lagrange factors, and their physical meaning will be explained below. Thus, it follows from (3.14) that factor λ_i^{H} characterizes the number of places filled by the adsorbate.

The free energy derivative in respect to particle number is, by definition, their chemical potential, and therefore $\lambda_{\mathrm{H}i} = \mu_{\mathrm{H}}$ is the hydrogen chemical potential. In the so-called regular approximation the chemical potentials can be expressed in the form:

$$\mu_{\mathrm{H}} = \mu_{\mathrm{H}}^0 + kT \ln a_{\mathrm{H}}, \tag{3.15}$$

where μ_{H}^0 are chemical potentials of the pure component and a_{H} is the hydrogen activity, connected either with its concentration or the pressure in gas phase:

$$a_{\mathrm{H}} = p_{\mathrm{H}_2}/p_s^{\mathrm{H}_2}. \tag{3.16}$$

The final expressions for the adsorbed molecule concentrations have the form:

$$N_{\mathrm{H}i}^{\mathrm{C}} = a_{\mathrm{H}}\left(N_i^{\mathrm{HC}} - N_{\mathrm{H}i}^{\mathrm{C}}\right) \exp\left(-\frac{g_i^{\mathrm{H}} - \mu_{\mathrm{H}}^0}{kT}\right). \tag{3.17}$$

From (3.17) the expression for the isotherm can be obtained, which is an analog of Langmuire's formula:

$$N_{\mathrm{H}i}^{C} = \frac{a_{\mathrm{H}} N_i^{\mathrm{HC}} \exp\left(-\frac{g_i}{kT}\right)}{a_{\mathrm{H}} \exp\left(-\frac{g_i}{kT}\right) + 1} = \frac{K p_{\mathrm{H}_2}}{1 + K p_{\mathrm{H}_2}} N_i^{\mathrm{HC}} \tag{3.18}$$

where $K = \frac{1}{p_s^{\mathrm{H}_2}} \exp\left(-\frac{g_i}{kT}\right)$ is the equilibrium constant; and $g_i = g_i^{\mathrm{H}} - \mu_{\mathrm{H}}^0$ is the partial Gibbs free energy of the hydrogen atom, adsorbed on a place with an index i, that is subtracted from the chemical potential of a pure component.

As opposed to Langmuire's formula, expression (3.18) accounts for adsorption on various places, differing in their adsorption partial energies.

Formulas (3.16)–(3.18) allow us to take into account the concentration of hydrogen atoms adsorbed on various places. For calculations it is necessary to know only the values of the corresponding partial free energy. For chemisorption this value can be sufficiently high and its determination can require high-temperature experiments. The results of such experiments are absent, and therefore we will demonstrate in the next section how this value can be defined using kinetics data for hydrogen desorption.

3.5 Hydrogen Desorption Kinetics (TGA)

As was mentioned above, the data for atom desorption from a carbon atom allows us to calculate kinetic coefficients, defining the parameters of molecule capture and release by CNTs. In the present section these procedures will be used for analysis of the hydrogen chemisorption process.

An experiment on gas desorption (TGA) was carried out at high vacuum conditions under continuous pumping out [91], and therefore the adsorbed gas pressure (the molecule concentration) tended to zero. In this case it is not necessary to take into account an inverse capture of desorbed molecules. Hydrogen desorption is observed under sufficiently high temperatures. In this case the electrons and hole concentrations are sufficiently high and near to characteristic values, and therefore it can be supposed that for every adsorption act an equilibrium regarding the electron–hole subsystem is established over time. The adsorption equation in accordance with [3] takes the form:

$$\frac{\mathrm{d}N_{\mathrm{H}i}^{\mathrm{C}}}{\mathrm{d}t} = -\nu_{\mathrm{H}i}^{\mathrm{C}} N_{\mathrm{H}i}^{\mathrm{C}} \exp\left(-\frac{g_i}{kT}\right). \tag{3.19}$$

Desorption from each place can be considered independently, and therefore in (3.19) it is sufficient to study the desorption process from one type of place.

The measuring of nanotube desorption rates, as a rule, happens after they are annealed at high vacuum pressures and temperatures of about 1,000–1,200 °C over

several hours to remove from them samples of amorphous carbon, low-molecular complexes, and undesirable adsorbents. After annealing the temperature is decreasing and the nanotubes are saturated with the adsorbent at a given temperature and at least the cryostat with the sample is cooling to helium temperatures. After equilibrium is achieved, the sample's temperature is linearly increased with time: $T = T_0 + \beta t$, where T_0 is the starting temperature of heating (as a rule, this point is selected long before the desorption process). Under this heating process, the desorbed substance amount is fixed in one or another way, and so the thermo-stimulated desorption of a given substance from the nanotube is recorded. For a description of the process it is necessary in formula (3.19) to pass the argument t (time) to T (temperature). Substituting the variable, we obtain the differential equation:

$$\frac{dN_{Hi}^{C}}{N_{Hi}^{C}} = -\frac{\nu_{Hi}^{C}}{\beta}\exp\left(-\frac{g_i}{kT}\right)dT, \tag{3.20}$$

where β is the sample heating rate.

The solution has the form:

$$N_{Hi}^{C} = N_{Hi0}^{C}\exp\left[-\frac{\nu_{Hi}^{C}T}{\beta}E_2\left(\frac{g_i}{kT}\right)\right], \tag{3.21}$$

where $E_2\left(\frac{g_i}{kT}\right)$ is an integral exponential function of second order.

Equation (3.21) allows us to find the next two kinetic coefficients (g_i is the molecule bond energy and ν_{Hi}^{C} is a desorption probability) by comparison of the analytical expression with experimental results. However, in actual practice it is more convenient to use the derivative in respect of the temperature from the desorbed gas concentration, which for a unique process presents a curve with a maximum, and for a process superposition—a curve with several maximums (their number is equal to the number of independent desorption processes). The derivative for several process superpositions has the form:

$$\sum_{i=1}^{m}\frac{dN_{Hi}^{C}}{dT} = -\sum_{i=1}^{m}\frac{\nu_{Hi}^{C}N_{Hi0}^{C}}{\beta}\exp\left(-\frac{g_i}{kT}\right)\exp\left[-\frac{\nu_{Hi}^{C}T}{\beta}E_2\left(\frac{g_i}{kT}\right)\right]. \tag{3.22}$$

It is easily seen, that when the molecule desorption probability value becomes comparable with the observation time, the derivative achieves its maximum. At the maximum temperature a desorption probability (with a systematic error of order k^2T^2/g_i^2) is equal to:

$$\nu_{Hi}^{C} = \frac{\beta g_i}{kT_{mi}^2}\exp\left(\frac{g_i}{kT_{mi}}\right). \tag{3.23}$$

Substituting (3.23) into (3.22) and using the exponential function approximation, we obtain for the DTGA:

$$dN = \sum_{i=1}^{m} \frac{g_i}{kT_{mi}} N_{\mathrm{Hi}}^{\mathrm{C}} Z \exp\left[-\frac{T^2}{T_{mi}^2}\left(1 - \frac{2g_i}{kT_{mi}}\right)Z\right], \tag{3.24}$$

where

$$Z = \exp\left[\frac{g_i}{k}\left(\frac{1}{T_{mi}} - \frac{1}{T}\right)\right].$$

We conducted our experiments measuring the TGA as explained in Sect. 3.2. A hydrogen adsorption was studied both just after CNT synthesis and after vacuum annealing at a temperature of 2,000 °C for 6 h followed by a slow cooling.

At first glance the DTGA process is running only from one place, but modeling with formula (3.24) showed that the process was not described only by Gibbs partial energy, because it had a more complex character. Formula (3.24) usage allowed us to divide the desorption process into its components, as shown in Fig. 3.14a, b. The results demonstrate that annealing changes DTGA process intensity, connected with a change in place concentration, from which annealing proceeds. The calculation results are presented in Table 3.1.

The results of Table 3.1 show that the bound energy per hydrogen atom is 2.6 eV.

Annealing leads to a sufficient decrease in hydrogen concentration, desorbed on places of type 1 and 2, that allows us to suppose that these places do not belong to

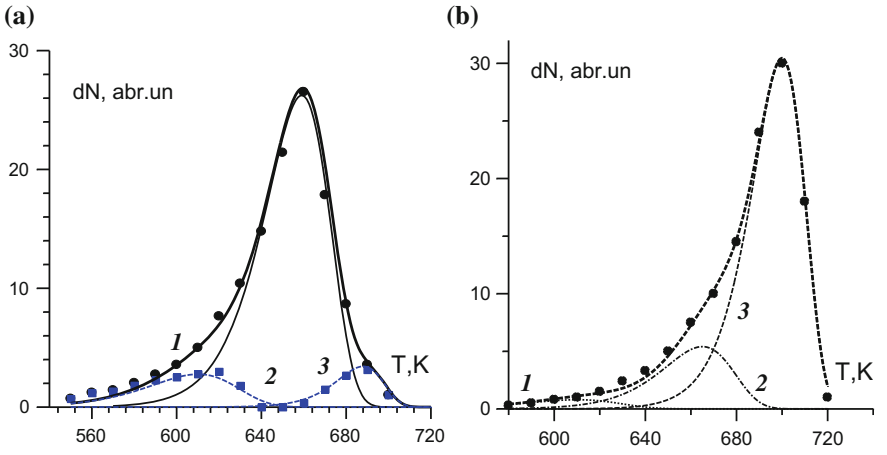

Fig. 3.14 The DTGA spectrum division of components in accordance with formula (2.86) (points correspond to experimental results): **a** immediately after the synthesis and **b** after annealing at a temperature of 2,000 °C over 6 h. The desorption process energies equal: *1* 1.5 eV; *2* 2.4 eV; *3* 3.6 eV

Table 3.1 Comparison of the desorption process intensities in SWCNTs before and after annealing

№	g_i (eV)	Desorbed hydrogen amount before annealing (%)	Desorbed hydrogen amount after annealing (%)
1	1.5	11	3
2	2.4	77	17
3	3.6	13	80

the CNT itself, but are connected with some residual synthesis products (e.g., to amorphous carbon or fullerenes, also being formed under the CNT synthesis).

Type-3 places, stipulated by adsorption on a SWCNT, have a very high chemisorption energy, arising for corresponding chemical bond rapture conditions. This makes it consistence with the model described above.

The above described chemisorption model demonstrates that on one elementary cell of a graphene latice can be adsorbed at most one hydrogen atom, and thus the adsorption place number is equal to the elementary cell number on the graphene plane, from which the CNT is formed. Since carbon has an atomic weight of 12 and receives two hydrogen atoms per one elementary cell, the weight ratio of the adsorbed hydrogen can achieve 4 wt%. This corresponds to literature data (given in Sect. 3.1) and is in accordance with the calculation results of [27]. However, this value can be achieved only at high temperatures (which are necessary to shorten an adsorption time) and sufficiently high pressures.

3.6 Experimental Studies of Hydrogen Adsorption on SWCNTs

It was reported in [86] that SWCNT adsorptive capacitance can be raised to 4.2 wt% (at room temperature and pressure of 10–12 MPa) and 8.25 wt% at cryogenic temperature and pressure of 7.18 MPa). Moreover, it is considered that the crucial factor for for hydrogen adsorption growth is an inter-planar distance into the nanotubes that equals 0.34 nm, a distance which is characteristic of a turbostrated carbon. In this case, nanotubes can retain hydrogen even at room temperature and their curved surface increases the molecule binding energy with a graphite surface. Moreover, during the single-wall fabrication there arises some “sheafs” or bundles, representing the close-packed triangular lattices from parallel arranged cylinders, the distance between which equals 3.4 Å. This value almost exactly corresponds to a distance between the neighboring layers in graphite. Such triangular nanotube packaging increases the total system accumulation capacitance at the expense of the voids arising in the system. The geometrical packing of the hydrogen molecules into the SWCNTs assures an accumulation at a level of 3.3 wt%. The void volumes increase this by 0.7 wt%, increasing the total accumulation value to 4 wt%.

It was noted in publications [92–96] that hydrogen desorption energy from carbon materials is ~20–40 kJ/mol. This is higher than the energy required for the

breaking of van der Waals forces, that are characteristic of physical adsorption, but are one order lower than the energy of the C–H bond rupture, which is characteristic of chemisorption.

There are various values of bond energy arising for various variants of hydrogen atom arrangements in the tube. This fact undoubtedly impedes calculations, and therefore the calculated bond energy value of 0.1 eV [81, 83] is an overstated one.

Adsorption is proceeding from a rarefied gas, which can be considered as an ideal one, and in this case we have $c_{\alpha 0}^{\beta} = 4.4 \times 10^{-15}$ cm^3 s^{-1}, i.e., ference with data on adsorption probability are apparently connected with the repulsion barriers present for physical adsorption. Formula (2.21) allows us to estimate these barrier values for different adsorption places. The results of calculations allow us to consider that hydrogen is added to the reaction of a CNT, overcoming the potential barrier.

Thus, we have succeeded to separate the desorption processes from three different places and for the first time been able to define desorption probability. The results of kinetic experiments are very consistent with thermodynamic calculations using the adsorption isotherm.

As was shown above, from the hydrogen storage point of view the problems of chemisorption on CNTs are very important. The energy of C–H chemical bond formation (a hydrogen atom with a carbon atom in a graphene layer) equals 243 kJ/mol [92], and is sufficiently high to retain hydrogen at room temperatures. The higher the value of the sorption energy, the more apparent becomes diffusion and a hydrogen interaction with the carbon material for hydrogen dissociation chemisorption on the boundary carbon atom positions in the "chair"-type and "zigzag"-type structures. In this case the C–H bond formation energy is 364 kJ/mol and the hydrogen molecule adsorption energy is 140 kJ/mol [92].

Considering the energy values in the previously described process they are near to the so-called dissociative–associative hydrogen chemisorption (from molecular H_2 gas) on superficial regions of graphite and carbon nanostructures (SWNT, MWNT). Chemisorption is due to two hydrogen atoms interacting with a carbon atom (2H=C) into a "chair" type or with two carbon atoms 2(H–C), arranged at alternating positions in a graphene layer. This process is characterized by a standard adsorption energy of one mole of hydrogen molecules being 20 kJ/mol, and the energy of the chemical bond formation for two hydrogen atoms with one carbon atom (2H=C) or two carbon atoms in the adsorbent surface layer, being 460 kJ/mol.

Table 3.2 The energies of outer hydrogen chemisorption (E_{ads}) and HOMO–LUMO gap width (E_g) for SWCNT (6, 0) with one or two SW defects

	(6,0) + 1 SW		(6,0) + 2 SW		(6,0)	
	E_{ads} (eV)	E_g (eV)	E_{ads} (eV)	E_g (eV)	E_{ads} (eV)	E_g (eV)
Pure SWCNT*		2.83		3.09		2.30
8 H	−2.31	3.00	−2.30	3.22	−2.81	3.64
16 H	−2.47	3.35	−2.42	3.24	−3.07	3.65

Note * represents a pure graphene surface without adsorbed hydrogen atoms

Under chemisorption, the chemical bond energy is usually rather great [27]. For SWCNT within the range 2.5–4 eV is observed a peak [27] connected with hydrogen chemisorption. The theoretical calculations confirm these energy values.

In a survey [93] the results obtained by various authors are summarized. It is shown that the bond energies under physical adsorption change from 0.05 to 0.08 eV, but under chemical adsorption lay from 1.5 to 2.4 eV. Undoubtedly, the results are only approximated, because in the overwhelming number of experiments the parameter calculation algorithms do not take into account the very complex adsorption processes and do not define separately adsorption from various types of places. To increase hydrogen storage capacitance some electrochemical methods were also used [97]. The most effective proved to be so-called oxidative annealing, that was carried out in a system with oxygen pressure at 1 mbar and temperature at 700 °C for 30 min.

Hydrogen adsorption in SWCNT bundles was studied [98], where the calculation simplification for the adsorption was considered for another limiting case, namely for a thin SWCNT bundle, fabricated from several densely packed (9, 9) nanotubes.

In this situation, the distance from hydrogen atom to SWCNT bundle could be changed over a wide range in accordance with their hydrogen interaction with the carbon atoms on the curved surfaces. The calculated molecular dynamic trajectories show that hydrogen molecules are rapidly diffusing around the bundle outward parts. Unlike the molecules on the inner centers, that are completely restricted in their motion, the molecules on external centers are able to move very far from the bundle. The highest hydrogen density values were observed at hydrogen intermolecular distances of about 2.7 Å for 1.51 and 6.5 wt% loading. At the highest loading there was a supplementary peak at about 5.4 Å, reflecting the laminated structure of inner adsorption [98]. We made the following conclusions:

- Hydrogen distribution into different nanotube bundles depends on the nanotube diameter and its filling. For low filling densities we have the tendency for hydrogen to be adsorbed on tube outer surfaces, but with a filling degree increase hydrogen accumulates on the inner surfaces. The greater the nanotube diameter, the higher is the relative completion of the inner centers. However, the hydrogen content ratio on the inner centers never exceeds 50% of the total adsorbed hydrogen for tubes with diameters up to 12 Å.
- Hydrogen adsorption energy increases with a nanotube diameter decrease. It was found that an essential extension of the SWCNT lattice proceeds under hydrogen adsorption with a loading of about 6.5 wt%. The high adsorbed hydrogen densities the adsorption energies decreases due a repulsion between the molecules.
- The diffusion coefficients for hydrogen into CNTs are sufficiently higher than in the microporous materials. This onece again demonstrates the excellent transport properties into nanotubes.
- The mean adsorption energy and an effective adsorption capacitance strongly depend on the hydrogen molecule distance from a SWCNT surface.

- Packing defects, arising with nanotube non-uniformity create significant channels between bundles of nanotubes, which play an important role under adsorption from a gaseous phase.
- The quantum mechanical calculations and experiments showed that zigzag-type nanotubes are less stable than armchair-type. The zigzag-type tubes are destroyed when more than two hydrogen atoms are adsorbed into a single cell of a graphene lattice.
- The adsorption energy of *zigzag*–type tubes is less stable than *armchair*-type tubes and therefore hydrogen adsorption in the former type must be stronger than in the latter.

The role of defects in hydrogen adsorption by carbon nanotubes

It was mentioned above that CNT structure defects could play a role in the adsorption process [30]. The defects, forming in the system under a hydrogen treatment were considered, namely the hydrogen adsorption centers and atomic vacancies. The common feature of the both these defects is a rebuilding of the long-range order of the state's local density, that is characterized by a superstructure with period of 5 nm order, and is connected with an electron states scattering on the point defects, that leads to an arising of steady electronic waves near the defect. In present work the hydrogen bond energies are calculated for different variants of hydrogen molecule arrangement with respect to CNTs both with and without defects.

Interesting theoretical results have been obtained in [74, 75]. In the former, was considered the atomic hydrogen chemisorption on graphite with Stone-Walles defects, and it was found, that hydrogen atom is preferably chemisorbed on the one of carbon atoms with a «turned» bond. Moreover, the formed conformation is stable and its adsorption energy equals 2.49 eV. The work [75] is devoted to the hydrogen molecular adsorption on SWNT with Stone–Wales defects. It was shown that adsorption on a tube with one Stone–Wales defect is more stable than one on an ideal tube, but at the same time adsorption on a tube with two symmetrical defects is not stable. It is worth noting that the first Stone–Wales defect introduced into a tube increases the HOMO–LUMO gap width, but the second symmetrical defect introduced decreases this width, but not to its original value. The hydrogen adsorption on an ideal SWCNT increased the HOMO–LUMO gap width at 0.19 eV, but adsorption on a tube with one defect does not change this gap.

In a theoretical study [82, 88] some fluorine chemisorption was modeled. In spite of the fact that the work was not devoted to hydrogen, the obtained results are very important for chemisorption of any substance, because they demonstrate the role of deformation. The authors showed that such regular chemisorption leads to an appearance of SWCNT prismatic modifications, when the tube cross-section obtains triangular or quadrangular forms. In this case, the atoms re-hybridization is regular and the SWCNT deformation can secure the most profitable conditions for conjugated subsystem formation on the tube's curved surface. In particular, they

established that: (1) the prismatic modifications of zigzag-type SWCNT lead to a energetic gap width increase and (2) in the energetic gap of the zigzag-type SWCNT (n, 0), under regular chemisorption, there can appear some additional discrete energy levels, and for n divisible by 3 these levels are located near zone edges, but in other cases they are placed near the energetic gap center. It must be noted, that peculiarities (1) and (2) are not observed for chair-type SWCNT.

In one piece of work [93] the chemical adsorption of atomic hydrogen or hydrogen ions was considered, as well as the adsorption energetic barrier dependence on carbon lattice curvature and the lattice local defects. As was said above, electronic envelope sp^2-hybridization takes place in graphite. The σ-bonds lying in the plane are responsible for a strong covalent connection between atoms, but the normally placed π-bonds are responsible for a weak interaction between the carbon layers in graphite. In this work is also shown that chemical hydrogen binding with an sp^2-bonded carbon network demands a local re-hybridization from sp^2 to sp^3 and therefore has a rather greater adsorption energetic barrier for the strictly planar sp^2 carbon network. The authors studied a hydrogen interaction with the sp^2 carbon as a function of the graphite network local curvature. The adsorption experiments on the graphite (0001), SWCNT, and multilayer C_{60} films cover a range of the carbon network local curvature radius values from $r = \infty$ (for graphite) to $r = 3.55$ Å (for C_{60}). It was found that the atomic hydrogen energy is not sufficient to overcome the hydrogen chemisorption energetic barriers on a graphite surface, but that situation changes after the carbon (0001) surface treatment by H_2 plasma. The doses $\sim 10^{14}$ ions/cm^2 induced modifications in the electronic structure and spectral analysis detected an increase in the π- and σ-state intensity ratios with an increase in plasma treatment duration.

The treatment by atomic hydrogen induces the changes in the SWCNT valence zone, appearing as an intensity shortening at pure π-bonds with bond energies of 2.5 eV. This means a change of the delocalized π-bonds on the C–H edge states with a σ-bond, having the bond energy ~ 10 eV. This can be achieved by atomic hydrogen treatment. A further increase of hydrogen adsorption can be achieved by the above mentioned H_2-plasma treatment.

Thus, an important parameter, changing the adsorption energetic barrier in the considered carbon structures, is local curvature at the sp^2 carbon network. An introduction of curvature can be considered as a partial tetra-hybridization at the local binding configuration, leading to an admixture, having sp^3. This decreases the adsorption energy barrier of hydrogen chemisorption, demanding a local re-hybridization (from sp^2 and sp^3). The decreased energetic barrier for the strongly curved structures is proof that atomic hydrogen can be adsorbed on C_{60} and SWCNT, but not on graphite.

The adsorption energetic barrier depends on, besides curvature, the hydrogen coating degree (i.e., on the adsorption process prehistory). It is proof that a coating degree, which can be achieved on SWCNT and C_{60} by atomic hydrogen, is limited, and further hydrogen adsorption in these systems can be realized by an affect of more highly energetic hydrogen species, namely hydrogen plasma. The authors of [98] reported on a quantum mechanical modeling where so-called ab initio methods (density functional theory) were used for the description of hydrogen adsorption on

SWCNT. It was noted that hydrogen adsorption energy on an *armchair*-type (9, 9) SWCNT lattice at different temperatures, with a hydrogen loading of 0.4 wt%, is sufficiently higher than on graphite and graphite intercalated mixtures. An attraction force, applied to the molecular hydrogen from the outer part of the curved carbon surface, explained this fact. The modeling results also showed that hydrogen adsorption on a SWCNT is a dynamic process with very high hydrogen mobility into a lattice and a marked deformation of the SWCNT structure at moderate temperatures.

The SWCNT lattice is deformed under adsorption and also the most noted lattice expansion was observed for nanotubes with small radiuses, because in these tubes the volume suitable for a hydrogen adsorption (both into the tubes and into the inter-tubular bundle channels) is very small and the lattice is expanded for hydrogen molecule "building-in" the system.

3.7 Modeling of a Nanotube with Stone–Wales Defects

It was noted in several publications that with the presence of structural defects in a SWCNT the admixture atoms are more easily adsorbed, namely on places with defects. In this section is considered one of the most important SWCNT defects, the so-called Stone–Wales (SW) defect, connected with a reversal of the chemical bond, where into a SWCNT arised two pentagons and two heptagons. For this study, two (6,0) and (8,0) tubes with lengths of 5 elementary cycles were selected. For the pure optimized SWCNT the length of the HOMO–LUMO gap width was defined equal to 2.3 and 2.6 eV, correspondingly. For every tube the following two situations were modeled: a one SW defect and two SW defects, located in a diametrically symmetric manner, as is shown in Fig. 3.15.

The calculations showed that for (6, 0) SWCNT + 1 SW defect the forbidden zone width is 2.8 eV, but for (6, 0) SWNT +2 SW defects—3.1 eV, i.e., the defects increase the forbidden zone width. For (8, 0) SWCNT + 1 SW defect the forbidden zone width is 2.64 eV, but for (8, 0) SWCNT + 2 SW defects—2.57 eV, i.e., one defect increased the forbidden zone width a little, but two symmetric defects practically do not change the width value.

In order to study hydrogen chemisorption on such defected nanotubes, we modeled a "regular" nanotube coating by hydrogen atoms along its axis in two situations: one pair of hydrogen atoms per one elementary cell and two pairs on the cell. The edge cells remained out of consideration. The calculations showed that for all possible coating variants (under the same coating value) the most preferable ones turn out to be the variants presented in Fig. 3.16.

The calculation results for the outer chemisorption of 8 and 16 hydrogen atoms on the tubes with chiral vector (6, 0) and defects are given in Table 3.2.

The results show that hydrogen chemisorption on the outer surface of a (6, 0) nanotube increases the HOMO–LUMO gap width, i.e., is decreasing the system conductivity as compared with a pure tube with the same defects. The next relations are valid for the considered systems:

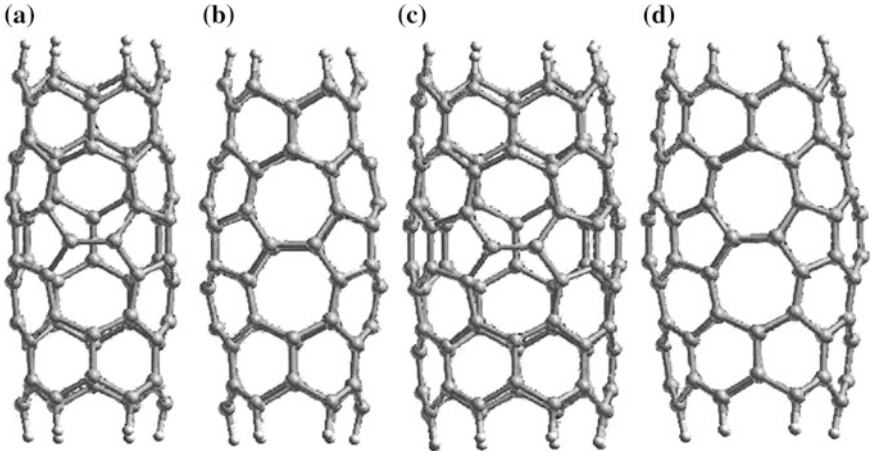

Fig. 3.15 Nanotubes with defects: **a** (6, 0) tube with one SW defect; **b** (6, 0) tube with two SW defects; **c** (8, 0) tube with one SW defect; and **d** (8, 0) tube with two SW defects

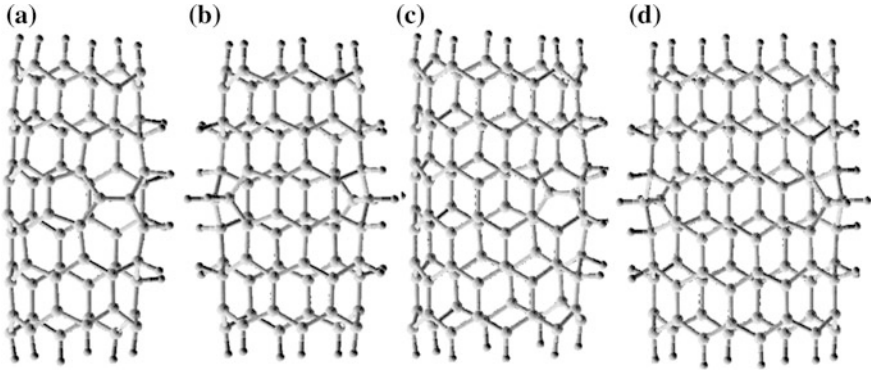

Fig. 3.16 Nanotube type from *left* to *right*: **a** (6, 0) tube with one SW defect and 8 atoms; **b** (6, 0) tube with two SW defects and 16 atoms; **c** (8, 0) tube with one SW defect and 8 atoms; and **d** (8, 0) tube with two SW defects and 16 atoms

- for a pure SWCNT: $E_g[(6,0)] < E_g[(6,0)+1SW] < E_g[(6,0)+2SW]$,
- for a SWCNT with 8 hydrogen atoms: $E_g[(6,0)+1SW] < E_g[(6,0)+2SW] < E_g[(6,0)]$,
- for a SWCNT with 16 hydrogen atoms: $E_g[(6,0)+2SW] < E_g[(6,0)+1SW] < E_g[(6,0)]$.

A SWCNT (6, 0) without adsorbed hydrogen atoms (i.e., a pure graphene surface) has a more narrow energy gap (and a bigger conductivity) than a SWCNT with defects. Hydrogen chemisorption is a changing situation: a tube without defects has a bigger energy gap (and a smaller conductivity), than defected tubes

with the same amount of adsorbed hydrogen atoms. The adsorption energy on the defected SWCNT (6, 0) decreases with coating value growth, but in all cases it remains bigger than the adsorption energy on a pure SWCNT (6, 0).

Thus, a Stone–Wales defect presence influenced the hydrogen chemisorption processes. The adsorption energy and HOMO–LUMO gap width for "regular" hydrogen chemisorption change qualitatively (as compared with defect-less tubes), but the general tendencies remain the same: the energy gap width is increasing, but the conductivity and adsorption energy are decreasing (with regard to sign) with outer hydrogen coating value growth.

The presence of a Stone–Wales defect affects the hydrogen chemisorption process. The chemisorption of hydrogen changes the adsorption energy and energetic gap as compared with the a SWC NT without defects, but overall tendencies remain the same: the energetic gap width increases, but the conductance and adsorption energy (with account the sign) decrease with growth in the external coating degree.

A stable hydrogen coating at room temperature can be created by chemisorption, which can be carried out under high temperatures and pressures. This indicates that there exists a repulsion barrier for carbon atom chemisorption on CNTs.

3.8 The Problem of Hydrogen Storage

Investigations of the hydrogen adsorption and storage on the CNTs is mainly devoted to the perspectives of CNT usage as "containers" for hydrogen storage [2, 99–103]. At present, there are some different technologies for hydrogen storage and usage (e.g., hydrogen storage in compressed forms, hydrogen transformation into metal hydrides, hydrogen adsorption on the surfaces of various carbon structures, etc.). All these technologies have their own disadvantages, e.g., the activated carbon has not a sufficient weight capacitance for gas storage; the technologies connected with the metal hydrides, are complex, etc. Cryogenic technologies in general are of limited utility due to the very low temperatures needed to store the gas (about 21 K), etc.

Compressed hydrogen is stored under pressures up to 2.5×10^4 Pa. Such storage requires the development of new types of storage tank made from expensive and light composite materials. The hydrogen volumetric density (the stored hydrogen weight per unit system volume) remains very low even at the above-mentioned pressures. Moreover, this high-pressure storage method is not profitable economically due to the high cost of the pressure equipment and some safety problems.

Another possibility is hydrogen transfer into a bound state in some inter-metallic compounds of forms of metal hydrides. The hydrogen charge/discharge is carried out simply by system compression/rarefaction. The technology is a very simple one, but it provided only a low capacitance. The hydrogen weight density in hydrides reaches only 1–1.5% in the best case. The compressed hydrogen demonstrates both a higher weight density (approximated to 20%) and volume density (50 kg H_2/m^3), but this

technology required expensive cryogenic cooling (21 K) with special equipment and great energy consumption. Moreover, this system has a very short service time (maximum two days without leakage).

Adsorption on carbon structures is considered to have great potential for hydrogen storage but (for the structures limited surface area and a high mass density) these carbon-adsorptive technologies have not progressed sufficiently. The weight capacitance of activated carbon does not exceed 2 wt% under pressures up to 1.4×10^4 Pa and room temperatures. In addition, it does not exceed 4.5 wt% under pressures up to 5.5×10^3 Pa and temperatures of 160 K [2]. The comparison of adsorptive capacitance of the various carbon-based materials (including CNT) demonstrated that CNTs are not the leading material in respect of their capacitance ability, but they do have other advantages.

Hydrogen storage in nanotubes provides many preferences. The method seems to be safe and economically profitable, because it does not demand the high pressures for gas compression and there is no giant disproportion between the gas and accumulative storage masses. The main difficulty is to obtain sufficiently high hydrogen content in the tubes. At present it is commonly supposed, that for the main industrial applications the hydrogen content level in SWCNT must be 6–7 wt%.

The important characteristics of hydrogen storage are the weight of hydrogen, which can hold 1 cm^3 storage, and gas retention time for certain temperatures. We will evaluate these options.

Chemisorption is one technique for hydrogen storage into carbon nanotubes. The calculations showed that for nanotubes under consideration (in spite of their chirality and diameter) at every coverage degree of outer adsorption there is a stable configuration, i.e., the tubes can be covered totally (by one layer) by hydrogen atoms—the accumulation capacitance in this case is about 8.3 wt% (this value exceeds the minimal limit established for industrial applications which equals 6–7 wt%). Total hydrogen coating is possible for a mixed chemisorption type, when hydrogen atoms are adsorbed on both inner and outer nanotube surfaces. At inner chemisorption the hydrogen accumulation is possible only for nanotubes with larger diameters than that of SWNT (4, 4), which equals 5.43 Å. In this case the weight percentage of hydrogen accumulation for a (4, 4) tube is 3.1 wt%, for a (7, 0) tube—3.6 wt%, for (8, 0) and (10, 0) tubes—4.2 wt%. The calculated values of bond energies for adsorbed hydrogen atoms with nanotubes for chemisorption are sufficiently bigger than the corresponding energies of hydrogen physical adsorption. Thus, although hydrogen accumulation by chemisorption in nanotube samples presented a barely realized process, it has some advantages over physical adsorption methods: high values of weight content and the possibilities of storage without leakage for long periods of time at normal environmental temperature.

The density of MWCNTs is 0.5–1.0 g/cm^{-3}; 1 cm^3 of storage can hold of 0.04 g of hydrogen on average. The same amount of hydrogen has 0.02 mol and takes of 0.45 l under normal conditions.

Thus, many experimental facts and quantum mechanical calculations made SWCNTs a prospective material for hydrogen storage at standard temperatures. It was found that hydrogen amounts increase with reducing tube diameters, something which can also be used to increase the partial content of the adsorbed substance. A substantial expansion of a SWCNT lattice is found to give a hydrogen adsorption loading of about 6.5 wt%, and the high adsorbed hydrogen densities reinforce the intermolecular repulsion and decreasing adsorption energies. Some other effects are worthy of mention:

- the hydrogen diffusion coefficients in SCNT are noticeably greater than these coefficients for many microporous materials, that confirms the excellent properties of the transport processes into the tubes;
- the mean adsorption energy and an effective adsorption capacity depend critically on the hydrogen molecule distance from the SWCNT surface; and
- the package defects, connected with nanotube non-uniformity, can create noticeable inter-tubular channels, that play an important role under adsorption from gaseous phase.

An important role for hydrogen storage sits with chemisorption (from initial state of molecular gas H_2) on the defect regions on graphite or other carbon nanostructures, including graphite nanofibers, deformed SWCNTs, and defective MWCNT samples. The process is characterized by a standard adsorption energy for one mole of hydrogen molecules—120 kJ/mol [63] (molar energy of the (2H=C) chemical bond formation for two hydrogen atoms with one carbon atom at an edge, "zigzag"-type position—570 kJ/mol).

To assure this high energy value CNT filling by hydrogen must proceed at high temperatures, because the characteristic time constant of the filling process decreases with a rise in real process temperature via the formula:

$$\tau^{-1} = \nu_{\mathrm{H}i}^{\mathrm{C}} \exp\left(-\frac{g_i}{kT}\right). \tag{3.25}$$

From another point of view, at low temperatures a bigger hydrogen amount can be retained. To estimate this amount, let us write down the expression of hydrogen capture kinetics not in a vacuum (as for desorption), but under an excessive hydrogen pressure in the form:

$$\frac{\mathrm{d}N_{\mathrm{H}i}^{\mathrm{C}}}{\mathrm{d}t} = -\nu_{\mathrm{H}i}^{\mathrm{C}} N_{\mathrm{H}i}^{\mathrm{C}} \exp\left(-\frac{g_i}{kT}\right) + c_{\mathrm{H}i}^{\mathrm{C}} N_{\mathrm{H}_2} N_i^{\mathrm{CH}}, \tag{3.26}$$

where $c_{\mathrm{H}i}^{\mathrm{C}}$ is a coefficient of hydrogen capture on a CNT. In accordance with the results of [97, 98] we have $c_{\mathrm{H}i}^{\mathrm{C}} = \nu_{\mathrm{H}i}^{\mathrm{C}}/N_i^{\mathrm{CH}}$.

In equilibrium, setting equal the expression (3.26) to zero, we obtain the formula for the maximal concentration of adsorbed hydrogen:

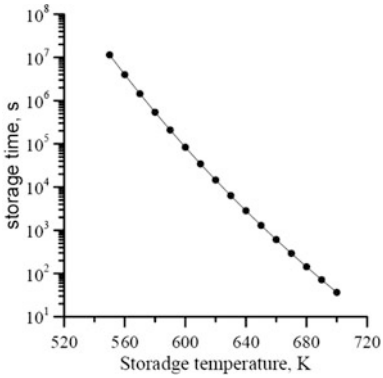

Fig. 3.17 Storage time for a certain temperature

$$N_{\mathrm{H}i}^{\mathrm{C}} = \frac{N_{\mathrm{H}_2} N_i^{\mathrm{CH}}}{N_i^{\mathrm{CH}} \exp\left(-\frac{g_i}{kT}\right) + N_{\mathrm{H}_2}} = \frac{p_{\mathrm{H}_2} N_i^{\mathrm{CH}}}{kTN_i^{\mathrm{CH}} \exp\left(-\frac{g_i}{kT}\right) + p_{\mathrm{H}_2}}. \tag{3.27}$$

Analysis of formula (3.27) shows that at sufficiently high pressure the adsorbed hydrogen concentration achieved the value of adsorption place concentration.

Formula (3.26) allows us to estimate the storage time at certain temperatures. The calculation results are shown in Fig. 3.17

Figure 3.17 shows that at room temperature hydrogen can be stored for a long time without loss. Therefore, such storage is not dangerous. Storage must be heated to remove hydrogen

3.9 Conclusion

Results from this chapter reveal the reasons for changing the electronic properties of CNTs. They are dependent on changing the size, doping, physical, and chemical adsorption. These factors make it possible to control the properties of nanotubes.

We also showed that chemisorption is a good mechanism for hydrogen storage. At room temperature storage is not dangerous, while heating allows the extraction of hydrogen.

References

1. T.K. Ghosh, M.A. Prelas, Energy Resources and Systems: Volume 2: Renewable Resources (Springer, Berlin, 2011), pp. 495—628
2. L.L. Vasiliev, L.E. Kanonchik, G. Kulakov, D.A. Mishkinis, Activated carbon and hydrogen adsorption storage. Hydrogen Mater. Sci. Chem. Carbon Nanomaterials, 633–651 (2007)
3. S.V. Bulyarskiy, Uglerodnye nanotrubky: techologya, upravlenie svoystvami, primenenie. Ulyanovsk, Streshen (2011), 479s. (Rus.)

4. V.A. Eletskiy, Sorption properties of carbon nanostructures. Adv. Phys. Sci. **174**(11), 1191–1231 (2004)
5. A.C. Dillon, K.M. Jonse, T.A. Bekkedhai, C.H. Kiang, Storage of hydrogen in single-walled carbon nanotubes. Nature **386**, 377–379 (1997)
6. K.K. Murata, K. Kaneko, Adsorption mechanism of supercritical hydrogen in internal and interstitial nanospaces of single-wall carbon nanohorn assembly. J. Phys. Chem. B. **106**, 1132–1138 (2002)
7. V. Gayathri, R. Geetha, Hydrogen adsorption in defected carbon nanotubes. Adsorption **13**, 53–60 (2007)
8. Y. Ye, C.C. Ahn, C. Witham, B. Fultz, J. Liu, A.G. Rinzler, D. Colbert, K.A. Smith, R.E. Smalley, Hydrogen adsorption and cohesive energy of single-walled carbon nanotubes. Appl. Phys. Lett. **74**, 2307—2309 (1999)
9. C. Liu, Y.Y. Fan, M. Liu, H.T. Conga, H.M. Cheng, M.S. Dresselhaus, Hydrogen in single-walled carbon nanotubes at room temperature. Science **286**, 1127—1132 (1999)
10. K.K. Murata, K. Kaneko, Adsorption mechanism of supercritical hydrogen in internal and interstitial nanospaces of single-wall carbon nanohorn assembly. J. Phys. Chem. B. **106**, 1132–1138 (2002)
11. Y. Ye, C.C. Ahn, C. Witham, B. Fultz, J. Liu, A.G. Rinzler, D. Colbert, K.A. Smith, R.E. Smalley, Hydrogen adsorption and cohesive energy of single-walled carbon nanotubes. Appl. Phys. Lett. **74**, 2307—2309 (1999)
12. A.G. Lipson, B.F. Lyakhov, E.I. Saunin, A.Y. Tsivadze, Hydrogen accumulation by single-walled carbon nanotubes encapsulated in the palladium matrix. Doklady Phys. Chem. **414**(2), 143–146 (2007)
13. H. Zhu, A. Cao, X. Li et al., Hydrogen adsorption in bundles of well-aligned carbon nanotubes at room temperature. Appl. Surf. Sci. **178**(1–4), 50–55 (2001)
14. Y. Ye, C. Ahn, C. Witham et al., Hydrogen adsorption and cohesive energy of single-walled carbon nanotubes. Appl. Phys. Lett. **74**(16), 2307–2309 (1999)
15. C. Liu, Y.Y. Fan, M. Liu et al., Hydrogen storage in single-walled carbon nanotubes at room temperature. Science **286**(5442), 1127–1129 (1999)
16. R.O. Loutfy, A. Moravsky, A. Franco et al., Physical hydrogen storage on nanotubes and nanocarbon materials, in *Perspectives of Fullerene Nanotechnology* ed. by E. Ōsawa (Springer, Berlin 2002) pp. 327—339
17. G.Q. Ning, F. Wei, G.H. Luo, Q.X. Wang, Y.L. Wu, H. Yu, Hydrogen storage in multi-wall carbon nanotubes using samples up to 85 g. Appl. Phys. A **78**(7), 955–959 (2004)
18. Dillon A. C., Gennett T., Alleman J. L., Jones K. M., Parilla P. A., Heben M. J., « Carbon Nanotube Materials for Hydrogen Storage »// Proceedings of the 2000 U.S. DOE Hydrogen Program Review, 9—11 May 2000, San Ramon, California. NREL/CP-570-28890. Golden, CO: National Renewable Energy Laboratory Vol. II: p. 421—440; NREL Report No. CP-570-32301
19. A.C. Dillon, T. Gennett, J.L. Alleman, K.M. Jones, P. Parilla, M.J. Heben, Carbon nanotube materials for hydrogen storage. Proceedings of the 1999 U.S. DOE Hydrogen Program Review, 4–6 May 1999, Lakewood, Colorado. NREL/CP-570-26938. Golden, CO: National Renewable Energy Laboratory Vol. II: pp. 422–438; NREL Report No. CP-570-32269
20. A.C. Dillon, K.E.H. Gilbert, J.L. Alleman, T. Gennett, K.M. Jones, P.A. Parilla, M.J. Heben, Carbon nanotube materials for hydrogen storage. Proceedings of the 2001 U.S. DOE Hydrogen Program Review, 17–19 April 2001, Baltimore, Maryland. NREL/CP-610-30535. Golden, CO: National Renewable Energy Laboratory pp. 478–494; NREL Report No. CP-610-32314
21. C. Nutzenadel, H. Zuttel, D. Chartouni, L. Schlaphach, Electrochemical storage of hydrogen in nanotube materials Electrochem. Solid State Lett. **2**(1), 30–32 (1999)
22. N. Rajalakshmi, K.S. Dhathathreyan, A. Govindaraj, B.C. Satishkumar, Electrochemical investigation of single-walled carbon nanotubes for hydrogen storage. Electrochim. Acta **45**(27), 4511–4525 (2000)

23. M.C. Gordillo, J. Boronat, J. Casulleras, Isotopic effects of hydrogen adsorption in carbon nanotubes. Phys. Rev. B. **65**(1), 014503 (2001)
24. K.A. Williams, P.C. Eklund, Monte Carlo simulations of H2 physisorption in finite-diameter carbon nanotube ropes. Chem. Phys. Lett. **320**(3–4), 352–358 (2000)
25. S. Hammes-Schiffer, J.C. Tully, Proton transfer in solution: Molecular dynamics with quantum transitions. J. Chem. Phys. **101**(6), 4657–4667 (1994)
26. J.C. Tully, Molecular dynamics with electronic transitions. J. Chem. Phys. **93**(2), 1061–1071 (1990)
27. A.S. Fedorov, P.B. Sorokin, Density and thermodynamics of hydrogen adsorbed on the surface of single-walled carbon nanotubes. Solid State Phys. **48**(2), 377–382 (2006)
28. H. Cheng, A.C. Cooper, G.P. Pez, M.K. Kostov et al., Molecular dynamics simulations of hydrogen adsorption in finite and infinite bundles of single walled carbon nanotubes. Mol. Mater. Specif. Interact. Model. Design. **4**, 469–485 (2007)
29. R. Zidan, A.M. Rao, M. Au, Doped carbon nanotubes for hydrogen storage. Hydrogen, Fuel Cells, and Infrastructure Technologie, FY 2003 Progress Report (2003)
30. Z. Zhang, K. Cho, Ab initio study of hydrogen interaction with pure and nitrogen-doped carbon nanotubes. Phys. Rev. B. **75**(7), 075420 (2007)
31. Y. Fujimoto, S. Saito, Structure and stability of hydrogen atom adsorbed on nitrogen-doped carbon nanotubes. J. Phys: Conf. Ser. **302**(1), 012006 (2011)
32. E. Rangel, G. Ruiz-Chavarria, L.F. Magana, J.S. Arellano, Hydrogen adsorption on N-decorated single wall carbon nanotubes. Phys. Lett. A. **373**(30), 2588–2591 (2009)
33. T. Yildirim, S. Ciraci, Titanium-decorated carbon nanotubes as a potential high-capacity hydrogen storage medium. Phys. Rev. Lett. **94**(17), 175501 (2005)
34. A. Sabir, W. Lu, C. Roland, J. Bernholc, Ab inito simulations of H2 in Li-doped carbon nanotube systems. J. Phys. Condens. Matter **19**(8), 086226 (2007)
35. X. Wu, Y. Gao, X.C. Zeng, Hydrogen storage in pillared Li-dispersed boron carbide nanotubes. J. Phys. Chem. C **112**(22), 8458–8463 (2008)
36. A. Allouche, Y. Ferro, T. Angot, C. Thomas, J.-M. Layet, Hydrogen adsorption on graphite (0001) surface: a combined spectroscopy-density-functional-theory study. J. Chem. Phys. **123**(12), 124701 (2005)
37. P. Ruffieux, O. Gröning, M. Bielmann, P. Mauron, L. Schlapbach, P. Gröning, Hydrogen adsorption on sp2-bonded carbon: influence of the local curvature. Phys. Rev. B. **66**(24), 245416 (2002)
38. P. Ruffieux, O. Gröning, P. Schwaller, L. Schlapbach, P. Gröning, Hydrogen atoms cause long-range electronic effects on graphite. Phys. Rev. Lett. **84**(21), 4910–4913 (2000)
39. L. Hornekær, Z. Sljivancanin, W. Xu, R. Otero, E. Rauls et al., Metastable structures and recombination pathways for atomic hydrogen on the graphite (0001) surface. Phys. Rev. Lett. **96**(15), 156104 (2006)
40. L. Hornekær, E. Rauls, W. Xu, Z. Sljivancanin, R. Otero, I. Stensgaard et al., Clustering of chemisorbed H(D) atoms on the graphite (0001) surface due to preferential sticking. Phys. Rev. Lett. **97**(18), 186102 (2006)
41. B.N. Khare, M. Meyyappan, A.M. Cassell et al., Functionalization of carbon nanotubes using atomic hydrogen from a glow discharge. Nano Lett. **2**(1), 73–77 (2002)
42. G. Chiarello, E. Maccallini, R.G. Agostino, T. Caruso, V. Formoso et al., Vibrational and electronic properties of hydrogen adsorbed on single-wall carbon nanotubes. Phys. Rev. B. **69**(15), 153409 (2004)
43. A. Nilsson, Nanoengineering of hybrid carbon nanotube-metal nanocluster composite materials for hydrogen storage. GCEP Technical Report (2006), http://gcep.stanford.edu/pdfs/QeJ5maLQQrugiSYMF3ATDA/2.1.4.4.nilsson_06.pdf
44. O. Wessely, M.I. Katsnelson, A. Nilsson et al., Dynamical core-hole screening in the x-ray absorption spectra of hydrogenated carbon nanotubes and grapheme. Phys. Rev. B. **76**(16), 161402 (2007)
45. G. Zhang, P. Qi, X. Wang et al., Hydrogenation and hydrocarbonation and etching of single-walled carbon nanotubes. J. Am. Chem. Soc. **128**(18), 6026–6027 (2006)

46. S. Pekker, J.-P. Salvetat, E. Jakab et al., Hydrogenation of carbon nanotubes and graphite in liquid ammonia. J. Phys. Chem. B. **105**(33), 7938–7943 (2001)
47. H. Takagi, H. Hatori, Y. Yamada, Desorption property of hydrogen chemisorbed on the surface of activated carbon. American Carbon Society. Carbon Conference Archive (2004), http://acs.omnibooksonline.com/data/papers/2004_L039.pdf
48. A.C. Dillon, T. Gennett, J.L. Alleman et al., Optimization of single-wall nanotube synthesis for hydrogen storage. IEA Task 12: Metal Hydrides and Carbon for Hydrogen Storage. NREL/CH-590-31288, pp. 91—95 (2001)
49. Y. Ye, C. Ahn, C. Witham et al., Hydrogen adsorption and cohesive energy of single-walled carbon nanotubes. Appl. Phys. Lett. **74**, 2307 (1999)
50. M. Yudasaka, Single-wall carbon nanotubes and single-wall carbon nanohorns. in *Perspectives of Fullerene Nanotechnology*, ed. by E. Osawa (Kluwer Akademic Publisher, USA, 2002), pp. 125–129; T. Yildirim, O. Gülseren, S. Ciraci, Exohydrogenated single-wall carbon nanotubes. Phys. Rev. B. **64**(7), 075404 (2001)
51. A.A. Bogdanov, On the limits of physical adsorption of hydrogen in carbon materials. Tech. Phys. **75**(9), 139 (2005)
52. S.D. Bondarenko, I.A. Alekseev, Study of isotopic effect for hydrogen and deuterium adsorption on nanoporous carbon. Hydrogen Mater. Sci. Chem. Carbon Nanomater. **3**, 493–497 (2006)
53. M.C. Gordillo, J. Boronat, J. Casulleras, Isotopic effects of hydrogen adsorption in carbon nanotubes. arXiv:cond-mat/0109480v1 (cond-mat.stat-mech), 26 Sep 2001
54. S.M. Lee, K.H. An, Y.H. Lee, G. Seifert, T. Frauenheim, A hydrogen storage mechanism in singlewalled carbon nanotubes. J. Am. Chem. Soc. **123**(21), 5059–5063 (2001)
55. Y. Ferro, F. Marinelli, A. Allouche, Density functional theory investigation of the diffusion and recombination of H on a graphite surface. Chem. Phys. Lett. **368**(5–6), 609–615 (2003)
56. A.S. Barnard, M.L. Terranova, M. Rossi, Density functional theory of H-induced defects as nucleation sites in hybrid carbon nanomaterials. Chem. Mater. **17**(3), 527–535 (2005)
57. G.U. Sumanesekera, C.K.W. Adu, S. Fang, P.C. Eklund, Effects of gas adsorption and collisions on electrical transport in single-walled carbon nanotubes. Phys. Rev. Lett. **85**(5), 1096–1099 (2000)
58. G. Buchs, A.V. Krasheninnikov, P. Ruffieux et al., Creation of paired electron states in the gap of semiconducting carbon nanotubes by correlated hydrogen adsorption. New J. Phys. **9**(8), 275 (2007)
59. W.L. Yim, T. Klüner. H2 carrying capacity by considering charging and discharging processes—Case Studies on Small Carbon—and Boron Nitride Nanotubes. High Performance Computing in Science and Engineering (Springer, Berlin, 2010), pp. 85–109
60. M.C. Gordillo, J. Boronat, J. Casulleras, Isotopic effects of hydrogen adsorption in carbon nanotubes. Phys. Rev. B. **65**(1), 014503 (2001)
61. K.A. Williams, P.C. Eklund, Monte Carlo simulations of H2 physisorption in finite-diameter carbon nanotube ropes. Chem. Phys. Lett. **320**, 352 (2000)
62. S. Hammes-Schiffer, J.C. Tully, Proton transfer in solution: Molecular dynamics with quantum transitions. J. Chem. Phys. **101**, 4657 (1994)
63. J.C. Tully, Molecular dynamics with electronic transitions. J. Chem. Phys. **93**, 1061 (1990)
64. A.S. Fedorov, S.G. Ovchinikov, Density and thermodynamics of hydrogen adsorbed inside narrow CNTs. Phys. Solid State **46**(3), 563 (2004)
65. M.J.S. Dewar, E.G. Zoebisch, E.F. Healy, J.J.P. Stewart, Development and use of quantum mechanical molecular models. 76. AM1: A new general purpose quantum mechanical molecular model. J. Am. Chem. Soc. **107**(13), 3902–3909 (1985)
66. B.C. Wanga, H.W. Wanga, I.C. Lina et al., A semiempirical study of carbon nanotubes with finite tubular length and various tubular diameters. J. Chin. Chem. Soc. **50**, 939—945 (2003)
67. D. Lu, Y. Li, S.V. Rotkin, U. Ravaioli, K. Schulten, Finite-size effect and wall polarization in a carbon nanotube channel. Nano Lett. **4**(12), 2383–2387 (2004)

68. A.C. Dillon, K.E.H. Gilbert, P.A. Parilla, C. Horbacewicz, J.L. Alleman, K.M. Jones, M. J. Heben, Hydrogen storage in carbon single-wall nanotubes. Hydrogen, Fuel Cells, and Infrastructure Technologies, FY 2003 Progress Report (2003)
69. P. Ruffieux, O. Groning, M. Bielmann, P. Groning, Hydrogen chemisorption on sp2-bonded carbon: Influence of the local curvature and local electronic effects. Appl. Phys. A **78**(7), 975–980 (2004)
70. E. Durgun, S. Dag, S. Ciraci, O. Gülseren, Energetics and electronic structures of individual atoms adsorbed on carbon nanotubes. J. Phys. Chem. B. **108**(2), 575–582 (2004)
71. O. Gulseren, T. Yildirim, S. Ciraci, Tunable adsorption on carbon nanotubes. Phys. Rev. Lett. **87**(1), 116802 (2011)
72. A.N. Andriotis, M. Menon, D. Srivastava, G. Froudakis, Extreme hydrogen sensitivity of the transport properties of single-wall carbon-nanotube capsules. Phys. Rev. B. **64**(19), 193401 (2001)
73. H. Scudder, G. Lu, N. Kioussis, Hydrogen-induced unzipping of single-walled carbon nanotubes. Phys. Rev. B. **68**(20), 205416 (2003)
74. S. Letardi, M. Celino, F. Cleri, V. Rosato, Atomic hydrogen adsorption on a Stone-Wales defect in graphite. Surf. Sci. **496**(1–2), 22–38 (2002)
75. C. Tabtimsai, S. Keawwangchai, N. Nunthaboot, V. Ruangpornvisuti, B. Wanno, Density functional investigation of hydrogen gas adsorption on Fedoped pristine and Stone–Wales defected single-walled carbon nanotubes. J. Mol. Model. **18**(8), 3941–3949 (2012)
76. O. Wessely, M.I. Katsnelson, A. Nilsson et al., Dynamical core-hole screening in the x-ray absorption spectra of hydrogenated carbon nanotubes and grapheme. Phys. Rev. B. **76**(16), 161402 (2007)
77. G. Zhang, P. Qi, X. Wang et al., Hydrogenation and hydrocarbonation and etching of single-walled carbon nanotubes. J. Am. Chem. Soc. **128**(18), 6026–6027 (2006)
78. S. Pekker, J.-P. Salvetat, E. Jakab et al., Hydrogenation of carbon nanotubes and graphite in liquid ammonia. J. Phys. Chem. B. **105**(33), 7938–7943 (2001)
79. R.E. Haufler, J. Conceicao, L.P.F. Chibante et al., Efficient production of C60 (buckminsterfullerene), C60H36, and the solvated buckide ion. J. Phys. Chem. **94**(24), 8634–8636 (1990)
80. G. Lu, H. Scudder, N. Kioussis, Hydrogen-induced unzipping of single-walled carbon nanotubes. Phys. Rev. B. **68**(20), 205416 (2003)
81. K.A. Park, S.J. Kim, K. Seo, Y.H. Lee, Adsorption of atomic hydrogen on single-walled carbon nanotubes. J. Phys. Chem. B. **109**(18), 8967–8972 (2005)
82. C.W. Bauschlicher Jr., Hydrogen and fluorine binding to the sidewalls of a (10, 0) carbon nanotube. Chem. Phys. Lett. **322**(3–4), 237–241 (2000)
83. S. Jalili, R. Majidi, The effect of atomic hydrogen adsorption on single-walled carbon nanotubes properties. J. Iran. Chem. Soc. **4**(4), 431–437 (2007)
84. P. Nikolaev, A. Thess, A.G. Rinzler, D.T. Colbert, R. Smalley, Diameter doubling of single-wall nanotubes. Chem. Phys. Lett. **266**(5–6), 422–426 (1997)
85. Б. Трепнел, « Хемосорбция » . М.: Иностранная лит., 1958. 327 с
86. Y.S. Nechaev, O chemosorbtchii i phyzicheskoy sorbtcii vodoroda uglerodnymi nanostructurami. Alternativnaya energetica i ecologya. **2**(22), 64–73 (2005)
87. O.B. Tomilin, U.U. Murumin, Adsorption on the graphene surface of carbon nanotubes and their energy spectrum. Phys. Solid State **48**(3), 563–571 (2006)
88. O.B. Tomilin, P.V. Avramov, A.A. Kuzovov, S.G. Ovchinikov, G.L.Pashkov, Connection the chemical properties of carbon nanotubes with their atomic and electronic structure. Phys. Solid State **46**(6), 1143–1146 (2004)
89. A. Yu, Zarifayntc. J. Phys. Chem. **38**, 2655–2664 (1964)
90. V.F. Kisilev, O.V. Krylov, Adsorption processes on the surface of semiconductors and dielectrics. Moscov. Sience, 255 (1978) (Rus.)
91. A.P. Popov, Bazhin influence of impurities and defects on electronic structure of carbon nanotubes. Hydrogen Mater. Sci. Chem. Carbon Nanomater., 795–799 (2007)

92. Y.S. Nechaev, O chemosorbtchii i phyzicheskoy sorbtcii vodoroda uglerodnymi nanostructurami. Alternativnaya energetica i ecologya. **2**(22), 64–73 (2005)
93. P. Ruffieux, O. Groning, M. Bielman, P. Groning, Hydrogen chemisorption on sp2-bonded carbon: influence of the local curvature and local electronic effects. Appl. Phys. A **78**, 975–980 (2004)
94. L. Sabir, W. Lu, C. Roland, J. Bernholc, Ab initio simulations of H2 in Li-doped carbon nanotube system. arXiv: cond-mat/ 0608432v1. 18 Aug. 2006
95. Y. Zhao, Y.H. Kim, A.C. Dillon, M.J. Heben, S.B. Zhang, Hydrogen storage in novel organometallic buckyballs. Phys. Rev. Lett. **94**(15), 155504 (2005)
96. T. Yildirim, S. Ciraci, Titanium-decorated carbon nanotubes as a potential high-capacity hydrogen storage medium. Phys. Rev. Lett. 94(17), 175501 (2005)
97. S.V. Bulyarskiy, V.V. Fistul, The thermodynamics and kinetics of the interaction of defects in semiconductors. Moscov. Sience, 351 (1997) (Rus.)
98. S.V. Bulyarskiy, V.V. Svetuhin, Physical basis of defect management in semiconductors. Ulianovsk 385 (2003) (Rus.)
99. A. Nikitin, H. Ogasawara, D. Mann, R. Denecke, Z. Zhang et al., Hydrogenation of single-walled carbon nanotubes. Phys. Rev. Lett. **95**, 225507 (2005)
100. S. Dhiman, R. Kumar, K. Dharamvir, A density functional study of zigzag carbon nanotubes. (2011), 141. http://physics.puchd.ac.in/events/2010-2011/chascon2011/full-papers/Shobhna.pdf
101. A. Rochefort, D.R. Salahub, P. Avouris, The effects of finite length on the electronic structure of carbon nanotubes. J. Phys. Chem. B. **103**(4), 641–646 (1999)
102. I. Cabria, M.J. Lopez, J.A. Alonso, Adsorption of hydrogen on normal and pentaheptite single wall carbon nanotubes. Eur. Phys. J. **34**, 279—282 (2005)
103. P.I. Meshkov, Hydrogen storage using nanomaterials (2008), www.nanometer.ru/2008/04/22/konkurs_statej_47267.html

Chapter 4
Oxygen Interaction with Electronic Nanotubes

Sergey Bulyarskiy, Alexandr S. Basaev, Darya A. Bogdanova and Alexandr Pavlov

Analysis of the scientific literature shows that oxygen reacts with CNTs by physical adsorption only—when semiconductor nanotubes have acceptor-type conductivity. A calculation, made by methods of quantum mechanics, indicate this may be chemical adsorption which has a partial free energy of >10 eV. Adsorption energy is big, so this phenomenon is not observed in practice. Analysis of experimental adsorption isotherms of oxygen and desorption thermogravimetric curves allow calculation of oxygen adsorption energy for three possible locations.

4.1 Simulation of the Oxygen Interaction with Electronic Nanotubes

The studies of oxygen adsorption [1–7] are important for understanding CNT conductivity type changes. It is known that oxygen adsorption by a nanotube leads to acceptor-type conductivity. On the other hand, usage of CNT as an adsorbent has allowed division of argon and oxygen, producing O_2 of very high purity [8, 9].

Oxygen cannot be built-in into the SWNT crystalline lattice, but it was shown experimentally that oxygen has a profound impact on nanotubes conductivity. In many

S. Bulyarskiy (✉) · A.S. Basaev · D.A. Bogdanova · A. Pavlov
Institute Nanotechnology of Microelectronics, Russian Academy of Sciences, Moscow, Russia
e-mail: bulyar2954@mail.ru

A.S. Basaev
e-mail: a.basaev@tcen.ru

D.A. Bogdanova
e-mail: bogdanovada8@gmail.com

A. Pavlov
e-mail: Alexander.a.pavlov@gmail.com

S. Bulyarskiy and A. Saurov (eds.), *Doping of Carbon Nanotubes*, NanoScience and Technology, DOI 10.1007/978-3-319-55883-7_4

studies the possible usage of the SWCNT adsorbed oxygen as a *p*-doping admixture was considered, because this process can proceed due to a charge transport between the adsorbed atoms and nanotube [10, 11]. Many investigators had pointed out that gaseous oxygen can appreciably change the various nanotube properties (such as conductivity, thermo-electromotive force, local state density, etc). In particular, the semiconductor nanotubes can be transformed into metallic ones under the action of oxygen even at low concentrations [12–14]. It has been shown experimentally that an oxygen adsorption practically always reduces SWCNT resistivity [12, 15].

It was found in an experimental study [16] that the nanotubes thermo-electromotive force increases under the action of ultraviolet in an air atmosphere. This is presumed to be a consequence of UV stimulated adsorption on CNTs. Authors of a theoretical study [17] have shown that the rise of oxygen adsorption under UV exposure is connected most likely with oxygen molecule excitation from their ground spin-triplet state into a more highly energetic spin-singlet state. Such excitation reduces the activation energy of the molecular oxygen adsorption on a nanotube, raises the adsorption energy, and creates conditions for charge transport from a tube to the oxygen molecule, i.e., the UV action can sufficiently increase the oxygen sorption on a CNT. The authors showed that Stone–Wales defects play a critical role in tube bounding with O_2 molecules and enforcemen of the charge transport process. The influence of CNT parameters (diameter, chirality, and wall number) on the adsorption process was found to be well below the influence of defects.

In one piece of work [2], molecular oxygen adsorption was modeled for an individual SWCNT and it was shown that under normal conditions oxygen is physically adsorbed on a CNT and the adsorption decreased the nanotube's resistance by about two orders of magnitude. The molecular oxygen adsorption on a (5,0) and (4,4) type SWCNT was modeled in [18] and the calculations showed a strong interaction between nanotubes and adsorbate. In this case the forbidden gap of (5,0)-type nanotubes also increased under the action of oxygen from 0.77 to 1.37–1.44 eV, but for (4,4)-type nanotubes changed from 2.79 to 1.47–2.9 eV, depending on adsorption center characteristics.

Atomic oxygen chemisorption on SWCNTs (that can be realized, e.g., by ionic implantation) was theoretically studied also in [19]. Here was used a density functional method the author had shown for individual oxygen atom chemisorption in a (10,0)-type nanotube—the adsorption more often proceeds over a C–C bond, being parallel to the nanotube axis with an adsorption energy of about 2.21–2.60 eV. The author also considered chemisorption processes of two, three, and four nitrogen atoms on a nanotube and found that the adsorption energy values are equal 2.57–2.93, 2.93–3.01, and 2.85–3.03 eV correspondingly (the energy intervals were taken for the possibility of several adsorption centers existening). In another theoretical study [20] of oxygen chemisorption for the same (10,0) nanotube the following adsorption energy values were found: for 1 oxygen atom −3.26 eV (Hartree–Fock method) and 5.21 eV (TGA method); and for 2 oxygen atoms −6.47 eV (Hartree–Fock method) and 10.37 eV (TGA method). In [21] it was theoretically calculated that the bound energy for individual oxygen atom

chemisorption on a (8,0)-type SWCNT is equal to 5.1 eV. The authors of [22], via modeling of molecular oxygen adsorption at a (8,0) nanotube, obtained a weak coupling with very low charge transport, but they pointed out that the adsorption was studied for the oxygen spin-triplet state only. In theoretical works [23, 24], where the oxygen singlet state was studied, authors showed that an in this case an interaction with the tube is sufficiently strong and the charge transport is considerable. Thus, it may be thought that oxygen is adsorbed and firmly retained on CNTs with a sufficiently great coupling energy, allowing a change from nanotube resistance type to acceptor type.

In this connection it is important to model the adsorption processes to detect their parameters and admixture mutual influences.

The simulation modeling of oxygen adsorption on (5,0), (6,0), (7,0), and (8,0) SWCNT tubes was carried out by the method used for hydrogen described in Chap. 3. Calculations were carried out for the adsorption on SWCNTs of one or two oxygen atoms. For the case of one atom the adsorption center locations are shown in Fig. 4.1.

The oxygen adsorption process has its own peculiarities. Because the spin of the studied isotope ^{16}O is equal zero, a system of "SWNT + O" can exhibit both the singlet and triplet properties even for adsorption of one oxygen atom. The system properties for one atom adsorption per one cell are presented in Table 4.1, with the data relating to steady conformations only, because for tubes (7,0) and (8,0) with bigger diameters the oxygen chemisorption results are stable only for the singlet system "atoms–SWCNT". For the smaller (5,0)-type and (6,0)-type tubes both singlet and triplet states are possible, and moreover the triplet states are energetically more preferable. The calculations showed that the energetic characteristics for the triplet state were similar to the energetic characteristics of the singlet, which are in Table 4.1. As one would expect, in the triplet system's forbidden band occur are two "impurity", "semi-forbidden" levels, and for both (5,0) and (6,0) nanotubes these states are located in the upper half of the energetic HOMO–LUMO gap, thus increasing the *n*-type conductivity of the structure under consideration. The adsorption energies for the most energetically stable systems are equal to: −4.5 eV for (5,0); +2.4 eV for (6,0); −4.1 eV for (7,0); and −1.7 eV for (8,0). This means that (by analogy with one nitrogen atom chemisorption) one oxygen atom chemisorption for a (6,0) tube is an endothermic process and its junction is an unstable one. The same situation is observed for a (7,0) tube with one chemisorbed oxygen atom (Table 4.1).

In all considered variants of one oxygen atom chemisorption on SWCNTs arises a change of system conductivity. In triplet (5,0) and (6,0) systems this change

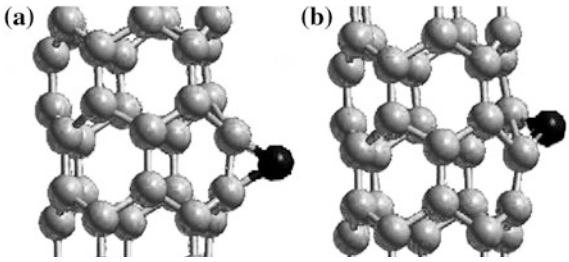

Fig. 4.1 Two variants of adsorption center locations for oxygen atom chemisorption on a (5,0) nanotube

proceeds at the expense of a new impurity states appearance into the HOMO–LUMO gap. For singlet systems (7,0) and (8,0) at the oxygen atom chemisorption a little reduction in the energy gap width is observed, and as a result the conductivity increases 1.2 times for the (7,0) nanotube and 2.2 times for the (8,0) nanotube.

In Fig. 4.2 the conformations, corresponding to the two-oxygen atom adsorption on one cell are shown and in Table 4.2 the results of chemisorption parameter calculations are presented for such SWCNT with two adsorbed oxygen atoms.

In Table 4.2 are data only for stable conformations. In general the behavior of oxygen in the systems with two adsorbed oxygen atoms is similar to the behavior of the described systems with one adsorbed atom.

Note the interesting difference between oxygen and nitrogen chemisorption, namely in oxygenic systems the adsorbed oxygen atom always carries a negative charge, but for nitrogen adsorption systems there can be observed positive charge transport too.

There is no one stable triplet conformation for SWCNT (8,0) and the system stable triplet states are also absent for the case (Fig. 4.2b) of a (5,0) tube and cases (Fig. 4.2a–c) of a (7,0) tube. Some distinctions were observed for a (6,0) tube, because for hydrogen chemisorption there are two possible triplet conformers—

Table 4.1 Parameters of a one oxygen atom adsorption process on (5,0), (6,0), (7,0), and (8,0) SWCNTs

		(5,0)	(6,0)	(7,0)	(8,0)
Center 1 (σ = 1)	E_{tot} (kcal/mol)	−190,000	−220,000	−260,000	−260,000
	Δq (e)	−0.14	−0.16	−0.15	−0.16
	E_g (eV)	4.5	2.7	3.1	2.5
	E_{HOMO} (eV)	−7.1	−6.5	−6.4	−6.5
	E_{LUMO} (eV)	−2.6	−3.8	−3.3	−4.0
Center 2 (σ = 1)	E_{tot} (kcal/mol)	−190,000	−220,000	−26,000	−290,000
	Δq (e)	−0.12	−0.17	−0.11	-0.20
	E_g (eV)	3.9	2.0	3.3	2.5
	E_{HOMO} (eV)	−6.8	−6.2	−6.7	−6.1
	E_{LUMO} (eV)	−2.9	−4.2	−3.4	−3.6

Notes E_{tot} the total energy of one oxygen atom system on a SWCNT; Δq the partial charge transport on the oxygen atom; *E*g the energy gap width; E_{HOMO} energy of HOMO; E_{LUMO} energy of LUMO. Center 1 corresponds to a location variant of Fig. 4.1a; Center 2 corresponds to the singlet state of Fig. 4.1b

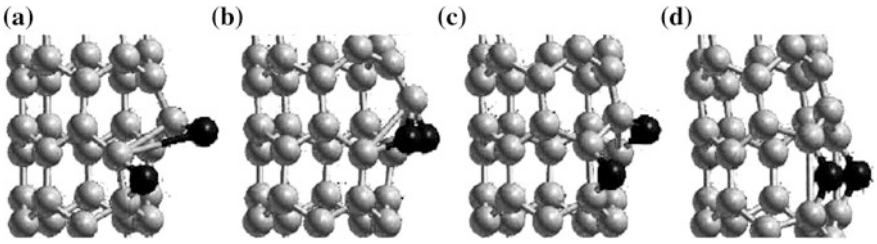

Fig. 4.2 Four variants of the two chemisorbed oxygen atom locations for a (5,0) nanotube

Table 4.2 Parameters of the two oxygen atom chemisorption process on (5,0), (6,0), (7,0), and (8,0) SWCNT (as seen in Fig. 4.2a–d)

	E_{tot} (kcal/Mol)	Δq (e)		E_g (eV)	E_{HOMO} (eV)	E_{LUMO} (eV)	E_O (L-SOMO) (eV)	E_O (H-SOMO) (eV)
(5,0), (a), σ = 1	−190,000	−0.15	−0.13	4.4	−7.1	−2.7		
(5,0), (a), σ = 3	−190,000	−0.15	−0.13	4.8	−7.4	−2.6	−4.86	−4.81
(5,0), (b), σ = 1	−190,000	−0.12	−0.13	4.2	−7.0	−2.8		
(5,0), (b), σ = 3	−190,000	−0.12	−0.12	3.9	−6.9	−2.9	−4.93	−4.78
(5,0), (c), σ = 1	−190,000	−0.13	−0.14	3.82	−6.81	−2.99		
(5,0), (d), σ = 1	−190,000	−0.14	−0.14	3.84	−6.93	−3.09		
(5,0), (d), σ = 3	−190,000	−0.15	−0.15	4.44	−7.24	−2.80	−5.01	−4.94
(6,0), (a), σ = 1	−230,000	−0.18	−0.20	2.91	−6.52	−3.60		
(6,0), (b), σ = 1	−230,000	−0.16	−0.16	1.98	−6.18	−4.19		
(6,0), (b), σ = 1	−230,000	−0.22	−0.13	2.10	−6.26	−4.16		
(6,0), (c), σ = 3	−230,000	−0.20	−0.15	3.98	−7.45	−3.47	−5.38	−5.07
(6,0), (d), σ = 1	−230,000	−0.19	−0.15	2.92	−6.47	−3.55		
(6,0), (d), σ = 3	−230,000	−0.16	−0.17	3.98	−7.39	−3.41	−5.19	−5.13
(7,0), (a), σ = 1	−270,000	−0.15	−0.14	3.21	−6.48	−3.27		
(7,0), (b), σ = 1	−270,000	−0.12	−0.12	3.21	−6.51	−3.29		
(7,0), (c), σ = 1	−270,000	−0.15	−0.15	3.28	−6.56	−3.27		
(7,0), (d), σ = 1	−270,000	−0.15	−0.15	2.86	−6.52	−3.65		
(7,0), (d), σ = 3	−270,000	−0.16	−0.17	3.08	−6.43	−3.35	−5.01	−4.87
(8,0), (a), σ = 1	−300,000	−0.17	−0.19	1.98	−6.02	−4.03		
(8,0), (b), σ = 1	−300,000	−0.16	−0.16	2.37	−6.27	−3.90		
(8,0), (c), σ = 1	−300,000	−0.18	−0.15	2.51	−6.56	−4.05		
(8,0), (d), σ = 1	−300,000	−0.21	−0.21	2.21	−6.28	−4.07		

Fig. 4.2c, d. The minimal energy states are as follows: triplet (Fig. 4.2b) for a (5,0) tube, singlet (Fig. 4.2b) for a (6,0) tube, singlet (Fig. 4.2b) for a (7,0) tube, and singlet (Fig. 4.2c) for a (8,0) tube.

The adsorption energy of two oxygen atoms on a SWCNT (calculated per one adsorbate atom) for the most energetically advantageous conformations is equal to: −4.2 eV for (5,0); −5.5 eV for (7,0); and −1.3 eV for (8,0), i.e., the system "SWNT (6,0) + 2O" is a metastable one.

In all considered cases, conductivity changes were observed. For the triplet systems, this fact is associated with the impurity states emergence into the energy gap, for singlet systems—with a change in the energy gap width. For the two oxygen atom chemisorption case the situation is opposite to that for the two nitrogen atom chemisorption (for the most stable singlet conformations). For tubes with even chiralities the conductivity increases 8.4 times for (6,0) and in 2.3 times for (8,0), whereas for tubes with chiralities which are odd it is decreasing by 3.5 times for (5,0) and 1.4 times for (7,0).

Substitution doping of SWCNTs with oxygen cannot be realized.

4.2 The Characteristic Parameters of Oxygen Adsorption

The experiments on oxygen physical adsorption [9] were carried out in this manner: the samples from activated carbon and CNTs were baked out for 4 h at a temperature of 523 K in a vacuum under desorbed gase which was continuously pumped out by molecular pump. Then the system was filled with oxygen at a certain pressure. The isotherms of oxygen and nitrogen adsorption by activated carbon and SWCNT (with mean diameter 3 nm) are presented in Fig. 4.3 for comparison, and it is easy to see that the activated carbon isotherms for oxygen and nitrogen are very close, whereas the isotherm difference for adsorption on CNTs achieves 40% for the same experimental conditions.

The theoretical models developed in [4, 5] allow the determination of the adsorption process parameters. For calculations the experimental results were recounted from weight percents to relative units (Fig. 4.3). As a result there arose some non-linear isotherms, demonstrating that the system's thermodynamic parameters depended on temperature.

Using the data from Fig. 4.3 the temperature dependencies of the Gibbs partial energy are defined (Table 4.3).

To obtain system kinetic coefficients and later on to calculate technological process dynamics it is necessary to study gas desorption kinetics. The thermodynamic parameters of oxygen TGA were determined by the method described in Sect. 2.5. The calculation results are presented in Table 4.4 and Fig. 4.4.

We succeeded in the separation of the desorption process for nanotubes from four different locations. For the first time we determined the probability of desorption of oxygen. Desorption from position *1* is the same as for amorphous carbon. In accordance with the data of work [3] oxygen adsorption heat on a carbon surface

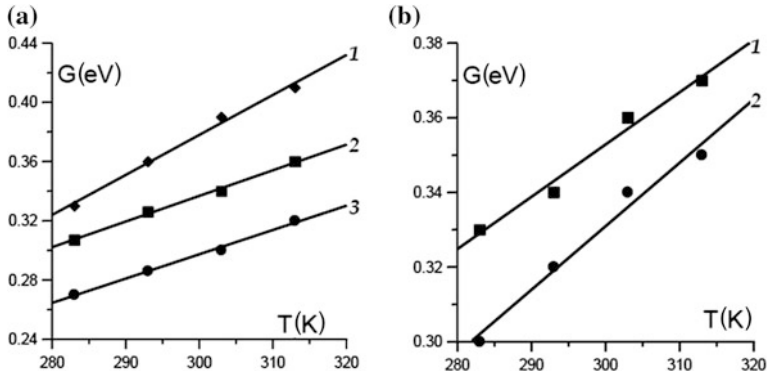

Fig. 4.3 Gibbs partial energy of molecular oxygen adsorption by activated carbon (**a**) and CNT (**b**) (*lines* approximation; *points* experimental results)

Table 4.3 Thermodynamic parameters of oxygen adsorption

Activated carbon			SWCNT		
Location	H (eV)	S (entropy units) (k)	Location	H (eV)	S (entropy units) (k)
1	−0.19	−19	1	−0.07	−15
2	−0.18	−20	2	−0.18	−19
3	−0.43	−43			

Table 4.4 The oxygen TGA parameters for four different localization points

Plase (*i*)	1	2	3	4
Coupling energy $G_{\alpha i}^{\beta}$ (eV)	0.02	0.05	0.06	0.07
Desorption probability $v_{\alpha i}^{\beta}$ (s^{-1})	12	1300	3000	2200
Probability of adsorbent capture, $c_{\alpha i}^{\beta}$ ($cm^3 s^{-1}$)	–	7.7×10^{-20}	1.7×10^{-19}	1.3×10^{-19}
The repulsion barrier energy for oxygen physical adsorption $\Delta_{\alpha i}^{\beta}$ (eV)	–	0.050	0.058	0.066

was changed between the range 1600–3800 cal/mol, corresponding to a coupling energy value of 0.017–0.038 eV.

It seems likely that process *1* is connected with desorption from the tube's external surface. The coupling energy of other locations is bigger, something which can be connected with a porosity effect. It can be supposed that in such cases the processes corresponds to desorption from the defects, the tubes inner surface, and pores formed by nanotube bundles. As can be judged from the desorbed oxygen amounts the desorption energy (0.059 eV) corresponds to the gas molecule location in the tube, because this peak is the most intense for the desorption process, and as

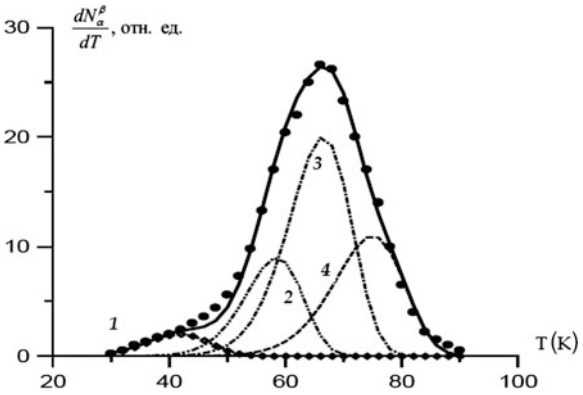

Fig. 4.4 Temperature dependence of the oxygen DTGA under heating at β = 0.25 K/s (*diamonds* experimental data for desorption from an amorphous graphite surface; *points* experimental data for desorption from CNTs; *continuous line* summary calculation curve; *dashed line* calculations using formula (2.86) for coupling energies N_α^β (eV): *1* 0.021; *2* 0.050, *3* 0.059; *4* 0.068

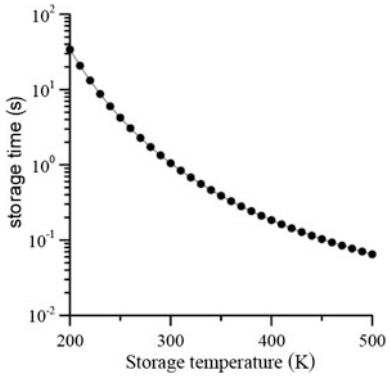

Fig. 4.5 Time to remove oxygen by heating under vacuum conditions at a certain temperature

one would expect the adsorbed molecule number is proportional to the desorption probability.

The results of calculations show that the oxygen can be easily removed by heating the samples in a vacuum (Fig. 4.5).

The values of capture probability, $c_{\alpha i}^\beta$, estimated by a calculation, are presented in Table 4.4. The number of possible adsorption places was calculated on the presumption that the mean tube radius equals 1.5 nm [1] and the distance between hydrogen atoms is 2.46 Å. Assuming that an oxygen molecule can be captured by every cell, one obtains values of 6.4×10^{14} cm^{-2} and 1.7×10^{22} cm^{-3} for the surface and volumetric seat concentrations correspondingly. The capture coefficients for the adsorption (assuming that a repulsing barrier is absent) can be estimated by formulae (2.31), where the multiplier 2 is chosen because molecule

rapture takes place on a hemisphere. The adsorption proceeds from a rarefied gas, which can be considered as ideal, giving: $c_{x0}^{\beta} = 4.4 \times 10^{-15}$.

4.3 Conclusion

The variations from Table 4.3 are connected supposedly with the existence of a repulsing barrier to physical adsorption. Formula (2.72) makes it possible to estimate these barrier heights for different places (Table 4.4). It must be noted also that the coupling energy values, calculated in work [3], are overestimated by more than 2 times, because the pre-exponential factor (in Table 3.4 it is the desorption probability) in the mentioned work was in fact chosen without any justification giving a substantial systematic error in the calculated coupling energy values. The oxygen adsorption leads to a change of CNT conductivity type from electronic to hole [8] and this fact allows us to control the CNT properties of adsorption. At the same time many different authors agree that the oxygen adsorption process has a physical character and therefore there are no charge exchanges between the adsorbed oxygen molecule and the CNT. The detailed theoretical analysis and experimental studies of this problem are presented in research work [3]. In experiments a CNT was placed between two Au/Ti contacts in a vacuum system (pumped out to a residual pressure of 10^{-7} Torr by molecular pump) at room temperature. During the pumping out process the SWCNT resistance was measured and the resistance was found to increase to 16×10^6 Ω, but later (after experimental volume filling by air) decrease to 2.5×10^6 Ω over 15 min.

We completed calculations using a spin-polarized model which showed that the energy of oxygen coupling with a nanotube is described by a potential, having a minimum (0.05 eV) at a distance of 0.35 nm from the tube surface. Such interaction potential is characteristic of van der Waals couplings, and this result is in very good agreement with the data of Table 4.4. We detected several such potential curves, suggesting that oxygen can captured on several physically non-equivalent places or sites, and nuances can be accounted by the used calculation method. The calculations showed that after oxygen atom adsorption the Fermi level of the carbon semiconductor nanotube (with a forbidden gap width 0.69 eV) shifted to the valence zone and was placed at a distance of 0.20–0.24 eV from this zone, creating conditions for hole conductivity in the system.

Such calculations for (5,0), (6,0), (7,0), and (8,0) nanotubes with one and two chemisorbed nitrogen or oxygen atoms demonstrated that in all cases there are observed changes in OCNTs conductivity nature, but the scales and mechanisms of these changes are different.

For an individual oxygen atom (^{16}O, $s = 0$) connection to the final system "tube + adsorbed atom" can be both a singlet and triplet one. For (5,0) and (6,0) SWCNTs with lesser diameters the most energetically profitable state is the triplet state, when into the nanotube energetic gap appear two near semi-filled "impurity" levels. They are located in the upper half of the HOMO–LUMO gap and at the cost

of these levels the *n*-type conductivity can be realized in the systems under consideration.

For SWCNTs with bigger diameters, namely (7,0) and (8,0), the only stable state is a singlet one, when the "impurity" levels as such do not appear in the energy gap, but the width of the gap itself decreases, and as a result the conductivity of SWCNT (7,0) and SWCNT (8,0) increases 1.2 and 2.2 times, correspondingly.

References

1. S.V. Bulyarskiy, Uglerodnye nanotrubky: techologya, upravlenie svoystvami, primenenie. Ulyanovsk, "Streshen" (2011), 479 s. (Rus)
2. A. Tchernatinsky, B. Nagabhinrava, S. Desai et al., Adsorption oxygen molecules on individual carbon single-walled nanotubes. arXiv: cond-mat/0502012 (2005)
3. H. Ulbricht, G. Moos, T. Hertel, Phys adsorption of molecular oxygen on single-walled Carbon nanotubes bundles and graphite. arXiv: cond-mat/0204525 (2005)
4. S.V. Bulyarskiy, A.S. Basaev, Thermodynamics and kinetics of adsorption of atoms and molecules with carbon nanotubes. ZhETF **135**(4), 788–799 (2009)
5. S.V. Bulyarskiy, A.S. Basaev, Adsorption by carbon nanotubes. Nano- and Microsyst. **12** (116), 16–55 (2009)
6. J. Sun, L. Gao, J. Electroceram. **17**, 91–94 (2006)
7. T. Roman, W.A. Dino, H. Nakanishi, H. Kasai, Eur. Phys. J. **D38**, 117–120 (2006)
8. B. Ho Kim, B. Reon Kim, Y.G. Seo, A Study on adsorption equilibrium for oxygen and nitrogen into carbon nanotubes. Adsorption **11**, 207–212 (2005)
9. S.U. Rege, R.T. Yang, Kinetic separation of oxygen and argon using molecular sieve carbon. Adsorption **6**, 15–22 (2000)
10. S.J. Tans, A.R.M. Verschueren, C. Dekker, Room-temperature transistor based on a single carbon nanotube. Nature **393** (1998). doi:10.1038/29954
11. R. Martel, T. Schmidt, H.R. Shea, et al. Appl. Phys. Lett. **73**(17), 2447 (1998)
12. P.G. Collins, K. Bradley, M. Ishigami, A. Zett, Extreme oxygen sensitivity of electronic properties of carbon nanotubes Science **287**(10), 1801–1804 (2000)
13. J. Hone, I. Ellwood, M. Muno et al., Thermoelectric power of single-walled carbon nanotubes. Phys. Rev. Lett. **80**(5), 1042–1045 (1998)
14. J. Kong, N.R. Franklin, C. Zhou et al., Nanotube molecular wires as chemical sensors. Science **287**(5453), 622–625 (2000)
15. K. Urita, S. Seki, S. Utsumi et al., Effects of gas adsorption on the electrical conductivity of single-wall carbon nanohorns. Nano Lett. **6**(7), 1325–1328 (2006)
16. T. Savage, S. Bhattacharya, B. Sadanadan et al., Photoinduced oxidation of carbon nanotubes. J. Phys.: Condens. Matter **15**(35), 5915 (2003)
17. M. Grujicic, G. Cao, A.M. Rao et al., UV-light enhanced oxidation of carbon nanotubes. Appl. Surf. Sci. **214**(1–4), 289–303 (2003)
18. S.A. Babanejad, F. Ashrafi, A. Ghasemi, et al., in *Comparison of NQR of O_2, N_2 and CO on Surface of Single-walled Carbon Nanotubes and Chemisorption of Oxygen-doped on the Surface of Single-walled Carbon Nanotubes: a DFT and Computational NMR Study*, ed. by S. Yellampalli, Carbon Nanotubes—Synthesis, Characterization Applications, ISBN 978-953-307-497-9, Published: July 20, 2011 under CC BY-NC-SA 3.0 license
19. J. Kroes, F. Pietrucci, W. Andreoni et al., Atomic oxygen chemisorption on carbon nanotubes. J. Phys. Chem. C **117**(4), 1948–1954 (2013)

20. M. Kia, V. Pourghasem, F. Niksolat, Ab initio calculations SWNTs and investigation of interaction atoms of oxygen with that by computational calculations. J. Phys. Theor. Chem. IAU Iran. **7**(4), 213–219 (2011)
21. E. Durgun, S. Dag, S. Ciraci, O. Gülseren, Energetics and electronic structures of individual atoms adsorbed on carbon nanotubes. J. Phys. Chem. B. **108**(2), 575–582 (2004)
22. P. Giannozzi, R. Car, G. Scoles, Oxygen adsorption on graphite and nanotubes. J. Chem. Phys. **118**(3), 1003–1006 (2003)
23. D.C. Sorescu, K.D. Jordan, P. Avouris, Theoretical study of oxygen adsorption on graphite and the (8,0) single-walled carbon nanotube. J. Phys. Chem. B. **105**(45), 11227–112232 (2001)
24. A. Ricca, J.D. Drocco, Interaction of O2 with a (9,0) carbon nanotube. Chem. Phys. Lett. **362** (3–4), 217–223 (2002)

Chapter 5
Nitrogen Interaction with Carbon Nanotubes: Adsorption and Doping

Alexandr Saurov, Sergey Bulyarskiy, Darya A. Bogdanova and Alexandr Pavlov

Abstract Nitrogen is an important impurity in CNTs. An overview of the interaction of nitrogen with impurities will be given in this chapter. The properties of a nitrogen atom depend on its place on the graphene lattice and on the closest neighboring particles. Nitrogen, which is located in the site of a graphene lattice, is a donor, however, if there is a vacancy nearby it becomes an acceptor. Processes of nitrogen interaction with the surface of nanotubes are complex. A detailed analysis is necessary to understand this interaction.

Nitrogen is an important impurity in CNTs. An overview of the interaction of nitrogen with impurities will be given in this chapter. The properties of a nitrogen atom depend on its place on the graphene lattice and on the closest neighboring particles. Nitrogen, which is located in the site of a graphene lattice, is a donor, however, if there is a vacancy nearby it becomes an acceptor. Processes of nitrogen interaction with the surface of nanotubes are complex. A detailed analysis is necessary to understand this interaction.

Analysis of the doping process was made using quantum mechanics, thermodynamics, and physical kinetics methods. The nitrogen atom may be attached to the graphene lattice by chemisorption. It is located above the sigma bond C–C (energy is 2.8 eV) or at Stone-Wales defects (energy is 1.4–1.7 eV and depends on the chirality of the nanotubes) in this case.

A. Saurov (✉) · S. Bulyarskiy · D.A. Bogdanova · A. Pavlov
Institute Nanotechnology of Microelectronics, Russian Academy of Sciences, Moscow, Russia
e-mail: a.saurov@tcen.ru

S. Bulyarskiy
e-mail: bulyar2954@mail.ru

D.A. Bogdanova
e-mail: bogdanovada8@gmai.com

A. Pavlov
e-mail: alexander.a.pavlov@gmail.com

S. Bulyarskiy and A. Saurov (eds.), *Doping of Carbon Nanotubes*, NanoScience and Technology, DOI 10.1007/978-3-319-55883-7_5

By thermodynamics method it has been calculated which formulas connect the main concentration of the doping centers, vacancies, and Stone-Walls defects, with the terms of nanotube growth. These calculations are compared with the results of a study of nanotube mean X-ray photo electronic spectroscopy (XPS) and thermogravimetric analysis. The results of the comparison are in the form of the partial free energy of defects that occur on the graphite and pyridine and the energy of chemisorption of nitrogen atoms.

5.1 Nitrogen Arrangement on Carbon Nanotubes

The problems of CNT property control are connected with many various internal and external factors. In previous chapters (using as an example hydrogen and oxygen) we have considered the adsorption processes influencing CNT property change. In this case as external factors doping conditions are considered, but the internal factors are linked to the nanotube's own parameters (chirality, diameter, length, wall number, etc.). In this chapter we consider the processes connected to CNT doping by nitrogen.

CNT doping by nitrogen has been studied intensively for many years, as evidenced by the number of publications in this field (Fig. 5.1), but the problem grows wider and deeper.

It was mentioned above that the difference between doping and sorption notions is a very conventional one, and it will become evident upon examination of the nitrogen interaction with CNTs, when these two physical effects combine with one another [1–19]. In the majority of publications only the two types of the SWCNTs are considered: a graphite-like doping (when a carbon atom is displaced by nitrogen atom) and a pyridine doping, which presents a nitrogen atom's chemisorption on some SWCNT defect. Under the graphite-like doping nitrogen substitutes all three-carbon bonds (couplings), leaving one non-divided bond. Pyridine doping has different forms, corresponding to different numbers of adsorbed nitrogen atoms per one vacancy, because under this doping the nitrogen atom forms two chemical bonds with the lattice with one bond remaining absent. This situation allows us to

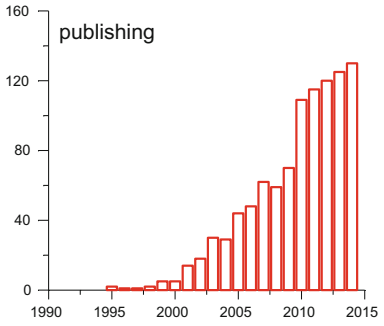

Fig. 5.1 Dynamics of the number of publications devoted to CNT doping by nitrogen

consider pyridine doping as a complex formation with a carbon vacancy in a nanotube lattice.

The nitrogen atoms can be located in the graphene and CNT lattices in various ways, creating the defects which are able to change the energetic and electrical properties of the carbonic structures under consideration. The change in their electrical properties is connected with the fact that the defect, introduced by the nitrogen atom, can exhibit both donor- and acceptor-type characteristics. The energetic property change is connected with a possible change of energetic states (levels), structure, and density. In the graphene lattice the doped nitrogen atom can be placed via more than 8 methods (i.e., positions), and therefore nitrogen in this situation can be called a super-amphoteric admixture.

The above mentioned features or peculiarities are connected with the great diversity of the nitrogen arrangement on the nanotube graphene surfaces, and it confirms a known fact that mesoscopic system properties are strongly dependent on their atoms arrangement [12, 20–28]. Nitrogen has one odd (excess) electron compared with carbon, and therefore its introduction into the lattice from the general point of view must lead to a donor-type conductivity appearance [27], but this is not a general rule [28], as is shown below.

The carbon atom lattice is formed by three σ-bonds and one π-bond. In this case graphite-like nitrogen, having five electrons, replaced a carbon atom in the graphene lattice. Such a substitution (because the last has four electrons) is a classic example of donor doping. Four from five electrons of such atom bonds create chemical bonds (three σ-bond and one π-bond), but the fifth electron remains free and gives rise to conditions of donor-type conductivity. With a pyridine-like arrangement two electrons form σ-bond and two others form p_x-bonds are filled, non-bounded states in the graphene lattice plane. The fifth electron creates a bond with neighbors and forms a filled valence zone, but without changing the conductivity characteristic. Under the pyridine-like arrangement there can arise an acceptor state due to nitrogens location near to a vacancy and loss of the carbon p_z bond under vacancy formation.

So a nitrogen atom, substituting carbon in the lattice, is similar to a donor-type atom—being located near a vacancy it is either neutral (if all vacancies are filled) or can create an acceptor state with vacancy free places. If doing so it traps hydrogen (and goes from a pyridine-like state to a pyrrole-like one) and again remains neutral. Similar conclusions were reached by other authors [10, 11, 13, 29].

It is known that nitrogen-doping can essentially affect CNT mechanical, electrical, and physical–chemical properties [7–12]. In some cases, nitrogen doping leads to a metallic conductivity [13], because the nitrogen electronic terms, as a rule, are located above the Fermi level.

From a morphological point of view nitrogen atom doping leads to the appearance and growth of so-called bamboo-type CNTs [14–19, 30]. Such nanotubes growth behavior arises because the chemical bond N–C is shorter than the C–C bond, and therefore under tube growth there arises some additional stress, that tends to decrease the growth of tube diameter [30].

The nanotube grows from a catalyst. The nanotube breaks away from it because of internal stresses. This stops the growth of the nanotube. For this reason into a formed tube a new one starts to grow and thus the tube gains a bamboo-type structure [31–41]. One of the first such growths was described by Saito [33], and later the analogous structures were observed for nanotube synthesis with the use of ammonium [35], pyridine [36], methylamine [37], thiazine [38], acetonitrile [39], dimethylformamide [40], zinc-phtalocyan [39], and cyanide [42]. One characteristic is that the structure period decreased with nitrogen concentration, as is shown in Fig. 5.6 [43]. The same explanation of the appearance of such structures was given in some other studies [44–46].

The CNT growth conditions under nitrogen doping are very different [44–54]. For example, the doped graphene layer growth was carried out by CVD-method, where temperature increased and stabilized every 20°. The prominent graphene growth was observed at 500 °C, and synchronously decreased the intensity of a peak characterizing namely the nitrogen pyridine-like substitution. Nitrogen in the graphene lattice knots appeared after annealing at a temperature of 500 °C for several hours.

In several cases some physical properties of nitrogen doped structures (e.g., emission) improved after doping [54], connected to a reduction of the yield work value for structures with a prominent π-type conductance, because in this case the Fermi level increases and changes the electronic bond characteristic (as well as lattice oscillations types too). The Raman (combination) scattering spectra are very sensitive to nitrogen presence [55–57].

The Raman scattering spectrum of CNTs is usually combined from several modes [58]. The oscillations, forming so-called radial breathing modes (RBM), seem to stretch the graphene lattice, similar to the human thorax under breathing. This mode is very sensitive to lattice diameter. The two carbon oscillations tangentially, and in opposing directions, lead to G-mode generation. It is characteristic for an ideal lattice and its intensity allows an estimate to be made of the lattice quality. This mode band consists of several near-located bands, which arise due to a non-equivalent arrangement of the lattice atoms. To these structures corresponds a two-photonic mode G'. There is a mode, arising due to defect, non-elastic interactions, denoted as D-mode. The defect number grows with nitrogen doping concentration increase, an therefore the modes intensity ratio, D/G, also grows with nitrogen concentration increase [56].

There are many methods of CNT doping during growth. Below we will consider some CVD processes and a treatment after tube fabrication. The growth conditions have an effect on the nitrogen concentration, doping the nanotube, including the fact that the content of different nitrogen types changes with CNT increased temperature change [57].

For conciseness the CVD process conditions are presented in Table 5.1. It is seen that CNTs are fabricated mostly using iron as a catalyst. The catalyst is prepared as a substrate in a form of a thin film or volatile compounds are used, such as ferrocene, etc.

Table 5.1 The conditions of CVD processes used for CNT fabrication by nitrogen doping during growth

No.	Catalyst	Gaseous mixture in reactor	T (°C)	References
1	Vermiculite:ferrous nitrate: ammonia:molybdanate in proportions: 20:100:5:1	Ar, H_2, C_2H_2, NH_3 10:5:5:3	650–800	[59]
2	MgO:Fe:Mo 20:1:0.1	CH_4:NH_3:Ar 50:10:500	850	[59]
3	Iron—10 nm	C_2H_2:NH_3:Ar	750	[60]
4	Nickel—5 nm	Ar, C_2H_2, NH_3	800	[61]
5	Iron—10 nm	Ar, C_2H_2, NH_3	800	[62]
6	Iron	Butylamine: N_2	600–900	[63]
7	Fe:Mo = 10:1	CH_4:NH_3: = 9:1	900	[64]

Often a mixture of Ar, C_2H_2, and NH_3 is used. The growth temperature changes in a wide range from 550 to 1000 °C. In this case with temperature increase the nitrogen substitution concentration increases too.

5.2 Determination of Nitrogen Atom Configuration on the Graphene Plane of a Carbon Nanotube

Nitrogen is an ideal material for substitution doping of SWCNTs, and therefore the preponderance of publications in the field of nitrogen doping of CNTs, are devoted namely to this case. As it was said above, most often, two types of nitrogen doping are considered: namely a graphite-type doping (when a carbon atom is replaced by a nitrogen atom) and pyridine doping, which is rather like a chemisorption of nitrogen atoms on a SWCNT defect. It was shown experimentally that the semiconducting SWCNT (doped by nitrogen to 2–10%) becomes metallic [66]. The authors of [67] also experimentally studied 1%-doped SWCNTs. It was found that although the graphite-type and pyridine-type nitrogen contents in samples were comparable under normal conditions, only substitution doping types can induce an *n*-type conductance in nanotubes at room temperature. In the low temperature ranges arises a factor, connected to pyridine-type doping, which suppresses *n*-type conductance. Namely, for this reason in some studies of nitrogen doped CNTs *p*-type conductance was experimentally observed. If the doping process is considered as a one carbon atom substitution (in a graphene "canvas") to a one nitrogen atom (graphite-type doping), the all sp^2-orbitals of penta-valent nitrogen are involved in the nitrogen covalent bond formation with the carbon neighboring atoms, and one remaining valent electron occupies the nitrogen p_z-orbital. This electron can easily be broken away from its parent atom and become a part of the delocalized π electrons. At room

temperature such "excessive" electrons are mostly localized (especially in semiconducting nanotubes). In the case of pyridine-type doping this nitrogen atom cannot be ionized under normal conditions, because there remains its non-divided electron pair, which does not take part in the conjugated pair formation. Thus, these two different doping types differently affect SWCNT properties.

The authors of [68] studied theoretically the nitrogen doped semiconducting SWCNT (10, 0). They found that with impurities in low concentrations (about 0.83%) the graphite-type substitution narrows the forbidden gap width. With substitution-type doping level growth, this forbidden gap width continually diminishes and finally (at 1.67% doping concentration) the SWCNT becomes metallic. The pyridine-type doping in this investigation also "transformed" the semiconducting SWCNT into metallic form—something confirmed in other studies [69]. On the other hand, studies of nitrogen doped CNT conductance in general does not allow an estimate to be made of the nitrogen concentration or a predominance of certain configurations in the doping process, because the conductivity has integral properties, characterizing only the total content of defects and impurities. For a more detailed control it is necessary to carry out some demands, connected with the regulation of growth conditions [70, 71], gas flows, and gaseous mixture content control [72–74], as well as considering a growth's defects [75]. In this connection some modern diagnostic methods were elaborated upon—these are described below.

Let us consider the methods which allow us to directly estimate the characteristics of the nitrogen interactions with a graphene plane.

Energy-filtered transmission electron microscopy (EFTEM) is a variant of transmission electron microscopy, when the image or diffraction pattern formation of the electrons, with a given range of kinetic energies, is used. The method can be used for chemical content analysis in combination with some additional techniques. In general, transmission electron microscopy is a very important method for studying the processes proceeding in nanomaterials, if they are presented in a form of thin foils, being transparent to electrons. The method gives an additional procedure for defining and analyzing the separate element arrangement on sample surfaces [69, 70, 76, 77], and is widely used for the study and analysis of CNTs [59].

The idea of the method consists of separation by filtering the scattered electrons with given energies and visualization of the scattering centers. The method's realization can be conditionally divided into several stages:

- the formation of the non-filtered scattered electron contrast;
- a contrast transformation into a spectrum;
- a separation of the spectrum by energetically selective filters;
- a transformation of the separated emission part into a non-filtered image; and
- detection of the image.

The scatterings on the different types of defects are different and therefore the results of EFTEM analysis allow us to obtain the distributions of the different defects (atoms of certain type) over the studied surface. As an example of EFTEM analysis for CNT we can consider the results of this study [59]. The experiments

demonstrate that nitrogen at the internal and external surfaces of MWCNTs is distributed uniformly

One another important analytical method, called ***X-ray photo electronic spectroscopy (XPS)***, is based on the fact that when an X-ray radiation photon is adsorbed by a substance, there is an electron with a given energy emitted, which is called photoelectron. This photoelectron's kinetic energy is defined by the bond energy onto the target atom. The photoelectron's energy can be measured using their trajectory inclinations in the electric and electromagnetic fields. Analyzing the obtained photoelectron energy spectra, one can draw certain conclusions about the predominating type of defects into the target, forming characteristic and definite chemical bonds. The kinetic energy in metals is measured from the Fermi level, but is difficult to carry out in semiconductors and dielectrics, not to mention that these substances are charging. Therefore, interpretation of the results in such cases must be performed very carefully. This relates to CNTs too.

The XPS is a standard method in doped CNT investigations. This effect spectra for nitrogen is given in many publications in the field [66, 79–101]. The method and results give a presentation about the chemical bonds arising due to an atoms interaction with CNT surfaces. Experimental results characterize nitrogen, oxygen, and phosphorus atom interaction with CNT surfaces [80]. In this study CNTs and substrate were subjected to an ionic bombardment by nitrogen molecules N_2^+ for 5 and 10 min.

One can separate several ranges of bond energies, relating and characterizing certain elements chemical bonds. At a region of 100–105 eV we see the peaks of chemical bonds, belonging to the substrate, where the nanotubes were grown. Silicon in 2p state has two peaks: 99.3 eV (connected with pure silicon) and 103.3 eV (corresponding to SiO_2). The transformation of these peaks is explained by a penetration of the element by small amounts into the substrate, where as a result Si_3N_4 compound is formed. Under a more prolonged bombardment (10 min) arises three peaks, characterizing silicon: 100.15 eV (pure silicon), 102.5 eV (silicon nitride), and 103.3 eV (silicon oxide). Thus, the bombardment affects not only the new compound formation (nitride), but transforms the pure silicon peak position. Probably it is connected with a surface defect increase, changing the pure silicon bond energy.

In the spectrum of the non-irradiated sample one can see a bond with energy 284.4 eV, characteristic of pure graphite lines, observed in CNTs. After the irradiation these lines show a small shift to the high energy region due to the advent of a covalent bond, C–N. This bond appears after nitrogen bombardment at its main energy of 398 eV. The line can be shifted up to 403 eV, due to the presence of an oxidized substrate, leading to N–O bond formation [86]. Oxygen in this case forms bonds with energies of 530–535 eV.

The studies of X-ray photoelectron spectroscopy allow us to obtain even more detailed information about the state of the nitrogen atom, interacting with the CNT, because the peaks characterizing the bonds have a fine structure which gives us a chance to judge the atom interactions and arrangement on a graphene plane [59].

The important information about solid body state and chemical bonds can be obtained from the data on the electron beam energy losses during their passage through the substance or reflections from the body surfaces. On the basis of this effect studies were elaborated using a method called ***electron energy loss spectroscopy*** **(*EELS*)** [66]. The main peak in the spectrum is connected with plasmonic losses. In the spectrum there are also observed steps (caused by ionization and atomic framework excitation) and other excitations because the energy transferred by the electron is usually small.

Thus, modern methods allow us to judge the defects and doped atom arrangements in the lattice, their interactions with each other, as well as their concentration change in connection with nanotube growing conditions. Such information allows us to carry out a fine control of the technological processes during CNT fabrication.

5.3 Analysis of Atomic Configurations and Nitrogen Electronic States on Graphene Planes of CNTs by Quantum Mechanical Methods

The authors of [66, 94–96], using the density functional method, have studied substitution type nitrogen doping of various SWNTs matrices. The simulation results have demonstrated, that for a metallic SWCNT with chiral vector (5, 5) and *armchair* structure, the impurity state is totally delocalized and the corresponding energy level is located into the nanotube conductance zone. In a semiconductor SWCNTs with chiral vector (8, 0) and *zigzag* structure, the doped nitrogen forms an impurity level, lying in the forbidden zone at 0.2 eV below the conductance zone bottom. This partially occupied (by only one electron) energy level creates an opportunity to connect two nanotubes, if they both have one carbon atom substituted by nitrogen and are converted to each other by their impurity centers. A bundle of nanotubes connected this way, can grow very quickly and tube interconnection can appreciably change the characteristics of tunneling between them.

In one study [97] the authors looked at two nitrogen doped SWCNTs (6, 0): $C_{90}N_6$ (carbon nanotube C_{96}, where 6 carbon atoms, located around one of the ends, are substituted by 6 nitrogen atoms) and $C_{84}N_{12}$ (carbon nanotube C_{96}, where 12 carbon atoms are substituted by 12 nitrogen atoms). It was shown, that nitrogen doped SWCNT (6, 0) are more stable than pure nanotubes. The authors carried out forbidden zone width calculations for two doped and one pure tube. In all three cases the HOMO–LUMO gap was so small that the tubes could be considered as conductors. However, the gap widens with a substitution of nitrogen atoms into the tube, allowing the proposition that with further nitrogen concentration growth the SWCNT can be transformed to a semiconducting state. At last, because nitrogen and carbon atom sizes are comparable, the nanotube diameter only changes a little near the nitrogen atom ring, remaining constant at some distance from ring.

From theoretical studies one interesting piece of work [98] is where the authors, using quantum mechanical methods, studied hydrogen atom chemisorption on a SWCNT (10, 0) with one carbon atom substituted by nitrogen. They found that hydrogen is preferentially adsorbed on the nitrogen atom. A pure tube is a semiconductor, and the substitution of one carbon atom to one nitrogen atom (with one weakly localized electron) leads to the appearance of a donor state near the conductance zone bottom. The hydrogen atom brings to the system one additional electron, which "fills" this semi-empty state near the conductance zone bottom with the donor state disappearing. Hence, hydrogen adsorption can make the SWNTs peculiarities "vanish", after substitution nitrogen doping.

However, not only nitrogen doping can affect nanotube conductance. Some studies showed that molecular nitrogen's physical adsorption on a CNT can also change resistance [99, 100], and this effect can be very useful for creating gas sensors on a carbon nanotube base. In an experimental investigation [101] it was found that a SWCNT array's electrical resistance increases a little after molecular nitrogen adsorption.

It was also found experimentally that an acidic treatment of a MWCNT sufficiently increased their nitrogen adsorbing energy, as well as is improving the MWCNT sorption capacitance with respect to nitrogen [102].

The calculation by quantum chemistry methods demonstrate that substitution doping is energetically more preferred than nitrogen chemisorption and pyridine doping, only for nanotubes with diameters greater than 8 nm [103].

In one piece of work [104] is theoretically considered various types of SWCNT nitrogen modification: graphite-like doping, pyridine-like doping (doping with a vacancy), external chemisorption of nitrogen atoms, and covalent $–NH_2$-functionalization. It was shown that not only doping, but chemisorption also, gives some stable conformations. It is interesting that under chemisorption the SWCNT obtains a magnetic moment.

Nitrogen and oxygen adsorption on finite length SWCNTs was simulated in [105, 106], and the authors showed that between nitrogen and the nanotube can exist a strong covalent or ionic interaction, and in this case the interaction between the nanotube and adsorbate becomes stronger with a growth in nanotube length. Moreover, it was shown that the adsorbed nitrogen increased the SWCNT conductance, but is not as evident as it is for oxygen. The possibility of a strong interaction between a SWCNT (4, 4) and oxygen, as well as a variety of nitrogen adsorption centers, was studied in [107]. The adsorption energy values were found to be 1.17 and 0.981 eV. It was shown also that there is a great influence played by the adsorbed nitrogen on SWCNT geometrical and electronic structures.

The quantum mechanical calculations from first principles [108] showed that under nitrogen doping a semiconducting nanotube becomes a metallic one. In this work nanotube stability under doping was also analyzed, as well as the change in nanotube electronic properties with pyridine-like doping by transient metal atoms.

In [109] was analyzed 15 different defect configurations, arising under the nitrogen doping. It was shown that formation of one or two, near place defects, increased the CNT forming energy, i.e., the vacancies stabilize the nanotubes.

Substitution doping by nitrogen led to the donor state appearance into a HOMO–LUMO gap, and a vacancy with three nitrogen atoms creating the acceptor states. Double vacancy with three nitrogen atoms created both acceptor and donor states.

Thus, the experimental tunneling spectroscopy method identified, just as theoretical studies demonstrated, that substitution nitrogen doping creates donor states [110]. The calculations for nanotubes (10, 10) showed electronic property strengthening of nanotubes under both pyridine-like and graphite-like doping.

Thus, all theoretical calculations carried out for nanotubes with different chirality, confirm that graphene substitution doping leads to a donor-type conductivity and can even transform a nanotube with semiconducting conductivity to one with metallic conductivity.

5.4 Simulation of Nitrogen Chemisorption on Single-Wall Carbon Nanotubes

For simulation of nitrogen chemisorption on CNTs the SWCNT (5, 0), (6, 0), (7, 0), and (8, 0) were selected. The simulation process was carried out by using a semi-empirical, quantum mechanical method (based on the framework of the Hyper Chem. Program). The length of all considered nanotubes was equal to five elementary crystalline cells (i.e., to five elementary hexagonal cycles along the tube axis). We studied the external chemisorption of one or two nitrogen atoms on SWCNTs. For the one nitrogen atom case two adsorption centers (location variants for adsorbed atoms) were proposed (Fig. 3.2, Chap. 3), and for two nitrogen atoms—four variants. The data for every such chemisorption center is presented in Table 5.2, only for stable configurations. For tubes with even chirality indices, (6, 0) and (8, 0), the nitrogen chemisorption at center 1 does not generate a stable state.

Table 5.2 Data for one nitrogen atom chemisorption on SWCNT (5, 0), (6, 0), (7, 0), and (8, 0) (center 1 corresponds to the variant in Fig. 3.2a, center 2—to the variant in Fig. 3.2b)

		(5, 0)	(6, 0)	(7, 0)	(8, 0)
Center 1	E_{tot} (kcal/mol)	−180,000		−250,000	
	Δq (e)	+0.05		−0.3	
	E_{HOMO} (eV)	−7.7		−6.2	
	E_{LUMO} (eV)	−2.9		−3.6	
	E_N (eV)	−5.7		−5.7	
Center 2	E_{tot} (kcal/mol)	−180,000	−220,172	−250,000	−290,000
	Δq (e)	−0.18	−0.32	−0.24	−0.26
	E_{HOMO} (eV)	−6.9	−7.2	−6.4	−6.1
	E_{LUMO} (eV)	−2.7	−3.9	−3.3	−3.7
	E_N (eV)	−5.0	−4.9	−5.0	−4.6

Notes: E_{tot} The total energy of the system (1N + SWCNT); Δ_q the partial charge transport to atom N; E_{HOMO} energy of HOMO; E_{LUMO} energy of LUMO; E_N the partially filled "impurity" level

Table 5.3 Total energy (E_{tot}), charge transport (Q), and HOMO–LUMO gap width (E_g) for SWCNTs (6, 0) and (8, 0)with two doping (dop) and two chemisorbed (ads) nitrogen atoms

(6, 0) + 2N-dop	**(6, 0) + 2N-ads**
E_{tot} = −202,283 (kcal/mol) Q = 0.34; 0.47 (e) E_g = 2.5	E_{tot} = −207,463 (kcal/mol) Q = −0.20; −0.01 (e) E_g = 2.3
(8, 0) + 2N-dop	**(8, 0) + 2N-ads**
E_{tot} = −269,270 (kcal/mol) Q = 0.65; 0.53 (e) E_g = 2.1	E_{tot} = −274,745 (kcal/mol) Q = −0.46; −0.20 (e) E_g = 2.6

It also follows from Table 5.3 data, that for tube (5, 0) nitrogen adsorption is energetically more preferable on center 2 and for tube (7, 0)—on center 1. From the table it can be seen that all types of nitrogen chemisorption are accompanied by a partial charge transport to the nitrogen atom, with the only exception at center 1 for tube (5, 0).

The most important implication is the fact that with the addition of one nitrogen atom to the nanotube in all cases there appears a partially filled (semi-filled) "impurity" level into forbidden zone and this sufficiently influences a tube's conductivity. For SWCNTs (5, 0) and (7, 0), in their more energetically profitable states, this "impurity" level is situated in the bottom-half of the forbidden zone, but for tubes (6, 0) and (8, 0)—it lies in the top-half. For the most stable states the adsorption energies were calculated, giving the following values: −5.89 eV for (5, 0), +2.67 for (6, 0), −2.80 for (7, 0), and −4.30 for (8, 0), i.e., for tube (6, 0) one nitrogen atom chemisorption is an endothermic process and the forming compound is a metastable one.

Below the results of calculations are presented for two nitrogen atom chemisorptions on a SWCNT. For the case of tube (5, 0) these variants are shown in Fig. 3.2 (Chap. 3). The most energetically preferable conformations for every tube are displayed in the table in bold type, and the adsorption energies are calculated per single nitrogen atom. The following values were obtained: −5.310 eV for tube (5, 0), +0.73 eV for (6, 0), −4.55 eV for (7, 0), and −4.773 eV for (8, 0). One can see, that for tube (6, 0) there again arises a situation earlier observed for one nitrogen atom.

When a state with two nitrogen atoms is characterized by a positive value of adsorption energy, it can be supposed that most likely nitrogen chemisorption on the tube (6, 0) is, in general, energetically non-profitable, i.e., it gives unstable conformations. For the all singlet states of the considered systems the "impurity" state itself was absent in the energy gap, i.e., these occupied "impurity" levels were adjoined to nanotube energetic zones.

In the systems with triplet states in the forbidden zone arises two closely located "impurity" partial filled levels, and their presence obviously changed the nanotube conductance characteristics. For the most stable (singlet) states we obtained conductances which decreased for tubes with even chirality indices (6, 0) and (8, 0) (by 30.6 and 8.7 times, correspondingly), and increased for tubes with odd chirality indices (5, 0) and (7, 0) (by 1.2 and 3.3 times).

Next, we studied substitution nitrogen doping of the above listed SWCNT types. The calculations showed that in contrast to chemisorption (when some negative charge transport to the adsorbed nitrogen atom takes place), substitution doping is connected with a positive (and greater by value) charge transport (Table 5.3).

The electronic property calculations for a lattice with a vacancy was carried out in [66] for nanotube (12, 0) with a *zigzag* structure. The vacancy generates various and sufficiently complex configurations of $V_{a,b}D_n(\sigma)$-type [66].

It was experimentally shown, that nitrogen doped (to 2–10%) semiconducting SWCNTs, become metallic [110], and graphite-like and pyridine-like nitrogen contents are comparable under standard conditions [111] in SWCNT samples with 1% nitrogen doping. It was shown also that a graphite-type substitution doping can induce, in a nanotube, an *n*-type conductance at room temperature. In the low-temperature range a dominant role is played by a factor connected with pyridine-type doping, suppressing the *n*-type conductance, and namely for this reason making it possible to observe experimentally a *p*-type conductance in nitrogen doped SWCNT samples. If nitrogen doping is considered as one carbon atom substitution in a graphene "canvas" of fabric (it is graphite-like doping), then all five valence electron sp^2-orbitals are involved in covalent bonds forming with neighboring carbon atoms, with the remaining valence electron occupying the nitrogen p_z-orbital. This electron can easily be removed from the atom. It becomes one of the delocalized π electrons. At room temperatures the large share of such "excess" electrons are localized (especially in semiconductive nanotubes). In the case of pyridine-type doping it is impossible to ionize nitrogen under normal conditions, because there remains a non-divided electron pair, which is not involved in the conjugated bond formation. Thus, these two different doping modes differently affect the SWCNT properties.

The nitrogen-doped semiconductive SWCNT (10, 0) behavior was theoretically studied in [112], and it was found that at low concentrations of doping admixture (about 0.83%) the graphite-like doping narrows the forbidden zone width. The following rise in substitution-type doping content led to a continued decrease in the forbidden zone width, and finally (at 1.67% doping) the SWCNT becomes "metallic". Pyridine-type doping in this investigation also "transfers" the semiconductive SWCNT into a metallic state.

The authors of [113] studied nitrogen substitution doping in various types of SWCNT, using the functional density method. The simulation results showed that for a metallic SWCNT (5, 5) with an *armchair* structure the impurity state is totally delocalized and the corresponding energy level is located into the nanotube conductance zone. This partially occupied (by one electron) energy level gives the possibility, for example, to connect two nanotubes as if they both have a common carbon atom (substituted by a nitrogen atom), and these tubes are directed to each other by impurity doped centers. Bundles of SWCNTs, where nanotubes are connected in this way, can be very strong. On the other hand, this bond between the tubes can very likely sufficiently change the characteristics of the tunneling processes between them.

In one piece of work [107] it was established that a nitrogen doped SWCNT (6, 0) is even more stable than a pure nanotube. The authors presented the calculated values of the forbidden energy gap width for doped and pure tubes. In all cases the HOMO–LUMO gap width was very small (and this fact allows consideration of the tubes as conductive), but it widened with an increase of the substitution of nitrogen atoms in the nanotube. Therefore, one can suppose that following nitrogen atom concentration growth in this SWCNT it will become a semiconductor substance. Finally, because the carbon and nitrogen atom sizes are comparable, the nanotube diameter changes only near nitrogen atom rings, remaining practically constant even at a small distance from it.

The quantum mechanical calculations showed also that substitution doping is energetically more preferable (as compared with nitrogen chemisorption and pyridine doping) only for nanotube diameters greater than 8 nm [64].

Various variants of SWCNT nitrogen modifications, such as graphite-like doping, pyridine doping (i.e., doping with a vacancy), external nitrogen chemisorption of adsorbed nitrogen atoms, and covalent $–NH_2$-functionalization, were studied theoretically in [109]. The authors [109] showed that not only doping, but chemisorption too, produces stable conformations. It is of interest that after nitrogen chemisorption SWCNTs obtain some magnetic moment.

Nitrogen and oxygen adsorption on finite length SWCNTs were simulated in papers [64, 107, 113], where it was shown that there exists a strong covalent or ionic interaction between a nitrogen atom and nanotube. As this takes place the interaction between nanotube and adsorbate strengthens with tube length increase. Moreover, it was found that the adsorbed nitrogen increases the conductivity of nanotubes, but not so obviously as oxygen. The possibility of a strong interaction between a SWCNT (4, 4) and nitrogen, as well as a variety of nitrogen adsorption centers was shown in [64]. The adsorption energy, depending on the distance from the adsorption center, was equal to 1.17 and 0.981 eV. It was shown also, that the adsorbed nitrogen can have a profound effect on the SWCNT's geometrical and electronic structures.

5.5 Nitrogen Chemisorption Simulation for Nanotubes with Stone-Wales Defects

It was shown above, that the impurity atoms, in the presence of structural defects in SWCNTs, are more likely adsorbed at defect places. In this chapter is considered one of the most important SWCNT defects, namely the so-called Stone-Wales defect (SW defect). They generate into the SWCNT structure a combination of two pentagons and two heptagons. For this study two nanotubes were chosen: (6, 0) and (8, 0), with every length of five elementary cycles considered. The HOMO–LUMO gap width (for pure, without defect, and optimized SWCNTs of this length) were found to be equal to 2.3 and 2.6 eV, correspondingly. For every tube two situations

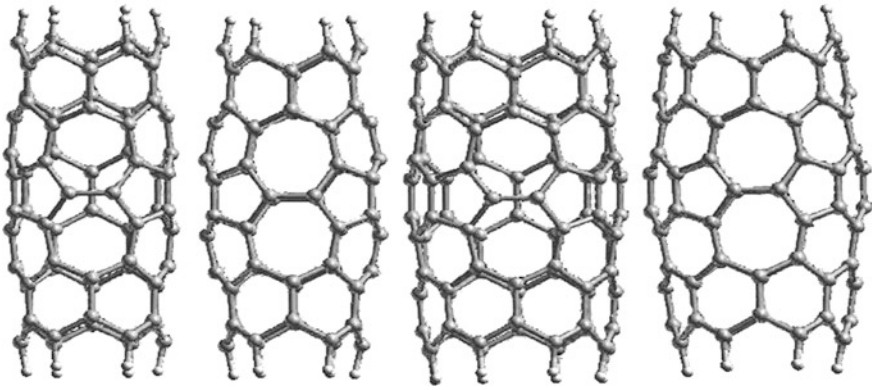

Fig. 5.2 The models of nanotubes with Stone-Wales defects. From *left* to *right* are presented nanotubes: (6, 0) with one SW defect; (6.0) with two SW defects; (8, 0) with one SW defect; (8, 0) with two SW defects

were simulated, namely with one SW defect and two SW defects, being arranged diametrically symmetrical (Fig. 5.2).

For a SWCNT–1SW (6, 0) tube the forbidden zone width equals 2.8 eV, for SWNT–2SW (6, 0) it was 3.1 eV, i.e., the defect presence really does increasing the forbidden zone width. Variants with two defects, SWNT–1SW (8, 0) and SWNT–2SW (8, 0), have values of 2.64 and 2.57 eV, i.e., one defect increased the gap width only a little, but two defects (arranged diametrically symmetrical) decrease this parameter.

Let us consider a chemisorption of one or two nitrogen atoms on a SWCNT (8, 0) with length of five elementary cells and one or two Stone-Wales defects. Initially, different adsorption centers for the nanotubes were considered. In Fig. 5.3 the three most energetically profitable configurations with one SW defect are

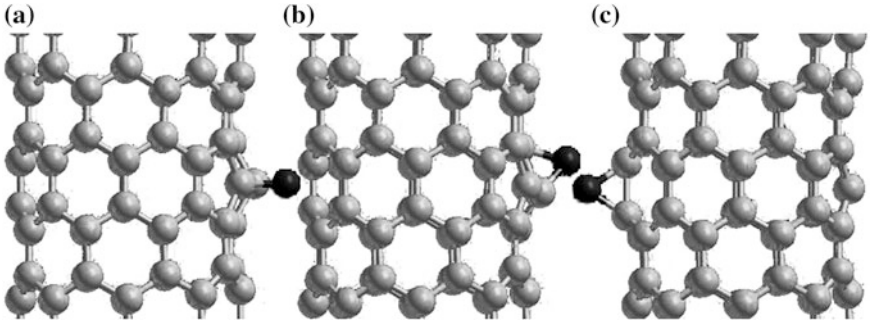

Fig. 5.3 Three different centers of nitrogen atom chemisorption on a SWCNT (8, 0) with one SW defect. Center (**a**) corresponds to the adsorption above the defect bond; center (**b**)—to adsorption over the heptagon surface, nearest to the defect bond; center (**c**)—to adsorption over the bond, C–C, located along the nanotube axis at the side, being diametrically opposite to the defect side

Table 5.4 Data for one nitrogen chemisorption on a SWCNT (8, 0) with one SW defect [(*a*), (*b*) and (*c*) correspond to atom location in Fig. 5.3]

	E_{tot} (Kcal/mol)	Δ_q (e)	E_g (eV)	E_{HOMO} (eV)	E_{LUMO} (eV)	E_N (eV)	E_{ads} (eV)
(*a*)	−290,000	−0.35	2.75	−6.48	−3.73	−5.10	−2.66
(*b*)	−290,000	−0.31	2.80	−6.54	−3.73	−4.86	−1.59
(*c*)	−290,000	−0.35	2.75	−6.48	−3.73	−5.18	−1.42

Notes: E_{tot} Total energy of system 1N + SCNT; Δq the partial charge transport to nitrogen atom; E_g energy gap width; E_{HOMO} energy of HOMO, E_{LUMO} energy of LUMO; E_N partially filled "impurity" energy level; E_{ads} adsorption energy

presented (the adsorption parameters of the corresponding configurations are given in Table 5.4).

The data presented in Table 5.4 shows that the most preferable place for adsorption into a nanotube with one SW defect is a center near the defect (*a*). Note, that the defect presence itself increases the tube adsorption capacitance. Because the system's multiplicity is equal to two, into the SWCNT forbidden zone appears a partially filled impurity level. In the most energetically preferred situation (*a*) this level is located practically in the middle, between HOMO and LUMO.

Let us study the chemisorption of two nitrogen atoms on a SWCNT (8, 0) with one SW defect. The most energetically preferable conformations and adsorption parameters are presented in Fig. 5.4, the calculation results are given in Table 5.5.

For each of these configurations we consider two states (singlet and triplet). It was established that only configuration (*b*) in Fig. 5.4 (where two nitrogen atoms are located on adjacent carbon lattice bonds) has a stable state with total spin equal to 1, whereas for the defect-less SWCNT, when there are two stable states: with spin $S = 1$ and spin $S = 0$, and also the former is energetically more profitable.

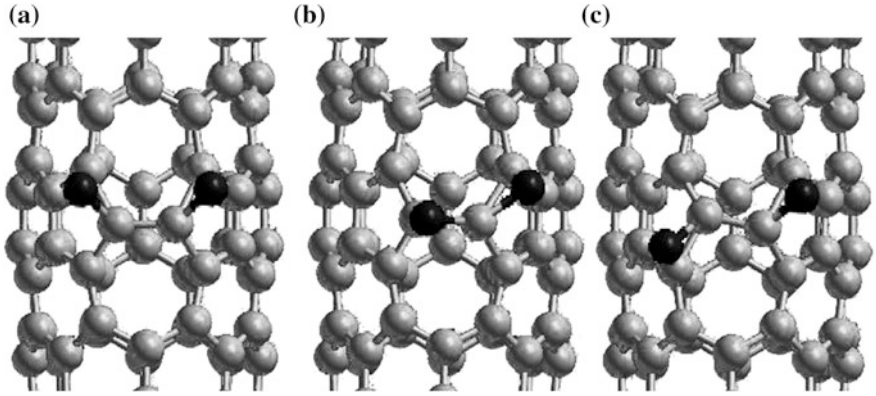

Fig. 5.4 The variants of two nitrogen atom chemisorption on a SWCNT (8, 0) with one SW defect

Table 5.5 Data describing two nitrogen atom chemisorption on a SWCNT (8, 0) with one SW defect [(a), (b), and (c) correspond to the atom arrangement in Fig. 5.4]

	E_{tot} (kcal/mol)	Δq (e)	E_g (eV)	E_{HOMO} (eV)	E_{LUMO} (eV)	E_{ads} (eV)	E_N (L-SOMO) (eV)	E_N (H-SOMO) (eV)
(*a*), $\sigma = 1$	−290,000	−0.32	2.38	−6.42	−4.04	−1.67		
(*b*), $\sigma = 1$	−290,000	−0.32	2.62	−6.48	−3.86	−1.42		
(*b*), $\sigma = 3$	−290,000	−0.33	3.02	−6.95	−3.94	−1.63	−5.21	−5.08
(*c*), $\sigma = 1$	−290,000	−0.23	2.70	−6.50	−3.80	−1.44		

Notes: E_{tot} Total energy of the system (1N–SWNT); Δq a partial charge transport to atom N; E_g energy gap width; E_{HOMO} energy of HOMO; E_{LUMO} energy of LUMO; E_N a partially filled "impurity" energetical level (for a singlet case); E_N (L-SOMO) lower partially filled level; E_N (H-SOMO) upper partially filled level

The results in Table 5.5 demonstrate that chemisorption on different centers of tube (8, 0) with defects can differently affect tube conductance, increasing and decreasing the energy gap width or creating within the gap a pair of closely located semi-filled levels. In general it is seen that for all conformations the energetically most preferable is a singlet (*a*), for which it is characteristic that the energy gap width decreases compared with a pure defect tube (8, 0). This is shown by a conductance increase of 10.1 times (in this connection it can be recalled that two nitrogen atom chemisorption on a defect-less tube (8, 0) decreases its conductance 8.7 times).

The data analysis showed that the presence of Stone-Wales defects affects both the SWCNT properties and nitrogen atom chemisorption on their surface. Moreover, not only do numerical values of parameters (HOMO-LUMO gap width, adsorption energy) change, but there is a general tendency toward change.

The presented results of our calculations indicate that in real conditions with any nitrogen chemisorption experimental study the presence of a defect will have a strong impact on the results. It is possible that the defect's influence can explain the wide scatter of existing published experimental data.

5.6 Thermodynamics of the Nitrogen Physical Adsorption Processes on Carbon Nanotubes

All the atoms in a nanotube are arranged on the surface and are in contact with the environment. This situation is preserved for multi-wall tubes, because the atoms and molecules of other substances can penetrate through the walls of different nanotubes. For this reason the nanotubes always have many non-equivalent sites of adsorption, and therefore their experimental adsorption isotherms can have several line segments.

In the model, proposed in Sect. 2.4, a situation is considered, when in the CNT environment medium has only one adsorbate of α-type (in our case it is molecular nitrogen). It is supposed also, that the medium, under given conditions, can contain only a fixed content of the adsorbate. In gaseous phase, this corresponds to the condensation start point; in solutions—to the saturation point. The limiting number of particles, able to be located in the external medium, we will call the places, N^{N}. The real particle number in gaseous phase is smaller and equals $N_{\mathrm{N}}^{\mathrm{N}}$. In an ideal gas medium the particle concentration can be expressed in terms of pressure in the following form:

$$N^{\mathrm{N}} = p_{\mathrm{s}}^{\mathrm{N}}/kT, \quad N_{\mathrm{N}}^{\mathrm{N}} = p^{\mathrm{N}}/kT, \tag{5.1}$$

where p^{N} is the nitrogen partial pressure and $p_{\mathrm{s}}^{\mathrm{N}}$ is the partial pressure of its saturated vapor.

As an adsorption consequence the adsorbate particles are trapped on the adsorbing surface places or on the places located over the nanotube's corresponding chemical bonds. The number of such places is equal to N^{β} (below we will consider the statistical probability of this process). The number of adsorbate particles trapped on these places is N_{N}^{β} (notation is demonstrating that the nitrogen molecule is occupying a place over the chemical bond of "β"-type.

In Sect. 2.4 the expressions for the adsorption isotherm were derived in the forms (Fig. 5.5):

$$N_{\mathrm{N}}^{\mathrm{N}} = a_{\mathrm{N}} N^{\mathrm{N}} \exp\left(-\frac{g_{\mathrm{N}}^{\mathrm{g}} - \mu_{\mathrm{N}}^{0}}{kT}\right), \tag{5.2}$$

$$N_{\mathrm{N}}^{\beta} = a_{\mathrm{N}} N^{\beta} \exp\left(-\frac{g_{\mathrm{N}}^{\beta} - \mu_{\mathrm{N}}^{0}}{kT}\right) \tag{5.3}$$

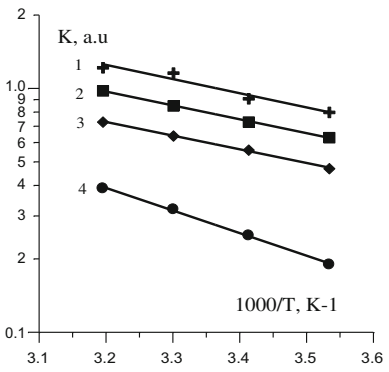

Fig. 5.5 Isotherms of nitrogen's physical adsorption at various external nitrogen pressures (atm): *1* 8; *2* 6; *3* 4; *4* 2

Thus, the adsorbed molecule concentration is proportional to the nitrogen activity in gaseous phase and depends on the adsorbate temperature and properties (which are defined by its partial free energy of adsorption and appearance in a gaseous phase). Formulas (5.2) and (5.3) allow us to obtain several other useful relationships.

In the first place, we can write out the coefficient of adsorbate molecule distribution between gaseous and condensed phases:

$$\frac{N_{\mathrm{N}}^{\beta}}{N_{\mathrm{N}}^{\mathrm{N}}} = \frac{N^{\beta}}{N^{\mathrm{N}}} \exp\left(- \frac{g_{\mathrm{N}}^{\beta} - g_{\mathrm{N}}^{\mathrm{g}}}{kT} \right) = kT \frac{N^{\beta}}{p_{\mathrm{s}}^{\mathrm{N}}} \exp\left(- \frac{g_{\mathrm{N}}^{\beta} - g_{\mathrm{N}}^{\mathrm{g}}}{kT} \right) \tag{5.4}$$

In the second part of the relationship given in (5.4) the Clapeyron formula is used. It follows from (5.4) that the distribution coefficient is defined by the saturation vapor pressure of the element in gaseous phase, the adsorption place number, and partial free energies of the adsorption element and its generation in a gaseous phase.

Second, relationship (5.4) allows us to obtain the adsorption isotherm:

$$C_{\alpha}^{\beta} = \frac{N_{\alpha}^{\beta}}{N^{\beta}} = p^{\alpha} K_{\alpha}^{\beta}. \tag{5.5}$$

We can define the parameters connected with nitrogen's physical adsorption using this formula. The calculated values are presented in Fig. 5.5.

The experimental data in Fig. 5.5 shows that adsorption proceeds at least on two types of place or site. At lower pressure the places are occupied with the activation energy of physical adsorption which equals 0.18 eV. With pressure increase these places fill, and there begins an adsorption on the other place, having an adsorption activation energy equal to 0.11 eV.

These results are a preposition, that CNTs under physical adsorption bind molecules in several places, being non-equivalent from an energy point of view.

5.7 Thermodynamics of Carbon Nanotube Doping by Nitrogen

The study of some process thermodynamics allows us to determine the conditions and parameters corresponding to stable state existence for a system under consideration. The conditions are technological process operating regimes, and the parameters are some fundamental properties of both adsorbent and adsorbate. Nitrogen doping of CNTs is characterized by several specific features: first, it can be carried out not only during the crystal growth process, but also by a treatment of ready nanotubes; second, nitrogen creatings a great number of the defect conformations with its own participation, and besides these defects can have a varying

nature (some of them are neutral, but there are donors and acceptors too). The problem of nitrogen doping in our case is difficult enough, but it can be solved by the Gibbs free energy minimization method [65, 115–118].

We will consider a thermodynamic system in equilibrium state, whose conditions (temperature and pressure) corresponding to nanotube growth. This system consists of two interconnected subsystems: gaseous phase and condensed phase (in a form of nanotubes).

Regardless of the molecules aggregate state, it is possible to separate the number of places and molecules. In a condensed solid phase (such as a system of increasing nanotubes), all the places are occupied by particles and therefore these numbers are equal. It must be noted also, that the process is run very slowly (as compared, for example, with pyrolysis), so that it does not violate the fully formed equilibrium of the system.

Let us consider the gaseous phase, where the pyrolysis processes are running, resulting in an equilibrium content (numbers) of carbon and nitrogen atoms. In an ideal gas medium these numbers can be expressed by the pressure values in the form:

$$N_{\mathrm{g}}^{\mathrm{C}} = p_{\mathrm{s}}^{\mathrm{C}}/kT, \quad N_{\mathrm{C}}^{\mathrm{g}} = p^{\mathrm{C}}/kT, \tag{5.6}$$

where p^{C} is the partial pressure and $p_{\mathrm{s}}^{\mathrm{C}}$ is the partial pressure of saturated vapor. Analogously for nitrogen, we have:

$$N_{\mathrm{g}}^{\mathrm{a}} = p_{\mathrm{s}}^{\mathrm{a}}/kT, \quad N_{\mathrm{a}}^{\mathrm{g}} = p^{\mathrm{a}}/kT \tag{5.7}$$

where p^{a} is the partial pressure and $p_{\mathrm{s}}^{\mathrm{a}}$ is the partial pressure of saturated vapor.

Formulas (5.6) and (5.7) are derived from the so-called gas cell model, in the framework of which every gaseous molecule occupies a certain volume. Saturation in the considered system is achieved when gas is condensing (it is called the dew point), i.e., all the volume is filled by a given type of molecules. At this moment, one can estimate the volume occupied by one molecule by dividing the total volume by the molecule number. The molecule number as a unit volume is defined by the gas saturated vapor pressure. Thus, the gas volume can be broken into some cells having volumes equal to one molecule's volume in saturated vapor. The gas molecules occupy a part of these cells, but a part remains free. Namely, the total cell number for the gas molecules is called the place number. This number, as was said above, is equal to the volume filled by the gas divided by one molecule's volume, defined by the saturated vapor pressure. This definition is very convenient because the saturated vapor pressure is a tabulated value.

A very important role is played by *conservation laws*. The nitrogen's behavior under doping is sufficiently complicated, because it can take various positions in the CNT graphene lattice and forms different types of complexes. Therefore, before identifying and describing the conservation laws, let us construct a table,

Table 5.6 Atoms and defects in gaseous phase and within the graphene lattice

Particles	Places				
	Gaseous phase		In the graphene lattice		Total particles number
	Carbon	Nitrogen	In lattice nodes	On bonds	
Point defects					
Carbon	N_C^g		N_C^C	N_{CSW}^{σ}	N_C
Nitrogen		N_a^g	$N_a^C + N_D^C + N_{pD}^C$	N_a^{σ}	N_a
Vacancies	N_V^{gC}	N_V^{ga}	$N_V^C + N_D^C$	N_V^{σ}	N_V
Total place number	N_g^C	N_g^a	N^C	N^{σ}	N

characterizing the place and position of the atoms and defects within the system (Table 5.6).

The gas phase is conveniently divided into cells, which can take carbon and nitrogen atoms independently. The method of gaseous phase division into the cell is itself is a very formal one. Such division allows us to separate the places available to be occupied by molecules. The cells, assigned to the different gas molecules, according Dalton's law, are independent from each other. The numbers of cells and carbon or nitrogen atoms are defined by (5.6) and (5.7). From a formal point of view, if there are filled cells in gaseous phase, there will be empty ones. Let us denote the number of nitrogen empty cells in a gaseous phase as: N_V^{ga}, then the number of the empty carbon cells is N_V^{gC}(these designations must not affect the calculation results). In the graphene lattice nodes are located at various atoms presented as independent structural units or as the parts of other complexes. Let us consider them.

N_C^C is a carbon atom located in the graphene lattice node. It is a component of the ideal lattice.

N_a^C is a doping nitrogen atom located in a lattice angle (graphite-like substitution). The above given analysis has shown that such atom is a donor.

N_V^C is a vacancy (an absence of a carbon atom in its own node). This defect is neutral itself, but promotes the complex formation processes, when other compound defects form.

N_D^C is double vacancy, this defect is occupying two nodes, but it can be consider as a defect having a center in one node and a second vacancy around it, occupying three equivalent positions. For the calculations of the configuration entropy it is necessary to account for the fact that this defect is a triple degenerated one (from a spatial point of view).

$N_{\mathrm{p}}^{\mathrm{C}}$ is a nitrogen atom location of pyridine-type, i.e., in the neighborhood of a carbon node. According to literature data, it is supposed that around such a vacancy are located three nitrogen atoms (in the nearest carbon nodes).

$N_{\mathrm{pD}}^{\mathrm{C}}$ is a nitrogen arrangement in the nodes, nearest to a double vacancy, leading to acceptor-type doping. This fact often is not taken into account during the analysis of experimental results, and therefore we singled it out separately.

N_{V}^{σ} is the vacancies on the bonds, which testifies that this bond is not taking part in the adsorption processes and is not deformed—as a result such bonds are characteristic for the ideal graphene lattice.

$N_{\mathrm{CSW}}^{\sigma}$ is a neutral defect (of SW type), connected with a bond turn, as was described above. Appearance of such effects change the lattice's energetics and promote an increase growth in doping atom concentration.

N_{a}^{σ} is a nitrogen chemisorbed on a graphene lattice bond. The lower index describes the place number where the defect can be located.

5.7.1 The Laws of Conservation of Place Number

It was said above, that objects under consideration can be located in the gas phase cells, the graphene lattice nodes of CNTs, and on the chemical bonds. Therefore, we can obtain the laws of place number conservation by summation over the columns of Table 5.6. There are three types of place (in gaseous phase, on nodes, and on chemical bonds), so the place number conservation laws are described by three equations, which can be formulated as additional conditions used for a free energy functional minimization:

$$\begin{aligned}
&\varphi^{\mathrm{ga}} = \lambda^{\mathrm{ga}}\left(N_{\mathrm{g}}^{\mathrm{a}} - N_{\mathrm{a}}^{\mathrm{g}} - N_{\mathrm{V}}^{\mathrm{ga}}\right); \varphi^{\mathrm{gC}} = \lambda^{\mathrm{gC}}\left(N_{\mathrm{g}}^{\mathrm{C}} - N_{\mathrm{C}}^{\mathrm{g}} - N_{\mathrm{V}}^{\mathrm{gC}}\right),\\
&\varphi^{\mathrm{C}} = \lambda^{\mathrm{C}}\left(N^{\mathrm{C}} - N_{\mathrm{C}}^{\mathrm{C}} - N_{\mathrm{a}}^{\mathrm{C}} - N_{\mathrm{V}}^{\mathrm{C}} - N_{\mathrm{p}}^{\mathrm{C}} - N_{\mathrm{D}}^{\mathrm{C}} - N_{\mathrm{pD}}^{\mathrm{C}}\right),\\
&\varphi^{\sigma} = \lambda^{\sigma}\left(N^{\sigma} - N_{\mathrm{a}}^{\sigma} - N_{\mathrm{V}}^{\sigma}\right),
\end{aligned} \tag{5.8}$$

where $\lambda^{\mathrm{ga}}, \lambda^{\mathrm{gC}}, \lambda^{\mathrm{C}}$, and λ^{σ} are the indefinite Lagrange multipliers, having in our problem the following meanings described below.

5.7.2 The Laws of Conservation of Particle Number

The arrangement of objects is presented in Table 5.6. They are the carbon atoms (occupying their places in nodes), nitrogen atoms (built in by a graphite-type substitution), and nitrogen atoms (build in by a pyridine-type substitution and forming a complex with a carbon vacancy), etc. Thus, the conservation law number is equal to the atom and defect type number. In the present case, we consider the arrangements of two atom types and four types of defects, so that the conservation laws can be written by summation over the rows of Table 5.6:

$$\begin{aligned}\varphi_{\mathrm{C}} &= \lambda_{\mathrm{C}}\left(N_{\mathrm{C}} - N_{\mathrm{C}}^{\mathrm{g}} - N_{\mathrm{C}}^{\mathrm{C}} - N_{\mathrm{CSW}}^{\sigma}\right),\\ \varphi_{\mathrm{V}} &= \lambda_{\mathrm{V}}\left(N_{\mathrm{V}} - N_{\mathrm{V}}^{\mathrm{g}} - N_{\mathrm{V}}^{\mathrm{C}} - N_{\mathrm{V}}^{\sigma} - N_{\mathrm{D}}^{\mathrm{C}}\right),\\ \varphi_{\mathrm{a}} &= \lambda_{\mathrm{a}}\left(N_{\mathrm{a}} - N_{\mathrm{a}}^{\mathrm{g}} - N_{\mathrm{a}}^{\mathrm{C}} - N_{\mathrm{a}}^{\sigma} - N_{\mathrm{p}}^{\mathrm{C}} - N_{\mathrm{pD}}^{\mathrm{C}}\right).\end{aligned} \tag{5.9}$$

5.7.3 The Law Charge Conservation

The graphite-type substituted nitrogen atom creates free electrons, but being substituted by a pyridine-type arrangement, creates free holes. Nitrogen chemisorption leads to donor-type doping. Accounting for all these features the charge conservation law must be written in the form:

$$\varphi_{\mathrm{e}} = \lambda_{\mathrm{e}}\left[n - p - \left(N_{\mathrm{a}}^{\mathrm{C}} - n_{\mathrm{a}}^{\mathrm{C}}\right) - \left(N_{\mathrm{a}}^{\sigma} - n_{\mathrm{a}}^{\sigma}\right) + n_{\mathrm{p}}^{\mathrm{C}} + n_{\mathrm{pD}}^{\mathrm{C}}\right] \tag{5.10}$$

5.7.4 Configuration Entropy of the System

Identifying the thermodynamic probability and further calculating the configuration entropy of our system, we must to take into account all the carbon and nitrogen atom arrangements over the places in gaseous phase, as well as all the above listed object arrangements over their positions in the CNT nodes and on the chemical bonds of these nodes. Moreover, it is necessary to account for the electron arrangements over the defects taking part in the formation of donor and acceptor bonds. The probabilities of such arrangements can be described by a product of several cofactors:

$$W = W^{\mathrm{g}} W W^{\sigma} W_{\mathrm{V}}^{\mathrm{p}} W_{\mathrm{p}}^{\mathrm{C}} W_{\mathrm{a}}^{\mathrm{C}} W_{\mathrm{a}}^{\sigma} W^{\mathrm{n}} W^{\mathrm{p}} \tag{5.11}$$

The factors meaning and concrete forms are explained below.

The first factor W^{g} is the probability of the carbon and nitrogen atom arrangement being in gaseous phase and has a form:

$$W^{g} = \frac{N_{g}^{C}!}{N_{C}^{g}!\left(N_{g}^{C} - N_{C}^{g}\right)!} \frac{N_{g}^{a}!}{N_{a}^{g}!\left(N_{g}^{a} - N_{a}^{g}\right)!} \tag{5.12}$$

In order to write the expression of the thermodynamic ability of an object's arrangement (or disposition) over a graphene lattice node it must be taken in account that nitrogen is displacing carbon from the graphene lattice, and therefore it must be arranged namely on the places occupied by carbon, which are denoted as N_{C}^{C}. In this case the required ability has the form:

$$W = \frac{N_{C}^{C}!}{\left(N_{C}^{C} - N_{a}^{C} - N_{V}^{C} - N_{D}^{C}\right)!N_{a}^{C}!N_{V}^{C}!N_{D}^{C}!} \tag{5.13}$$

The thermodynamic ability of the object's arrangement over the places on the chemical bonds of a graphene lattice has the form:

$$W^{\sigma} = \frac{N^{\sigma}!}{N_{CSW}^{\sigma}!N_{a}^{\sigma}!\left(N^{\sigma} - N_{CSW}^{\sigma} - N_{a}^{\sigma}\right)!} \tag{5.14}$$

The probability of the pyridine-type arrangement complex formation for vacancies and double vacancies is equal to:

$$W_{V}^{p} = \frac{N_{V}^{C}!}{N_{p}^{C}!\left(N_{V}^{C} - N_{p}^{C}\right)!} \frac{N_{D}^{C}!}{N_{pD}^{C}!\left(N_{D}^{C} - N_{pD}^{C}\right)!} \tag{5.15}$$

The probability of the electron arrangement over the donors and acceptors is equal to:

$$W_{p}^{C}W_{a}^{C}W_{a}^{\sigma}W^{n}W^{p} = \frac{N_{H}^{n}}{n!}\frac{N_{L}^{p}}{p!}\frac{N_{p}^{C}!}{n_{p}^{C}!\left(N_{p}^{C} - n_{p}^{C}\right)!}\frac{N_{pD}^{C}!}{n_{pD}^{C}!\left(N_{pD}^{C} - n_{pD}^{C}\right)!}\frac{N_{a}^{C}!}{n_{a}^{C}!\left(N_{a}^{C} - n_{a}^{C}\right)!}\frac{N_{a}^{\sigma}!}{n_{a}^{\sigma}!\left(N_{a}^{\sigma} - n_{a}^{\sigma}\right)!} \tag{5.16}$$

The configuration entropy of the system, according to Boltzmann's formula, is defined by the thermodynamic probability (5.11) in the form:

$$S_{conf} = k \ln W.$$

The free energy of the system can be written as:

$$G = H - TS = g_{\mathrm{C}}^{\mathrm{g}} N_{\mathrm{C}}^{\mathrm{g}} + g_{\mathrm{a}}^{\mathrm{G}} N_{\mathrm{a}}^{\mathrm{g}} + g_{\mathrm{C}}^{\mathrm{C}} N_{\mathrm{C}}^{\mathrm{C}} + g_{\mathrm{a}}^{\mathrm{C}} N_{\mathrm{a}}^{\mathrm{C}} + g_{\mathrm{V}}^{\mathrm{C}} N_{\mathrm{V}}^{\mathrm{C}} + g_{\mathrm{D}}^{\mathrm{C}} N_{\mathrm{D}}^{\mathrm{C}} + g_{\mathrm{p}}^{\mathrm{C}} N_{\mathrm{p}}^{\mathrm{C}} + g_{\mathrm{pD}}^{\mathrm{C}} N_{\mathrm{pD}}^{\mathrm{C}} + g_{\mathrm{CSW}}^{\sigma} N_{\mathrm{CSW}}^{\sigma} + g_{\mathrm{CSW}}^{\xi} N_{\mathrm{CSW}}^{\sigma} + \varepsilon_{\mathrm{a}}^{\mathrm{C}} \left(N_{\mathrm{a}}^{\mathrm{C}} - n_{\mathrm{a}}^{\mathrm{C}} \right) + \varepsilon_{\mathrm{a}}^{\sigma} \left(N_{\mathrm{a}}^{\sigma} - n_{\mathrm{a}}^{\sigma} \right) - n_{\mathrm{p}}^{\mathrm{C}} \varepsilon_{\mathrm{p}}^{\mathrm{C}} - n_{\mathrm{pD}}^{\mathrm{C}} \varepsilon_{\mathrm{pD}}^{\mathrm{C}} - TS_{\mathrm{conf}} \quad (5.17)$$

In formula (5.17), for every object, the partial Gibbs potentials are introduced, which characterize the growth of the system energy per single object of the types listed below:

$g_{\mathrm{C}}^{\mathrm{C}}$ is the Gibbs partial potential chemical bond of the graphene lattice;

$g_{\mathrm{a}}^{\mathrm{C}}$ is the Gibbs partial potential of the graphite-type substitution; $g_{\mathrm{p}}^{\mathrm{C}}, g_{\mathrm{pD}}^{\mathrm{C}}$ is the Gibbs partial potential of the pyridine-type defect with vacancy and divacancy;

$g_{\mathrm{V}}^{\mathrm{C}}$, $g_{\mathrm{D}}^{\mathrm{C}}$ is the Gibbs partial potential of the formation of a vacancy and double vacancies on the nanotube lattice node;

g_{a}^{σ} is the Gibbs partial potential of chemisorptions, t;

$g_{\mathrm{CSW}}^{\mathrm{C}}$ is the Gibbs partial potential of Stone-Wales defect formation;

$\varepsilon_{\mathrm{a}}^{\mathrm{C}}, \varepsilon_{\mathrm{a}}^{\sigma}$ is the energy of donor-type defect ionization under nitrogen addition by graphite-type substitution or under chemisorption; and

$\varepsilon_{\mathrm{p}}^{\mathrm{C}}$, $\varepsilon_{\mathrm{pD}}^{\mathrm{C}}$ is the energy of acceptor defect ionization under nitrogen addition by pyridine-type substitution at a vacancy or divacancy.

Let us consider the *Gibbs energy minimization* problem. The method used was earlier repeatedly described in publications [58, 115–118]. In order to get the functional, for which a minimization procedure must be carried out, it is necessary to add to the free energy expression (5.17) some functional conditions with the indefinite Lagrange multipliers. These conditions are following from the conservation laws (5.8), (5.9), and (5.10):

$$\Phi = G + \varphi^{ga} + \varphi^{\mathrm{gC}} + \varphi^{\mathrm{C}} + \varphi^{\sigma} + \varphi_{\mathrm{c}} + \varphi_{\mathrm{a}} + \varphi_{\mathrm{V}} + \varphi_{\mathrm{D}} + \varphi_{\mathrm{p}} + \varphi_{\mathrm{pD}} + \varphi_{e}. \quad (5.18)$$

Let us rewrite the entropy expression in line with formulas (5.11)–(5.16), for which purpose let us take away the factorials, using Stirling's formula. The functional, that must be minimized, has the form:

$$
\begin{aligned}
\Phi = {} & g_{\mathrm{C}}^{\mathrm{g}} N_{\mathrm{C}}^{\mathrm{g}} + g_{\mathrm{a}}^{\mathrm{g}} N_{\mathrm{a}}^{\mathrm{g}} + g_{\mathrm{C}}^{\mathrm{C}} N_{\mathrm{C}}^{\mathrm{C}} + g_{\mathrm{a}}^{\mathrm{C}} N_{\mathrm{a}}^{\mathrm{C}} + g_{\mathrm{V}}^{\mathrm{C}} N_{\mathrm{V}}^{\mathrm{C}} + g_{\mathrm{D}}^{\mathrm{C}} N_{\mathrm{D}}^{\mathrm{C}} + g_{\mathrm{p}}^{\mathrm{C}} N_{\mathrm{p}}^{\mathrm{C}} \\
& + g_{\mathrm{pD}}^{\mathrm{C}} N_{\mathrm{pD}}^{\mathrm{C}} + g_{\mathrm{a}}^{\sigma} N_{\mathrm{a}}^{\sigma} + g_{CSW}^{\sigma} N_{CSW}^{\sigma} + \varepsilon_{\mathrm{a}}^{\mathrm{C}} \left(N_{\mathrm{a}}^{\mathrm{C}} - n_{\mathrm{a}}^{\mathrm{C}} \right) + \varepsilon_{\mathrm{a}}^{\sigma} \left(N_{\mathrm{a}}^{\sigma} - n_{\mathrm{a}}^{\sigma} \right) \\
& - n_{\mathrm{p}}^{\mathrm{C}} \varepsilon_{\mathrm{p}}^{\mathrm{C}} - n_{\mathrm{pD}}^{\mathrm{C}} \varepsilon_{\mathrm{pD}}^{\mathrm{C}} \\
& - kT \left[N_{\mathrm{g}}^{\mathrm{a}} \ln N_{\mathrm{g}}^{\mathrm{a}} + N_{\mathrm{g}}^{\mathrm{C}} \ln N_{\mathrm{g}}^{\mathrm{C}} + N_{\mathrm{C}}^{\mathrm{C}} \ln N_{\mathrm{C}}^{\mathrm{C}} + N^{\sigma} \ln N^{\sigma} + n \ln N_{\mathrm{H}} + p \ln N_{\mathrm{L}} \right] \\
& - kT \left[- \left(N_{\mathrm{g}}^{\mathrm{a}} - N_{\mathrm{a}}^{\mathrm{g}} \right) \ln \left(N_{\mathrm{g}}^{\mathrm{a}} - N_{\mathrm{a}}^{\mathrm{g}} \right) - \left(N_{\mathrm{g}}^{\mathrm{C}} - N_{\mathrm{C}}^{\mathrm{g}} \right) \ln \left(N_{\mathrm{g}}^{\mathrm{C}} - N_{\mathrm{C}}^{\mathrm{g}} \right) - N_{\mathrm{C}}^{\mathrm{g}} \ln N_{\mathrm{C}}^{\mathrm{g}} - N_{\mathrm{a}}^{\mathrm{g}} \ln N_{\mathrm{a}}^{\mathrm{g}} \right] \\
& - kT \left[- \left(N_{\mathrm{C}}^{\mathrm{C}} - N_{\mathrm{a}}^{\mathrm{C}} - N_{\mathrm{V}}^{\mathrm{C}} - N_{\mathrm{D}}^{\mathrm{C}} \right) \ln \left(N_{\mathrm{C}}^{\mathrm{C}} - N_{\mathrm{a}}^{\mathrm{C}} - N_{\mathrm{V}}^{\mathrm{C}} - N_{\mathrm{D}}^{\mathrm{C}} \right) \right] \\
& - kT \left[- \left(N^{\sigma} - N_{\mathrm{a}}^{\sigma} - N_{CSW}^{\sigma} \right) \ln \left(N^{\sigma} - N_{\mathrm{a}}^{\sigma} - N_{CSW}^{\sigma} \right) - N_{CSW}^{\sigma} \ln N_{CSW}^{\sigma} \right] \\
& - kT \left[- \left(N_{\mathrm{V}}^{\mathrm{C}} - N_{\mathrm{p}}^{\mathrm{C}} \right) \ln \left(N_{\mathrm{V}}^{\mathrm{C}} - N_{\mathrm{p}}^{\mathrm{C}} \right) \right] - kT \left[- \left(N_{\mathrm{D}}^{\mathrm{C}} - N_{\mathrm{pD}}^{\mathrm{C}} \right) \ln \left(N_{\mathrm{D}}^{\mathrm{C}} - N_{\mathrm{pD}}^{\mathrm{C}} \right) \right] \\
& - kT \left[- \left(N_{\mathrm{a}}^{\mathrm{C}} - n_{\mathrm{a}}^{\mathrm{C}} \right) \ln \left(N_{\mathrm{a}}^{\mathrm{C}} - n_{\mathrm{a}}^{\mathrm{C}} \right) - n_{\mathrm{a}}^{\mathrm{C}} \ln n_{\mathrm{a}}^{\mathrm{C}} - n \ln n + n - p \ln p + p \right] \\
& - kT \left[- \left(N_{\mathrm{a}}^{\sigma} - n_{\mathrm{a}}^{\sigma} \right) \ln \left(N_{\mathrm{a}}^{\sigma} - n_{\mathrm{a}}^{\sigma} \right) - n_{\mathrm{a}}^{\sigma} \ln n_{\mathrm{a}}^{\sigma} - \left(N_{\mathrm{p}}^{\mathrm{C}} - n_{\mathrm{p}}^{\mathrm{C}} \right) \ln \left(N_{\mathrm{p}}^{\mathrm{C}} - n_{\mathrm{p}}^{\mathrm{C}} \right) - n_{\mathrm{p}}^{\mathrm{C}} \ln n_{\mathrm{p}}^{\mathrm{C}} \right] \\
& - kT \left[- \left(N_{\mathrm{pD}}^{\mathrm{C}} - n_{\mathrm{pD}}^{\mathrm{C}} \right) \ln \left(N_{\mathrm{pD}}^{\mathrm{C}} - n_{\mathrm{pD}}^{\mathrm{C}} \right) - n_{\mathrm{pD}}^{\mathrm{C}} \ln n_{\mathrm{pD}}^{\mathrm{C}} \right] \\
& + \lambda_{\mathrm{g}}^{\mathrm{a}} \left(N_{\mathrm{g}}^{\mathrm{a}} - N_{\mathrm{a}}^{\mathrm{g}} - N_{\mathrm{V}}^{ga} \right) + \lambda_{\mathrm{g}}^{\mathrm{C}} \left(N_{\mathrm{g}}^{\mathrm{C}} - N_{\mathrm{C}}^{\mathrm{g}} - N_{\mathrm{V}}^{\mathrm{gC}} \right) \\
& + \lambda^{\mathrm{C}} \left(N^{\mathrm{C}} - N_{\mathrm{C}}^{\mathrm{C}} - N_{\mathrm{a}}^{\mathrm{C}} - N_{\mathrm{V}}^{\mathrm{C}} - N_{\mathrm{p}}^{\mathrm{C}} - N_{\mathrm{D}}^{\mathrm{C}} - N_{\mathrm{pD}}^{\mathrm{C}} \right) + \lambda^{\sigma} \left(N^{\sigma} - N_{\mathrm{a}}^{\sigma} - N_{\mathrm{V}}^{\sigma} \right) \\
& + \lambda_{\mathrm{C}} \left(N_{\mathrm{C}} - N_{\mathrm{C}}^{\mathrm{g}} - N_{\mathrm{C}}^{\mathrm{C}} - N_{CSW}^{\sigma} \right) + \lambda_{\mathrm{V}} \left(N_{\mathrm{V}} - N_{\mathrm{V}}^{\mathrm{g}} - N_{\mathrm{V}}^{\mathrm{C}} - N_{\mathrm{V}}^{\sigma} - N_{\mathrm{D}}^{\mathrm{C}} \right) \\
& + \lambda_{\mathrm{a}} \left(N_{\mathrm{a}} - N_{\mathrm{a}}^{\mathrm{g}} - N_{\mathrm{a}}^{\mathrm{C}} - N_{\mathrm{a}}^{\sigma} - N_{\mathrm{p}}^{\mathrm{C}} - N_{\mathrm{pD}}^{\mathrm{C}} \right) \\
& + \lambda_{e} \left[n - p - \left(N_{\mathrm{a}}^{\mathrm{C}} - n_{\mathrm{a}}^{\mathrm{C}} \right) - \left(N_{\mathrm{a}}^{\sigma} - n_{\mathrm{a}}^{\sigma} \right) + n_{\mathrm{p}}^{\mathrm{C}} + n_{\mathrm{pD}}^{\mathrm{C}} \right]
\end{aligned}
\tag{5.19}
$$

The minimization procedure allows us to calculate the equilibrium concentrations of the given sort defects. The procedure consists of taking the partial derivatives of functional (5.19). It should be taken into account that the derivative with respect to the place number is equal to zero, and the derivative with respect to the particle number equal to the corresponding particle chemical potential. For example, the derivative with respect to nitrogen atom number in gaseous phase equals the nitrogen chemical potential in this phase. The nitrogen chemical potential in the gaseous phase equals:

$$\mu_{a}^{\mathrm{g}} = \mu_{\mathrm{a}}^{0} + kT \ln \left(a_{\mathrm{a}}^{\mathrm{g}} \right),$$

where μ_{a}^{0} is the nitrogen chemical potential under normal conditions and $a_{\mathrm{a}}^{\mathrm{g}}$ is the nitrogen activity in gaseous phase. The analogous denotations will be introduced for carbon (with a natural change of index a to index c).

In ideal nanotubes the all carbon atoms are arranged in their places in the graphene lattice nodes, and therefore the tube free energy is equal to:

$$G_{u\partial} = N_{\mathrm{C}} g_{\mathrm{C}}^{\mathrm{C}}. \tag{5.20}$$

The free energy partial derivative with respect to particles equals their chemical potential, and allows us to find the partial free energy, $g_{\mathrm{C}}^{\mathrm{C}}$, in the form:

$$\frac{\partial G_{u\partial}}{\partial N_{\mathrm{C}}} = g_{\mathrm{C}}^{\mathrm{C}} = \mu_{\mathrm{C}}. \tag{5.21}$$

The results of such derivatives taken from the given functional (5.19) presents a system of algebraic equations, the solution of which allows us to obtain the desired concentrations of the defects and electrons on them, that forming during the tube growth process in a condensed phase. Some results of thermodynamic calculations and analyses are given below:

$$\frac{\partial \Phi}{\partial N_{\mathrm{a}}} = \lambda_{\mathrm{a}} = \mu_{\mathrm{a}}, \frac{\partial \Phi}{\partial N_{\mathrm{C}}} = \lambda_{\mathrm{C}} = \mu_{\mathrm{C}}, \tag{5.22}$$

$$\frac{\partial \Phi}{\partial N_{\mathrm{g}}^{\mathrm{a}}} = -kT \ln N_{\mathrm{g}}^{\mathrm{a}} + kT \ln \left(N_{\mathrm{g}}^{\mathrm{a}} - N_{\mathrm{a}}^{\mathrm{g}}\right) + \lambda_{\mathrm{g}}^{\mathrm{a}} = 0, \tag{5.23}$$

$$\frac{\partial \Phi}{\partial N_{\mathrm{a}}^{\mathrm{g}}} = g_{\mathrm{a}}^{\mathrm{g}} + kT \ln N_{\mathrm{a}}^{\mathrm{g}} - kT \ln \left(N_{\mathrm{g}}^{\mathrm{a}} - N_{\mathrm{a}}^{\mathrm{g}}\right) - \lambda_{\mathrm{g}}^{\mathrm{a}} - \lambda_{\mathrm{a}} = 0. \tag{5.24}$$

Solving the system of (5.22)–(5.24), we find the nitrogen atom concentration in gaseous phase:

$$N_{\mathrm{a}}^{\mathrm{g}} = N_{\mathrm{g}}^{\mathrm{a}} \exp\left(\frac{\mu_{\mathrm{a}}}{kT}\right) \exp\left(-\frac{g_{\mathrm{a}}^{\mathrm{g}}}{kT}\right). \tag{5.25}$$

And analogously for carbon atoms:

$$N_{\mathrm{C}}^{\mathrm{g}} = N_{\mathrm{g}}^{\mathrm{C}} \exp\left(\frac{\mu_{\mathrm{C}}}{kT}\right) \exp\left(-\frac{g_{\mathrm{C}}^{\mathrm{g}}}{kT}\right). \tag{5.26}$$

We can calculate nitrogen atom concentration, being introduced by a graphite-type substitution, and the number of electrons on them, giving a value:

$$\frac{\partial \Phi}{\partial N_{\mathrm{C}}^{\mathrm{C}}} = g_{\mathrm{C}}^{\mathrm{C}} - kT \ln N_{\mathrm{C}}^{\mathrm{C}} + kT \ln \left(N_{\mathrm{C}}^{\mathrm{C}} - N_{\mathrm{a}}^{\mathrm{C}} - N_{\mathrm{V}}^{\mathrm{C}} - N_{\mathrm{D}}^{\mathrm{C}}\right) - \lambda^{\mathrm{C}} - \lambda_{\mathrm{C}} = 0 \tag{5.27}$$

With respect to (5.21) and (5.22) we obtain an expression for the Lagrange indefinite multiplier, λ^{C}:

$$\lambda^{C} = -kT \ln N_{C}^{C} + kT \ln \left(N_{C}^{C} - N_{a}^{C} - N_{V}^{C} - N_{D}^{C}\right). \tag{5.28}$$

$$\frac{\partial \Phi}{\partial N_{a}^{C}} = g_{a}^{C} + kT \ln \left(N_{a}^{C} - n_{a}^{C}\right) - kT \ln \left(N_{C}^{C} - N_{a}^{C} - N_{V}^{C} - N_{D}^{C}\right) - \lambda^{C} - \lambda_{a} - \lambda_{e} = 0, \tag{5.29}$$

$$\frac{\partial \Phi}{\partial n_{a}^{C}} = -\varepsilon_{a}^{C} - kT \ln \left(N_{a}^{C} - n_{a}^{C}\right) - kT \ln n_{a}^{C} + \lambda_{C} = 0, \tag{5.30}$$

$$\frac{\partial \Phi}{\partial n} = -kT \ln N_{H} + kT \ln n + \lambda_{e} = 0; \quad \lambda_{e} = kT \ln N_{H} - kT \ln n = -E_{F}, \tag{5.31}$$

where E_F is the Fermi energy.

Solving the system of (5.28)–(5.31), we can find the concentration of nitrogen atoms being arranged by graphite-type substitution in the form:

$$N_{a}^{C} = \frac{\left(N_{C}^{C} - N_{a}^{C} - N_{V}^{C} - N_{D}^{C}\right)^{2}}{N_{C}^{C}} \exp\left(-\frac{g_{a}^{C} - \mu_{a}}{kT}\right)\left[1 + \frac{N_{H}}{n}\exp\left(-\frac{\varepsilon_{a}^{C}}{kT}\right)\right], \tag{5.32}$$

$$n_{a}^{C} = \frac{\left(N_{C}^{C} - N_{a}^{C} - N_{V}^{C} - N_{D}^{C}\right)^{2}}{N_{C}^{C}} \exp\left(-\frac{g_{a}^{C} - \mu_{a}}{kT}\right). \tag{5.33}$$

If the place number in graphene lattice nodes, occupied by the defects, is sufficiently less than the place number occupied by carbon, then formulas (5.32) and (5.33) can be simplified and take the form:

$$N_{a}^{C} = N^{C} \exp\left(-\frac{g_{a}^{C} - \mu_{a}}{kT}\right)\left[1 + \frac{N_{H}}{n}\exp\left(-\frac{\varepsilon_{a}^{C}}{kT}\right)\right], \tag{5.34}$$

$$n_{a}^{C} = N^{C} \exp\left(-\frac{g_{a}^{C} - \mu_{a}}{kT}\right). \tag{5.35}$$

It is possible to calculate the concentration of carbon vacancies, nitrogen atoms doped by pyridine-type substitution, and the electron number on these atoms:

$$\frac{\partial \Phi}{\partial N_{\mathrm{V}}^{\mathrm{C}}} = g_{\mathrm{V}}^{\mathrm{C}} - kT \ln\left(N_{\mathrm{V}}^{\mathrm{C}} - N_{\mathrm{p}}^{\mathrm{C}}\right) + kT \ln\left(N_{\mathrm{C}}^{\mathrm{C}} - N_{\mathrm{a}}^{\mathrm{C}} - N_{\mathrm{V}}^{\mathrm{C}} - N_{\mathrm{D}}^{\mathrm{C}}\right) - \lambda^{\mathrm{C}} - \lambda_{\mathrm{V}} = 0. \tag{5.36}$$

Taking into account expression (5.28) and the fact that vacancy also is a quasi-particle (with chemical potential equal to zero), one can obtain:

$$\frac{\partial \Phi}{\partial N_{\mathrm{V}}^{\mathrm{C}}} = g_{\mathrm{V}}^{\mathrm{C}} + kT \ln\left(N_{\mathrm{V}}^{\mathrm{C}} - N_{\mathrm{p}}^{\mathrm{C}}\right) - 2kT \ln\left(N_{\mathrm{C}}^{\mathrm{C}} - N_{\mathrm{a}}^{\mathrm{C}} - N_{\mathrm{V}}^{\mathrm{C}} - N_{\mathrm{D}}^{\mathrm{C}}\right) - kT \ln N_{\mathrm{C}}^{\mathrm{C}} = 0, \tag{5.37}$$

The concentration of nitrogen, doped by pyridine-type substitution, can be calculated and gives the relationships:

$$\frac{\partial \Phi}{\partial N_{\mathrm{p}}^{\mathrm{C}}} = g_{\mathrm{p}}^{\mathrm{C}} - kT \ln\left(N_{\mathrm{V}}^{\mathrm{C}} - N_{\mathrm{p}}^{\mathrm{C}}\right) + kT \ln\left(N_{\mathrm{p}}^{\mathrm{C}} - n_{\mathrm{p}}^{\mathrm{C}}\right) - \lambda^{\mathrm{C}} - \lambda_{\mathrm{a}} = 0, \tag{5.38}$$

$$\frac{\partial \Phi}{\partial n_{\mathrm{p}}^{\mathrm{C}}} = -\varepsilon_{\mathrm{p}}^{\mathrm{C}} + kT \ln n_{\mathrm{p}}^{\mathrm{C}} - kT \ln\left(N_{\mathrm{p}}^{\mathrm{C}} - n_{\mathrm{p}}^{\mathrm{C}}\right) + \lambda_e = 0 \tag{5.39}$$

Accounting for (5.22) and (5.28), we obtain:

$$N_{\mathrm{p}}^{\mathrm{C}} = \frac{\left(N_{\mathrm{C}}^{\mathrm{C}} - N_{\mathrm{a}}^{\mathrm{C}} - N_{\mathrm{V}}^{\mathrm{C}} - N_{\mathrm{D}}^{\mathrm{C}}\right)^3}{\left(N_{\mathrm{C}}^{\mathrm{C}}\right)^2} \exp\left(\frac{\mu_{\mathrm{a}} - g_{\mathrm{V}}^{\mathrm{C}} - g_{\mathrm{p}}^{\mathrm{C}}}{kT}\right)\left[1 + \frac{n}{N_{\mathrm{H}}} \exp\left(\frac{\varepsilon_{\mathrm{p}}^{\mathrm{C}}}{kT}\right)\right], \tag{5.40}$$

$$n_{\mathrm{p}}^{\mathrm{C}} = \frac{\left(N_{\mathrm{C}}^{\mathrm{C}} - N_{\mathrm{a}}^{\mathrm{C}} - N_{\mathrm{V}}^{\mathrm{C}} - N_{\mathrm{D}}^{\mathrm{C}}\right)^3}{\left(N_{\mathrm{C}}^{\mathrm{C}}\right)^2} \exp\left(\frac{\mu_{\mathrm{a}} - g_{\mathrm{V}}^{\mathrm{C}} - g_{\mathrm{p}}^{\mathrm{C}}}{kT}\right). \tag{5.41}$$

After using (5.37) and (5.41), we can calculate the vacancy concentration:

$$N_{\mathrm{V}}^{\mathrm{C}} = N^{\mathrm{C}} \exp\left(-\frac{g_{\mathrm{V}}^{\mathrm{C}}}{kT}\right)\left[1 + \exp\left(\frac{\mu_{\mathrm{a}} - g_{\mathrm{p}}^{\mathrm{C}}}{kT}\right)\left[1 + \frac{n}{N_{\mathrm{L}}} \exp\left(\frac{\varepsilon_{\mathrm{p}}^{\mathrm{C}}}{kT}\right)\right]\right]. \tag{5.42}$$

The concentration of nitrogen, chemisorbed on carbon chemical bonds, and electron number on these atoms, can be calculated by formulas:

$$N_{\mathrm{a}}^{\sigma} = N^{\sigma} \exp\left(-\frac{g_{\mathrm{a}}^{\sigma} - \mu_{\mathrm{a}}}{kT}\right)\left[1 + \frac{N_{\mathrm{H}}}{n}\exp\left(-\frac{\varepsilon_{\mathrm{a}}^{\sigma}}{kT}\right)\right], \tag{5.43}$$

$$n_{\mathrm{a}}^{\sigma} = N^{\sigma} \exp\left(-\frac{g_{\mathrm{a}}^{\sigma} - \mu_{\mathrm{a}}}{kT}\right). \tag{5.44}$$

The calculated values of nitrogen atoms, doped Nitrogen atoms by pyridine-type substitution with a double vacancy participation, and electron number on these atoms, are equal to:

$$N_{\mathrm{pD}}^{\mathrm{C}} = \frac{\left(N_{\mathrm{C}}^{\mathrm{C}} - N_{\mathrm{a}}^{\mathrm{C}} - N_{\mathrm{V}}^{\mathrm{C}} - N_{\mathrm{D}}^{\mathrm{C}}\right)^3}{\left(N_{\mathrm{C}}^{\mathrm{C}}\right)^2} \exp\left(\frac{\mu_{\mathrm{a}} - g_{\mathrm{V}}^{\mathrm{C}} - g_{\mathrm{pD}}^{\mathrm{C}}}{kT}\right)\left[1 + \frac{n}{N_{\mathrm{L}}}\exp\left(\frac{\varepsilon_{\mathrm{pD}}^{\mathrm{C}}}{kT}\right)\right], \tag{5.45}$$

$$n_{\mathrm{pD}}^{\mathrm{C}} = \frac{\left(N_{\mathrm{C}}^{\mathrm{C}} - N_{\mathrm{a}}^{\mathrm{C}} - N_{\mathrm{V}}^{\mathrm{C}} - N_{\mathrm{D}}^{\mathrm{C}}\right)^3}{\left(N_{\mathrm{C}}^{\mathrm{C}}\right)^2} \exp\left(\frac{\mu_{\mathrm{a}} - g_{\mathrm{V}}^{\mathrm{C}} - g_{\mathrm{pD}}^{\mathrm{C}}}{kT}\right). \tag{5.46}$$

The Stone-Wales defect concentration is defined by the next expression:

$$N_{CSW}^{\sigma} = a_{\mathrm{C}} N^{\sigma} \exp\left(-\frac{g_{CSW}^{\sigma} - \mu_{\mathrm{C}}^{0}}{kT}\right). \tag{5.47}$$

Thus, in this section on the basis of the free energy analysis of the system, containing the gas phase and growing nanotubes, we have obtained the system of equations describing defect formation, including both the doping and adsorption. The nitrogen atoms introduction into CNT nodes is connected with many technological factors and thermodynamic parameters. First, the nitrogen concentration is defined by the Gibbs partial potential for a defect formation process. It is difficult to calculate these partial potentials. Therefore, they must be defined by a comparison of the theoretical results with experimental data. Second, the nanotube growth temperature is also an important factor of the process. Third, we must take into account the nitrogen and carbon activities, characterized by the gaseous molecule concentration in the reactor. The increase of nitrogen-containing molecule concentration leads to an increase in introduced nitrogen atom numbers. Note, that the amount of nanotube graphene lattice nodes, N^{C}, is a fixed number, as is the amount of the chemical bonds there are between them, N^{σ}, something which is connected with nanotube chirality and some other parameters. For this reason the carbon activity does not affect the building-in of nitrogen atoms.

5.8 Calculations of Doped Carbon Nanotube Conductance

The law of charge conservation (5.10) allows us to calculate the electron and hole concentrations and define the system Fermi level value, i.e., the parameters characterizing the doped nanotube's conductance. Let us substitute into (5.10) the theoretical expressions for the electron and hole concentrations on them. After some transformations one can obtain:

$$n = \sqrt{\frac{n_i^2 - A}{1 + B}}, \tag{5.48}$$

where n_i^2 is the carrier concentration in the nanotube. The coefficients A and B are connected with technological conditions of nanotube fabrication, as well as with other parameters and characteristics linked to increasing nanotubes and defects, by:

$$\begin{aligned} A &= a_a N_H \left[N^C \exp\left(-\frac{g_a^C + \varepsilon_a^C - \mu_a^o}{kT} \right) + N^\sigma \exp\left(-\frac{g_a^\sigma + \varepsilon_a^\sigma - \mu_a^o}{kT} \right) \right], \\ B &= \frac{a_a N^C N_L}{n_i^2} \left[\exp\left(-\frac{g_p^C + \varepsilon_p^C - \mu_a^o}{kT} \right) \right] + \exp\left(-\frac{g_{pD}^C + \varepsilon_{pD}^C - \mu_a^o}{kT} \right). \end{aligned} \tag{5.49}$$

It is necessary to note, that formula (5.48) describes the electron concentration value, which forms with increasing temperatures. Under a cooling process there begins the secondary processes of defect formation or generation, and this fact must be without fail accounted for when considering the electron concentration. On the other hand, formula (5.48) demonstrated a tendency of increasing nanotube conductance change under doping. For metallic nanotubes (when their own electron concentration is higher than the doping admixture concentration) we can neglect coefficients A and B, and the concentration, defined by formula (5.48), becomes equal to the intrinsic electron concentration, that indirectly confirms the reliability of this expression.

5.9 Analysis of Thermogravimetric Curves of Carbon Nanotubes, Doped by Nitrogen

One of the most important methods for nitrogen-doped carbon nanotube content control is thermogravimetric analysis [119–122], and therefore it is necessary to properly and correctly interpret the mass changes registered by this method. Let us consider the method application, just for nitrogen-doped CNTs.

Once more let us analyze the base conditions of the method's mathematical model, developed in Sect. 1.3:

- the desorption proceeds from certain adsorption centers;
- the dopant molecules do not interact with each other and can pass directly in a vacuum;
- the dopant molecule number is a constant value, prescribed by a prehistory of sample preparation; and
- every dopant molecule bounded by to only one adsorbent molecule.

Let us raise attention to the fact that the adsorption proceeds in a vacuum and the desorbed molecule is removed from the CNT surface. Thus, the desorption process itself is irreversible, i.e., if a defect is destroyed and emitted an adsorbent, the defect will never arise again. With this fact is connected the so-called mass loss effect, studied below. The effect is described by (2.83), which specifically for nitrogen desorption takes the form:

$$\frac{dN_{\mathrm{N}}}{dt} = \sum_{\beta,i=1}^{m} \frac{dN_{\mathrm{N}i}^{\beta}}{dt} = -\sum_{i=1}^{m} v_{\mathrm{N}i}^{\beta} N_{\mathrm{N}i}^{\beta} \exp\left(-\frac{g_{\mathrm{N}i}^{\beta}}{kT}\right) dt, \tag{5.50}$$

where $N_{\mathrm{N}i}^{\beta}$ is the nitrogen atom concentration, being bounded at i-type sites or positions; N_i^{β} is the concentration of the i-type sites, with coefficient β having meanings "c" and "σ" (the latter relates to such cases when nitrogen is volatilizing from the grapheme lattice nodes and chemical bonds, which are denoted by these symbols); $N_{\mathrm{N}}^{\mathrm{g}}$ is the dopant molecule concentration in gaseous phase, defining its partial pressure; $c_{\mathrm{N}i}^{\beta}$ is the probability of dopant capture by i-type adsorption centers under unitary dopant concentration in a gaseous phase; and $e_{\mathrm{N}i}^{\beta}$ is the probability of dopant molecule desorption.

In order to solve (5.50) it is necessary to know the kinetic coefficients that define the gaseous component adsorption and desorption probabilities. In an equilibrium state the right-hand side of (5.50) becomes equal to zero. Substituting into this equation the dopant molecule concentration value, we get for nitrogen adsorption probability the expression:

$$e_{\mathrm{N}i}^{\beta} = c_{\mathrm{N}i}^{\beta} N^{ga} \exp\left(-g_{\mathrm{N}i}^{\beta}/kT\right), \tag{5.51}$$

where $v_{\mathrm{N}i}^{\beta} = c_{\mathrm{N}i}^{\beta} N^{ga}$ and $g_{\mathrm{N}i}^{\beta}$ is the partial free dopant energy.

To obtain the adsorption rate, it is necessary to cool down the cryostat (with a sample) to helium temperatures. After achieving an equilibrium state the samples must be heated up at a constant rate (e.g., $\gamma = 0.2\,\mathrm{K/s}$), with temperature rising

linearly with time, i.e., $T = T_0 + \gamma t$, where T_0 is an initial temperature, chosen usually long before the start of desorption. The amount of the desorbed substance is recorded for to control the thermo-stimulated desorption process.

The problem of heating at a constant rate was solved in Sect. 1.3 and has the form:

$$N_{\mathrm{N}i}^{\beta} = N_{\mathrm{N}0i}^{\beta} \exp\left[-\frac{\nu_{\mathrm{N}i}^{\beta} T}{\gamma} E_2\left(\frac{g_{\mathrm{N}i}^{\beta}}{kT}\right)\right], \tag{5.52}$$

where $N_{\mathrm{N}0i}^{\beta}$ is an initial concentration of a given type of defect and $E_2(x)$ is the second order integral exponential function.

Equation (5.52) allows us to obtain the next two kinetic coefficients: $g_{\mathrm{N}i}^{\beta}$—the adsorption free energy (molecule bonds) and $\nu_{\mathrm{N}i}^{\beta}$—a desorption probability. For their determination it is necessary to compare the analytical expressions with experimental results. Some simple formulas, which allow us to carry out the comparison, are also given in Sect. 1.3 and have the form:

$$\nu_{\mathrm{N}i}^{\beta} = c_{\mathrm{N}i}^{\beta} N^{g\alpha} = \frac{\gamma g_{\mathrm{N}i}^{\beta}}{kT_{mi}^2} \exp\left(\frac{g_{\mathrm{N}i}^{\beta}}{kT_{mi}}\right). \tag{5.53}$$

$$\frac{dN_{\mathrm{N}}}{dT} = \sum_{i=1}^{m} \frac{g_{ni}^{\beta}}{kT_{mi}} N_{\mathrm{N}0i}^{\beta} Z \exp\left[-\frac{T^2}{T_{mi}^2}\left(1 - \frac{2g_{\mathrm{N}i}^{\beta}}{kT_{mi}}\right) Z\right], \tag{5.54}$$

Where

$$Z = \exp\left[\frac{g_{\mathrm{N}i}^{\beta}}{k}\left(\frac{1}{T_{mi}} - \frac{1}{T}\right)\right].$$

Formulas (5.53) and (5.54) are very convenient for analysis of desorption kinetics, because they allow us to divide desorption processes into their stages with great accuracy in order to calculate desorption parameters separately. In Fig. 5.6 are shown the experimental results, processed by the above described method. The kinetic coefficients are presented in Table 5.7.

The next problem is identification of the process data with regards to the nature of defect concerning them.

Table 5.7 Averaged values of kinetic coefficients for nitrogen desorption processes, obtained by the treatment of experimental data from [119–122]

No. of desorption processes	1	2	3	4	1	2	3
	Fig. 5.21a				Fig. 5.21b		
Desorption process via partial Gibbs energy, g_{Ni}^{β} (eV)	0.68 ± 0.03	0.85 ± 0.03	1.10 ± 0.03	1.7 ± 0.05	2.00 ± 0.05	2.20 ± 0.05	2.40 ± 0.05
Desorption process probability, ν_{Ni}^{β} (sec^{-1})	$(3 \pm 1) \times 10^5$	$(3 \pm 2) \times 10^6$	$(4 \pm 1) \times 10^8$	$(3 \pm 1) \times 10^{10}$	$(3 \pm 1) \times 10^{12}$	$(4 \pm 1) \times 10^{12}$	$(6 \pm 1) \times 10^{12}$

5.10 Calculation of Nitrogen Fugacity Under Plasmochemical Synthesis

X-ray photoelectron spectroscopy (XPS) is one of the most developed and widely used methods for determining the nitrogen concentration, introduced into a grapheme lattice by various techniques [114, 123–127]. The experimental results, obtained by this method, showed that a nanotube increase in temperature leads to nitrogen concentration in the tubes decreasing [114], and this fact in general corresponds to mass decreasing effects, which are usually observed and recorded by TGA. It must be noted, that nitrogen concentration depends on growing or annealing the temperature and presents an equilibrium quantity, so that the XPS results must be made consistent with formulas found in Sect. 5.7. For these analyses it is necessary to calculate the nitrogen atom fugacity under plasmochemical synthesis.

The plasmochemical technology involved in the nanotube epitaxial chemical vapor deposition method (PECVD) has many advantages over a standard CVD method [128]. In the first place, the plasma temperature is defined by the current density and the gaseous discharge source power (an applied voltage). This temperature exceeds the substrate temperature, so that the nanotube's temperature decreases. Second, the electrical field presence allows growth of aligned CNTs. At present, there exist several variants of this method: HF PECVD [129], SHF PECVD [130], PECVD with inductive coupling [131], and DC PECVD [132, 133]. In general, they have the same mechanism of the pyrolysis activation energy lowering on account of the electron elastic interaction with dissociated molecules. This property of the process presents an important advantage. In experiments this energy was decreasing practically by 4 times [134], down to 390 °C (temperature of bamboo-type tube growth) and even to 120 °C (amorphous twist growth) [135].

Hydrocarbon pyrolysis is a sufficiently complex process of hydrocarbon transformation under a molecule heating and an excitation of their vibrational subsystem. Pyrolysis as a rule proceeds in the presence of a catalyst, with a note, that the pyrolysis process catalyst and CNT growth catalyst are not always the same substance. The pyrolysis promoting catalyst is presenting in a gaseous phase, but the CNT growth catalyst is a substrate. Some substances (e.g., ferrocene) can simultaneously take part in both processes, however because these processes are different the catalytic chain reactions also differ. So, pyrolysis processes cannot be reduced to a set or collection of consequent and parallel chemical deposition reactions, because, along with decomposition, there proceeds a synthesis with a lot of reactions, mainly monomolecular ones. During these reactions there is a change not only the hydrocarbon molecule structure (i.e., isomerization), but also the molecular mass (dissociation). In this work we take into account these complex processes.

An important characteristic of CNT growth is fugitiveness of the atomic carbon in gaseous phase. This parameter which defines the particles current to a catalyst, influences the carbon atom solubility in the catalyst substance and thus affects the

CNT growth rate. The aim of our work is to calculate this value under plasmochemical pyrolysis processes. Taking into account the complexity of the proceeding processes and a great number of reactions, we use the Gibbs free energy minimization method [115, 117], which allows us to consider the diversity of the processes.

The method used assumes that the system is an equilibrium state, i.e., the temperature and pressure are equilibrated and all kinetic processes are stationary. In this case (at constant temperature and pressure) the system's Gibbs free energy is:

$$G = H - TS.$$

This must have a minimal value. The calculation algorithm is based on the system's free energy component analysis with a following energy minimization, using several additional conditions in the capacity of which are used the conservation laws.

The conservation laws are defined by a balance of particle and molecule numbers in a system. Let us denote each substances atom as a subscript. For example, the total content of nitrogen, being both in gaseous phase and free state, will be denoted as N_α, where index "α" corresponds to the simple substance's atom. We will use the index k for any compound of this substance, regardless of its composition. The number of one type of compound's molecules, presented in gaseous phase, will be denoted N_k. For further analysis let us use the cell model of a gas, developed in [117]. In this model one can separate the place number, which corresponds to the cell number in gaseous phase. The cell presents the same volume, occupied by one atom or molecule in gaseous phase, and therefore, if a saturated vapor is formed in gaseous phase, every cell will be occupied just by one gaseous atom or molecule. Thus, the cell number is equal to the gas unit volume, divided by the saturated vapor atom number. We will call the place number a maximal number of a single gas particles (atoms or compounds), and will denote it as a superscript. Thus, for a simple substance this number will be denoted N^α, and for compounds, N^k.

The place number in a system is defined by the saturated vapor pressure at a given temperature. It is a tabular value and can be found from the state diagram of a given type gas:

$$N^\alpha = p_{\text{as}}/kT \quad \text{N}^k = p_{\text{ks}}/kT \tag{5.55}$$

The total place number in a gas phase is defined by the sum of the values given by expressions (4.10.1):

$$N = \sum_\alpha p_{\text{as}}/kT + \sum_k p_{\text{ks}}/kT = \sum_\alpha N^\alpha + \sum_k N^k. \tag{5.56}$$

5.10.1 The Place Number Conservation Laws

It was said above, that the place number corresponds to a maximal number of a given type of molecules, which can simultaneously be located in gas phase for given conditions. By definition the number can be calculated from the value of saturated vapor, consisting completely of gas molecules of the considered type. This number is equal to the number of system chemical components, each of which can be written down as a law of place conservation. For simple substances, we have:

$$\varphi^{\alpha} = N^{\alpha} - N_{\alpha} - N_{\alpha}^{0} = 0, \tag{5.57}$$

In addition, for the nitrogen compounds:

$$\varphi^{k} = N^{k} - N_{k} - N_{k}^{0} = 0, \tag{5.58}$$

where $N_{\alpha,\mathrm{k}}^{0}$ is the number of places in gaseous phase, that remain free.

5.10.2 The Particles Number Conservation Laws

The nitrogen molecules can unite and create new compounds. From a thermodynamic point of view, these complex objects can be described in a single way. Moreover, the atoms and molecules of every substance can exist in either free ionized state. Let us designate the number of nitrogen atoms, being able to form some ions, by $N_{\alpha q}$, where the index q (defining a charge state) can have discrete values. For example, for an ionized double-charged molecule this index can take values "0" and "+1" or "0" and "−1", but for a multiple-ionized molecule the index value combinations number is increasing and equals the molecule total charge state number. Using the notion of "charge state" allows us in a unique way to describe and consider both the positively and negatively charged ions, as well as the ionized or multiple-ionized molecules. The atoms of every element can be present in both free and connected states. Under a pyrolysis process the compound's composition and the number of free atoms of nitrogen or other substances can change, bur their sum remains constant due to system closure. This condition is based on a certain atom and molecule number conservation law, in the form:

$$\begin{aligned} \varphi_{\alpha} &= N_{\alpha} - \sum_{\alpha q} N_{\alpha q} - \sum_{\alpha,k} N_{k} m_{\alpha k} = 0 \\ \varphi_{k} &= N_{k} - \sum_{kq} N_{kq} = 0, \end{aligned} \tag{5.59}$$

where m_{α} is the simple substance (carbon or hydrogen) number in a hydrocarbon molecule.

5.10.3 Charge Conservation Law

The plasma pseudo-neutrality condition implies that there exists a balance between the positive and negative charges, i.e., the charge conservation law is fulfilled in the form:

$$\varphi_e = n - \sum_{\alpha q} q_\alpha N_{\alpha q} - \sum_{q,k} q_k N_k = 0. \tag{5.60}$$

Note, that the index q may be positive or negative. Moreover, the single atoms or compounds in the system can be ionized, taken into account by formula (5.60), written in a common form.

5.10.4 Free Energy of the System

The Gibbs free energy of the system has a form:

$$G = G^{\mathrm{G}}\left(N^{\mathrm{G}}_{\alpha q}, N_{kq}\right) + G^e, \tag{5.61}$$

where G^{G} is the free energy of the gaseous phase; $N_{\alpha q}$ is the concentration of α-type atoms in gaseous phase, being in a charge state q; N_{kq} is the compound concentration in a certain charge state; and G^e is the free energy of the electronic subsystem with contributions from all charge carrying elements (both the atoms and molecules).

To find an explicit form of the free energy dependence on atom and molecule concentration, let us introduce the Gibbs partial potential per atom or molecule of a compound:

$$\begin{aligned} g_{\alpha q} &= g_\alpha = H_\alpha - TS_\alpha \\ g_{kq} &= g_k = H_k - TS_k + \sum_{\alpha kq} m_{\alpha k}(H_k - TS_k), \end{aligned} \tag{5.62}$$

where $H_{\alpha(k)}$ is the free energy of a neutral atom's (or compound's) formation; $S_{\alpha(q)}$ is an oscillating (thermal) entropy, connected with the atom (compound); and $\varepsilon_{\alpha(k)q}$ is the energy, that is necessary for transfer the atom (compound) into a charge state, q.

Formula (5.52) accounts for the compound formation from the separate atoms. For the sake of notation economy we use a parenthesis: thus, the index α relates to an atom, the letter in parenthesis (i.e., k) relates to a compound. In formula (5.62) these values are given separately.

Let us consider the thermal part of the system free energy as a product of the atom and molecule partial free energies by their concentrations:

$$G_T = \sum_{\alpha} g_{\alpha} N_{\alpha} + \sum_{k} g_k N_k + G^e \tag{5.63}$$

The configuration part of the free energy is expressed by Boltzmann's formula:

$$G_K = -kT \ln W, \tag{5.64}$$

where W is the thermodynamic probability of the states (i.e., the number of realization variants for this macroscopic state):

$$W = \prod_{\alpha,k} \frac{N^{\alpha}!}{N_{\alpha q}!(N^{\alpha} - N_{\alpha})!\left(N_{\alpha} - \sum\limits_{q} N_{\alpha q}\right)!} \frac{N^{k}!}{N_{kq}!(N^{k} - N_{k})!\left(N_{k} - \sum\limits_{q} N_{kq}\right)!} \tag{5.65}$$

The W value accounts for all permutations (rearrangements) of identical atoms and molecules regarding their place, as well as the charge state permutations by elements. The total amount of paticales of the one kinde is equal to:

$$N_{\alpha} = \sum_{\alpha,q} N_{\alpha q} + \sum_{\alpha,k,q} N_{kq} m_{\alpha k} \tag{5.66}$$

The electronic subsystem free energy can be written in the form:

$$G^e = \sum_{\alpha,q} N_{\alpha q} \varepsilon_{\alpha q} + \sum_{k,q} N_{kq} \varepsilon_{kq} \tag{5.67}$$

The electrons in the system arise as a result of atom and molecule ionization, and therefore the charge conservation law can be formulated as:

$$\varphi_e = n - \sum_{\alpha,q} q N_{\alpha q} - \sum_{k,q} q N_{kq} \tag{5.68}$$

The equilibrium concentration of carbon and hydrogen atoms, as well as compounds generated under pyrolysis, can be found via the Lagrange indefinite multipliers (factors) method. The equilibrium corresponds to the minimum of the functional:

$$\Psi = G_T + G_K + \sum_{\alpha} \lambda_{\alpha} \varphi_{\alpha} + \sum_{\alpha} \lambda^{\alpha} \varphi^{\alpha} + \lambda_e \varphi_e + \sum_{k} \lambda_k \varphi_k + \sum_{k} \lambda^k \varphi^k. \tag{5.69}$$

The resultant expression for the free energy functional has the form:

$$\begin{aligned}\Psi = &\sum_{\alpha} g_{\alpha} N_{\alpha} + \sum_{k} g_k N_k + \sum_{\alpha,q} N_{\alpha q}\varepsilon_{\alpha q} + \sum_{k,q} q N_{kq}\varepsilon_{kq} \\ &- kT \ln \prod_{\alpha,k} \frac{N^{\alpha}!}{\prod_{\alpha} N_{\alpha q}!(N^{\alpha} - N_{\alpha})!\left(N_{\alpha} - \sum_{q} N_{\alpha q}\right)!} \frac{N^{k}!}{\prod_{k} N_{kq}!(N^{k} - N_k)!\left(N_k - \sum_{q} N_{kq}\right)!} \\ &+ \lambda^{p}\left(N - \sum_{\alpha} N^{\alpha} - \sum_{k} N^{k}\right) + \sum_{\alpha,k,q} \lambda_{\alpha}\left(N_{\alpha} - \sum_{\alpha q} N_{\alpha q} - \sum_{\alpha,k} N_k m_{\alpha k}\right) \\ &+ \lambda_e\left(n - \sum_{\alpha q} q_{\alpha} N_{\alpha q} - \sum_{q,k} q_k N_{kq}\right) + \lambda_k \sum_{q,k}\left(N_k - \sum_{kq} N_{kq}\right) \\ &+ \lambda^{k} \sum_{k}\left(N^{k} - N_k - N_k^{0}\right) + \lambda^{\alpha} \sum_{\alpha}\left(N^{\alpha} - N_{\alpha} - N_{\alpha}^{0}\right)\end{aligned} \tag{5.70}$$

According to the Fermi level definition (electron chemical potential) we find the meaning of the multiplier λ_e:

$$E_F = \frac{\partial G}{\partial n} = \frac{\partial \Psi}{\partial n} = \lambda_e, \tag{5.71}$$

coinciding with the Fermi level energy value.

The free energy derivative with respect to given type of atom or molecule number is by definition called the chemical potential of the substance. It was said above, that the system is in thermodynamic equilibrium, and this means that the chemical potential of all the species (dislocated molecules and free atoms arising during pyrolysis, etc.) are equal to one another, i.e., for every particle type we have the condition:

$$\mu_{\alpha}^{\mathrm{g}} = \mu_{\alpha}^{\mathrm{mol}},$$

where $\mu_{\alpha}^{\mathrm{g}}$ is the chemical potential of any atom in gaseous phase and $\mu_{\alpha}^{\mathrm{mol}}$ is the atom's chemical potential into a molecule:

$$\mu_{\alpha}^{\mathrm{mol}} = \mu_{\alpha}^{0} + \ln m_{k\alpha} x_{k\alpha} \approx \mu_{\alpha}^{0} + \ln m_{k\alpha} f_{k\alpha}, \tag{5.72}$$

where $x_{k\alpha}$ is the number of gaseous phase molecules, which can produce α-type atoms under the pyrolysis and $f_{k\alpha}$ is the molecule's fugitiveness.

Differentiating the functional Ψ with respect to N^{α} we obtain a relationship between the Lagrange multiplier and concentrations:

$$\lambda_\alpha = -kT \ln N^\alpha + kT \ln (N^\alpha - N_\alpha) \tag{5.73}$$

On the other hand, differentiating the functional Ψ with respect to N_a we obtain the result that the chemical potential of the α-element in gaseous phase is expressed itself through the Lagrange multipliers for place and particle conservation:

$$\lambda_\alpha = \mu_\alpha^0 + \ln m_{k\alpha} f_{k\alpha} - \left[g_\alpha + kT \ln (N_\alpha - \sum_q N_{q\alpha}) - kT \ln \left(N^\alpha - N_\alpha\right) \right]. \tag{5.74}$$

The usual presentation is used for nitrogen chemical potential: $\mu_\alpha^0 + kT \ln a$, where μ_α^0 is the nitrogen chemical potential under standard conditions.

Taking the derivative of functional Ψ with respect to $N_{q\alpha}$, one can, after some calculations, arrive at the expression:

$$N_{q\alpha} = f_{k\alpha} N^\alpha \exp\left(-\frac{g_\alpha + \varepsilon_{q\alpha} - \mu_\alpha^0 - q_\alpha E_F}{kT} \right) = f_{k\alpha} N^\alpha \exp\left(-\frac{E_a - q_\alpha E_F}{kT} \right), \tag{5.75}$$

where $E_a = g_\alpha + \varepsilon_{q\alpha} - \mu_\alpha^0$ is the activation energy of the usual, not plasmochemical, pyrolysis.

The fugitiveness of α-type atoms in a system equals the relationship of their partial pressure to the their saturation vapor pressure. Taking into account that pressure is connected with molecule concentration by the Clapeyron equation $p = kTN$, we obtain for nitrogen:

$$f_\alpha = \frac{\sum_q N_{q\alpha}}{N^\alpha} = f_{k\alpha} \sum_q \exp\left(-\frac{E_a - q_\alpha E_F}{kT} \right) \tag{5.76}$$

Replacing the index α in (5.76) with carbon, we obtain its fugitiveness, i.e., for carbon atom fugacity in a gaseous phase under plasmochemical pyrolysis we have the expression:

$$f_C = f_{kC} \sum_q \exp\left(-\frac{E_C - q_C E_F}{kT} \right), \tag{5.77}$$

where f_{kC} is the hydrocarbon fugacity, being pyrolyzed into the reactor. This value is connected with the gas current fed (conveyed) into reactor to carry out the CNT synthesis.

Formulas (5.76) and (5.77) show that when the Fermi energy of the plasma electrons is rising (this energy is rising with a growth of the free electrons

concentration), the activation energy of the plasmochemical process decrease—something that was observed in experiments [135].

Thus, in the present work the most common expressions are obtained for the fugitiveness of carbon and nitrogen atoms, arising during plasmochemical pyrolysis. The calculations obviously demonstrate that the activation energy of plasmochemical processes depends on the free electron concentration in the plasma. This fact corresponds to the assumption that activation energy decreases due to the molecule excitation under the inelastic interactions with electrons. The Fermi energy in the plasma equals $E_F = 3,64 \cdot 10^{-15}(n)^{2/3}$ eV. In an experimental study [135] the Fermi energy was found to be equal to 0.9 eV. This value corresponds to the concentration of electrons in nanotubes, confirming sufficient accuracy in the presented calculations.

5.11 Analysis of X-Ray Photoelectron Spectra of Nitrogen Doped Carbon Nanotubes

In the scientific literature, related to XPS studies of carbon doped nanotubes are most often found the analyses of the next three methods of nitrogen interaction with a graphene lattice: graphite-like, pyridine substitution and chemisorption on chemical bonds. The equilibrium nitrogen concentrations in these three cases are defined by (5.34), (5.40), and (5.43), which we repeating there for convenience:

Graphite-type integrated nitrogen:

$$N_{\mathrm{a}}^{\mathrm{C}} = N^{\mathrm{C}} \exp\left(-\frac{g_{\mathrm{a}}^{\mathrm{C}} - \mu_{\mathrm{a}}}{kT}\right)\left[1 + \frac{N_{\mathrm{H}}}{n}\exp\left(-\frac{\varepsilon_{\mathrm{a}}^{\mathrm{C}}}{kT}\right)\right] \tag{5.78}$$

Pyridine-type integrated nitrogen:

$$N_{\mathrm{p}}^{\mathrm{C}} = N^{\mathrm{C}} \exp\left(\frac{\mu^{\mathrm{a}} - g_{\mathrm{V}}^{\mathrm{C}} - g_{\mathrm{p}}^{\mathrm{C}}}{kT}\right)\left[1 + \frac{n}{N_{\mathrm{H}}}\exp\left(\frac{\varepsilon_{\mathrm{p}}^{\mathrm{C}}}{kT}\right)\right] \tag{5.79}$$

Molecular nitrogen, chemisorbed on chemical bonds:

$$N_{\mathrm{a}}^{\sigma} = N^{\sigma} \exp\left(-\frac{g_{\mathrm{a}}^{\sigma} - \mu^{\mathrm{a}}}{kT}\right)\left[1 + \frac{N_{\mathrm{H}}}{n}\exp\left(-\frac{\varepsilon_{\mathrm{a}}^{\sigma}}{kT}\right)\right] \tag{5.80}$$

We will also use the formula for nitrogen concentration in gaseous phase (5.25):

$$N_{\mathrm{a}}^{\mathrm{g}} = N_{\mathrm{g}}^{\mathrm{a}} \exp\left(\frac{\mu_{\mathrm{a}}}{kT}\right) \exp\left(-\frac{g_{\mathrm{a}}^{\mathrm{g}}}{kT}\right) \tag{5.81}$$

and the formula for nitrogen fugitiveness in the plasmochemical process (5.76). From (5.81) we obtain for the factor, containing the nitrogen chemical potential, the expression:

$$\exp\left(\frac{\mu_{\mathrm{a}}}{kT}\right) = \frac{N_{\mathrm{a}}^{\mathrm{g}}}{N_{\mathrm{g}}^{\mathrm{a}}} \exp\left(\frac{g_{\mathrm{a}}^{\mathrm{g}}}{kT}\right) = \frac{p_{\mathrm{a}}}{p_{\mathrm{a}}^{s}} \exp\left(\frac{g_{\mathrm{a}}^{\mathrm{g}}}{kT}\right) = f_{ak} \exp\left(\frac{g_{\mathrm{a}}^{\mathrm{g}}}{kT}\right), \tag{5.82}$$

defining the nitrogen chemical potential under pyrolysis without plasma. Thus, namely for the plasmochemical process from (5.82) we obtain:

$$\exp\left(\frac{\mu_{\mathrm{a}}}{kT}\right) = \frac{N_{\mathrm{a}}^{\mathrm{g}}}{N_{\mathrm{g}}^{\mathrm{a}}} \exp\left(\frac{g_{\mathrm{a}}^{\mathrm{g}}}{kT}\right) = \frac{p_{\mathrm{a}}}{p_{\mathrm{a}}^{s}} \exp\left(\frac{g_{\mathrm{a}}^{\mathrm{g}}}{kT}\right) = f_{ak} \exp\left(\frac{g_{\mathrm{a}}^{\mathrm{g}} - q_{\alpha} E_{Fp}}{kT}\right) \tag{5.83}$$

The fugitiveness, f_{ak}, is characterized by the initial gas content (i.e., ammonia), that presents sources of both atomic and molecular nitrogen under the pyrolysis process. In the scientific literature their concentrations in the reactor are specified by the corresponding current values, which can be easily recalculated and converted into pressure and fugitiveness values. The Gibbs partial potential ($g_{\mathrm{a}}^{\mathrm{g}}$) characterized the pyrolysis process, and namely the energy losses, that are connected with atomic and molecular nitrogen generation. Undoubtedly, the pyrolysis process is a very complex one, during which form many intermediate compounds, including polymer-type substances. For example, it is known that during acetylene pyrolysis there can be named more than 68 various compounds and reaction products taking part in processes within the reactor, and therefore formula (5.54) presents a sum. Any detailed analysis is impossible due to experimental data insufficiency in the literature, and therefore we will restrict ourselves to the simple expression (5.83) whilst discussing the primary estimations of the process parameters. The Fermi energy of the plasma (E_{Fp}) depends on the plasma discharge conditions, as well as on the applied voltage and reactor construction. Therefore, this value is only evaluated for concrete-type reactors. At a first approximation it can be said that the dissociation energy decreased with a growth of electrical power used for discharge excitation in plasma. It can be supposed that these experimental and theoretical data comparisons are only qualitative and valuating, but we nevertheless can substitute (5.83) into expressions (5.78)–(5.79) and obtain formulas for the experimental data analysis in the forms:

Graphite-type integrated nitrogen:

$$N_{\mathrm{a}}^{\mathrm{C}} = N^{\mathrm{C}} f_{ak} \exp\left(\frac{g_{\mathrm{a}}^{\mathrm{g}} - q_{\alpha} E_{Fp}}{kT}\right) \exp\left(-\frac{g_{\mathrm{a}}^{\mathrm{C}}}{kT}\right)\left[1 + \frac{N_{\mathrm{H}}}{n} \exp\left(-\frac{\varepsilon_{\mathrm{a}}^{\mathrm{C}}}{kT}\right)\right]. \quad (5.84)$$

Pyridine-type integrated nitrogen:

$$N_{\mathrm{p}}^{\mathrm{C}} = N^{\mathrm{C}} f_{ak} \exp\left(\frac{g_{\mathrm{a}}^{\mathrm{g}} - q_{\alpha} E_{Fp}}{kT}\right) \exp\left(-\frac{g_{\mathrm{V}}^{\mathrm{C}} + g_{\mathrm{p}}^{\mathrm{C}}}{kT}\right)\left[1 + \frac{n}{N_{\mathrm{L}}} \exp\left(\frac{\varepsilon_{\mathrm{p}}^{\mathrm{C}}}{kT}\right)\right]. \quad (5.85)$$

Molecular nitrogen, chemisorbed on chemical bonds:

$$N_{\mathrm{a}}^{\sigma} = N^{\sigma} f_{ak} \exp\left(\frac{g_{\mathrm{a}}^{\mathrm{g}} - q_{\alpha} E_{Fp}}{kT}\right) \exp\left(-\frac{g_{\mathrm{a}}^{\sigma}}{kT}\right)\left[1 + \frac{N_{\mathrm{H}}}{n} \exp\left(-\frac{\varepsilon_{\mathrm{a}}^{\sigma}}{kT}\right)\right]. \quad (5.86)$$

In one experimental study [114] relationships between the equilibrium concentrations were obtained for nitrogen, integrated by graphene-type and pyridine-type substitution changes exponentially, approximated using the Arrhenius formula. The Arrhenius activation energy is 0.57 eV. In [125] the authors obtained a value of this energy of 0.63 eV. The middle value of activation energy is equal 0.60 ± 0.03 eV. From (5.84) and (5.85) (assuming, that the nitrogen admixture is only slightly ionized) we obtain:

$$\frac{N_{\mathrm{a}}^{\mathrm{C}}}{N_{\mathrm{p}}^{\mathrm{C}}} = \exp\left(-\frac{g_{\mathrm{a}}^{\mathrm{C}} - g_{\mathrm{V}}^{\mathrm{C}} - g_{\mathrm{p}}^{\mathrm{C}}}{kT}\right), \quad \text{then} \quad g_{\mathrm{a}}^{\mathrm{C}} - g_{\mathrm{V}}^{\mathrm{C}} - g_{\mathrm{p}}^{\mathrm{C}} = 0.60 \text{ ev} \quad (5.87)$$

This fact can explain why in studies [114, 126–128] as a whole it was observed that there was a tendency for an increase in nitrogen concentration, introduced by graphene-type substitution, and a decrease in pyridine-type substituted nitrogen when the temperature of the CNT synthesis increased under simultaneous doping.

The activation energy, obtained from experimental data of CNT doping, is equal to 1.4 eV for graphene substitution and 1.7 eV for molecular nitrogen, chemisorbed on chemical bonds. In these studies doping with ammonia was used, for which the pyrolysis activation energy was about 0.7 eV. From these results follow the values $g_{\mathrm{a}}^{\mathrm{C}}$ = 2.1 eV and g_{a}^{σ} = 2.4 eV, which are in accordance with the data in Table 5.10. The comparison allows us to return to the pyrolysis stage problems and conclude that the process or stage 4 (in Fig. 5.6a) for this table relates to the nitrogen integration by pyridine-type substitution, and processes 1 and 2 (in Fig. 5.6b) relate to the integration by graphene-type, with process 3 (in Fig. 5.6b) describing nitrogen chemisorption. Other processes are perhaps connected with the reaction product desorption, leading to the CNT growth and doping. The results of the analysis are summarized in the Table 5.8.

Thus, the above given theoretical analysis allows us to adequately describe CNT doping by nitrogen. It must be noted also, that the results of the Gibbs partial

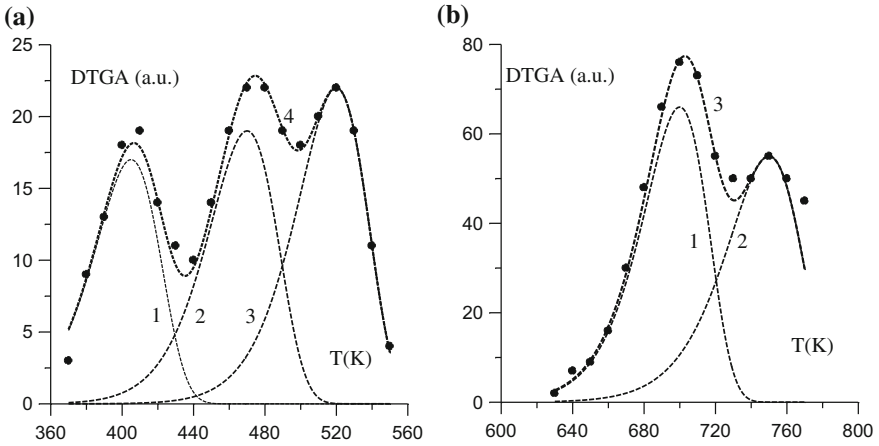

Fig. 5.6 The results of experimental curve division on separate adsorption processes with the use of formula (5.54) (the calculations were carried out using the following values of Gibbs partial energy (eV): **a** *1* 0.68; *2* 0.85; *3* 1.1; *4* summary curve; **b** *1* 2.0; *2* 2.2; *3* summary curve; *points* experimental data)

Table 5.8 Kinetic coefficients for the processes of CNT doping by nitrogen

Doping process	Kinetic coefficient
Piridine-type doping	$(3 \pm 1) \times 10^{10} \exp\left(-\frac{1.7}{kT}\right)$
Graphite-type doping	$(3 \pm 1) \times 10^{12} \exp\left(-\frac{2.1}{kT}\right)$
Nitrogen chemisorption	$(6 \pm 1) \times 10^{12} \exp\left(-\frac{2.4}{kT}\right)$

energies for chemisorption are in accordance with the quantum mechanical calculations.

5.12 Applications of Nitrogen Doped Carbon Nanotubes

5.12.1 Improvement of Emissive Properties

Carbon nanotubes are a good prospect for use as materials for so-called auto-emission cathodes, because they have many advantages over metallic needle based cathodes, for example, aspect ratio, the small curvature radius of the emitting surface, and lower yield work [136–142]. Due to the extended CNT structure and their possible orientation with respect to emitting surface, auto-emission initiation

requires a significantly lower voltage (1–3 V/mcm) compared with metals (10^4 V/mcm). The main CNT shortfalls are their rapid degradation under auto-emission processes and the limitations of the running current values. Local tube heating (and a partial tube material evaporation) causes degradation initially and then additionally by the formation of residual gases from radicals and ions, which interact with the surface and change its composition (and hence the yield work). The CNT yield work value must also be noted (4.5–5 eV). Approaches to decrease the yield work value are developed below.

It must be noted that CNT bunches, used as cold emitters, are non-uniform because nanotubes have various chiralities and conductance-types. To increase bunch uniformity nitrogen atom doping was used [143]. The nanotube growth was carried out by CVD method from a methane and ammonium mixture with use of a combined catalyst, based on ferrum and molybdenum. The nitrogen content in nanotubes was controlled by X-ray photoelectron spectroscopy method and was equal 1.2 and 1.5%. Judging this spectra, it appears that nitrogen was introducing into nanotubes by pyridine-type substitution. The Raman light scattering showed nanotubes to be of high quality. The I_G/I_D ratio of non-doped tubes was 13.5, but after nitrogen introduction this value decreased to 5.5. The morphological studies showed a growth of nanotube diameter after nitrogen introduction and corresponds to the results of other work [144, 145].

Nitrogen doping essentially influences emission current values. The threshold emission voltage falling, but the current density values rise. These results can be connected with the fact that a higher electron concentration in the structure corresponds to a lower distance between the vacuum level end Fermi level, that characterizes the system yield work [146–152]. Nitrogen doping is also connected with another factors (except the yield work), which can improve emission characteristics. Some effect is produced also by the bamboo-type morphology of nitrogen doped CNTs.

Thus, nitrogen doping allows a decrease in the threshold values of the emisission field to 2.65—3.55 V/mcm.

5.12.2 Electrodes for Ionic-Lithium Batteries

Nitrogen doped CNTs have a big prospect in nanoelectronics [153]. One of the most important applied directions is lithium-ionic cell production [153–155]. The development in this field demands for studies of CNT surface functionalization and development of the technology used for this purpose [156–158]. The most general processes of CNT surface modification are connected with oxidation [159]. Until now they have been studied sufficiently well [160–164], and are connected firstly with a heating in HNO_3, as well as in a mixture of sulfuric acid with hydrogen peroxide and other oxidizers [165–169]. As a result of this treatment the first stage of surface functionalizing can proceed—the surface becomming covered by radicals –COOH, which can adjoin some other radicals, ensuring the necessary CNT functions.

For cell and battery production the second and third functionalizing stages are carrying out by the Friedel–Grafts scheme [170], under which nanotubes are successively treated by a mixture of $AlCl_3$, PhCOCl, and $C_6H_5NO_2$ at a temperature of 180 °C for 3 h. In the third stage the surface is saturated by lithium in the course of a holding process realized in a $Li/NH_3,BrCH_2COOC_2H_5$ mixture at a temperature of 78 °C.

The commercially produced lithium-ionic cells were developed in the 1990s [171–174]. The growth of their capacitance (with conservation of compactness and lightness) demands the production of electrodes with branched surfaces, and for this purpose CNTs are very convenient. The nanotubes doped with nitrogen are used to negatively charge electrodes.

5.13 Conclusion

We have proposed a method for calculating the concentration of the dopant in nanotubes and graphene in Chap. 2, which is based on the minimization of the Gibbs free energy. This method has successfully coped with the difficult problem of the behavior of superamphoteric nitrogen during its interaction with the graphene plane. We have calculated the concentration of impurity states and major defects, which create nitrogen. This calculation represents a possible explaination for the experimental conditions required for the concentration of nitrogen occuring whilst doping nanotubes. This chapter gives an example of a successful combination of thermodynamic and kinetic approaches to solving the problem of solid-state doping.

References

1. T. Maiyalagan, B. Viswanathan, Template synthesis and characterization of well-aligned nitrogen containing carbon nanotubes. Mater. Chem. Phys. **93**, 291–295 (2005)
2. O. Stephen, P.M. Ajayan, C. Colliex, Ph Redlich, J.M. Lambert, P. Bernier, P. Letin, Doping graphitic and carbon nanotube structures with boron and nitrogen. Science **266**, 1683–1685 (1994)
3. J. Feng, Y. Li, F. Hou, X. Zhong, Controlled growth of high quality bamboo carbon nanotube arrays by the double injection chemical vapor deposition process. Mater. Sci. Eng. A **473**, 238—243 (2008); Materials **3**, 2162 (2010)
4. E.N. Nxumalo, V.O. Nyamori, N.J. Coville, CVD synthesis of nitrogen doped carbon nanotubes using ferrocene/aniline mixtures. J. Organomet. Chem. **693**, 2942–2948 (2008)
5. X.Y. Tao, X.B. Zhang, F.Y. Sun, J.P. Cheng, F. Liu, Z.Q. Luo, Large-scale CVD synthesis of nitrogen-doped multi-walled carbon nanotubes with controllable nitrogen content on a $Co_xMg_{1-x}MoO_4$ catalyst. Diamond Relat. Mater. **16**, 425–430 (2007)
6. D. Usachov, O. Vilkov, A. Guneis, D. Haberer, A. Fedorov, V.K. Adamchuk, A.B. Preobrajenski, P. Dudin, A. Barinov, M. Oehzelt, C. Laubschat, D.V. Vyalikh, Nitrogen-doped graphene: efficient growth, structure, and electronic properties. Nano Lett. **11**, 5401–5407 (2011)

7. K. Mondal, N.J. Coville, M.J. Witcomb, J. Havel, G. Tejral, Boron mediated synthesis of multiwalled carbon nanotubes by chemical vapor deposition. Chem. Phys. Lett. **43**, 787–791 (2007)
8. C.P. Ewels, M. Glerup, Nitrogen doping in carbon nanotubes. J. Nanosci. Nanotechnol. **5**, 1345–1363 (2005)
9. S. Van Dommele, K.P. Van de Jong, J.H. Bitter, Nitrogen-containing carbon nanotubes as solid base catalysts. Chem. Commun. 4859–4861 (2006)
10. S. Van Dommele, A. Romero-Izquirdo, R. Brydson, K.P. de Jong, J.H. Bittera, Tuning nitrogen functionalities in catalytically grown nitrogen-containing carbon nanotubes. Carbon **46**, 138–148 (2008)
11. P. Ayala, R. Arenal, M. Rummeli, A. Rubio, T. Pichler, The doping of carbon nanotubes with nitrogen and their potential applications. Carbon **48**, 575–586 (2010)
12. J. Robertson, C.A. Davis, Nitrogen doping of tetrahedral amorphous carbon. Diamond Relat. Mater. **4**, 441–444 (1995)
13. E.J. Biddinger, D. von Deak, U.S. Ozkan, Nitrogen-containing carbon nanostructures as oxygen-reduction catalysts. Top. Catal. **52**, 1566–1574 (2009)
14. P.J. Letsoala, L.M. Cele, E.N. Nxumalo, N.J. Coville, The influence of nitrogen sources on nitrogen doped multi-walled carbon nanotubes. Unpublished work
15. P. Ghosh, M. Zamri, M. Subramanian, T. Soga, T. Jimbo, R. Katoh, M. Tanemura, Bamboo-shaped aligned CN_x nanotubes synthesized using single feedstock at different temperatures and study of their field electron emission. J. Phys. D Appl. Phys. **41**, 155405–155412 (2008)
16. X.X. Zhang, Z.Q. Li, G.H. Wen, K.K. Fung, J. Chen, Y. Li, Microstructure and growth of bamboo-shaped carbon nanotubes. Chem. Phys. Lett. **333**, 509–514 (2001)
17. Y.Y. Wang, G.Y. Tang, F.A.M. Koeck, B. Brown, J.M. Garguilo, R.J. Nemanich, Experimental studies of the formation process and morphologies of carbon nanotubes with bamboo mode structures. Diamond Relat. Mater. **13**, 1287–1291 (2004)
18. A.G. Kudashov, A.V. Okotrub, L.G. Bulusheva, I.P. Asanov, Y.V. Shubin, N.F. Yudanov, L.I. Yudanova, V.S. Danilovich, O.G. Abrosimov, Influence of Ni-Co catalyst composition on nitrogen content in carbon nanotubes. J. Phys. Chem. B **108**, 9048—9053 (2004); Materials 32163 (2010)
19. C.H. Lin, H.L. Chang, C.M. Hsu, A.Y. Lo, C.T. Kuo, The role of nitrogen in carbon nanotube formation. Diamond Relat. Mater. **12**, 1851—1857 (2003); H. Choi, J. Ihm, S. Louie, M. Cohen, Defects, quasibound states, and quantum conductance in metallic carbon nanotubes. Phys. Rev. Lett. **84**, 2917—20 (2000)
20. X. Liu, T. Pichler, M. Knupfer, J. Fink, H. Kataura, Electronic properties of $FeCl_3$-intercalated single-wall carbon nanotubes. Phys. Rev. B **70**, 205405 (2004)
21. J. Ma, S. Guan, C.H. Lai, Disorder effect on electronic and optical properties of doped carbon nanotubes. Phys. Rev. B **74**, 205401 (2006)
22. K.Y. Chun, C.J. Lee, Potassium doping in the double-walled carbon nanotubes at room temperature. J. Phys. Chem. C **112**, 4492–4497 (2008)
23. B. Smith, M. Monthioux, D. Luzzi, Encapsulated C_{60} in carbon nanotubes. Nature **396**, 323–324 (1998)
24. H. Shinohara, Endohedral metalofullerenes. Rep. Prog. Phys. **64**, 843—892 (2000)
25. B.L.V. Prasad, H. Sato, T. Enoki, Y. Hishiyama, Y. Kaburagi, A.M. Rao et al., Intercalated nanographite: structure and electronic properties. Phys. Rev. B **64**, 235407 (2001)
26. X. Liu, T. Pichler, M. Knupfer, J. Fink, Electronic and optical properties of alkali-metal-intercalated single-wall carbon nanotubes. Phys. Rev. B **67**, 125403 (2003)
27. O. Stephan, P. Ajayan, Doping graphitic and carbon nanotube structures with boron and nitrogen. Science **266**, 1863–1865 (1994)

28. C. Ewels, M. Glerup, V. Krstić, Nitrogen and boron doping in carbon nanotubes. In *Chemistry of Carbon Nanotubes*, ed. by V. A. Basiuk, E.V. Basiuk (American Scientific Publishers, 2007)
29. S. Van Dommele, K.P. Van de Jong, J.H. Bitter, Nitrogen-containing carbon nanotubes as solid base catalysts. Chem. Commun. 4859—4861 (2006)
30. B.G. Sumpter, V. Meunier, J.M. Romo-Herrera, E. Cruz-Silva, D.A. Cullen, H. Terrones et al., Nitrogen-mediated carbon nanotube growth: diameter reduction, metallicity, bundle dispersability, and bamboo-like structure formation. Acs Nano. **1**(4), 369–375 (2007)
31. C.H. Lin, H.L. Chang, C.M. Hsu, A.Y. Lo, C.T. Kuo, The role of nitrogen in carbon nanotube formation. Diamond Relat. Mater. **12**, 1851–1857 (2003)
32. V. Bajpai, L. Dai, T. Ohashi, Large-scale synthesis of perpendicularly aligned helical carbon nanotubes. J. Am. Chem. Soc. **126**, 5070–5071 (2004)
33. Y. Saito, T. Yoshikawa, Bamboo-shaped carbon tube filled partially with nickel. J. Cryst. Growth **134**(1–2), 154–156 (1993)
34. R. Andrews, D. Jacques, A.M. Rao, F. Derbyshire, D. Qian, X. Fan et al., Continuous production of aligned carbon nanotubes: a step closer to commercial realization. Chem. Phys. Lett. **303**(5–6), 467–474 (1999)
35. C.J. Lee, S.C. Lyu, H.W. Kim, J.H. Lee, K.I. Cho, Synthesis of bamboo-shaped carbon–nitrogen nanotubes using C_2H_2–NH_3–$Fe(CO)_5$ system. Chem. Phys. Lett. **359**, 115–120 (2002)
36. D. Qian, R. Andrews, D. Jacques, P. Kichambare, G. Lian, E.C.Dickey, Low-temperature synthesis of large-area CN_x nanotube arrays. J. Nanosci. Nanotech. **3**, 93–97 (2003)
37. M. Terrones, H. Terrones, N. Grobert, W.K. Hsu, Y.Q. Zhu, J.P. Hare et al., Efficient route to large arrays of CN_x nanofibers by pyrolysis of ferrocene/melamine mixtures. Appl. Phys. Lett. **75**, 3932–3934 (1999)
38. M. Terrones, N. Grobert, J. Olivares, J.P. Zhang, H. Terrones, K. Kordatos et al., Controlled production of aligned-nanotube bundles. Nature **388**(6637), 52–55 (1997)
39. R. Che, L.-M. Peng, Q. Chen, X.F. Duan, Z.N. Gu, Fe_2O_3 particles encapsulated inside aligned CN_x nanotubes. Appl. Phys. Lett. **82**, 3319–3321 (2003)
40. C.C. Tang, Y. Bando, D. Golberg, F.F. Xu, «Structure and nitrogen incorporation of carbon nanotubes synthesized by catalytic pyrolysis of dimethylformamide. Carbon **42**(12–13), 2625–2633 (2004)
41. X.B. Wang, W.P. Hu, Y.Q. Liu, C.F. Long, Y. Xu, S.Q. Zhou et al., Bamboo-like carbon nanotubes produced by pyrolysis of iron(II) phthalocyanine. Carbon **39**(10), 1533–1536 (2001)
42. M. Becker, H. Bender, M. Jansen, L. Kienle, W. Assenmacher, Efficient access to bamboo-like carbon micro and nanofibres by pyrolysis of zinc cyanamide. J. Phys. Chem. Solids **62**(8), 1431–1433 (2001)
43. R.M. Yadav, P.S. Dobal, T. Shripathi, R.S. Katiyar, O.N. Srivastava, Effect of growth temperature on bamboo-shaped carbon–nitrogen (C–N) nanotubes synthesized using ferrocene acetonitrile precursor. Nanoscale Res. Lett. **4**, 197–203 (2009)
44. J. Jiang, T. Feng, X. Cheng, L. Dai, G. Cao, B. Jiang, X. Wang, X. Liu, S. Zou, Synthesis and growth mechanism of Fe-catalyzed carbon nanotubes by plasma-enhanced chemical vapor deposition. Nucl. Instrum. Meth. B **244**, 327–332 (2006)
45. C.J. Lee, J. Park, Growth model of bamboo-shaped carbon nanotubes by thermal chemical vapordeposition. Appl. Phys. Lett. **77**, 3397–3399 (2000)
46. S. Trasobares, O. Stephan, C. Colliex, W.K. Hsu, H.W. Kroto, D.R.M. Walton, Compartmentalized CN_x nanotubes: chemistry, morphology, and growth. J. Chem. Phys. **116**, 8966—8972 (2002); S.B. Sinnot, R. Andrews, D. Qian, A.M. Rao, Z. Mao, E.C. Dickey, F. Derbyshire, Model of carbon nanotube growth through chemical vapor deposition. Chem. Phys. Lett. **315**, 25—30 (1999)

47. R. Czerw, M. Terrones, J.C. Charlier, X. Blase, B. Foley, R. Kamalakaran, N. Grobert, H. Terrones, D. Tekleab, P.M. Ajayan, W. Blau, M. Ruhle, D.L. Carroll, Identification of electron donor states in N-doped carbon nanotubes. Nano Lett. **1**, 457—460 (2001)
48. K. Xiao, Y.Q. Liu, P.A. Hu, G. Yu, Y.M. Sun, D.B. Zhu, n-Type field-effect transistors made of an individual nitrogen-doped multiwalled carbon nanotube. J. Am. Chem. Soc. **127**, 8614–8617 (2005)
49. M. Terrones, N. Grobert, H. Terrones, Synthetic routes to nanoscale $B_xC_yN_z$ architectures. Carbon **40**, 1665—1684 (2002); J.J. Velázquez-Salazar, E. Munoz-Sandoval, J.M. Romo-Herrera, F. Lupo, M. Ruhle, H. Terrones, M. Terrones, Synthesis and state of art characterization of BN bamboo-like nanotubes: evidence of a root growth mechanism catalyzed by Fe. Chem. Phys. Lett. **416**, 342—348 (2005)
50. P.E. Lammert, V.H. Crespi, Stochastic heterostructures and diodium in B/N-doped carbon nanotubes. Phys. Rev. Lett. **87**, 136402:1—136402:4 (2001)
51. B.Q. Wei, R. Spolenak, P.K. Redlich, M. Ruhle, E. Arzt, Electrical transport in pure and boron-doped carbon nanotubes. Appl. Phys. Lett. **74**, 3149–3151 (1999)
52. D.L. Carroll, P. Redlich, X. Blase, J.C. Charlier, S. Curran, P.M. Ajayan, S. Roth, M. Ruhle, Effects of nanodomain formation on the electronic structure of doped carbon nanotubes. Phys. Rev. Lett. **81**, 2332–2335 (1998)
53. D. Golberg, Y. Bando, C.C. Tang, C.Y. Zhi, Boron nitride nanotubes. Adv. Mater. **19**, 2413–2432 (2007)
54. R.B. Sharma, D.J. Late, D.S. Joag, A. Govindaraj, C.N.R. Rao, Field emission properties of boron and nitrogen doped carbon nanotubes. Chem. Phys. Lett. **428**, 102—108 (2006); M.S. Dresselhaus, F. Dresselhaus, R. Saito, A. Jorio, Raman spectroscopy of carbon nanotubes. Phys. Rep. **409**, 47—99 (2005)
55. Y. Li, B. Zhang, X.Y. Tao, J.M. Xu, W.Z. Huang, J.H. Luo, T. Li, Y. Bao, H.J. Geise, Mass production of high-quality multi-walled carbon nanotube bundles on a Ni/Mo/MgO catalyst. Carbon **43**, 295–301 (2005)
56. P. Tan, L. An, L. Liu, Z. Guo, R. Czerw, D.L. Carroll, P.M. Ajayan, N. Zhang, H. Guo, Probing the phonon dispersion relations of graphite from the double-resonance process of Stokes and anti-stokes Raman scatterings in multiwalled carbon nanotubes. Phys. Rev. B. **66**, 245410–245418 (2002)
57. W. Lv, K. Shi, L. Li, S. Shao, Nitrogen-doped multiwalled carbon nanotubes and their electrocatalysis towards oxidation of NO. Microchim Acta **170**, 91 (2010)
58. H.D. Zhao, Q. Wagner, Raman spectroscopy of carbon-nanotube-based composites. Phil. Trans. R. Soc. Lond. A. **362**, 2407—2424 (2004)
59. J.-Q. Huang, M.-Q. Zhao, Q. Zhang, J.-Q. Nie, L.-D.Yao, D.S. Su, F. Wei, Efficient synthesis of aligned nitrogen-doped carbon nanotubes in a fluidized-bed reactor. Catalysis Today **186** 83–92 (2012)
60. S.Y. Kim, J. Lee, C.W. Na, J. Park, K. Seo, B. Kim, N-doped double-walled carbon nanotubes synthesized by chemical vapor deposition. Chem. Phys. Lett. **413**, 300–305 (2005)
61. B.C. Bayer, C. Baehtz, P.R. Kidambi, R.S. Weatherup, C. Mangler, J. Kotakoski, C.J.L. Goddard, S. Caneva, A. Cabrero-Vilatela, J.C. Meyer, S. Hofmann, Nitrogen controlled iron catalyst phase during carbon nanotube growth. Appl. Phys. Lett. **105**, 143111–143115 (2014)
62. T.-Y. Kim, K.-R. Lee, K.Y. Eun, K.-H. Oh, Carbon nanotube growth enhanced by nitrogen incorporation. Chem. Phys. Lett. **372**, 603—607 (2003)
63. J.W. Jang, C.E. Lee, S.C. Lyu, T.J. Lee, C.J. Lee, Structural study of nitrogen-doping effects in bamboo-shaped multiwalled carbon nanotubes. Appl. Phys. Lett. **84**(15), 2877–2879 (2004); H. Jin, N. Bing, L. Wang, L. Wang, Synthesis of nitrogen incorporated carbon nanotubes with different diameters by catalytic pyrolysis of butylamine. Chem. Res. Chinese Univ. **27**(6), 903—905 (2011)

64. M.-H. Wu, X. Li, D. Pan, L. Liu, X.-X. Yang, Z. Xu, W.-L. Wang, Y. Sui, X.-D. Bai, Synthesis of nitrogen-doped single-walled carbon nanotubes and monitoring of doping by Raman spectroscopy. Chin. Phys. B **22**(8) 086101 (2013)
65. S.V. Bulyarskiy, Uglerodnye nanotrubky: techologya, upravlenie svoystvami, primenenie. Ulyanovsk, Streshen, 479 s. (Rus.) (2011)
66. J.C. Charlier, Defects in carbon nanotubes. Acc. Chem. Res. **35**(12), 1063–1069 (2002)
67. V. Krstić, G.L.J.A. Rikken, P. Bernier, S. Roth, M. Glerup, Nitrogen doping of metallic single-walled carbon nanotubes: n-type conduction and dipole scattering. EPL (Europhysics Letters). **77**(3), 37001 (2007)
68. M. Mananghaya, E. Rodulfo, G.N. Santos et al. Theoretical investigation on single-wall carbon nanotubes doped with nitrogen, pyridine-like nitrogen defects, and transition metal atoms. J. Nanomater. **2012**, 104891 2012
69. S.H. Lim, H.I. Elim, X.Y. Gao, A.T.S. Wee, W. Ji, J.Y. Lee, J. Lin, Electronic and optical properties of nitrogen doped multiwalled carbon nanotubes. Phys. Rev. B. 73045402 (2006)
70. X. Yang, L. Yuan, V.K. Peterson, A.I. Minett, Y. Yin, A.T. Harris, Facile preparation of free-standing carbon nanotube arrays produced using two-step floating-ferrocene chemical vapor deposition. ACS Appl. Mater. Inter. **4**, 1417–1422 (2012)
71. M. Xu, D.N. Futaba, M. Yumura, K. Hata, Alignment control of carbon nanotube forest from random to nearly perfectly aligned by utilizing the crowding effect. ACS Nano **6**, 5837–5844 (2012)
72. S.P. Patole, P.S. Alegaonkar, H.-C. Shin, J.-B.Yoo, Alignment and wall control of ultra long carbon nanotubes in water assisted chemical vapour deposition. J. Phys. D: Appl. Phys. **41** 155311 (2008)
73. X. Yang, L. Yuan, V.K. Peterson, Y. Yin, A.I. Minett, A.T. Harris, Open-ended aligned carbon nanotube arrays produced using CO_2-assisted floating-ferrocene chemical vapor deposition. J. Phys. Chem. C **115**, 14093–14097 (2011)
74. S. Esconjauregui, M. Fouquet, B. Bayer, J. Robertson, Carbon nanotubes growth: from entanglement to vertical alignment. Phys. Status Solidi. B **247**, 2656–2974 (2010)
75. Z. Yang, X. Chen, H. Nie, K. Zhang, W. Li, B. Yi, L. Xu, Direct synthesis of ultralong carbon nanotube bundles by spray pyrolysis and investigation of growth mechanism. Nanotechnology **19**, 085606 (2008)
76. H. Liu, Y. Zhang, R. Li, X. Sun, S. Desilets, H. Abou-Rachid, M. Jaidann, L.-S. Lussier, Structural and morphological control of aligned nitrogen-doped carbon nanotubes. Carbon **48**, 1498–1507 (2010)
77. W. Grogger, M. Varela, R. Ristau, B. Schaffer, F. Hofer, K.M. Krishnan, Energy-filtering transmission electron microscopy on the nanometer length scale. J. Electron Spectrosc. Relat. Phenom. **143**, 139–147 (2005)
78. C.P. Liu, C.B. Boothroyd, C.J. Humphreys, Energy-filtered transmission electron microscopy of multilayers in semiconductors. J. Microsc. **194**(Pt 1), 58–70 (1999)
79. W. Deng, X. Chen, X. Chen, Z. Liu, Y. Zeng, A. Hu, Y. Xiong, Z. Li, Q. Tang, Alignment and structural control of nitrogen doped carbon nanotubes by utilizing precursor concentration effect. Nanotechnology **25**, 475601, 10 p (2014)
80. R. Arenal, K. March, C.P. Ewels, X. Rocquefelte, M. Kociak, A. Loiseau, O. Stéphan, Atomic configuration of nitrogen-doped single-walled carbon nanotubes. arenal@unizar.es
81. C. Morant, R. Torres, I. Jimenez, J.M. Sanz, E. Elizalde, Characterization of nitrogen-doped carbon nanotubes by atomic force microscopy, X-ray photoelectron spectroscopy and X-ray absorption near edge spectroscopy. J. Nanosci. Nanotechnol. **8**, 1–6 (2008)
82. C.P. Ewels, M. Glerup, Nitrogen doping in carbon nanotubes. J. Nanosci. Nanotech. **5**(9), 1345–1363 (2005)
83. T. Xing, Y. Zheng, L.H. Li, B.C.C. Cowie, D. Gunzelmann, S.Z. Qiao, S. Huang, Y. Chen, Observation of active sites for oxygen reduction reaction on nitrogen-doped multilayer graphene. ACS Nano **8**(7), 6856–6862 (2014)

84. Z. Luo, S. Lim, Z. Tian, J. Shang, L. Lai, B. MacDonald, C. Fu, Z. Shen, T. Yu, Jianyi Lin, Pyridinic N doped graphene: synthesis, electronic structure, and electrocatalytic property. J. Mater. Chem. **21**, 8038–8044 (2011)
85. Z. Yang, H. Nie, X. Chen, X. Chen, S. Huang, Recent progress in doped carbon nanomaterials as effective cathode catalysts for fuel cell oxygen reduction reaction. J. Power Sources **236**, 238–249 (2013)
86. D.Q. Duy, H.S. Kim, D.M. Yoon, J.W. Ha, K.J. Lee, Y.G. Hwang, C.H. Lee, Role of atomic and molecular nitrogen in carbon nanotube formation. J. Korean Phys. Soc. **54**(4), 1554–1558 (2009)
87. S.-C. Chang, T.-S. Li, T.-C. Lin, Significant morphology dependence on nitrogen proportion in growing carbon nanotubes. Mater. Lett. **62**, 1893–1895 (2008)
88. J.W. Jang, C.E. Lee, S.C. Lyu, T.J. Lee, C.J. Lee, Structural study of nitrogen-doping effects in bamboo-shaped multiwalled carbon nanotubes. Appl. Phys. Lett. **84**(15), 2877—2879 (2004)
89. C.H. Lin, H.L. Chang, C.M. Hsu, A.Y. Lo, C.T. Kuo, The role of nitrogen in carbon nanotube formation. Diamond Relat. Mater. **12**, 1851–1857 (2003)
90. D. Srivastava, M. Menon, C. Daraio, S. Jin, Vacancy-mediated mechanism of nitrogen substitution in carbon nanotubes. Phys. Rev. B **69**, 153414-4 (2004)
91. R. Ohta, K.H. Lee, N. Saito, Y. Inoue, H. Sugimura, O. Takai, Origin of N 1s spectrum in amorphous carbon nitride obtained by X-ray photoelectron spectroscopy. Thin Solid Films **434**, 296–302 (2003)
92. H. Liu, Y. Zhang, R. Li, X. Sun, S. Désilets, H. Abou-Rachid, M. Jaidann, L.-S. Lussier, Structural and morphological control of aligned nitrogen doped carbon nanotubes. Carbon **48**, 1498—1507 (2010)
93. D. Yu, Y. Xue, L. Dai, Vertically aligned carbon nanotube arrays co-doped with phosphorus and nitrogen as efficient metal-free electrocatalysts for oxygen reduction. J. Phys. Chem. Lett. **3**, 2863–2870 (2012)
94. V. Krstić, G.L.J.A. Rikken, P. Bernier, S. Roth, M. Glerup, Nitrogen doping of metallic single-walled carbon nanotubes: n-type conduction and dipole scattering. EPL (Europhys. Lett.) **77**(3), 37001 (2007)
95. M. Mananghaya, E. Rodulfo, G.N. Santos et al., Theoretical investigation on single-wall carbon nanotubes doped with nitrogen, pyridine-like nitrogen defects, and transition metal atoms. J. Nanomater. **2012**, 104891 (2012)
96. A.H. Nevidomskyy, G. Csanyi, M.C. Payne, Chemically active substitutional nitrogen impurity in carbon nanotubes. Phys. Rev. Lett. **91**(10), 1055021–1055024 (2003)
97. О.Е. Глухова, О.А. Терентьев, Теоретическое исследование электронных и механических свойств C-N однослойных нанотрубок. Физика волновых процессов и радиотехнические системы. Т. **10**(4), С. 85—89 (2007)
98. Y. Fujimoto, S. Saito, Structure and stability of hydrogen atom adsorbed on nitrogen-doped carbon nanotubes. J. Phys. Conf. Ser. **302**(1), 012006 (2011)
99. J. Zhao, A. Buldum, J. Han, J.P. Lu, Gas molecule adsorption in carbon nanotubes and nanotube bundles. Nanotechnology **13**(2), 195–200 (2002)
100. G.U. Sumanesekera, C.K.W. Adu, S. Fang, P.C. Eklund, Effects of gas adsorption and collisions on electrical transport in single-walled carbon nanotubes. Phys. Rev. Lett. **85**(5), 1096–1099 (2000)
101. C. Marliere, P. Poncharal, L. Vaccarini, A. Zahab, Effect of gas adsorption on the electrical properties of single-walled carbon nanotubes mats. MRS Online Proc. Libr. **593** (1999). doi: http://dx.doi.org/10.1557/PROC-593-173
102. Z. Li, Z. Pan, S. Dai, Nitrogen adsorption characterization of aligned multiwalled carbon nanotubes and their acid modification. J. Colloid Interface Sci. **277**(1), 35–42 (2004)
103. D. Srivastava, M. Menon, B. Sadanadan et al., Vacancy mediated mechanism of nitrogen substitution in carbon nanotubes. Phys. Rev. B **69**(15), 153414 (2004)
104. S.H. Lim, R. Li, W. Ji, J. Lin, Effects of nitrogenation on single-walled carbon nanotubes within density functional theory. Phys. Rev. B **76**(19), 195406 (2007)

105. X.M. Min, D.X. Lan, F. Cheng, Study on oxygen and nitrogen adsorption in carbon nanotube. Department of Applied Chemistry, Wuhan University of Technology, Wuhan. Published in: *2nd IEEE International Nanoelectronics Conference*. INEC (2008)
106. M. Xin-min, X. Rui-juan, H. Han-lie, Quantum chemistry calculation on oxygen and nitrogen adsorption in carbon nanotube. J. Wuhan Univ. Technol. Mater. Sci. Ed. **18**(1), 1–3 (2003)
107. A.S. Ghsemi, F. Ashrafi, Density functional theory (DFT) study of O_2, N_2 adsorptions on H-capped (4,4) single-walled carbon nanotube. J. Appl. Sci. Eng. Technol. **4**(15), 2523–2528 (2012)
108. M.R. Mananghaya, Carbon nanotubes doped with nitrogen, pyridine-like nitrogen defects, and transition metal atoms. J. Korean Chem. Soc. **56**(1), 34–46 (2012)
109. M. Rossi, A. Fazzio, A.J.R. da Silva, Theoretical study of N-complexes in carbon nanotubes. ajrsilva@if.usp.br
110. R. Czerw, M. Terrones, J.-C. Charlier, X. Blase, B. Foley, R. Kamalakaran, N. Grobert, H. Terrones, P. M. Ajayan, W. Blau, D. Tekleab, M. Rühle, D. L. Carroll, Identification of electron donor states in N-doped carbon nanotubes. arXiv:cond-mat/0011318v1 [cond-mat.mtrl-sci] 20 Nov 2000
111. W.J. Mendes Lima, D.L. Azevedo, S. Guerini, B and N-doped double walled carbon nanotube: a theoretical study. Cent. Eur. J. Phys. **8**(5), 811—818 (2010)
112. A.P. Popov, I.V. Bazhin, Influence of impurities and defects on electronic structure of carbon nanotubes. Hydrogen Mater. Sci. Chem. Carbon Nanomater. 795—799 (2007)
113. X.M. Min, D.X. Lan, F. Cheng, Study on oxygen and nitrogen adsorption in carbon nanotube. Department of Applied Chemistry, Wuhan University of Technology, Wuhan; Published in*: 2nd IEEE International Nanoelectronics Conference*. INEC (2008)
114. J. Liu, S. Webster, D.L. Carroll, Temperature and flow rate of NH_3 effects on nitrogen content and doping environments of carbon nanotubes grown by injection CVD method. J. Phys. Chem. B **109**, 15769–15774 (2005)
115. S.V. Bulyarsky, V.P. Oleinicov, Thermodynamically evaluation of point defect density and impurity solubility in component semiconductor. Phys. Stat. Sol. (b) **141**, K7–K10 (1987)
116. S.V. Bulyarsky, V.P. Oleinicov, Thermodynamics of defect interaction in compound semiconductors. Phys. Stat. Sol. (b) **146**, 439—444 (1988)
117. S.V. Bulyarskiy, Uglerodnye nanotrubky: techologya, upravlenie svoystvami, primenenie. Ulyanovsk, Streshen, 479 s (2011)
118. S.V. Bulyarskiy, A.S. Basaev, Thermodynamics and kinetics of adsorption of atoms and molecules with carbon nanotubes. ZhETF **135**(4), 788–799 (2009)
119. Q. Ding, X. Song, X. Yao, X. Qi, C.-T. Au, W. Zhong, Y. Du, Large-scale and controllable synthesis of metal-free nitrogen-doped carbon nanofibers and nanocoils over water-soluble Na_2CO_3. Nanoscale Res. Lett. **8**, 545–563 (2013)
120. E.N. Nxumalo, V.O. Nyamori, N.J. Coville, CVD synthesis of nitrogen doped carbon nanotubes using ferrocene/aniline mixtures. J. Organomet. Chem. **693**, 2942–2948 (2008)
121. F. Villalpando-Paez, A. Zamudio, A.L. Elias, H. Son, E.B. Barros, S.G. Chou, Y.A. Kim, H. Muramatsu, T. Hayashi, J. Kong, H. Terrones, G. Dresselhaus, M. Endo, M. Terrones, M.S. Dresselhaus, Synthesis and characterization of long strands of nitrogen-doped single-walled carbon nanotubes. Chem. Phys. Lett. **424**, 345–352 (2006)
122. J. Hai-ying, B. Nai-ci, W. Ling-ling, W. Li-jun, Synthesis of nitrogen incorporated carbon nanotubes with different diameters by catalytic pyrolysis of butylamine. Chem. Res. Chin. Univ. **27**(6), 903–905 (2011)
123. T-Feng Hung, M.-H. Tu, C.-W. Tsai, C.-J. Chen, R.-S. Liu, W.-R. Liu, M.-Y. Lo, Influence of pyrolysis temperature on oxygen reduction reaction activity of carbon-incorporating iron nitride nitrogen-doped graphene nanosheets catalyst. Int. J. Hydrogen Energy **38**, 3956–3962 (2013)
124. Y. Mao, H. Duan, L. Zhang, Y. Hu, C. Zhao, Z. Wang, L. Chen, Y. Yang, Lithium storage in nitrogen-rich mesoporous carbon materials. Energy Environ. Sci. **5**, 7950–7955 (2012)

125. W. Lv, K. Shi, L. Li, S. Shao, Nitrogen-doped multiwalled carbon nanotubes and their electrocatalysis towards oxidation of NO. Microchim Acta, **170**, 91–98 (2010)
126. A. Dorjgotov, J. Ok, Y. Jeon, S.-H. Yoon, Y.G. Shul, Activity and active sites of nitrogen-doped carbon nanotubes for oxygen reduction reaction. J. Appl. Electrochem. **43,** 387–397 (2013)
127. W.-X. Lv, R. Zhang, T.-L. Xia, H.-M. Bi, K.-Y. Shi, Influence of NH_3 flow rate on pyridine-like N content and NO electrocatalytic oxidation of N-doped multiwalled carbon nanotubes. J. Nanopart. Res. **13**, 2351–2360 (2011)
128. M.S. Bell, R.G. Lacerda, K.B.K. Teo, W.I. Milne, Characterisation of the growth mechanism during PECVD of multiwalled carbon nanotubes. Top. Appl. Phys. **100**, 77–93 (2006)
129. M. Okai, T. Muneyoshi, T. Yaguchi, S. Sasaki, Structure of carbon nanotubes grown by microwave-plasma-enhanced chemical vapor deposition. Appl. Phys. Lett. **77**(21), 3468–3470 (2000)
130. C. Bower, W. Zhu, S. Jin, O. Zhou, Plasma-induced alignment of carbon nanotubes. Appl. Phys. Lett. **77**(6), 830–832 (2000)
131. J. Li, R. Stevens, L. Delzeit, H.T. Ng, A. Cassell, J. Han, M. Meyyappan, Nucleation and growth of carbon nanotubes by microwave plasma enhanced chemical vapor deposition. Appl. Phys. Lett. **81**, 910–914 (2002)
132. V.I. Merkulov, A.V. Melechko, M.A. Guillorn, D.H. Lowndes, M.L. Simpson, Effects of spatial separation on the growth of vertically aligned carbon nanofibers produced by plasma-enhanced chemical vapor deposition. Appl. Phys. Lett. **80**, 476–478 (2002)
133. Z. Ren et al., Physics of direct current plasma-enhanced chemical vapor deposition. In *Aligned Carbon Nanotubes, NanoScience and Technology* (Springer, Berlin, 2013). C. pp. 93–109
134. Z.F. Ren, Z.P. Huang, J.W. Xu, J.H. Wang, P. Bush, M.P. Siegal, P.N. Provencio, Synthesis of large arrays of well-aligned carbon nanotubes on glass. Science **282**, 1105–1107 (1998)
135. Y. Wang, S.H. Jo, S. Chen, D.Z. Wang, Z.F. Ren, Aligned carbon nanofibres by a low-energy dark discharge for field emission and optoelectronics. Nanotechnology **17**(2), 501–505 (2006)
136. W.A. De Heer, A. Chatelain, D. Ugarte, Carbon nanotube field emission electron source. Science **270**(5239), 1179–1180 (1995)
137. N. De Jonge, Y. Lamy, K. Schoots, R.H. Oosterkamp, High brightness electron beam from a multi-walled carbon nanotube. Nature **420**(6914), 393–395 (2002)
138. J.M. Bonard, K.A. Dean, B.F. Coll, C. Klinke, Field emission of individual carbon nanotubes in the scanning electron microscope. Phys. Rev. Lett. **89**(19), 197602–197605 (2002)
139. V. Meunier, C. Roland, J. Bemholc, M.B. Nardelli, Electronic and field emission properties of boron nitride/carbon nanotube superlattices. Appl. Phys. Lett. **81**(1), 46–48 (2002)
140. Y.J. Li, Z. Sun, S.P. Lau, G.Y. Chen, B.K. Tay, Carbon nanotube films prepared by thermal chemical vapor deposition at low temperature for field emission applications. Appl. Phys. Lett. **79**(11), 1670–1672 (2001)
141. N.G. Shang, C.P. Li, W.K. Wong, C.S. Lee, I. Bello, S.T. Lee, Microstructure and field emission properties of coral-like carbon nanotubes. Appl. Phys. Lett. **81**(26), 5024–5026 (2002)
142. Y. Saito, S. Uemura, Field emission from carbon nanotubes and its application to electron sources. Carbon **38**(2), 169–182 (2000)
143. K.-Y. Chuna, H.S. Leeb, C.J. Lee, Nitrogen doping effects on the structure behavior and the field emission performance of double-walled carbon nanotubes. Carbon **47**, 169–177 (2009)
144. S.H. Lim, H.I. Elim, X.Y. Gao, A.T.S. Wee, W. Ji, J.Y. Lee et al. Electronic and optical properties of nitrogen-doped multiwalled carbon nanotubes. Phys. Rev. B **73**(4), 045402-1–045402-6 (2006)
145. S. Maldonado, S. Morin, J. Stevenson, Structure, composition, and chemical reactivity of carbon nanotubes by selective nitrogen doping. Carbon **44**(8), 1429–1437 (2006)

146. S.K. Srivastava, V.D. Vankar, D.V. Sridhar Rao, V. Kumar, Enhanced field emission characteristics of nitrogen-doped carbon nanotube films grown by microwave plasma enhanced chemical vapor deposition process. Thin Solid Films **515**(4), 1851–1856 (2006)
147. S.H. Ahna, K.R. Lee, D.Y. Kim, S. Han, Field emission of doped carbon nanotubes. Appl. Phys. Lett. **88**(9), 093122-1–093122-3 (2006)
148. L. Qiao, W.T. Zheng, H. Xu, L. Zhang, Q. Jiang, Field emission properties of N-doped capped single-walled carbon nanotubes: a first-principles density-functional study. J. Chem. Phys. **126**(16), 164702-1–164702-7 (2007)
149. K.A. Dean, O. Groening, O.M. Kuttel, L. Schlapbach, Nanotube electronic states observed with thermal field emission electron spectroscopy. Appl. Phys. Lett. **75**(18), 2773–2775 (1999)
150. D. Lovall, M. Buss, E. Graugnard, R.P. Andres, R. Reifenberger, Electron emission and structural characterization of a rope of single-walled carbon nanotubes. Phys. Rev. B **61**(8), 5683–5691 (2000)
151. S.W. Yoon, S.Y. Kim, J. Park, C.J. Park, C.J. Lee, Electronic structure and field emission of multi-walled carbon nanotubes depending on growth temperature. J. Phys. Chem. B **109**(43), 20403–20406 (2005)
152. B. Ha, C.J. Lee, Electronic structure and field emission properties of in situ potassium-doped single-walled carbon nanotubes. Appl. Phys. Lett. **90**(2), 023108-1–023108-3 (2007)
153. T. Maiyalagan, B. Viswanathan, U.V. Varadaraju, Nitrogen containing carbon nanotubes as supports for Pt—alternate anodes for fuel cell applications. Electrochem. Commun. **7**(9), 905–912 (2005)
154. X. Li, J. Liu, Y. Zhang, Y. Li, H. Liu, X. Meng et al., High concentration nitrogen doped carbon nanotube anodes with superior Li^+ storage performance for lithium rechargeable battery application. J. Power Sources **197**, 238–245 (2012)
155. F. Villalpando-Páez, A.H. Romero, E. Muñoz-Sandoval, L.M. Martí et al., Fabrication of vapor and gas sensors using films of aligned CN_x nanotubes. Chem. Phys. Lett. **386**(1–3), 137–143 (2004)
156. C.R. Martin, P. Kohli, The emerging field of nanotube biotechnology. Nat. Rev. Drug Discovery **2**(1), 29–37 (2003)
157. R. Andrews, M.C. Weisenberger, Carbon nanotube polymer composites. Curr. Opin. Solid State Mater. Sci. **8**(1), 31–37 (2004)
158. A. Hirsch, O. Vostrowsky, Functionalization of carbon nanotubes. Top. Curr. Chem. **245**, 193–237 (2005)
159. J. Liu, A.G. Rinzler, H. Dai, J.H. Hafner, R.K. Bradley, P.J. Boul et al., Fullerene pipes. Science **280**(5367), 1253–1256 (1998)
160. K.J. Ziegler, Z. Gu, H. Peng, E.L. Flor, R.H. Hauge, R.E. Smalley, Controlled oxidative cutting of single-walled carbon nanotubes. J. Am. Chem. Soc. **127**(5), 1541–1547 (2005)
161. V. Datsyuk, M. Kalyva, K. Papagelis, J. Parthenios, D. Tasis, A. Siokou et al., Chemical oxidation of multiwalled carbon nanotubes. Carbon **46**(6), 833–840 (2008)
162. J. Zhang, H. Zou, Q. Qing, Y. Yang, Q. Li, Z. Liu et al., Effect of chemical oxidation on the structure of single-walled carbon nanotubes. J. Phys. Chem. B **107**(16), 3712–3718 (2003)
163. Z. Spitalský, C.A. Krontiras, S.N. Georga, C. Galiotis, Effect of oxidation treatment of multiwalled carbon nanotubes on the mechanical and electrical properties of their epoxy composites. composites part A. Appl. Sci. Manuf. **40**(6–7), 778–783
164. C.-C. Hu, J.-H. Su, T.-C. Wen, Modification of multi-walled carbon nanotubes for electric double-layer capacitors: tube opening and surface functionalization. J. Phys. Chem. Solids **68**(12), 2353–2362 (2007)
165. H. Hu, B. Zhao, M.E. Itkis, R.C. Haddon, Nitric acid purification of single-walled carbon nanotubes. J. Phys. Chem. B **107**(50), 13838–13842 (2003)
166. I.D. Rosca, F. Watari, M. Uo, T. Akasaka, Oxidation of multiwalled carbon nanotubes by nitric acid. Carbon **43**(15), 3124–3131 (2005)

167. D.V. Kosynkin, A.L. Higginbotham, A. Sinitskii, J.R. Lomeda, A. Dimiev, B.K. Price et al., Longitudinal unzipping of carbon nanotubes to form graphene nanoribbons. Nature **458** (7240), 872–876 (2009)
168. H. Hiura, T.W. Ebbesen, K. Tanigaki, Opening and purification of carbon nanotubes in high yields. Adv. Mater. **7**(3), 275–276 (1995)
169. J.M. Simmons, B.M. Nichols, S.E. Baker, M.S. Marcus, O.M. Castellini, C.S. Lee et al., Effect of ozone oxidation on single-walled carbon nanotubes. J Phys Chem B **110**(14), 7113–7118 (2006)
170. T.S. Alaban, M.C. Alaban, S. Malik, F.Hennrich, H. Fischer Sner, Polyacylation of single-walled carbon nanotubes under Friedel–crafts conditions: an efficient method for functionalizing. Purifying, decorating, and linking carbon allotropes. Adv. Mater. **18**, 2763–2767 (2006)
171. T. Nagaura, K. Tozawa, Prog. Batteries Sol. Cells **9**, 209 (1990)
172. E. Stura, C. Nicolini, New nanomaterials for light weight lithium batteries. Anal. Chim. Acta **568**(1–2), 57–64 (2006)
173. M. Armand, J.M. Tarascon, Building better batteries. Nature **451**(7179), 652–657 (2008)
174. J.M. Tarascon, M. Armand, Issues and challenges facing rechargeable lithium batteries. Nature **414**(6861), 359–367 (2001)

Chapter 6
Carbon Nanotube Doping by Acceptors. The *p–n* Junction Formation

Alexandr Saurov, Sergey Bulyarskiy and Alexandr Pavlov

Abstract This chapter investigates the interaction of boron with CNTs. A brief analysis of the scientific literature shows that for data for calculation of boron concentration, one can use formulas from the previous chapter.

This chapter investigates the interaction of boron with CNTs. A brief analysis of the scientific literature shows that for data for calculation of boron concentration, one can use formulas from the previous chapter.

In this chapter we discuss the prospects of creating *p–n* junctions in the arrays of CNTs.

6.1 The Electronic Properties of Boron-Doped Nanotubes

Under the doping process boron substitutes carbon in a node on a carbon lattice. This carbon atom has an electronic configuration $2s^2 2p^1$, and therefore at substitution boron is producing an acceptor effect. The Fermi level in such a boron-doped CNT decreases, bringing it nearer to the valence zone. The calculations, carried out using pseudopotential methods [1], allow us to find the parameters of CNTs with chiralities of [8,0], [10,0], and [16,0], which correspond to the total energy minimum along with their zone structure and electron state spectrum.

For calculations high concentration boron was used, which promoted a more obvious change in nanotube electronic characteristics. The calculations showed a

A. Saurov (✉) · S. Bulyarskiy · A. Pavlov
Institute Nanotechnology of Microelectronics, Russian Academy of Sciences, Moscow, Russia
e-mail: a.saurov@tcen.ru

S. Bulyarskiy
e-mail: bulyar2954@mail.ru

A. Pavlov
e-mail: alexander.a.pavlov@gmail.com

S. Bulyarskiy and A. Saurov (eds.), *Doping of Carbon Nanotubes*, NanoScience and Technology, DOI 10.1007/978-3-319-55883-7_6

state density rise near the CNT valence zone, and this density increased with boron concentration rise. The appearance of acceptor properties represented an important component of CNT doping by boron, attracting the attention of researchers [2–6].

The Raman light scattering spectrum demonstrated the intensity rise for lines corresponding to defects formation due to a rise in doping boron concentration [7]. In on piece of work [8] the optical properties of boron and nitrogen doped carbon nanotubes, grown by electric arc method, were studied. The measurements of tube diameter distribution showed that non-doped and nitrogen doped nanotubes have roughly the same diameters, of the order of 13 nm, but under boron doping the diameter decreased by about 20% [8].

The boron-doped CNT absorption peak, connected with the Wan Hoff first singularity, shifted to the high-energy region, demonstrating a decrease in Fermi level [9, 10], corresponding to an acceptor-type conductivity.

The studies of boron-doped CNT electric properties [11] showed a difference between the boron-doped single- and multi-wall tubes. For multi-wall tubes it is characteristic to note an appearance of acceptor states, defining *p*-type conductance. In the single-wall nanotubes under doping processes there is a marked change in the valence zone structure, which can be a result of substitution doping product action. The results of [11, 12] showed that the conductivity value of boron-doped SWCNTs rises more weakly compared with non-doped nanotubes, and the conductance is of an activation, semiconductor character.

Thus, under doping boron is substituting carbon into the graphene lattice nodes and has an acceptor action, creating activation *p*-type conductance.

6.2 Technology and Thermodynamics of Boron-Doped Carbon Nanotubes

The nitrogen-doped and boron-doped CNTs can be grown in different ways: a laser deposition method [13], a high-temperature electric arc method [14–16], and a substitution reaction method [17, 18]. The substitution reaction method consists of nanotubes already treated with B_2O_3 vapor. Within the tube proceeds a reaction of carbon atom substitution by a boron atom. A doping can be carried out during the well-known CVD method, which is very similar to nanoelectronic technologies and we therefore can consider it in detail. In CVD methods various precursors are used, such as three-boron-chloride [19], $C_9H_{21}BO_3$ [20], etc.

The energies of X-ray photoelectron spectroscopy (XPS) peaks are within the range 190–202 eV and are well recorded [21]. In one piece of work [19] the content of boron-doped nanotubes was estimated by XPS for a tube's growth at different temperatures. We investigated the dependencies of the concentration of nitrogen temperature by TGA (Fig. 6.1). Our results are consistent with that work [19].

The boron and nitrogen atoms behavior is analogous and therefore experimental results analysis can be made via the procedure described in Sect. 5.11. Boron is an

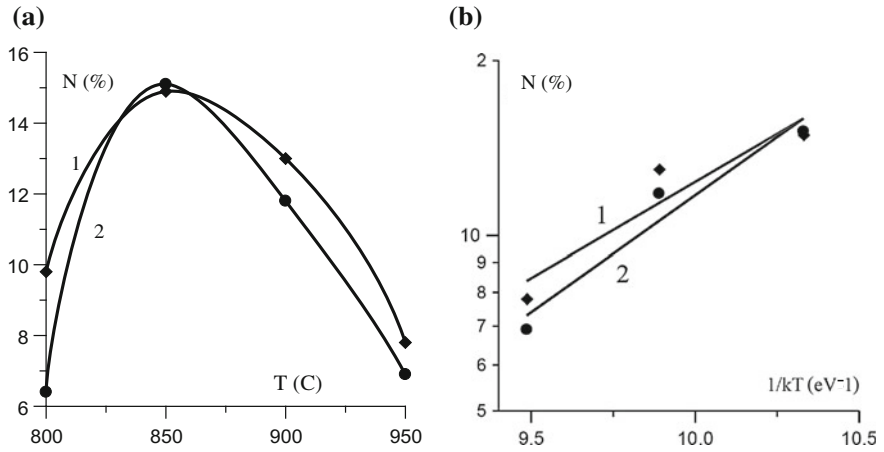

Fig. 6.1 Percentage content of nitrogen (*1*) and boron (*2*) into carbon nanotubes, defined by TGA method: **a** linear scale; **b** semi-logarithmic scale

acceptor and its thermodynamic estimation is similar to that of nitrogen, made in the section above.

The concentration of boron, substituting carbon in the graphene lattice nodes, is in thermodynamic equilibrium and can be defined by the XPS method, using the expression:

$$N_{\mathrm{Br}}^{C} = N^{C} \exp\left(-\frac{g_{\mathrm{Br}}^{C} - \mu_{\mathrm{Br}}}{kT}\right)\left[1 + \frac{n}{N_H}\exp\left(\frac{\varepsilon_{\mathrm{Br}}^{C}}{kT}\right)\right]. \tag{6.1}$$

The activation energy is equal $\left(g_{\mathrm{Br}}^{C} - \mu_{\mathrm{Br}}\right)$. As a boron source $NaBH_4$ compound was used, and using the calculated boron activity values for this compound's decomposition, we estimated the partial free energy of the boron incorporation into the graphene lattice nodes.

6.3 Boron-Doped Carbon Nanotube Usage

The high sorption characteristics of nanostructures (including CNTs) are very important from both a theoretical and practical point of view [22, 23]. As was said above, the adsorption changes the tube's electronic structure and hence its electronic properties too [24]. For example, in one piece of work [25] it was shown that CNT doping by boron strengthens their adsorptive power with regard to gases: H_2, H_2O, O_2, CO, CO_2, NO, NO_2, NH_3, and CH_3OH. Similar results were obtained elsewhere [26–29]. The comparative theoretical calculations also showed that for

boron-doped nanotubes the adsorption energy is higher (but the chemical bond length is smaller) than for non-doped tubes.

Under gas adsorption the electron state density is essentially changing. The calculations by the molecular dynamics method also confirmed that boron-doped CNTs represent a very good prospect in terms of material for gas sensor fabrication [25].

There are some other phenomena, connected with adsorption, for example it was reported that in boron-doped CNTs a superconductivity effect was recorded [30]. The emission processes in such nanotubes are hampered, because in materials with *p*-type conductance the electron yield work is higher than in *n*-type materials [31, 32].

Doping by boron can be used to create the *p–n* junction in single nanotubes.

6.4 The *p–n* Junction Forming Carbon Nanotubes

One good prospect in the field of applications of CNT is microelectronic device elements and device fabrications. Therefore, a realization of this (to create a *p–n* junction on the single, separated nanotube) holds great interest for researchers. Doping presents a standard way to create electron and hole conductivity in many materials, and *p–n* junctions are often formed by combining regions with different conductance types in a single-substance piece. These transitions have many advantages over metal semiconductor contacts. Note, that the *p–n* junction and metal semiconductor contacts present variants of semiconductor devices which contain a control region of strong field (so called the space charge region, SCR)—such formation of a region is a main feature of semiconductor devices. The external electric field, applied to the space charge region, changes the main electric field parameters into SCR (the geometric dimensions, potential distribution, and field voltage) and leads correspondingly to changes of current flowing along or across this region. This current can be transformed (including its amplification) by different constructive methods. The formation of SCR allows an increased efficiency of non-electric quantity's (As: light, radiation, heat, etc.,) transformation into electric current. Namely, the transformation is the main goal of the semiconductor devices creation and usage.

The main difference between the metal semiconductor contacts and the *p–n* junction is the condition of the charge injection process. An injection is a physical effect, which resides in the creation of a non-equilibrium free charge carrier concentration into the mentioned space charge region and adjoining quasi-neutral domain. The charge carrier injection proceeds under an external electric field application in such a way that the field (already existing in a region due to the constructive features of a given semiconductor device) decreased. The injections from the metal semiconductor contact are practically unipolar, meaning that in the process involves the majority of charge carriers, namely, in an electron's region (with *n*-type conductance) the electrons are injecting, but in a hole's region (with *p*-type conductance) the holes are injecting. On the contrary, in the *p–n* junction

situation the minority charge carriers are injected, namely, the electrons are injected into a hole's conductance region and the holes into an electron's conductance region. The phenomenon of minority carrier injection appears in work based on emitting devices, such as the photodiodes and injection lasers.

The electric field of the *p–n* junction is stronger compared with the field of a metal semiconductor contact, and this fact is connected with a potential barrier height on the contact boundary. Into the *p–n* junction a potential barrier height can achieve the order of the forbidden zone width, although in a metal semiconductor contacts this value, as a rule, is below two-thirds or even one-half the zone width. The lower potentials create weaker electric fields, which decrease the effectiveness of the non-electric quantities into electric ones (e.g., the effectiveness of photodetectors with a *p–n* junction is higher than for devices with metal semiconductor contacts).

We reproduce this well-known data, because within the scientific literature, related to CNT-based structures with a space charge region, sometimes appear the wrong expressions, reflecting the erroneous perceptions relative to the processes in these devices. For example, in some other publications, the metal contact with CNTs is named the Shottky diode. In fact, the Shottky diode presents a metal semiconductor contact, where the charge carrier transport through the contact is carried out due to a thermoelectric emission effect. A dominant preference of thermoelectronic emission over other transport effects must be especially proved in every case. It can be made by measuring the contact's current–voltage characteristics at various temperatures. Then it is necessary to construct a temperature dependence curve for the saturation current at standard coordinates for these procedures and to find the potential barrier height. If the barrier height, defined by this method, coincided with the height calculated from the saturation current data, one can say that a thermoelectric emission really takes place and the given device can be called a Shottky diode. Otherwise this metal and semiconductor contact cannot be named a Shottky diode.

It is well known that in a metal dielectric semiconductor structure you can create a region with a charge carrier inversion. The inversion effect arises into a channel of such a structure, fabricated on the basis of one type of conductance semiconductor (e.g., electronic conductance), when a combination of the external fields are applied near the dielectric semiconductor interface boundary by such a way, that the boundary forms a layer with the opposite conductance type (e.g., holes conductance). In the scientific literature, devoted to the CNT based devices, conductance inversion is sometimes mistakedly named an "electrostatic *p–n* junction" creation method. This notation is wrong for two reasons: first, every space charge region is formed and regulated by an electrostatic manner, and second, in such a structure it is impossible to carry out a minority charge carrier injection, which is a very important feature of the *p–n* junction.

Therefore, considering *p–n* junction formation, it is necessary to take into account the method of contact between the regions with *p*- and *n*-type conductance. These methods can be based on material doping or structural treatment by different actions (light irradiation, surface annealing, high-energy particle beam

bombardment). In every case the type of conductance, obtained under the action, must be retained after treatment without any influence of the external electric fields.

6.4.1 *Features of* p–n *Junction Formation in Carbon Nanotubes by a Mutual Acceptors and Donor Doping*

This method of *p–n* junction formation is well known in microelectronics, but in the case of CNTs there are some peculiarities which must be considered. A SWCNT is a graphene plane, convoluted into a tube, where all the atoms are arranged on a plane and therefore the traditional diffusion methods of region formation are ineligible.

As it was said above, the nitrogen and oxygen atom chemisorption on SWCNTs is connected with a negative charge transport, meanwhile SWCNT substitution doping by nitrogen is connected with a positive charge transport (substitution SWCNT doping by oxygen is energetically non-profitable). In theory it allows the

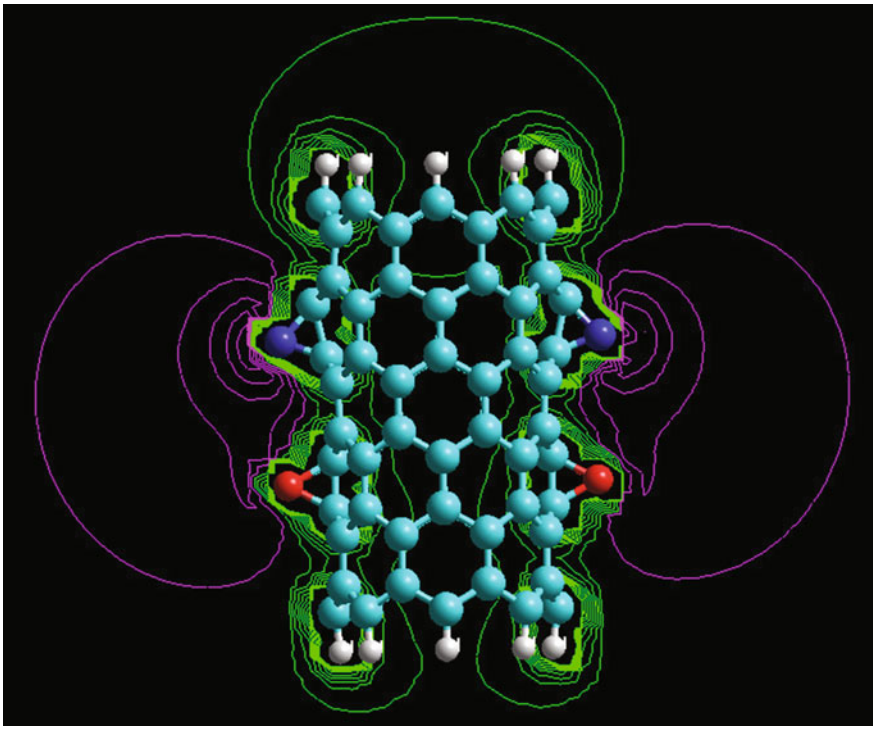

Fig. 6.2 Spatial distribution of electrostatic potential under chemisorption of two nitrogen and two oxygen atoms on a SWCNT with chirality (8.0). The calculated configuration characteristics are: $Q(N) = -0.48$; $Q(O) = -0.20$; $Eg = 2.48$ eV

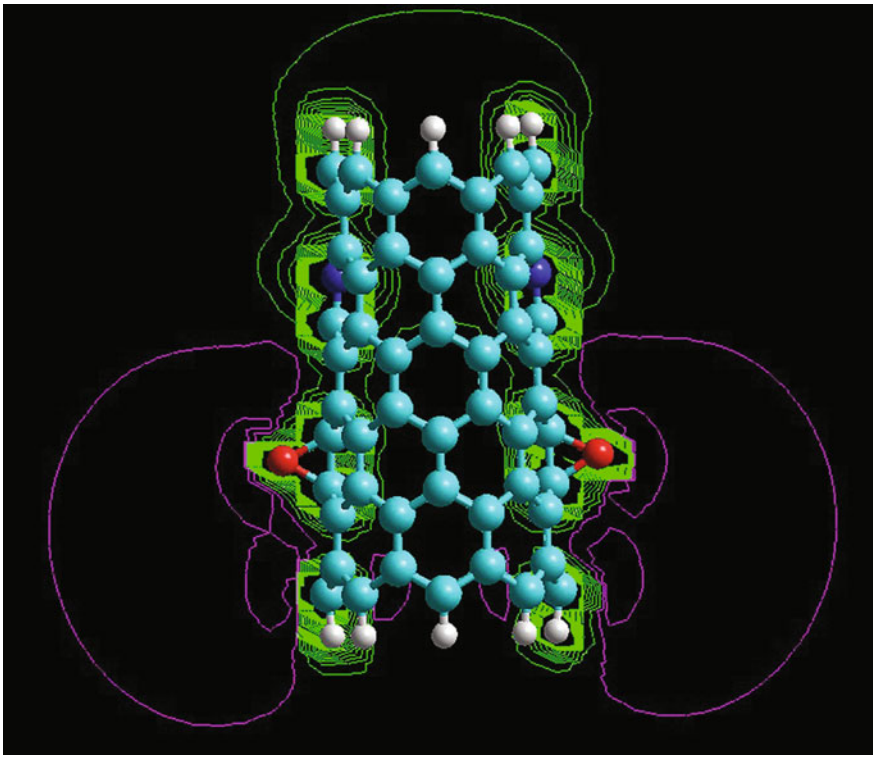

Fig. 6.3 Spatial distribution of electrostatic potential under chemisorption of two oxygen atoms and substitution doping by two nitrogen atoms on a SWCNT with chirality (8.0). The calculated configuration characteristics are: $QQ(N) = +1.08$; $Q(O) = -0.25$; $Eg = 1.87$ eV

creation, at one SWCNT region, of positive and negative charges and realization on the tube of a *p–n* junction. Below on the example of an (8,0) tube, the results of modeling are presented for a SWCNT with two chemisorbed nitrogen and oxygen atoms (Fig. 6.2) and a SWCNT with two chemisorbed oxygen atoms and two doped nitrogen atoms in a graphene substitution configuration (Fig. 6.3).

The second case really demonstrates the separation of positive and negative charge regions (Fig. 6.3) and indicates the theoretical possibility to create a *p–n* junction on the base of one SWCNT.

The problem is how to realize an ordered arrangement of atoms, when practically all atoms are in the same conditions. Therefore, regions with different conductance types are formed in a stochastic manner in view of the doping admixture's random location on the nanotube surface. In the present study the authors are correctly noting that the admixture distribution fluctuations are forming local regions with different conductance types. With a doping level growth the potential fluctuations value increases, but their sizes decrease. This well-known fact is earlier observed in the

highly doped, compensation semiconductors and so-called glass-like semiconductors. The impurities and defects fluctuations lead to electronic states localization.

Thus, the main problem of the *p–n* junction formation in a nanotube is to fabricate an equivalent surface arrangement of carbon atoms forming the graphene lattice. In view of this fact, the doping admixture takes its place in a random manner in an arbitrary place on the tube, and therefore it is difficult to form the relatively large and extended regions with the same type of conductance.

6.4.2 Carbon Nanotube Arrays as a Volume Crystal Analog

On a silicon substrate one can grow not a separate nanotube, but a sufficiently ordered array (Fig. 6.4).

The single nanotubes within the array can be located very closely, and moreover they consist in the form of bundles, growing from a same catalyst drop. The array is a continual medium, which (with some assumptions) is subordinating to diffusion laws. This fact allows certain treatments, leading to the formation into the array of a *p–n* junction, which grows parallel to the surface. Let us consider the perspective methods which can induce this effect.

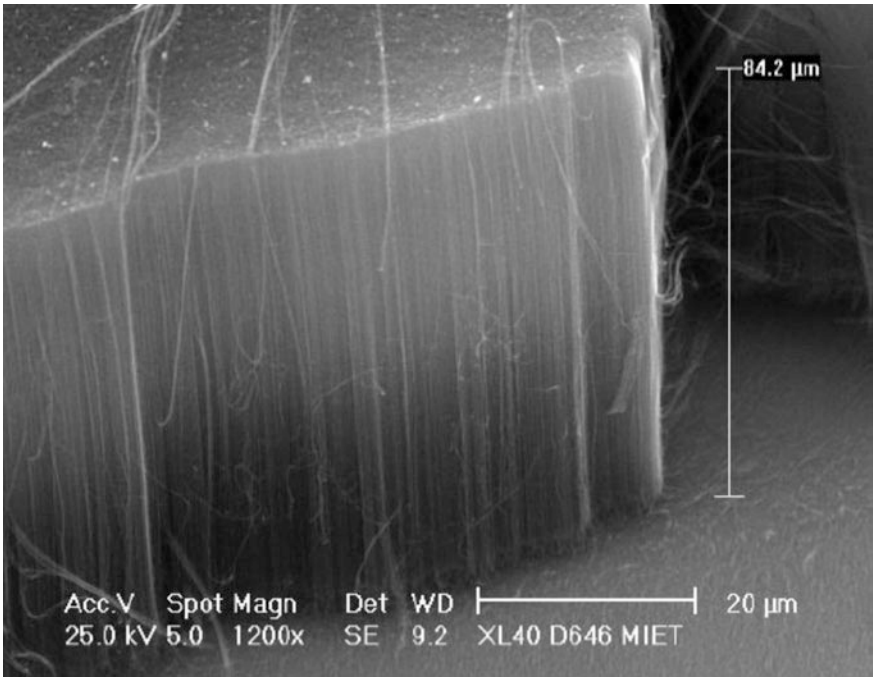

Fig. 6.4 Nanotube array, grown on a silicon substrate with a hard catalyst

6.4.3 *The Formation of a* p–n *Junction, Under Changing Temperatures, in a Nitrogen-Doped Carbon Nanotube Array*

It was shown in Chap. 5, that nitrogen introduced into a tube has amphoteric properties, i.e., can create both donor and acceptor admixtures. A nitrogen atom, substituting carbon in a lattice node, forms a donor admixture, but, being introduced by pyridine method, side by side with a vacancy, forms an acceptor admixture. In reference [136] of the Chap. 5 the growth temperature regions are shown for nanotubes doped by the various dominating nitrogen arrangement methods. For example, let us suppose that we begin growth at a temperature of 750 °C, and (after growing the rather dense array) then shut down the process, decreasing the temperature to 650 °C, and then continue the process once more. At a temperature of about 750 °C the nitrogen atoms are preferentially introduced by substitution method and this array's mass will have *n*-type conductance. The vacancies, formed under these conditions, are already occupied by nitrogen, being introduced by the pyridine method. Under a growth temperature decrease there must not arise any sufficient changes in the array growth zone. The volume the pyridine-type content will be increase then growth temperature decrease. The array will become *p*-type material. Thus, in a unique growth process a *p–n* junction region, parallel to the substrate, arises, due only to the change in conditions defining nitrogen introduction into the CNTs.

The analogous method can be used for tube growth under simultaneous doping by boron and nitrogen. By growing the array at a temperature of 845 °C, we form a *p*-region in the array, but then by decreasing the growth temperature to 780 °C, and forming an *n*-region in the array, we create a *p–n* junction.

6.4.4 *Doping Admixture Change During the Growth Process*

A similar result can be achieved by changing not only the growth temperature, but also the gas mixture composition, e.g., introducing to it a gaseous component, creating the donor or acceptor admixtures. The array grows sufficiently fast and therefore the gas, containing a new component, makes progress in penetrating the grown part of the array, forming a *p–n* junction.

6.4.5 *Ionic Doping of an Array*

It was shown that CNTs can be doped by ionic implantation method. The implanted ions with energy of several MeV destroy the CNTs, and such ionic etching can result in the array's total destruction. Therefore, the authors used nitrogen, argon,

and oxygen ions, accelerated at low voltages (about 20 V of order). The gas ionization proceeded on a heated tungsten filament. Studies of field transistors and Raman light scattering showed successful gaseous ion penetration into the CNT.

When the method is used with dense arrays, any ion flying into the array will be subjected to numerous scattering acts into the upper layer and therefore will not penetrate array regions near the substrate. If a dense nitrogen-doped array matrix is used for penetration, grown at a temperature of 750 °C, it will have *n*-type conductance. Oxygen ion penetration at low temperatures creates, in the upper layer of the array, a new region with *p*-type conductance, and thus will arise a *p*–*n* junction. Apparently, the same situation can arise under a doping by boron under certain conditions.

6.4.6 *Carbon Nanotube Array Oxidation Under Ultraviolet Irradiation*

In one piece of work changes of the CNT electromotive force at room temperature were studied for two types of irradiation: usual scattered light (i.e., found in lodgings and premises) and ultraviolet radiation with a wavelength of 240 nm and irradiation power per unit surface of 4 mW/mm^2. The oxidation intensity under ultraviolet radiation was sufficiently greater, the oxidation time (to a conductance inversion achievement) was shortened by 15 times, and the thermo-electromotive force value increased 5 times. This effect also can be used for *p*–*n* junction formation in an array. The upper part of the array is always rather deformed and the tube ends are chaotically bent. This fact leads to an additional light scattering namely in the array upper part and therefore this part must be oxidized faster, leading to a *p*–*n* junction. Thus, we listed several physical effects, which can form a *p*–*n* junction in a CNT array whilst the plane is parallel to the substrate surface.

6.5 Summary

We analyzed the results of doping with boron nanotubes and the prospect of creating *p*–*n* junctions in arrays of CNTs.

References

1. E. Tetik, The electronic properties of doped single walled carbon nanotubes and carbon nanotube sensors. Condens. Matter Phys. 17(4), 43301: 1–12 (2014)
2. P. Ayala, M.H. Rummeli, T. Gemming, E. Kauppinen, E. Kauppinen, H. Kuzmany, T. Pichler, CVD growth of singlewalled B-doped carbon nanotubes. Phys. Stat. Sol. (b) **245**(10), 1935–1938 (2008)
3. S. Ishii, T. Watanabe, S. Ueda, S. Tsuda, T. Yamaguchi, Y. Takano, Resistivity reduction of boron-doped multiwalled carbon nanotubes synthesized from a methanol solution containing boric acid. Appl. Phys. Lett. **92**, 202116 (2008)
4. W.L. Wang, X.D. Bai, E.G. Wang, Towards the singlewalled B- and/or N-doped carbon nantubes. Int. J. Nanosci. **6**, 431–442 (2007)
5. L. Williams Quinton, X. Liu, W. Walters Jr., J.G. Zhou, Y. Edwards Tylvia, L. Smith Franchesca, Boron-doped carbon nanotube coating for transparent, conducting, flexible photonic devices. Appl. Phys. Lett. **91**, 143116 (2007)
6. C. Ling-Na, M. Song-Shan, O. Fang-Ping, X. Jin, X. Hui, First-principles study of metallic carbon nanotubes with boron/nitrogen co-doping. Chin. Phys. B **20**(1), 017103 (2011)
7. J. Maultzsch, S. Reich, C. Thomsen, S. Webster, R. Czerw, D.L. Carroll, S.M.C. Vieira, P.R. Birkett, C.A. Rego, Raman characterization of boron-doped multiwalled carbon nanotubes. Appl. Phys. Lett. **81**, 2647–2648 (2002)
8. L.-J. Li, M. Glerup, A.N. Khlobystov, J.G. Wiltshire, J.-L. Sauvajol, R.A. Taylor, R. J. Nicholas, The effects of nitrogen and boron doping on the optical emission and diameters of single-walled carbon nanotubes. Carbon **44**, 2752–2757 (2006)
9. L.J. Li, R.J. Nicholas, Bandgap-selective chemical doping of semiconducting single-walled carbon nanotubes. Nanotechnology **15**(12), 1844–1847 (2004)
10. P. Petit, C. Mathis, C. Journet, P. Bernier, Tuning and monitoring the electronic structure of carbon nanotubes. Chem. Phys. Lett. **305**(5–6), 370–374 (1999)
11. R. Czerw, P.-W. Chiu, Y.-M. Choi, D.-S. Lee, D.L. Carroll, S. Roth, Y.-W. Park, Substitutional boron-doping of carbon nanotubes. Curr. Appl. Phys. **2**, 473–477 (2002)
12. B. Wei, R. Spolenak, P. Kohler-Redlich, M. Ruhle, E. Arzt, Electrical transport in pure and boron-doped carbon nanotubes. Appl. Phys. Lett. **74**(21), 3149–3151 (1999)
13. P.L. Gai, O. Stephan, K. Mc Guire, A.M. Rao, M.S. Dresselhaus, G. Dresselhaus, Structural systematics in boron-doped single wall carbon nanotubes. J. Mater. Chem. **14**(4), 669–675 (2004)
14. R. Droppa, P. Hammer, A.C.M. Caryalho, M.C. Santos, F. Alvarez, Incorporation of nitrogen in carbon nanotubes. J. Non-Cryst. Solids **299**, 874–879 (2002)
15. M. Glerup, J. Steinmetz, D. Samaille, O. Sterphan, S. Enouz, A. Loiseau, Synthesis of N-doped SWNT using the arc-discharge procedure. Chem. Phys. Lett. **387**(1–3), 193–197 (2004)
16. K. McGuire, N. Gothard, P.L. Gai, M.S. Dresselhaus, G. Sumanasekera, A.M. Rao, Synthesis and Raman characterization of boron-doped single-walled carbon nanotubes. Carbon **43**(2), 219–227 (2005)
17. D. Golberg, Y. Bando, W. Han, K. Kurashima, T. Sato, Single-walled B-doped carbon, B/N-doped carbon and BN nanotubes synthesized from single-walled carbon nanotubes through a substitution reaction. Chem. Phys. Lett. **308**(3–4), 337–342 (1999)
18. W. Han, Y. Bando, K. Kurashima, T. Sato, Synthesis of boron nitride nanotubes from carbon nanotubes by a substitution reaction. Appl. Phys. Lett. **73**(21), 3085–3087 (1998)
19. G. Zhang, Z. Liu, L. Zhang, L. Jin, K. Shi, Growth and characterization of BCN nanotubes with high boron and nitrogen content. J. Chem. Sci. **125**(5), 1169–1176
20. P. Ayala, W. Plank, A. Gruneis, E.I. Kauppinen, M.H. Rummeli, H. Kuzmany, T. Pichler, A one step approach to B-doped single-walled carbon nanotubes. J. Mater. Chem. **18**, 5676–5681 (2008)

21. P. Ayala, W. Plank, A. Gruneis, E.I. Kauppinen, M.H. Rummeli, H. Kuzmany, T. Pichler, A one step approach to B-doped single-walled carbon nanotubes. J. Mater. Chem. (2008). doi:10.1039/b809050e
22. S.V. Bulyarskiy, A.S. Basaev, Thermodynamics and kinetics of adsorption of atoms and molecules with carbon nanotubes. ZhETF **135**(4), 788–799 (2009)
23. S.V. Bulyarskiy, A.S. Basaev, Adsorption by carbon nanotubes. Nano Microsyst. **12**(116), 16–55 (2009)
24. S.V. Bulyarskiy, *Uglerodnye nanotrubky: techologya, upravlenie svoystvami, primenenie* (Streshen, Ulyanovsk, 2011), 479 p (Rus.)
25. P.A. Gowri Sankar, K. Udhayakumar, Electronic properties of boron and silicon doped (10, 25). Zigzag single-walled carbon nanotube upon gas molecular adsorption: a DFT comparative study. J. Nanomater. Article ID 293936, 12 p (2013)
26. L. Bai, Z. Zhou, Computational study of B- or N-doped single-walled carbon nanotubes as NH_3 and NO_2 sensors. Carbon **45**(10), 2105–2110 (2007)
27. W. An, C.H. Turner, Electronic structure calculations of gas adsorption on boron-doped carbon nanotubes sensitized with tungsten. Chem. Phys. Lett. **482**(4–6), 274–280 (2009)
28. J.A. Talla, First principles modeling of boron-doped carbon nanotube sensors. Phys. B **407** (6), 966–970 (2012)
29. J. Debnarayan, S. Chia-Liang, C. Li-Chyong, C. Kuei-Hsien, Effect of chemical doping of boron and nitrogen on the electronic, optical, and electrochemical properties of carbon nanotubes. Prog. Mater Sci. **58**, 565–635 (2013)
30. J. Haruyayma, V. Matsudaria, J. Reppert, A. Rao, Superconductivity in boron-doped nanotubes. J. Supercond. Nov. Magn. **24**, 111–120 (2011)
31. U.A. Palnitkar, R.V. Kashid, M.A. More, D.S. Joag, L.S. Panchakarla, C.N.R. Rao, Remarkably low turn-on field emission in undoped, nitrogen-doped, and boron-doped grapheme. Appl. Phys. Lett. 97, 063102, 97, 063102-1 (2010)
32. H.-S. Ahn, K.-R. Lee, D.-Y. Kim, S. Han, Field emission of doped carbon nanotubes. Appl. Phys. Lett. **88**, 093122 (2006)

Conclusions

What Was Known in the Field Before the Book Was Written?

The book writing process began in 2008, when new prospective materials, based on CNTs, "burst" into microelectronics. These materials appeared to hold great promise, but nanotubes in most cases presented themselves as conglomerates, which were interesting to study, but allowed only a glimpse of any practical applications on a scientific basis. At this time the first work was published, devoted to CNT array growth on silicon substrates.

It became clear, that the most promising direction for up-to-date nanoelectronics was the creation of hybrid structures, where CNTs would be grown on silicon integrated circuits. In this combination modern microelectronic achievements could be joined with CNT advantages and a new, unique type of integrated circuits could be fabricated, having the additional possibilities use in radiation and cold emission, UHF-range built-in receivers and emitters, as well as various magnetic, chemical, and biological sensors. Thus, there arose a new direction of electronics development, namely, silicon–carbon nanoelectronics, allowing the combination, in one crystal, of the characteristics of silicon and carbon structures, enlarging the usual planar integrated circuit properties by using unique carbon structure preferences for digital signal treatment.

This book's authors are actively involved in the realization of this approach. The main problem turns out to be a search for methods and conditions of nanotube property control both during their growth and subsequent to it. These problems remain for silicon–carbon nanoelectronic elements.

What Was Identified Whilst Writing the Book?

Carbon nanotube peculiarities were studied with regard to their role in system property regulation. The quantum mechanical analysis of impurity interaction with a graphene nanotube surface and its defects was carried out. The mathematical

S. Bulyarskiy and A. Saurov (eds.), *Doping of Carbon Nanotubes*,
NanoScience and Technology, DOI 10.1007/978-3-319-55883-7

models of gaseous phase atom interaction with the growth in reactor CNTs were elaborated in order to develop the thermodynamics of CNT behavior and control.

The comparison of theoretical models and experimental results demonstrated the validity of the developed theory and the numerical experiments resulting on its basis.

The analysis of the experimental results and theoretical models showed that a dominant role in the doping and adsorption processes is played by the free energy of the system, consisting of the gas mixture within the reactor, its temperature, and nanotube surface energy. The methods of admixture content calculation, based on this energy minimization, were developed.

Many scientific studies in the field of various admixture doping and adsorption processes (including works concerning the main admixtures: hydrogen, oxygen, and nitrogen) have been analyzed and estimated, as well as various methods and procedures for CNT property control, etc.

What is Clear After Completion of Writing the Book?

The conditions and methods of nanotube doping have been studied and the partial Gibbs potentials defined for the main admixture (hydrogen, oxygen and nitrogen) arrangements into the graphene lattice. This has the potential to help develop controlling technologies for nanoelectronic element production.

The problem of CNT property control seems easy, but is connected with significant technological difficulties, especially regarding the organization of the terminal technology operations. These operations must exclude any CNT interactions with oxygen and other admixtures. The difficulties to be surmounted are serious. It is first necessary to design and construct new technological equipment.

What Lies Ahead in this Field?

The accumulated knowledge on CNT doping and adsorption processes makes it possible to create and organize the controlling technologies for nanoelectronic element production.

Index

S. Bulyarskiy and A. Saurov (eds.), *Doping of Carbon Nanotubes*,
NanoScience and Technology, DOI 10.1007/978-3-319-55883-7